Design and fabrication of advanced microdevices for stem cell and cancer cell studies

Yadong Tang

THESE DE DOCTORAT DE

L'UNIVERSITE PIERRE ET MARIE CURIE

Spécialité :

Chimie Physique et Chimie Analytique

(Ecole doctorale ED388)

Présentée par

Yadong TANG

Pour obtenir le grade de

DOCTEUR de l'UNIVERSITÉ PIERRE ET MARIE CURIE

Sujet de la thèse :

Conception et étude de microsystèmes avancés pour la recherche de cellules souches et de cellules cancéreuses

Soutenue le 29 février 2016 devant le jury composé de :

M. Vincent TORRE	Rapporteur
M. Jean-francois BERRET	Rapporteur
M. Onnik AGBULUT	Examinateur
M. Ludovic JULLIEN	Examinateur
M. David PEYRADE	Examinateur
M. Yong CHEN	Directeur de thèse

Acknowledgement

Finally, I come to the end of my PhD work and I am really glad to have the opportunity to work on this thesis topic at the interface of several scientific disciplines. Although only my name appears on the cover of this thesis, a great many people have contributed to its production. I owe my gratitude to all those people who have made this dissertation possible, and because of whom, my PhD experience has been one that I will cherish forever.

Before all, I would like to present my gratitude to Chinese Scholar Council (CSC) for supporting me to study abroad during the whole three years, to Ecole Normal Supérieure (ENS) for providing me the best working conditions and excellent research environment to work on my thesis, to the Université Pierre et Marie Curie (UPMC) for accepting me as a doctor candidate, and the Institute for Integrated Cell-Material Sciences (iCeMS) of Kyoto University for hosting me as a visiting student during this thesis work.

Then, I would like to express my gratitude to my supervisor Prof. Yong CHEN, for his expert guidance, suggestion and support. Under his guidance, I learned how to think more logically facing a scientific problem and how to solve a problem more efficiently. Under his suggestion, I could be able to explore several important fields in the cross-disciplinary areas related to microengineering, cell biology, and biomedical applications. Under his support, I could have the chance to visit several laboratories in China and in Japan and to meet many talent peoples come from different countries. I believe all the experience and knowledges I gained from him will benefit my future career and life.

Next, I am also grateful to the professors, colleagues and friends in France for their kindly help, support and encouragement. They are: Dr. Jian Shi, Dr. Yvon E. Cayre, Dr. Li Wang, Dr. Jacques Fattaccioli, Dr. Jianmiao Liu, Dr. Weikang Wang, Dr. Sandrine Quignard, Dr. Diana Molino, Dr. Yohan Farouz, Dr. Kalthoum Ben M'barek, Dr. Ian Broadwell, Dr. Maria Kitsara, Dr. Timothee Houssin, Dr. Sisi Li, Dr. Li Yun, Dr. Lili Wang, Francesco Paolo Ulloa Severino, Absetou Atou Sow, Momoko Yoshioka, Jin Wei, Bin Wang, Xiaolong Tu, Olivier Mesdjian, Xiaoqing Liu, Chenge Li, Lihui Hu.

I would also like to thank my colleagues in iCeMS of Kyoto University. I would like to specially thank Dr. Li Liu, Dr. Junjun Li, Leqian Yu and their families for

their warm welcome and kind care, to Dr. Ken-Ichiro Kamei, Ayano Tabata, Nanae Fujimoto, Minako Nakajima for their kind help and suggestions.

My gratitude also goes to Auguste Filippi, Mme Anne Halloppe, Mr. Stéphane Paties-Gorizza, Mme Katy Seloi, Mme Marie Chayla in ENS and Mme Soobrayen Koonavadee in UPMC, who were always so kind to arrange everything for me in student affairs management.

Last but not least, I would like to thank my family. I am especially grateful to my husband Wenlong Wang, who gave me so many encouragement and support, even accompanied me every time I need to come to the laboratory during weekend/holidays. I am also grateful to my parents and parents-in-law for their support and understanding on our study abroad.

Yadong TANG

Table of Contents

Outline

Biomaterial and device engineering was in rapid development during the past decades and led to new perspectives for a large variety of applications in drug development, regenerative medicine and healthcare. In particular, microengineering tools and methods are now widely used to fabricate either two or three dimensions culture substrate or scaffolds to mimic the extracellular matrix for both *in vitro* and *in vivo* assays. Microengineering tools and methods are also used to fabricate microfluidic devices to more efficiently control the cell factors and physiological conditions *in vitro*.

The purpose of this thesis work is to develop new tools and methods which can solve the current problems encountered in stem cells and cancer studies.

Stem cells and pluripotent stem cells in particular are powerful for the development of new methods and new tools in tissue engineering and regenerative medicine. Yamanaka and John Gurdon were awarded the Nobel Prize in 2012 for the discovery that mature cells can be converted to embryonic-like stem cells (induced pluripotent stem cells or iPSCs), which can be differentiated into various specialized cell types. Their discovery holds very high potential for tissue engineering and transplantation therapy. So far, the studies on iPSCs are mostly based on conventional culture methods, i.e. the *culture dish methods*, which are not appropriate for most of envisaged applications. Therefore, there is a clear need for devices and methods for iPSC culture and handing under optimal physiological conditions and highly compatible to both *in vitro* and *in vivo* assays. In this work, we developed a *culture patch method*, which is based on the fabrication of crosslinked monolayer gelatin nanofibers, for iPSCs culture and differentiation. We show that both cardiomyocytes and neurons can be obtained on the culture patch under *off-ground culture* conditions and that the derived cardiac and neural patches can be used for removable electrophysiological measurements.

Cancer cells and circulation tumor cells in particular are objectives of a huge number of investigations since many decades. In this work we focus on cancer diagnosis since the early diagnosis is significant to decrease mortality, which will also benefit for the further therapy. Capture of circulating tumor cells (CTCs), which have strong relation to metastasis, was chosen as the method for cancer diagnosis due to its ease of operation and non-invasion. In this thesis, we propose a new

microdevice to solve the main problems in the field of CTCs capture, including improving efficiency and viability, as well as minimizing contamination. Besides, building *in vitro* solid tumor model is significant for deep understanding the complexity and mechanism of tumor and anti-cancer drug studies. Multicellular tumor spheroid model has been proved to be an efficient model for evaluations of drug sensitivity and resistance compared to 2D monolayer cell culture. In this work, we develop a multi-well array with millimeter size for tumor spheroids formation and anti-cancer drug tests.

Accordingly, this thesis is organized as follows:

In chapter one, we first introduce the basic concepts of cell and cellular microenvironment. Then, we focus on two types of cells, i.e. induced pluripotent stem cells (iPSCs) and circulating tumor cells (CTCs), and the needs of advanced microdevice technologies for their *in vitro* manipulation. Next, we describe the state of the art developments of patterned substrates and scaffolds as well as microfluidics techniques. Finally, we outline the objectives of this thesis work.

In chapter two, we present the technological development of this thesis work. Firstly, we describe the electrospinning technique for the fabrication of gelatin nanofiber scaffolds. Then, we introduce hydrogel formation techniques, with special focus on poly (ethylene glycol) (PEG) based hydrogel. Afterwards, we present several lithography techniques for surface patterning and microfluidic device fabrications.

In chapter three, we present a study of culture and differentiation of induced pluripotent stem cells by using culture patch method. We first describe the fabrication of the culture patch which consists of a monolayer of crosslinked gelatin nanofibers formed on a honeycomb frame made of biocompatible polymer. Then, we present the results of cell proliferation on culture patch under off-ground culture condition. Next, we show how human pluripotent stem cells (hiPSCs) can be differentiated into cardiomyocytes and neurons on the culture patch under off-ground culture conditions and how this method is advantageous comparing to the conventional culture dish method.

In chapter four, we present a study of isolation and culture of cancer cells. We first describe the development of a CTCs isolation technique by using conical shape holes and microfluidic device. The processing parameters such as flow rate and cell density are studied for different types of tumor cells. Cell culture is also performed

after isolation to show the post-isolation capability of the proposed device. Afterward, clinical trials are performed and mechanical analysis is used to theoretically demonstrate the advantages of the conical shape holes of the filter and the microfluidic design. Finally, we descried a multi-well device for tumor spheroids formation. The performances of the culture with three different types of materials are compared, showing the suitability of agarose formed device. Then, we show the drug effects on the tumor spheroids formation.

In chapter five, a summary of the present thesis is given, together with a perspective of this work.

In appendix, we present a method for depositing graphene dioxide (GO) on gelatin nanofiber patch. Raman spectra is applied to characterize the incorporation of GO on nanofibers.

Chapter 1

Introduction

In this chapter, we first introduce the basic concepts of cell and cellular microenvironment. Then, we focus on two types of cells, i.e. induced pluripotent stem cells (iPSCs) and circulating tumor cells (CTCs), and the needs of advanced microdevice technologies for their *in vitro* manipulation. Next, we describe the state of the art developments of patterned substrates and scaffolds as well as microfluidics techniques. Finally, we outline the objectives of this thesis work.

1.1 Cell and cellular microenvironment

1.1.1 Cell

The human body is made of eight interacting systems, including motor system, respiratory system, nervous system, circulating system, digestive system, endocrine system, urinary system and reproductive system. And each of them is functioning with specific and cooperative organs, such as heart and vessel in circulating system, ensuring the major activities of the body. The organs are formed by body tissues and each of them is composed of different types of cells, for instance, cardiomyocytes constitutes cardiac muscle tissue. Therefore, cells are the basic structural and functional units of the human body. **Fig. 1.1** shows the levels of nervous system.

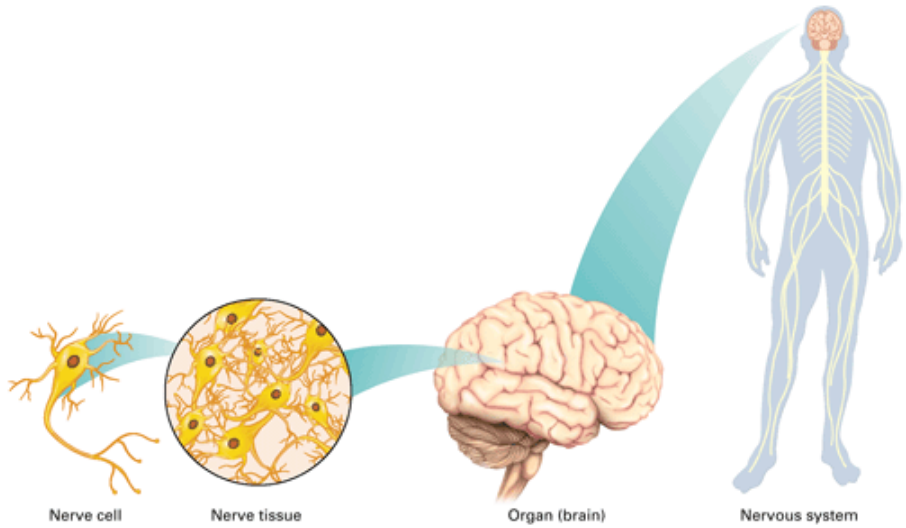

Fig. 1.1 The human brain, like other body organs, is made of a huge number of cells of many types in a sophisticated but highly complex way [1].

As the smallest unit of life, cells are considered as "building blocks of life". The number of cells in human is more than 10 trillion [2]. The structure and the organization of cells are also sophisticated and highly complex, as shown as **Fig. 1.2**.

Each cell has a membrane, called plasma membrane and made mostly from a double layer of phospholipids. The membrane surrounds the cytoplasm of a cell, divides the interior of cell from its outside environment, regulates that move different molecules into and out of the cell, and maintains the electric potential of the cell. Inside the membrane, a salty cytoplasm takes up most of the cell volume and acts to organize and maintain the shape of cell. The eukaryotic cytoskeleton contains microfilaments, intermediate filaments and microtubules. There are numbers of proteins associated with them, and regulate the structure of cells by directing, bundling, and aligning filaments. Cell nucleus is the information center, containing most of genetic material of cell. The nucleus offers a place for genetic transcription which is segregated from the location of translation in the cytoplasm, allowing levels of gene regulation. The main function of the cell nucleus is to regulate gene expression and DNA replication during the cell cycle.

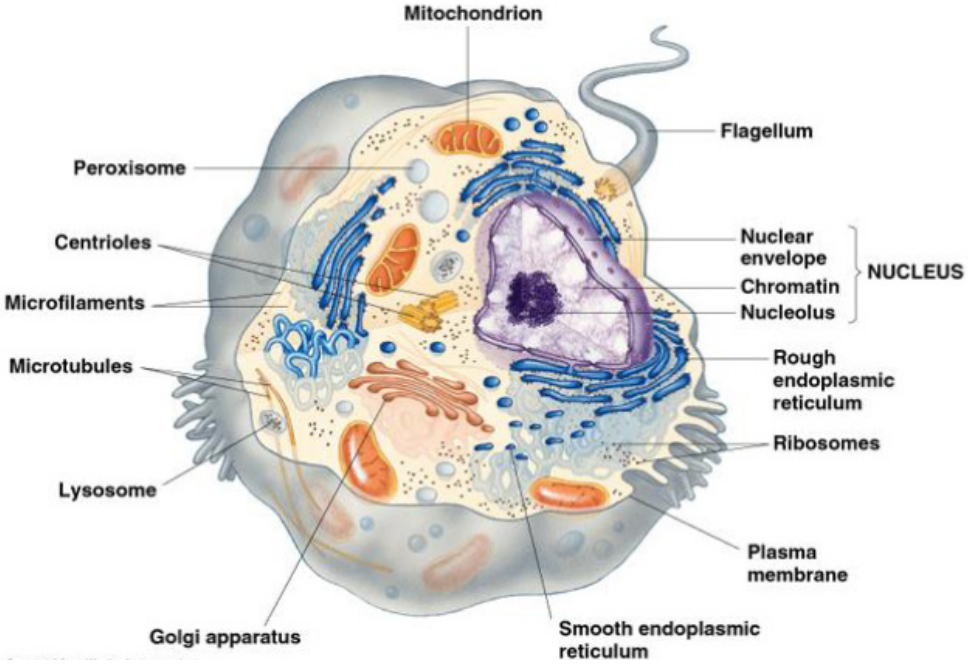

Fig. 1.2 Scheme of the intracellular structure of a typical animal cell [3].

1.1.2 Cellular microenvironment

The behavior and function of a cell are influenced by the immediate environment of the cell, named the cellular microenvironment. The structure and composition of the cellular microenvironment are also sophisticated and complex, which are coupled with cells as via biophysical, biochemical and other routes.

Considering an adhesion cell in a body, its cell microenvironment is composed of (i) extracellular matrix (ECM), (ii) homotypic or heterotypic cells surrounding the single cell, (iii) cytokines, hormones, and other bioactive agents around the cells due to autocrine, endocrine, and paracrine secretions, (iv) nano/microscale topography and physical properties of the adjuvant cells and the ECM, and (v) mechanical and dynamic forces caused by the movement of the organism or the movement of the physiological fluids such as blood. All these have a compound effect on the behavior of the cells, where the relative importance of each component is tissue and cell type dependent [4]. The controlling of the cellular microenvironment is a key aspect for understanding cell biology. And the cues derived from the surrounding microenvironment regulate cellular behaviors such as attachment, spreading, proliferation, migration and differentiation.

a) Extracellular Matrix

The extracellular Matrix (ECM) is the extracellular part of the body tissue providing the structural and biochemical support to the cell and regulating the cell behaviors such as cell adhesion, proliferation, migration and differentiation [5-8].

Fig. 1.3 shows the composition of ECM. Generally, it is considered that the ECM consists of two classes of insoluble biomacromolecules. One predominant component is the insoluble macromolecules, protein fibers including collagen and elastin which are structural fibers providing tensile strength to the ECM, as well as other proteins such as fibronectin, laminin and vitronectin which are adhesive fibers defining ECM function by acting as adhesive ligands.

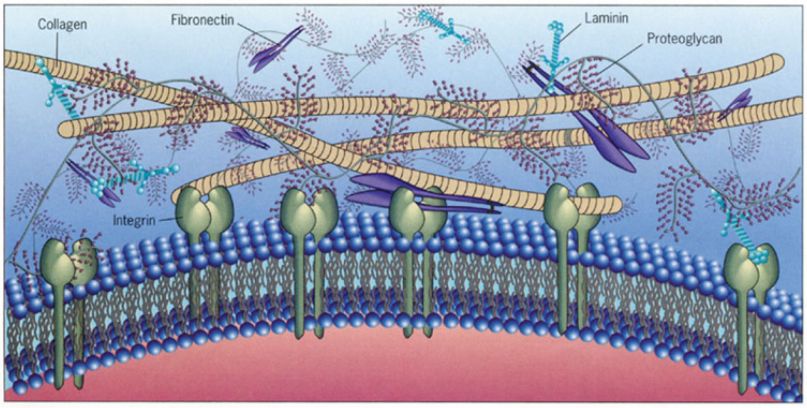

Fig. 1.3 Schematic of the composition of ECM [9].

Among them, collagen is the most abundant protein in ECM (accounts for 90% of bone matrix protein content), with more than 20 types of structures supporting the fibrin structure for cells [10-14]. Elastin, in contrast to collagens, give elasticity to tissues, is found in large quantities in tissues requiring elastic properties such as artery and bladder tissues [15]. Fibronectin and laminin are mainly in charge of adhesion to ECM, which are also widely used for substrate treatment before cell culture [16]. Another class of biomacromolecule is glycosaminoglycans, only playing roles in structure network and tissue resilience, but not deciding cell fate. In addition, proteoglycans have negative charge which can attract positive charged sodium ions (Na+), and help trap and store water molecules and keeps the ECM hydrated. Besides, growth factors are also an essential component in the matrix of ECM, such as fibroblast growth factor (FGF), epithelial growth factor (EGF) and vascular endothelial growth factor (VEGF). Typically growth factors as signaling molecules between cells are important for regulating a variety of cellular processes, including stimulating cellular growth, proliferation, healing, and differentiation [17]. **Table 1.1** summarizes the ECM components and their role in ECM dynamics.

Table 1.1 ECM components and their role [18].

Component	Function	Location
Collagens	Tissue scaffolding, tensile strength Cell-ECM interactions Cell-cell interactions Fibroblast activation	Ubiquitous
Proteoglycans	Collagen embedding Tissue resistance to compressive forces Transport of nutrients Fibroblast and chondrocyte proliferation Endothelial and epithelial cell differentiation	Ubiquitous
Hyaluronic acid	Transport of metabolites and nutrients Tissue resistance to compressive forces Cell migration Cell proliferation	Ubiquitous
Laminins	Intracellular signalling Cell differentiation Cell shape/movement	Basement membranes
Fibronectin	Cell attachment to ECM Cell migration Cell proliferation	Ubiquitous
Growth factors	Cellular signalling	Ubiquitous

b) Cell-ECM interaction

The interaction between cell and ECM is mainly controlled by specific cell-surface cellular adhesion molecules (CAM) known as integrin (shown in **Fig. 1.3**), which is a family of cell surface receptors attaching cells to the ECM and mediating mechanical and chemical signals from it. These integrin signals control the activities of growth factors receptors, ion channels, cytoplasmic kinases, and the intracellular actin cytoskeleton organization, directing cells to live or die, to proliferate, or to exit the cell cycle and differentiate. There are two subunits of integrin, α and β, which are bound covalently together. During their inactive state, integrin are freely diffusive within the cell membrane until they encounter an available binding domain in the ECM [19]. Once ligand binding, there will be a conformational change within integrin leading to the cytoplasmic proteins recruitment. These larger and clustered structures of integrin, such as fibronectin and laminin, and cytoplasmic proteins are generally called cell adhesions. The attachment of fibronectin to the ECM domain recruits intracellular signaling pathways as well as association with the cellular cytoskeleton via a set of adaptor molecules such as actin [20]. Therefore, integrin-mediated cell adhesions provide dynamic, bidirectional links between the cytoskeleton and the ECM, promoting cytoskeleton rearrangement and also inducing changes in cell shape which in turn alter the ability of cell proliferation or differentiation [21].

c) Cell-Cell interaction

The cell–cell interaction refers to the direct interactions between cell surfaces, playing a critical role in the function and development of multicellular organisms. This interaction between cells allows cells to communicate with each other in response to the changes in their microenvironment. The capacity of sending and receiving signals is crucial for the cell survival. The loss of communication between cells can result in uncontrollable cell growth and cancer. The cell-cell interactions involve cell junctions which are multiprotein complexes. Cell junctions can be divided into three categories, based upon the functions they serve (**Fig. 1.4**): tight junctions, anchoring junctions, and communicating junctions (called gap junction in animal) [22]. Tight junctions are multi-protein complexes that hold cells of a same tissue together and prevent movement of water and water-soluble molecules between

cells. Gap junction, which is composed of transmembrane proteins called connexins, is the main site of cell-cell signaling or communication allowing small molecules to diffuse between neighboring cells. Cell-cell interactions for adhesion can be mediated by cadherin, which is a family of adhesion receptors, and essential for anchoring cells to their niche directing cell behaviors.

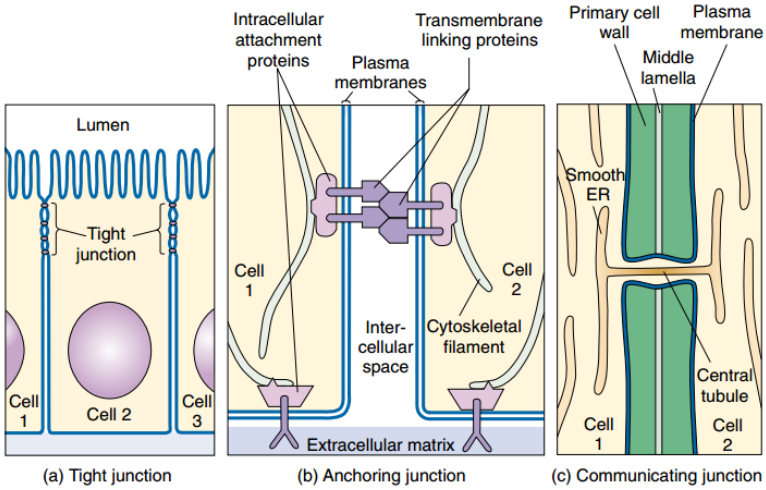

Fig. 1.4 Three major types of cell junctions: (a) tight junction; (b) anchoring junction; (c) communicating junction [22].

d) Extracellular fluid

The native extracellular microenvironments are extremely heterogeneous in three-dimension and they undergo dynamic and continuous remodeling with time. Therefore, biomechanical forces indisputably play a significant role within cellular microenvironment. Extracellular fluid (ECF) is one of these forces that can drive biochemical and biophysical changes with the cellular microenvironment. Typically, ECF represents all body fluid outside of the cells. ECF provides the cells of the body with nutrients and a means of waste removal. In mammals, the ECF can be divided into two main components: interstitial fluid and blood plasma. The interstitial fluid is found in the spaces between cells, which plays an important role in cellular behavior, signaling, lymphangiogenesis and angiogenesis. Blood and lymphatic vessels are continually exposed to mechanical forces. ECF plays a crucial role in various physiological and disease systems. In cancer, interstitial fluid flow may cause reorganization of the ECM and promote the invasion of tumor cells regulated by autologous chemotaxis. When tumor reach a critical size, new blood vessel is generated via secretion of VEGF, leading to an increase in interstitial fluid pressure

in tumors. Due to the high dynamic and complex condition of the cell-ECM interaction, a detailed understanding of the dynamic aspects of cellular microenvironment in terms of spatial and temporal variations of different chemical, mechanical, and biological stimuli is highly important in tissue or organ engineering [23].

1.1.3 Cell culture

Cells can be isolated from a body tissue and cultured outside their natural environments *in vitro*. By controlling the conditions in culture, the complex cellular processes can be maintained or changed by design. The mammalian cell cultured *in vitro* was demonstrated for the first time in the early 20th century [24]. Afterwards, this technique was widely developed and applied in biological laboratories, pharmaceutical companies and hospitals for fundamental research, diagnosis, drug screening and therapeutic purposes. The development of a culture beyond the primary culture results in a "cell line." The importance of a cell line lies in its ability to provide a renewable source of cell material for repeat studies. Currently, various cell lines, the corresponding culture medium and protocols are available commercially. A number of biological therapeutics such as antibodies, clotting factors, hormones, immune-adhesions, and vaccines have been produced by the cell culture related bio-production systems.

Basically, cells can be cultured under certain temperature and gas mixture conditions which could mimic the *in vivo* environment of cells by an incubator (ex. 37°C, 5% CO_2 for mammalian cells). Culture medium is one of the critical factors for cell culture, which is in specific pH and normally contains the essential nutrients, glucose and growth factors. The growth factors are usually derived from animal blood, such as calf serum [25].

Conventionally, cells are cultured in culture dishes, flasks, multi-well plates, etc., the surfaces in such culture platforms are commonly flat in two dimension and treated by surface coating or other methods to provide a better cell adhesion and proliferation. However, this *in vitro* environment for cells is still different from that *in vivo*. *In vitro*, the *in vivo* cell-cell interaction may lost and cells may have some kinds of genetic and phenotypic instability. To mimic the natural environment *in vivo*, various sophisticated methods and instruments have been developed to modulate cell behaviors by supplying appropriate conditions, and a mass of research has been

developed to culture cells on more complex substrates with physical or chemical topographic cues. Before introducing the state of the art of these approaches, we briefly describe the stem cell technologies since their behaviors and functions are more critically depending on the cellular microenvironment.

1.2 Stem cell and induced pluripotent stem cells

1.2.1 Stem cell

Stem cells are undifferentiated cells with capacities of differentiation into specialized cell types and division to produce more stem cells. Due to their outstanding properties they hold great potential as tools for the application in tissue engineering, regenerative medicine as well as *in vitro* modeling for disease study, drug screening and toxicity tests [26].

Typically, a stem cell is required to possess two main properties:

Self-renewal: defined as the capacity to go through numerous cycles of cell division while maintaining the undifferentiated state.

Potency: defined as the ability to differentiate into specialized cell types, which requires stem cells to be either totipotent or pluripotent—to be able to generate any type of mature cells.

Stem cells are rare in most tissues. Accordingly, in order to study their properties, stem cells have to be identified prospectively and purified carefully. However, the rigorous identification and purification of these somatic stem cells has only been achieved in a few occasions [27]. For instance, hematopoietic stem cells (HSCs) have been isolated from mice and humans [28, 29], and have been proved to be responsible for the generation and regeneration of the blood-forming and immune systems.

Basically, by different differentiation potentials, stem cells can be classified into three types: totipotent, pluripotent, and multipotent stem cells, as shown in **Table 1.2** [30].Tissue-specific multipotent adult stem cells have been isolated from various adult tissues in many species. Besides, embryonic stem cells (ESCs) have been isolated from embryos, which have the ability to differentiate into all types of cells in an adult organism. In recent years induced pluripotent stem cells (iPSC) have drawn increasing attention to be the substitution of ESCs [31].

Table 1.2 Classification of stem cells according to their differentiation potentiality (totipotent, pluripotent, and multipotent)[30].

Potency	Description	Examples
Totipotent	Each cell is able to develop into any cell types.	Cells from early (1–3 days) embryos
Pluripotent	Cells can form most of the cell types except placental tissues.	Some cells of blastocyst (5–14 days)
Multipotent	Cells differentiated, but can make a range of other particular tissues.	Fetal tissue, cord blood, and adult stem cells

1.2.2 Induced pluripotent stem cells

The investigation of induced pluripotent stem cells, also known as iPS cells or iPSCs, which can be generated directly from somatic cells and differentiated into almost any kind of cell types, were pioneered by Shinya Yamanaka in 2006 at Kyoto University, who was awarded the 2012 Nobel Prize "for the discovery that mature cells can be reprogrammed to become pluripotent"[31, 32]. In their work, Yamanaka et al introduced four specific genes encoding transcription factors, also dubbed "reprogramming factors" or "Yamanaka factors", including Oct4 (Pou5f1), Sox2, cMyc, and Klf4, into a given cell type to derive iPSCs.

iPSCs are able to be differentiated into ectodermal, mesodermal and endodermal cells (**Fig. 1.5**), which are extremely similar to natural pluripotent stem cells, such as embryonic stem cells (ESCs) in many aspects, including the expression of certain stem cell genes and proteins, doubling time, chromatin methylation patterns, embryonic body formation, viable chimera formation, potency and differentiability, but the full extent of their relation to natural pluripotent stem cells is still being assessed [33]. However, ESCs derived from human embryo are strictly prohibited in many countries, so the number of ES cell lines that are approved for research usage is very limited. This ban constrains the possibility to solve some of the most urgent questions, especially those relating to the modeling and curing disease [34]. iPSCs may probably be supplements to ESCs on the regenerative medical application. iPSCs from patient provide a specific platform from which to get mechanistic information of various diseases, to carry out *in vitro* drug screening, to evaluate potential therapeutics and to explore gene repair coupled with cell-replacement therapy. Additionally, most ESCs represented generic cells isolated from presumably

normal embryos. And they are genetically foreign to any particular patient, then during transplantation process, immune rejection can occur because recipient's body does not recognize the transplanted cells or require that the recipient take lifelong therapy with toxic immunosuppressive medication, while the iPSCs generated by reprogramming could avoid the immune rejection risk [35]. Thus iPSCs are now studied more and more for prospective applications in disease modeling, cell therapy and regenerative medicine [36, 37].

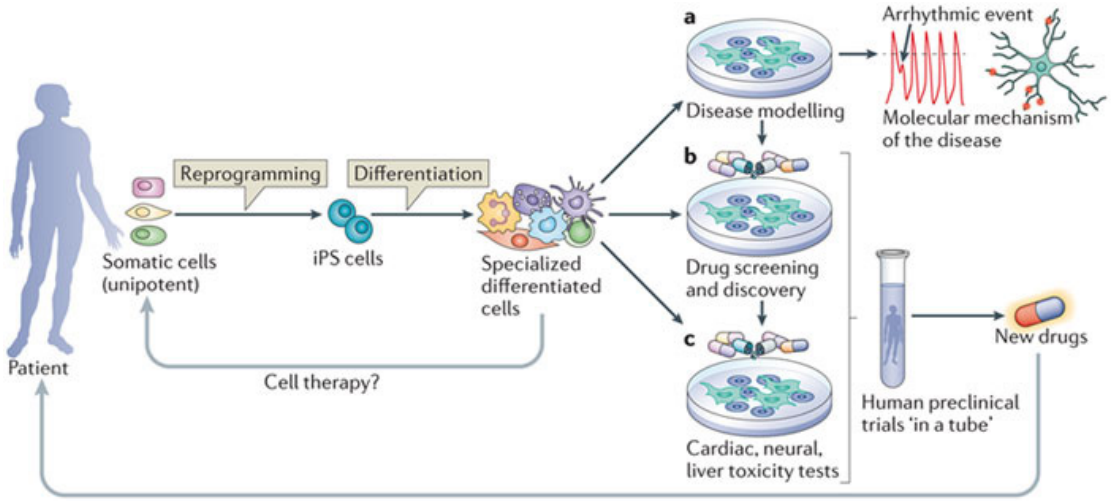

Fig. 1.5 Human iPSCs derivation, differentiation and applications. [38]

However, no general method is yet available for mass production of high quality hiPSCs with minimized risks of genetic instability and tumorigenicity. Previous studies have shown that both culture medium and culture substrate affect the cell fate decision of hiPSCs but only limited efforts have been devoted to the effects of culture stadium and it is not clear what are the best material stiffness and the best surface morphology of the stadium for clinic grade applications.

The first concern of iPSCs culture is the proliferation, i.e., iPSCs have to be propagated over many generations without losing their pluripotency, their purity and quality. Under conventional culture conditions, hiPSCs are impure and show often important chromosomal abnormalities and high tumorigenic risk. By adding feeder cells [39] or using Matrigel coated substrate [40], the quality of hiPSCs could be largely improved but both are not relevant for clinic applications because of the presence of animal factors. Xeno-free conditions have been achieved using culture substrates coated with recombinant proteins such as laminin, vitronectin, E-cadherin

or synthetic polymers culture substrates [41]. These studies, together with additional assays using non flat substrates [41], highlight the importance of using appropriate extracellular matrix (ECM) proteins /molecules and textured surfaces which take into account some of the specificity of *in vivo* stadium but not allow regulating other aspects of cellular microenvironments, i.e., soluble factors and cell-cell interaction.

The second concern of iPSC culture is the controlled differentiation. iPSCs have been re-differentiated into several somatic tissues, including active motor neurons [42-44], insulin-secreting islet-like clusters [45], hepatocyte cells[46, 47] and a number of cardiovascular cells (arterial endothelium, venous endothelium, lymphatic endothelium, and cardiomyocytes) [48, 49]. However, how to efficiently derive iPSCs into well-defined cellular lineages with high yields and high purity becomes the primary point. Since adult cells such as cardiac and neurons have different morphology and different physiochemical and biochemical responses which impose different organization and different mechanic stiffness. In many cases, the differentiated stem cells have better to be organized in form of tissues for easy applications which suggestion the importance of cell-cell interaction under less imposed conditions. In this thesis, we are mainly focusing on cardiomyocytes and motor neuron differentiation.

1.3 Cancer and circulating tumor cells

1.3.1 Cancer

Cancer, also known as malignant tumor or malignant neoplasm, is a group of diseases involving abnormal cell growth with the potential to invade or spread to other parts of the body [50]. The progression from normal cells to cells that can form a detectable mass to outright cancer involves multiple steps known as malignant progression and it accounts for millions of deaths every year worldwide. In 2008, the death due to cancer was around 13% of all human deaths (7.6 million), and this number is projected to pass 13 million in 2030 [51, 52].

All tumor cells show six hallmarks of cancer, including i) Cell growth and division without the proper signals to do so; ii) Continuous growth and division even when there are signals telling them to stop; iii) Avoidance of programmed cell death; iv) Limitless number of cell divisions; v) Promoting blood vessel construction; vi)

Invasion of tissue and formation of metastases [53].

Despite all efforts by scientists, cancer is still one of the leading causes of death. In 2012 about 14.1 million new cases of cancer occurred globally (not including skin cancer other than melanoma)[54]. However, among all the cancer related mortalities, metastasized cancer accounts for 90%. So complete understanding metastasis is significant for decreasing cancer resulted death and conquering cancer.

1.3.2 Metastasis and circulating tumor cells

Metastasis, or metastatic disease, is the spread of a cancer or other disease from one organ or part to another not directly connected with it. Cancer metastasis is a complex process, which is still not completed understood. But it has been proved that during metastasis, circulating tumor cells (CTCs) play a critical role.

CTCs were discovered firstly by the Australian pathologist Thomas Ashworth in 1869 in the blood of a patient with metastatic cancer, who noted that some cells present in the blood did not look like normal blood cells, while appeared similar to those in the patient's solid tumors. He postulated in the article in *Australian Medical Journal* that “cells identical with those of the cancer itself being seen in the blood may tend to throw some light upon the mode of origin of multiple tumors existing in the same person”. A whole comparison of the morphology of the circulating cells to cancer cells led Ashworth to conclude that “One thing is certain, that if they (CTCs) came from an existing cancer structure, they must have passed through the greater part of the circulatory system to have arrived at the internal saphena vein of the sound leg”[52, 55-57]. Over one hundred and forty years, cancer research has indeed confirmed that the critical role of CTCs in the metastasis of carcinomas [58].

The dominate perception consists that metastasis includes three steps: epithelial to mesenchymal transition (EMT) and invasion, hematogeneous spread and extravasation, and then metastatic colonization, as shown as **Fig. 1.6**.

a) Epithelial to mesenchymal transition (EMT)

In 2005, Elizabeth Hay (Harvard University, Boston, MA), first described the EMT [59], a morphogenetic process in which cells lose their epithelial characteristics and gain mesenchymal properties during embryogenesis, wound healing, and carcinoma invasion and acquire a fibroblast-like morphology [60, 61].

One critical event in EMT is the downregulation of E-cadherin with the phenotypic change of tumor cells, which will reduce the cell-cell adhesion and improve the motility of cancer cells in primary tumor [62]. The EMT process in cancer metastasis is highly complex and still mostly not understood but it is believed that it is a hallmark of metastasis and proposed to induce cancer stem cell (CSC) properties in non-CSCs [63, 64].

a) Hematogeneous spread and extravasation

After EMT process, cancer cells exhibit a motile, invasive phenotype, which enable them to detach from the tumor body and enter into circulation, but it is believed that CTCs could not proliferate in circulation system [58, 65]. Then following with blood flow, CTCs could travel to other part of body until they are captured at capillary beds of specific organs [66, 67]. Then CTCs penetrate through endothelial cells layer and invade into the secondary organ.

b) Metastatic colonization and secondary tumor formation

Once CTCs successfully invade into secondary host organ, they will undergo the mesenchymal to epithelial transition (MET) [68, 69]. As opposed to EMT, the converse MET is associated with the downregulating of mesenchymal phenotypes and upregulation of epithelial phenotypes. Then the cancer cells start to proliferate and colonize in the new environment to form secondary tumor.

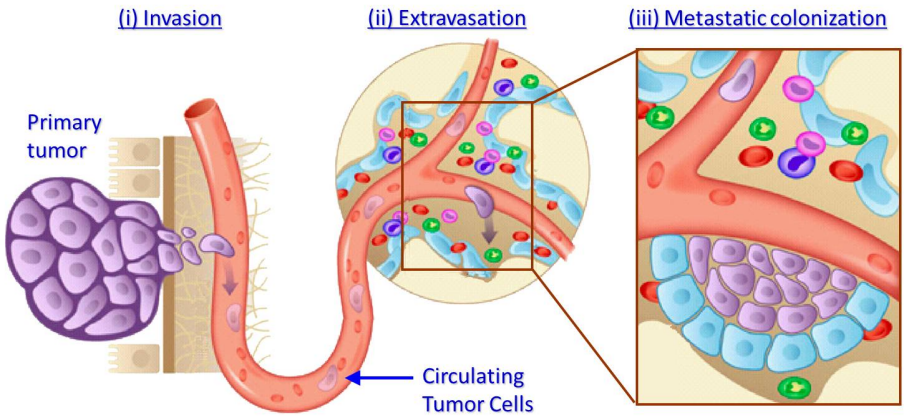

Fig. 1.6 Process of cancer metastasis. Tumor cells shed into the vasculature from a primary tumor and circulate in the bloodstream. Then CTCs extravasate into a distant area and form new metastatic colony [70].

1.3.3 Cancer diagnosis techniques

The earlier diagnosis of primary tumor, which will warn the further metastasis, is believed to be the key weapon to win the war on cancer. Currently, there are three main techniques for cancer diagnosis (**Fig. 1.7**), including imaging, bio-spy and blood analysis [71]:

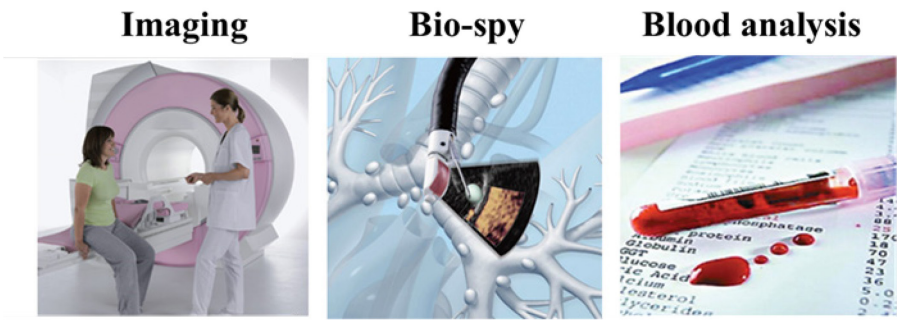

Fig. 1.7 Cancer diagnosis techniques

a) Imaging

Oncologists use imaging methods to detect the visible signs of tumors. Normally it relies on a series of diagnostic imaging tests, including:

i. X-Rays: by using X-Rays, the basic images of dense areas in the body (such as tumors) could be obtained.
ii. CT Scans: by using electromagnetic imagery, the detail images of internal structures can be created.
iii. Magnetic resonance imaging (MRI): it can produce images of highly active internal structures by magnets and radio waves.
iv. Positron emission tomography (PET) scans: by PET scanning, the areas of the body which have abnormally high and potentially cancerous metabolic activity.

However, some of the early tumors are too small to be detected by the techniques mentioned above, which will delay the illness and make wrong diagnosis.

b) Bio-spy

Bio-spy means that doctors have to take out some tissue samples from the patient body and send to a laboratory for evaluations by microscope or other machines. It can reveal that whether a growth is cancerous or benign and where the cancer originates and what type of cancer cells, which plays a significant role for the

treatment plan decision.

There are several ways for the doctors to obtain the samples for bio-spy, such as:

i. Fine-needle aspiration, which could extract cells through a thin, hollow needle;
ii. Excisional bio-spy, which removes the whole tumor from the body and test the certain samples of the tumor.
iii. Thoracoscopy or Mediastinoscopies: doctors insert a camera-equipped tube into the chest of patients for sampling.

Although bio-spy normally results into a more accurate diagnosis, tissue damage could be happened during the sampling process, which may lead some cancer cells to run out from the original tumor and cause metastasis[72].

c) Blood analysis

In recent years, researchers have spent a considerable amount of time to develop blood test methods for cancer diagnosis. Part of them focuses on detecting tumor specific biomolecules, such as specific-proteins which are present in certain cancer patients.

Another part of blood analysis focused on cancer cells, especially circulating tumor cells (CTCs). CTCs are derived from primary tumor and penetrate into circulating systems, such as blood vessel, which are significant markers to real-time monitor the metastasis of cancer patients. Therefore, more and more attentions have been paid to explore cancer diagnosis methods based on CTCs.

1.3.4 CTCs isolation

The major challenge of CTCs isolation is the rarity of CTCs in blood (**Fig. 1.8**), even in patients with advanced metastatic cancer, CTCs are in the range of a few cells per milliliter blood [73]. Besides, there are also estimated a few million white blood cells (WBCs), a few billion red blood cells (RBCs) and some other kinds of cells surrounding one CTC in 1 ml of whole blood [74]. Thus, high efficiency and high purity of isolating of CTCs is the primary step for the further CTCs analysis.

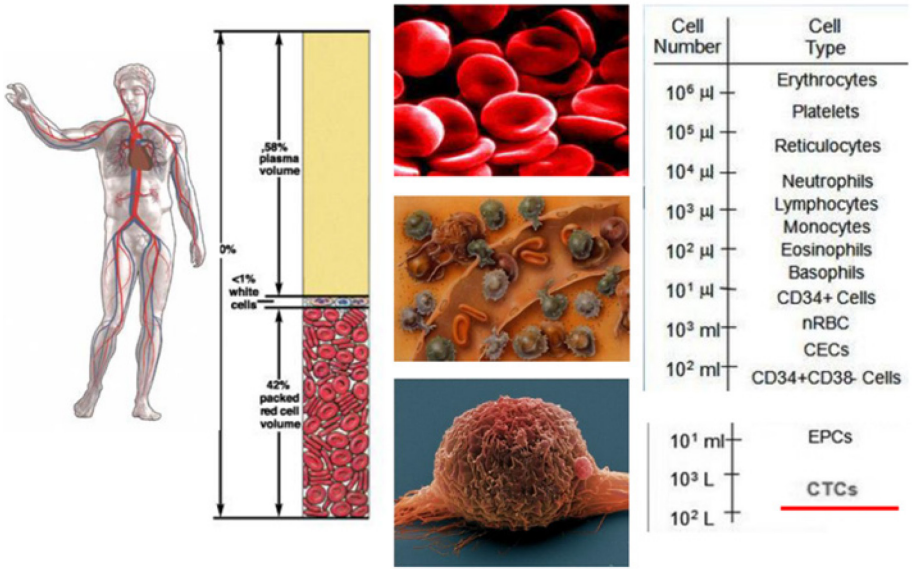

Fig. 1.8 The rarity of CTCs in blood [75].

Recent years, there are numerous techniques developed for CTCs capture (**Fig. 1.9**). Currently, two approaches are in competition, depending on whether or not the capture is affinity-based. The affinity-based capture relies on immunochemical interaction between magnetic beads [72, 76-80] or patterned structures [81-84] and tumor cells that express special surface markers such as EpCAM, an epithelial cell adhesion molecule over expressed by majority of tumor cells. These methods are efficient for capturing CTCs of epithelial phenotypes but not applicable to those with down-regulated or lost epithelial markers. It is known that when epithelial cells of solid tumors enter into a blood stream they may undergo epithelial to mesenchymal transition [85, 86]. In contrast, the non-affinity methods, including centrifuging deflection [87-91], dielectrophoretic separation [92-94] and size-based filtration [76, 95-108] are able to isolate both epithelial and mesenchymal phenotypes, which are more appropriate for analyses of tumor heterogeneity, tumor drug resistance, etc. However, these approaches are technologically biased and it is often difficult to reach a trade-off between capture efficiency, purity and cell viability which are all important criteria for both fundamental and clinical studies. For example, the size-based filtration has been developed for more than several decades but the most of reported results were obtained by using track-etched polycarbonate filters [76, 95-99]. The main problem of this approach is contamination: the track-etched cylindrical holes of the filter have generally high retention ratio of non-tumor cells if the size of the holes is sufficiently small to reach high tumor cell capture efficiency.

Furthermore, the randomly distributed holes are prone to significant coalescence of two or more holes allowing tumor cells to escape from the filter. More recent studies have shown that a variety of microfabrication techniques could be used to manufacture filters of different hole-types and densities [36-45], but none of them were able to meet the critical requirements for both clinical application and fundamental studies.

1.3.5 Cancer cell culture

With many recent advances, cancer cell culture research is more important than ever before. Due to the limitation of CTCs sources, most of current cultured cancer cells are either isolated from primary tumor or specific cancer cell lines. There are various methods to characterize and authenticate cell lines, to isolate and develop specific types of cancer cells, and to develop new cell line models. Functional assays are provided for the evaluation of clonogenicity, cell proliferation, apoptosis, adhesion, migration, invasion, senescence, angiogenesis, and cell cycle parameters. Other methods permit the modification of cells for transfection, drug resistance, immortalization, and transfer *in vivo*.

As we know that before metastasis, a primary tumor was formed at the anatomical site where tumor progression started to yield a cancerous mass. Therefore, one strategy in drug discovery is to against the tumor progression. However, the most previously used cell based assays for cancer drug studies are based two-dimensional (2D) culture which does not take properly into account the three dimensional (3D) characteristics of tumor formation *in vivo* [109, 110]. And it is becoming more and more apparent that 2D monolayer cultures of tumor cells cannot completely represent the characteristics of three-dimensional solid tumors. Consequently, the multicellular tumor spheroid model, which is of intermediate complexity between *in vivo* tumors and monolayer cultures, was developed [111].

Suspension culture is frequently used for multicellular spheroid formation but it is not easy to control the size consistency of the spheroids and to handle them for systematic studies [112, 113]. Suspension culture using spinning flask or rotating bioreactors can improve the size uniformity of the spheroids but undesired shear stress can be introduced during the spheroid formation. Culture with hanging drops can also improve the size uniformity and overcome the problem of mechanical disturbance. This technique is however time-consuming and not easy to perform

drug tests during spheroid progression. More recently 2D and 3D patterned substrates are used to support spheroid formation [114, 115]. In particular, various micro-well arrays are proposed for 3D cell aggregation, depending on microfabrication techniques [116, 117]. To facilitate the diffusion of nutrients, drugs and other factors into the spheroid area, it is also important to form the 3D assays with the materials of high permeability [118]. This approach allows controlling cell population in each spheroid as well as high-throughput screening. However, the available systems are mostly appropriate for small size spheroid formation, which cannot efficiently recapture the spheroid complexity of solid tumours.

1.4 Improved culture substrates and bio-scaffolds

Coming back to the general cases of cell culture, when cells are placed in a petri dish, a flask and a multi-well plate, where their *in vivo* physiological conditions are lost without surrounding organization of extracellular matrix proteins and blood capillary and they are forced to adapt a two-dimensional support where both underneath diffusion and cell-cell become less efficient. The problem arises when this change of scenario becomes critical, which is the case of pluripotent stem cells such as embryonic stem cells and iPSCs. So far, the most of studies on iPSCs, including their creation, their renewal and their differentiation have been based on the use of conventional culture techniques, which poses a problem of quality control and the risk of genetic instability, tumorigenicity, etc. [119-121].

Before going into more details, we put forward the great potential of iPSC derived tissues for regenerative medicine [122]. To this regard, the three-dimensional structuration or bio-scaffold fabrication is needed. Therefore, we introduce in the following notions of the materials and methods that are used for the fabrication of culture substrate and tissue scaffolds. For the design of substrates and scaffolds, the most central and primary factor is biomaterial.

1.4.1 Biomaterials

Over the past few decades, biomaterials have transformed from simply interacting with the body to influencing biological processes for the goal of tissue regeneration [123]. Basically, there are three main groups of biocompatible materials

for tissue engineering, including inorganic materials such as metals and ceramics, natural polymers and synthetic polymers. Each of these three types of biomaterials has specific advantages and disadvantages for a certain application. So currently more and more composite scaffolds which are composed of different types of materials are studied.

a) Inorganic materials

The inorganic materials such as metals and ceramics have been widely used in the medical field, particularly in orthopedic tissue replacement, especially the ceramic scaffolds such as hydroxyapatite (HA) and tri-calcium phosphate (TCP), which have been widespread applied for bone regeneration. The special properties of ceramic scaffolds, such as high mechanic stiffness, low elasticity, a hard brittle surface, as well as the outstanding biocompatibility due to their similar chemical and structural property to the mineral phase of natural bone, make them exhibit excellent in bone regeneration field [123]. Additionally, it has been reported that the interaction of osteogenic cells with the ceramic scaffolds can enhance the proliferation and differentiation of osteoblasts, which will improve bone regeneration [124, 125]. Titanium and titanium alloy have also been largely applied for not only implants, such as artificial limbs, but also dental products like crowns, dentures, etc. are also getting much attention in dentistry [126, 127].

However, due to the non-biodegradation and the limitation in processability, the application of metals and ceramics is still very limited in tissue engineering. So currently, polymer biomaterials have drawn increasing attention and are in rapid development, including natural polymers and synthetic polymers.

b) Natural polymer materials

The naturally derived polymers including polysaccharides, alginic acid, chitosan, gelatin and proteins of natural extracellular matrices such as collagen in particular and so on, are widely applied in tissue engineering [128-131]. Although generally natural polymer materials have poor mechanical strength, they are increasingly studied because of their biodegradation, less host response and the increased recognition for cells and tissues [18].

As one of the key structural proteins found in the ECM of many tissues in

mammals, collagen has been shown to be a suitable material for many of clinical medicine applications in the past several years, such as injectable collagen for the augmentation of tissue defects, hemostasis, burn and wound dressings and nerve regeneration [132, 133]. However the main disadvantage of collagen is the potential antigenic and immunogenic response that can be provoked during its *in vivo* application [134]. Gelatin is the product of collagen after thermal denaturation or disintegration, which has been reported with a lower immunogenicity *in vivo* [135, 136]. Due to the biodegradation, biocompatibility, as well as the lower cost in commercial use compared to collagen, gelatin has been increasingly utilized in many areas of tissue engineering, which is also one of the materials we chose in this work in Chapter 3.

c) Synthetic polymer materials

In the past several decades, many synthetic biocompatible polymers have been applied in the attempt to produce scaffolds, such as poly-l-lactic acid (PLLA), polyglycolic acid (PGA), poly(lactic acid) (PLA), poly-dl-lactic-co-glycolic acid (PLGA) and poly(ε-caprolactone) (PCL) [137]. PGA, PLA and their copolymer PLGA have been widely used as scaffolds for bone and cartilage repair [138, 139]. PCL-based materials are mostly used for skin, vascular as well as neural tissue engineering [140-142]. The main advantages of these synthetic polymer materials are the easy tailored architecture and controllable degradation property by flexible adjustment of the polymers and composition of different polymers[123, 143]. However, the main drawback of synthetic polymers compared to natural polymers is the risk of immunogenic rejection because of the lower bioactivity.

Among the various synthetic polymers, poly(ethylene glycol) (PEG) based hydrogels drawn increasingly attentions because of their water content controllability, hydrophilicity, and biocompatibility, especially lithographically-fabricated PEG based hydrogels, such as poly(ethylene glycol) diacrylate (PEGDA) and poly(ethylene glycol) dimethacrylates (PEGDMA), which can be easily tailored with the designed and controllable regular structures based on microfabrication techniques [144-146]. We chose also PEGDA as one of the materials for the scaffold in Chapter 3.

1.4.2 Culture substrate

A variety of substrates have been proposed to improve the culture performance of iPSCs. Matrigel [147] or recombinant proteins such as laminin [148] are commonly used to generate a gel layer on the flat surface of substrate to promote the adhesion of iPSCs. These methods are versatile but not allow mimicking the organization of the extracellular matrix proteins. To obtain a patterned substrate with appropriate surface stiffness which are more interesting for the control of stem fate of iPSCs [149], synthetic polymers such as PCL, PLGA, PLLA, etc. and natural biopolymers such as collagen, chitosan, alginate, hyaluronic acid, etc. have been used. In addition to the lithography defined substrate patterning which *will be described in the next chapter*, oxygen plasma etched substrates [150], porous materials [151, 152], electrospun nanofibers [153] have been successfully employed for iPSC culture but none of them fully take into account the specificity of the cellular microenvironment in term of three dimensional permeability and protein organization.

In parallel, suspension culture of iPSCs has been studied using bio-reactors such as shaker, rotator, etc.[154]. These methods can efficiently increase the yields but the agitation of the solution can introduce undesired shear forces on the cells. Microfluidic devices with minimized shear forces have also been used for iPSC culture [155] but it showed no advantage on the cell fate control due to the fact that they are not flexible for iPSC handling and the exogenous contact with the support material is always large. Alternatively, suspension culture can be done using carriers such as microspheres. This type of off-ground culture could be applied to iPSCs culture [156, 157] but it is limited by the difficulty of cell harvesting and uncontrollable exogenous contact with the carrier materials. Therefore, there is a clear need for devices and methods for iPSC culture and handing under optimal physiological conditions and highly compatible to both *in vitro* and *in vivo* assays.

1.4.3 Bio-scaffolds

Tissue engineering, as one of the main purposes of cell culture, has emerged in the development of biological substitutes which can restore, maintain, or improve function of tissue or organs [158-162]. As an interdisciplinary field, tissue engineering involves the combining of cell, scaffold, and bioactive agents to

fabricate functional new tissue to replace damaged tissue [163, 164], as shown as **Fig. 1.9**. In this approach, a well-designed scaffold is one of the critical tools to serve as an extracellular matrix (ECM) mimic substrate for the implanted cells adhesion and to guide actively the tissue regeneration process *in vitro* and *in vivo*.

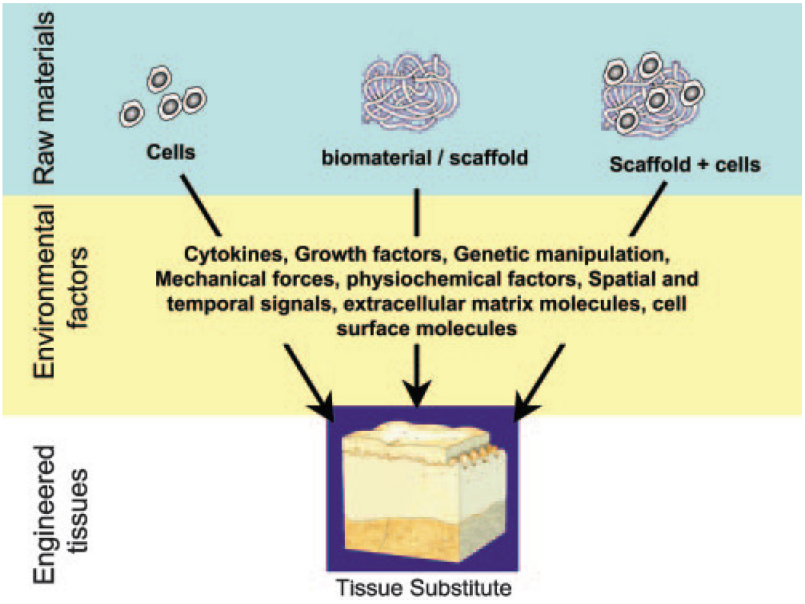

Fig. 1.9 Tissue engineering can be relied on (i) cells alone, (ii) cells with scaffolds, and (iii) scaffolds alone. In all cases, the micro-environmental factors are important for the quality of the tissue substitute [165].

For tissue engineering, scaffold design plays an important role in manipulating cells behavior and guidance of tissue formation [123, 166-169]. The best scaffold should be mimicking the ECM of the target tissue in its native state, intuitively. However, normally it is difficult to mimic exactly the complex composition and the multiple functions of the ECM in native tissues [170]. Therefore, the current concept of scaffold design in tissue engineering is to mimic the functions of native ECM as much as possible. Although the final requirements depend on the specific purpose of the scaffold, a number of key considerations and requirements are significant when designing or determining the suitability of a scaffold for a specific application in tissue engineering:

- **Biocompatibility**

The first and basic criterion is the scaffolds should be biocompatible for cell and tissue, which can allow cells adhesion, migration and proliferation on the surface and

prevent any immune rejection of the surrounding tissue after implantation [171, 172].

- **Suitable mechanical properties**

The strength of scaffold should be comparable to the *in vivo* tissue at the specific implantation area. For instance, a scaffold requires more flexibility or rigidity depending on the application in cardiovascular and bone respectively [173, 174].

- **Good permeability**

Based on a sufficient mechanical strength, the porosity of scaffold should be large enough to provide sufficient space for sufficient nutrient transport and waste products removal for cells [173, 175-177].

- **Suitable surface**

The surface should permit cell adhesion, promote cell growth, and allow the retention of differentiated cell functions. Besides, it has been reported a lot that the topography introduction of scaffold surface can enhance tissue organization resulted into promoted tissue function [178-180].

- **Manufacture possibility**

For clinical and commercial applications, the scaffold should have possibility of scale-up production from laboratory scale to larger batch production [181]. The development of scalable manufacturing processes to good manufacturing practice standard is critically essential for ensuring successful conversion of tissue engineering strategies to the clinic [182].

According to the criterions above, in the past decades, there have been many novel methods to shape biomaterials into complex architectures to achieve scaffolds with desired properties for specific tissue engineering applications.

a) Solvent casting

Solvent casting is a very simple, easy and inexpensive method, which consists of dissolving a polymer in a volatile solvent and casting it on a solution that will provide support to the polymer while the solvent is evaporating [183]. However the

main drawback is the induction of residual solvents which may retain some toxicity for the scaffold. Drying in vacuum may overcome this problem, but it will be very time consuming. Therefore some researchers developed particulate leaching method, which could be also combined with solvent casting.

b) Particulate-leaching

Particulate leaching is one of the most popular techniques which has been widely applied for scaffolding in tissue engineering [184]. Porogens such as salt, wax or sugars can be introduced to create pores or channels in the resulting scaffold. The process is easy to carry out: porogens with desired size are poured into a mold, then a polymer solution is cast into the porogen-filled mold, after evaporation, the porogens can be leach out to form the pores, which can be size-controlled by the size of porogens. Injection of high pressure CO_2 can also create pores, without utilization of organic solvents and high temperature, which is called gas foaming method [185].

c) Phase separation

The general principle of phase separation is to dissolve polymer in a solvent and to then extract the solvent by liquid-liquid phase seperation or solid-liquid demixing. These techniques have been largely used to fabricate porous membranes for filtration and separation [186]. But the main problem for this method is the not uniform distributed and not controllable pore size, which makes it limited used in tissue engineering.

d) 3D printing

3D printing can be used for rapid prototyping of scaffolds, by which the biomimetic architectures (size, shape, inter connectivity, branching, geometry and orientation) can be designed with the help of computer added design software. **Fig. 1.10** shows a 3D printer machine in our lab in ENS (a), a 3D-printed Eiffel tower (b), a 3D-printed PEGDA scaffold before (c) and after (d) integration of porous gelatin structure. However, the main drawbacks of rapid prototyping techniques are the limited material selection and low achieved resolution.

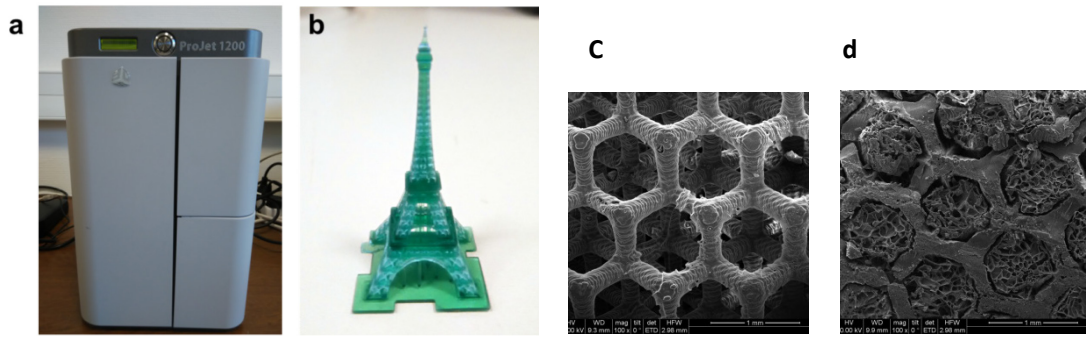

Fig. 1.10 (a) 3D printer (ProJet® 1200, 3D Systems) in ENS; (b) 3D-printed Eiffel tower; (c) 3D-printed PEGDA scaffold; (d) Porous gelatin PEGDA scaffold.

e) Hydrogel formation methods

Hydrogels are three dimensional crosslinked polymer networks with the ability to absorb large amounts of water, which have been demonstrated as outstanding scaffolds for 3D cell culture and played an ever increasing role in tissue engineering field in the last decade [187]. In biomedical engineering field, biocompatible hydrogels have been successfully applied to wound dressings, cartilage wound healing, bone regeneration and especially drug delivery systems development [188-191]. Hydrogel scaffolds have been increasingly studied for the application in tissue engineering for the connective tissue replacement, and have been proved to improve cell migration, enhance angiogenesis, and increase nutrient diffusion [192]. More details of the hydrogel formation technique used in this work *will be described in chapter 2*.

f) Electrospinning

To realize effective tissue engineering, it is crucial to apply as many biomimetic scaffolds as possible [193]. With the increasing development of nanotechnology, nanofibers fabrication attracts more attentions, because nanofiber scaffolds can mimic native ECM structure at nanoscale [194-196]. There are several methods for the fabrication of nanofibers, including anisotropic crystal growth, molecular self-assembly, lithography, atomic deposition and template. Among all these techniques, electrospinning, which was observed first in 1897 by Rayleigh [197], holds high potential due to the easy operation, low cost and well-control of nanofiber morphology and chemical compositions. **Fig. 1.11** shows the schematic of typical

electrospinning. More details of the electrospinning technique used in this work *will be described in chapter 2*.

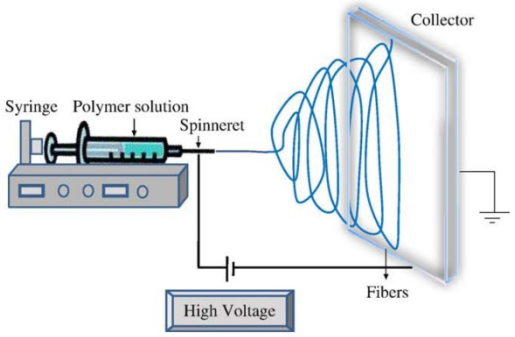

Fig. 1.11 Schematic of typical electrospinning [198].

1.5 Microfluidic device technologies

Microfluidic device techniques have been widely studied to improve biological and biomedical studies, due to their unique advantages of fast sample processing and precise fluid manipulation [199].

1.5.1 Introduction of microfluidic device

Microfluidic technology has passed a long way since the first application by Terry et al. in 1979, which was a miniature gas chromatographic analyzer [200], while the first cell culture in a microchannel was achieved by Doroszewski et al. in 1977 [201]. In concept, microfluidic is to manipulate fluids precisely by microscale devices, which was firstly established by semiconductor industry and later expanded in the field of micro-electromechanical systems (MEMS). Commonly these devices were called "miniaturized total chemical analysis system" (μTAS) [202] or lab-on-a-chip, which show a number of advantages such as cost effectiveness, low consumption of reagents, high sensitivity, high resolution and so on [203].

For biological applications, there are several reasons to choose microfluidic as the tool [204]: a) the increased interests in biochemical analysis of single cells, such as for drug evaluations, external stimuli on cell behavior, etc.; b) possibility of integration of all kinds of analytical standard operations into microfluidic systems; c) several techniques for manipulating large quantity of cells simultaneously can be

applied to microfluidic systems; d) the size of cells fits very well with that of commonly used microfluidic devices (10~100 μm); e) micromechanical devices are very well capable of manipulating single objects with cellular dimensions; f) small dimensions geometries with large electrical field strengths can be obtained with small voltages; g) fast transfer of heat and mass in microfluidic systems.

There are two main methods to produce fluid flow in microfluidic device: pressure driven flow and voltage driven electrokinetic flow (**Fig. 1.12**). And in different microscale channels, the behaviors of fluids are different, which are mainly related to several factors, such as laminar versus turbulent flow, surface and interfacial tension, capillary forces (**Fig. 1.13**) [199]:

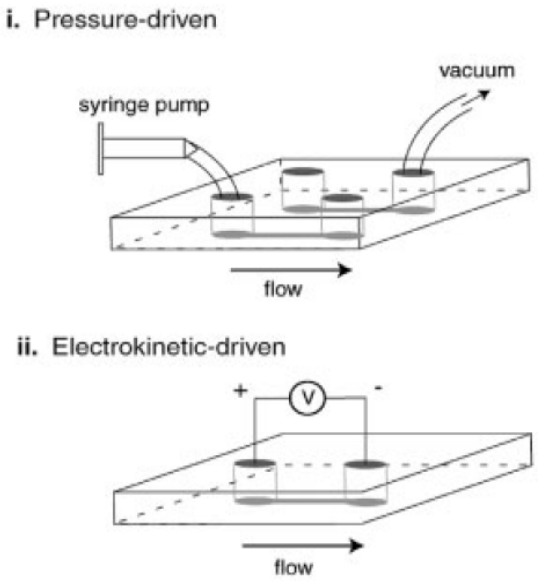

Fig. 1.12 Methods for driving a flow. (i) Pressure-driven flow using a vacuum at the outlet or a syringe pump at the inlet. (ii) Electrokinetic flow using a voltage applied across the microchannel[205].

(a) Laminar versus turbulent flow

The Reynolds number (Re) is a dimensionless value that represents the ratio of inertial to viscous forces in a fluid. Re is proportional to the characteristic velocity of the fluid and the length scale of the system, while inversely proportional to the viscosity of fluid. Turbulent flow is normally with high-Re number (~2000) having flow profiles that increasingly mix stochastically. For highly predictable fluid dynamics, Re is normally in the laminar flow regime in microfluidic systems.

Molecular transport also changes dramatically at microscale because convective mixing does not occur, enabling predictable diffusion kinetics.

(b) Surface and interfacial tension

Compared to gravity, surface and interfacial tension plays more dominant role on the microscale, which is much more critical on the macroscale. Surface tension represents the tendency of a fluid in a surface to reduce the free energy by contracting at the surface–air interface. Interfacial tension is a similar phenomenon, but is generally applied to two immiscible fluids (ex. oil and water). There have been lots of studies using these phenomena to conduct protein and cell sorting, perform nanoreactions for protein crystallization, and passively drive fluids through microchannel.

(c) Capillary forces

Capillary effect refers to the movement of a fluid through a thin restriction, such as in narrow tube or porous material, which is a more dominant in microscale. In microfluidic, capillary force can even force fluids to spread in opposition to gravity. Thus, capillary effect has been used to control fluids in many applications, such as at-home pregnancy test and portable glucometers to monitor blood glucose levels.

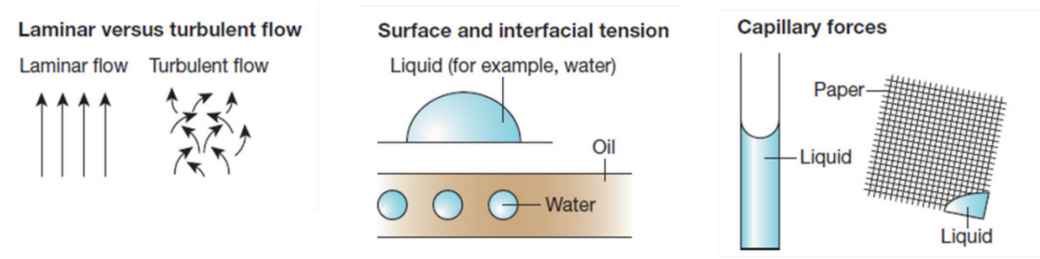

Fig. 1.13 Useful microfluidics concepts: laminar versus turbulent flow; surface and interfacial tension; capillary forces [199].

1.5.2 Biological applications of microfluidic

Intrinsically, microfluidic techniques have so many benefits and hold high

potential to influence variety of research fields. By combining different techniques from other areas, such as optical trapping for bio-particle manipulation and single-molecule detection, the rapid development of multifunctional microfluidic devices offers various opportunities for biological and biomedical studies [206], including tissue organization, culture and analysis (**Fig. 1.14**). In this section, several biological applications of microfluidic in recent years are highlighted.

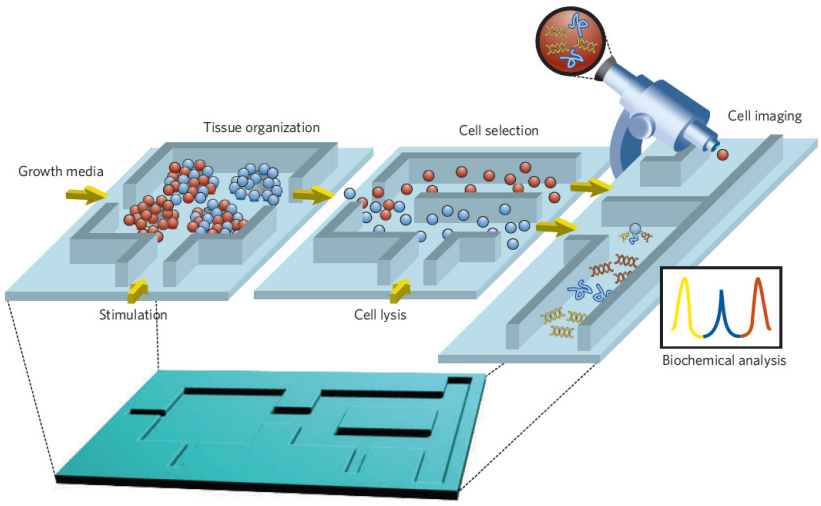

Fig. 1.14 Tissue organization, culture and analysis in microsystems [207].

a) Cell sorting

Cell sorting and purification is an essential preparatory step in many biological and medical assays. Over the past two decades, there has been several microscale separation techniques developed, such as optical tweezers, fluorescence or magnetic activated cell sorting, centrifugation, filtration and electric field-based manipulations based on cell size, morphology, magnetic and dielectric properties [204].

Fluorescence-activated cell sorting (FACS), also called flow cytometry has been widely used by biologists for cell sorting. A throughput of 10^4 cells/s is common with available FACS systems, however, the machines in present are normally large and high-cost, and the viability of cells after sorting is usually compromised. It has been reported to integrate miniaturized FACS sorters into microfluidic devices, which was restricted to handle one order of magnitude of cells per second because of the small microliter volumes they are able to manipulate, but with good cell viability

after sorting [208]. Magnetic based cell trapping which has low power requirement has also been used for isolating cells with magnetic susceptibility or with magnetic nanoparticles in microfluidics [209].

Due to the relative ease of microscale generation and structuring, electric field-based approaches are well suited to be miniaturized in microfluidic chips. And the cell sorting and manipulation by electric field shows high speed, flexibility and easy controllability. Especially dielectrophoresis based methods, have been successfully applied in microfluidics to manipulate and isolate various biological cells, such as bacteria, yeast and mammalian cells [204].

Size-based cell filtration is the most popular and easiest method in microfluidic systems, especially for rare cell isolation of blood samples. Yu-Chong Tai et al developed a parylene microfilter and integrated it into a PDMS microsystem for capturing circulating tumor cells (CTCs) in human blood, which reached ~90% CTCs recovery under pressure driven [100]. Microcavities in microfluidic have also been utilized to isolate lung carcinoma cells based size and deformability of cells [102]. The main limitations for these methods are the clogging and contaminations. Nagrath et al. [210] produced a micro-posts array in microfluidic system coated with specific antibody of CTCs (EpCAM), which can achieve high efficient separation of viable CTCs from peripheral whole blood samples, by the interaction of target CTCs with the antibody. However, this method is not applicable to those with down-regulated or lost epithelial markers and it is well known that when epithelial cells of solid tumors enter into a blood stream they may undergo epithelial to mesenchymal transition, which will make some of the tumor cells lose their surface marker [85, 211].There are also other techniques for CTCs capture in microfluidic, such as spiral centrifuge channels [88], Herringbone-chip [82] and so on, shown as **Fig. 1.15**. In this thesis, we design and fabricate a microfluidic device with integrated microfilter for CTCs capture to overcome all the drawbacks.

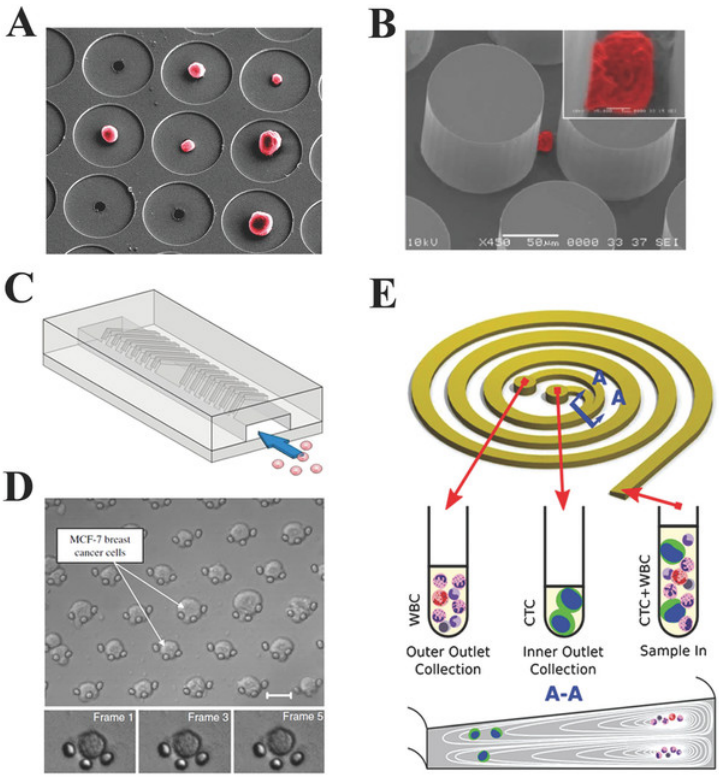

Fig. 1.15 Microfluidics-based CTCs capture and enrichment: A) Microcavity filter. B) CTC-chip. C) Herringbone-chip. D) Arc-shaped trap. E) Spiral microfluidic channel [212].

b) Cell analysis

Performing cellular analysis in microfluidic devices has many advantages, including less cell consumption, automated reagent supply, as well as controllable and reproducible mixing of reagents to cells [204]. There are many approaches for analyzing cells in microfluidic chips. Patch clamp and optical probes can be used to monitor intracellular signaling. Patch clamp has been widely used for the measurement of action potential or ion channels of cells, such as cardiac and neuron cells. Cell morphology variation can be detected with electrical impedance spectroscopy. Thermometric calorimeters can be used for cell metabolism monitoring. Genetic analysis can also be performed in microfluidic devices. Pal et al.[213] designed an integrated genetic analysis microdevice which can perform two independent serial biochemical reactions: polymerase chain reaction (PCR) amplification of a sample followed by restriction endonuclease digestion (RD).

Among many others, electrode-based techniques such as multi-electrode array (MEA) are the most common tools for real-time monitoring of cell

electrophysiological activities (shown as **Fig. 1.16**). Compared to patch clamp, electrophysiological measurement with MEA is non-invasive to cells because it does not require breaching of the cell membrane. With respect to *in vivo* arrays, the major advantage over patch clamping is the high spatial resolution. Besides, large-scale, parallel recordings with tens of implanted electrodes are possible, which make such extracellular recordings the method of choice to identify of neural circuits and to study their functions. In this thesis, MEA is used to record the electrical signals (field potential) of cardiomyocytes and motor neurons differentiated from human induced pluripotent stem cells (hiPSCs), as well as the reaction of cardiac sheet to cardiac drugs. In the following chapters, the impedance measurement as well as MEA will be introduced in detail.

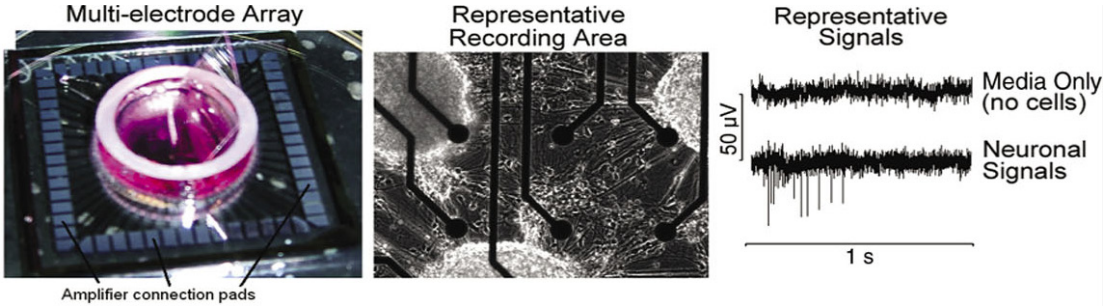

Fig. 1.16 The multi-electrode array (MEA) with embryonic cortical neurons after 14 d in culture, noting the elaborate axonal network and the recorded representative neuron signals. Electrodes and wires appear as black dots and lines, respectively [214].

c) Cell culture and organ on chip

Compared to the conventional culture using culture dishes, flasks or multi-well plates, microfluidic culture provides a controllable micro-environment to guide cell migration and differentiation, facilitating cell manipulation and analysis at single-cell level. Microfluidic culture can also be used to regulate the cell-substrate interactions and cell-cell coupling [206, 215]. Numerous studies have shown that the cell morphology can be modulated by changing the surface topography [216, 217] while a microfluidic controlled biomolecular gradient has been widely used to control the biological pattern formation and morphogenesis, including angiogenesis and axon path finding [218].

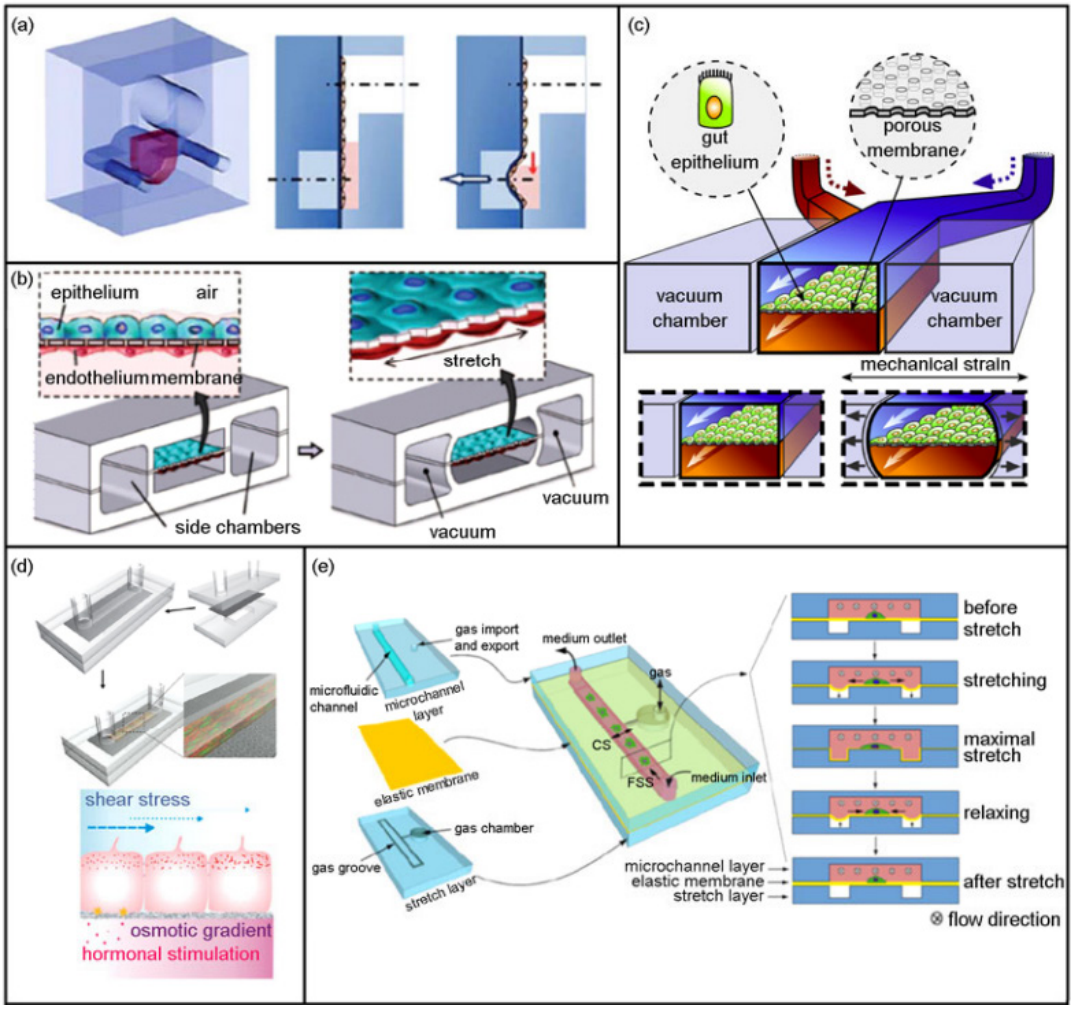

Fig. 1.17 Organs-on-chips. (a) Microfluidic "alveoli-on-a-chip". (b) Biologically inspired design of a human breathing lung-on-a-chip microdevice. (c) The human gut-on-a-chip. (d) Kidney-on-a-chip. (e) Microfluidic flow-stretch chip that mimics the cardiovascular systems [219].

However, 2D cell culture in microfluidic cannot mimic the aspects of the *in vivo* tissues. Thus in recent years, 3D microfluidic tissue engineering attracted increasing attentions because of the more *in vivo* mimic cell culture conditions compared to 2D culture. Vukasinovic et al.[220] designed a simple and scalable microfluidic perfusion system and cultured 700 μm thick neural-astrocytic (1:1) constructs at cell density approaching that of the brain (50,000 cells/mm^3). They found that with forced convection interstitial perfusion, cell viability reached 90% over 2 days, whereas unperfused controls exhibited widespread cell death. One of the main

application fields of 3D microfluidic cell culture is tissue engineering in microfluidics. Many researchers tried to combine various techniques with the microfluidics to control not only cell behaviors but also tissue organization, soluble gradients and mechanical stimulation. These micro engineered *in vitro* models are called "organs-on-chips" [219]. Compared to other conventional techniques, microfluidic tissue engineering can achieve the dynamic control of nutrients and reagents supply much conveniently. Organs-on-chips provide a significant tool to the researchers to study the physiological and pathophysiological processes in living organs, to operate drug screening and to assess the efficiency of treatment. Various organ models on chips have been developed currently, such as lung, heart, brain, gut, liver, and even body-on-chip composed of several linked tissues (**Fig. 1.17**).

The fundamental element of lung is the layer of epithelial and endothelial cells which allows the exchange of gas between air and blood. Douville et al.[221] developed a microfluidic "alveoli-on-chip" composed of a flexible PDMS membrane that provides a more physiologic recreation of the stresses, which is the first *in vitro* technique to systematically study the role of both solid and fluid mechanical forces in ventilator-induced lung injury (**Fig. 1.17a**). Huh et al.[222] described a biomimetic microsystem that reconstitutes the critical functional alveolar-capillary interface of the human lung (**Fig. 1.17b**). By using this system, they studied bacteria and inflammatory effect as well as nanotoxicology.

Grosberg et al.[223] reported a ''heart on a chip'' that exploits muscular thin film technology to measure contractility, combined with a quantification of action potential propagation, and cytoskeletal architecture in multiple tissues, which allowing real-time data collection and analysis during pharmacological intervention.

Brain is one of the most complex organs *in vivo*, in which blood-brain barrier (BBB) is a unique feature of human the key structure of the brain, not only protects brain homeostasis, but also prevents toxic substances to enter the brain. Griep et al.[224] reported a small model of BBB-on-chip by the well combination of fluidic shear stress and thin membrane, which was suited to study barrier function in detail and evaluate drug passage to finally gain more insight into the treatment of neurodegenerative diseases.

Microvasculature is an essential component for organ-on-chip systems. Miller et al.[225] printed rigid 3D filament networks of carbohydrate glass and used it as a sacrificial template to achieve cylindrical networks (microvascular structures) with

endothelial cells and perfused with blood under high-pressure pulsatile flow.

One of the major goals of organs-on-chip technique is to replace animal models due to the high cost, time-consumption, and the requirement of large amount of compounds of animal tests. Additionally, the traditional animal testing approaches often fail to predict human toxicity and efficiency, and often question the ethics of sacrificing animals if they cannot predict clinical outcomes reliably [219]. Thus in recent years, human induced pluripotent stem cells (hiPSCs) generated from the somatic cells of human are becoming more promising cell sources for organs-on-chip study, which not only are identified as suitable alternatives to supplant the need for animal studies but also largely improve the accuracy of drug assessment due to the in situ cell source compared to animal cells or embryonic stem cells (ESC). And in theory, hiPSCs are able to be differentiated into any type of human cells. So far, hiPSCs have been successfully differentiated into various types of cells, such as multi subtypes of neurons, cardiomyocytes, hepatocytes, endothelial cells and so on. Thus the organs-on-chips based on hiPSCs have high potential to provide more and reliable organ models of human and be more precisely predictive human relevant models for toxicity and efficacy test.

1.6 Research objectives

The purpose of this thesis work is to develop cell devices and methods for advanced biological and biomedical studies. More specifically, we were interested in cell processing which rely critically on the progress of the microdevice engineering. We have chosen to study culture and differentiation of induced pluripotent stem cells by using as well as isolation and culture of circulating tumor cells, since both are critically depending on the progress of *in vitro* cell processing.

For induced pluripotent stem cells, the primary importance is to prepare ECM mimic scaffolds for high quality processing, including stem cell proliferation and differentiation as well as stem cell derived tissue formation. These scaffolds have also to be appropriate for drug test and regeneration medicine. Therefore, we firstly developed a new type of substrate by considering the requests of versatility and flexibility for both *in vitro* and *in vivo* assays. Unlike conventional 2D culture and some so called 3D culture, we wish to design and fabricate a monolayer nanofiber

scaffold to provide a 3D permeability environment for cells like *in vivo* condition, which should be also convenient for handling for downstream analysis and implantation. The emerging hiPSCs were chosen as the cell source because of its pluripotency which provides diversity and genomic homogeneity which leading to more reliable models and the more accurate assessment for drugs as well as the non-immune rejection during further implantation. Due to the importance of cardiac and motor neuron cells in drug screening and disease therapy, we mostly wish to different hiPSCs into cardiac and motor neurons for generating cardiac patch and motor neuron patch. The promoting role of this scaffold for both differentiations will be discussed according to both various qualitative and quantitative characterizations. In particular, we wish to achieve electrical signals of cardiac and neuron patches by simply transferring onto multi-electrode array and then perform drug test by monitoring the changes of electrical signals.

For circulating tumor cells, great effort has been devoted to the methodical development of the high efficiency isolation. Clearly, their culture and studies after isolation are also important not only for diagnosis but also mechanistic understanding of cancer metastasis as well as disease modeling, drug assay and development. This importance of post-CTC isolation processing would require more careful design of the isolation and culture devices. The current methods for CTCs capture have various drawbacks such as contamination, clogging, low efficiency and low viability of captured cells. Therefore, we firstly designed and fabricated conical hole membranes for high efficiency and high selectively filtration of CTCs. Then, we used microfluidic channels to introduce cross flow for further decreasing the contamination effect and improving the cell viability. Both theoretical and experimental investigations were performed to optimize the device design and the flow rate. Our results showed that CTCs could not only be efficiently isolated at high selectivity but also be cultivated at a reasonable proliferation rate, thereby providing a new perspective for many interesting studies. In parallel, we undertook a primary study of 3D tumor spheroids culture to mimic the *in vivo* tumor by simply using cancer cell line U87 instead of isolated CTCs. Here, we developed a multi-well assay form by agarose molding for millimeter size tumor spheroid generation and maintaining and we succeeded to show anti-cancer drug effects based on such a tumor spheroid assay form.

Reference

[1] Pines M. Inside the cell: DIANE Publishing; 1993.

[2] http://homepage.smc.edu/wissmann_paul/cell.

[3] Barthes J, Özçelik H, Hindié M, Ndreu-Halili A, Hasan A, Vrana NE. Cell microenvironment engineering and monitoring for tissue engineering and regenerative medicine: the recent advances. BioMed research international. 2014;2014.

[4] Labat-Robert J, Bihari-Varga M, Robert L. Extracellular matrix. FEBS letters. 1990;268:386-93.

[5] Rozario T, DeSimone DW. The extracellular matrix in development and morphogenesis: a dynamic view. Developmental biology. 2010;341:126-40.

[6] Scott JE. Extracellular matrix, supramolecular organisation and shape. Journal of anatomy. 1995;187:259.

[7] Schultz GS, Ladwig G, Wysocki A. Extracellular matrix: review of its roles in acute and chronic wounds. World Wide Wounds. 2005;2005.

[8] http://jpkc.scu.edu.cn/ywwy/zbsw(E)/edetail4.htm.

[9] Peach RJ, Hollenbaugh D, Stamenkovic I, Aruffo A. Identification of hyaluronic acid binding sites in the extracellular domain of CD44. The Journal of cell biology. 1993;122:257-64.

[10] Di Lullo GA, Sweeney SM, Körkkö J, Ala-Kokko L, San Antonio JD. Mapping the ligand-binding sites and disease-associated mutations on the most abundant protein in the human, type I collagen. Journal of Biological Chemistry. 2002;277:4223-31.

[11] Karsenty G, Park R-W. Regulation of type I collagen genes expression. International reviews of immunology. 1995;12:177-85.

[12] Kern B, Shen J, Starbuck M, Karsenty G. Cbfa1 contributes to the osteoblast-specific expression of type I collagen genes. Journal of Biological Chemistry. 2001;276:7101-7.

[13] Emsley J, Knight CG, Farndale RW, Barnes MJ. Structure of the integrin α2β1-binding collagen peptide. Journal of molecular biology. 2004;335:1019-28.

[14] von der Mark K, Park J, Bauer S, Schmuki P. Nanoscale engineering of biomimetic surfaces: cues from the extracellular matrix. Cell and tissue research. 2010;339:131-53.

[15] Vakonakis I, Campbell ID. Extracellular matrix: from atomic resolution to ultrastructure. Current opinion in cell biology. 2007;19:578-83.

[16] Laiho M, Keski-Oja J. Growth factors in the regulation of pericellular proteolysis: a review. Cancer research. 1989;49:2533-53.

[17] Ungaro F, Biondi M, Indolfi L, De Rosa G, La Rotonda M, Quaglia F, et al. Bioactivated polymer scaffolds for tissue engineering. Topics in Tissue engineering. 2005;2.

[18] Théry M, Racine V, Pépin A, Piel M, Chen Y, Sibarita J-B, et al. The extracellular matrix guides the orientation of the cell division axis. Nature cell biology. 2005;7:947-53.

[19] Alberts B, Bray D, Hopkin K, Johnson A, Lewis J, Raff M, et al. Essential cell biology: Garland Science; 2013.

[20] Giannone G, Sheetz MP. Substrate rigidity and force define form through tyrosine phosphatase and kinase pathways. Trends in cell biology. 2006;16:213-23.

[21] Hay ED. Cell biology of extracellular matrix: Springer Science & Business Media; 2013.

[22] Cuerrier CMP, Andrew E. Cells, Forces, and the Microenvironment: CRC press; 2015.

[23] Merten O-W. Introduction to animal cell culture technology—past, present and future. Cytotechnology. 2006;50:1-7.

[24] Deutsch HF. Fetuin: the mucoprotein of fetal calf serum. Journal of Biological Chemistry. 1954;208:669-78.

[25] Mooney DJ, Vandenburgh H. Cell delivery mechanisms for tissue repair. Cell stem cell. 2008;2:205-13.

[26] Reya T, Morrison SJ, Clarke MF, Weissman IL. Stem cells, cancer, and cancer stem cells. Nature. 2001;414:105-11.

[27] Spangrude GJ, Heimfeld S, Weissman IL. Purification and characterization of mouse hematopoietic stem cells. Science. 1988;241:58-62.

[28] Baum CM, Weissman IL, Tsukamoto AS, Buckle A-M, Peault B. Isolation of a candidate human hematopoietic stem-cell population. Proceedings of the National Academy of Sciences. 1992;89:2804-8.

[29] da Conceição DS. Stem Cells in Microfluidics. 2011.

[30] Takahashi K, Yamanaka S. Induction of pluripotent stem cells from mouse embryonic and adult fibroblast cultures by defined factors. Cell. 2006;126:663-76.

[31] Kotton DN. The 2012 Nobel Prize in Physiology or Medicine.

[32] e Castro VP, Carbolante EMdSR. Reprogramming of Human Fibroblasts into Pluripotent Cells: Role of Lentiviral Mediated Transcription Factors. Stem Cells and Cancer Stem Cells, Volume 5: Springer; 2012. p. 201-11.

[33] Robertson JA. Embryo stem cell research: ten years of controversy. The Journal of Law, Medicine & Ethics. 2010;38:191-203.

[34] Daley GQ. Customized human embryonic stem cells. Nature biotechnology. 2005;23:826-8.

[35] Yamanaka S. Induced pluripotent stem cells: past, present, and future. Cell stem cell. 2012;10:678-84.

[36] Inoue H, Nagata N, Kurokawa H, Yamanaka S. iPS cells: a game changer for future medicine. The EMBO journal. 2014;33:409-17.

[37] Bellin M, Marchetto MC, Gage FH, Mummery CL. Induced pluripotent stem cells: the new patient? Nature reviews Molecular cell biology. 2012;13:713-26.

[38] Takahashi K, Tanabe K, Ohnuki M, Narita M, Ichisaka T, Tomoda K, et al. Induction of pluripotent stem cells from adult human fibroblasts by defined factors. Cell. 2007;131:861-72.

[39] Hughes CS, Postovit LM, Lajoie GA. Matrigel: a complex protein mixture required for optimal growth of cell culture. Proteomics. 2010;10:1886-90.

[40] Higuchi A, Ling Q-D, Kumar SS, Munusamy M, Alarfajj AA, Umezawa A, et al. Design of polymeric materials for culturing human pluripotent stem cells: Progress toward feeder-free and xeno-free culturing. Progress in Polymer Science. 2014;39:1348-74.

[41] Li XJ, Du ZW, Zarnowska ED, Pankratz M, Hansen LO, Pearce RA, et al. Specification of motoneurons from human embryonic stem cells. Nature biotechnology. 2005;23:215-21.

[42] Chambers SM, Fasano CA, Papapetrou EP, Tomishima M, Sadelain M, Studer L. Highly efficient neural conversion of human ES and iPS cells by dual inhibition of SMAD signaling. Nature biotechnology. 2009;27:275-80.

[43] Hu W, He Y, Xiong Y, Lu H, Chen H, Hou L, et al. Derivation, Expansion, and Motor Neuron Differentiation of Human-Induced Pluripotent Stem Cells with Non-Integrating Episomal Vectors and a Defined Xenogeneic-free Culture System. Molecular neurobiology. 2015.

[44] Tateishi K, He J, Taranova O, Liang G, D'Alessio AC, Zhang Y. Generation of

insulin-secreting islet-like clusters from human skin fibroblasts. Journal of Biological Chemistry. 2008;283:31601-7.

[45] Si‐Tayeb K, Noto FK, Nagaoka M, Li J, Battle MA, Duris C, et al. Highly efficient generation of human hepatocyte–like cells from induced pluripotent stem cells. Hepatology. 2010;51:297-305.

[46] Iwamuro M, Komaki T, Kubota Y, Seita M, Kawamoto H, Yuasa T, et al. Hepatic differentiation of mouse iPS cells in vitro. Cell transplantation. 2010;19:841-7.

[47] Kamp TJ, Lyons GE. On the road to iPS cell cardiovascular applications. Circulation research. 2009;105:617-9.

[48] Yang L, Soonpaa MH, Adler ED, Roepke TK, Kattman SJ, Kennedy M, et al. Human cardiovascular progenitor cells develop from a KDR+ embryonic-stem-cell-derived population. Nature. 2008;453:524-8.

[49] Organization WH. Cancer Fact sheet N 297.[Cited 2014 Nov; updated 2015 Feb].

[50] Jemal A, Bray F, Center MM, Ferlay J, Ward E, Forman D. Global cancer statistics. CA: a cancer journal for clinicians. 2011;61:69-90.

[51] Esmaeilsabzali H, Beischlag TV, Cox ME, Parameswaran AM, Park EJ. Detection and isolation of circulating tumor cells: principles and methods. Biotechnology advances. 2013;31:1063-84.

[52] Hanahan D, Weinberg RA. The hallmarks of cancer. Cell. 2000;100:57-70.

[53] Cancer IAfRo. World cancer report 2014. Geneva: WHO. 2014.

[54] den Toonder J. Circulating tumor cells: the Grand Challenge. Lab on a chip. 2011;11:375-7.

[55] Miller MC, Doyle GV, Terstappen LW. Significance of Circulating Tumor Cells Detected by the CellSearch System in Patients with Metastatic Breast Colorectal and Prostate Cancer. Journal of oncology. 2010;2010:617421.

[56] R.Ashworth T. A case of cancer in which cells similar to those in the tumourswere seen in the blood after death. TheMedical Journal of Australia. 1869;14:146-7.

[57] Fidler IJ. The pathogenesis of cancer metastasis: the'seed and soil'hypothesis revisited. Nature Reviews Cancer. 2003;3:453-8.

[58] Hay ED. The mesenchymal cell, its role in the embryo, and the remarkable signaling mechanisms that create it. Developmental dynamics. 2005;233:706-20.

[59] Barriere G, Tartary M, Rigaud M. Epithelial mesenchymal transition: a new insight into the detection of circulating tumor cells. ISRN oncology. 2012;2012:382010.

[60] Lee JM, Dedhar S, Kalluri R, Thompson EW. The epithelial-mesenchymal transition: new insights in signaling, development, and disease. The Journal of cell biology. 2006;172:973-81.

[61] Pouysségur J, Dayan F, Mazure NM. Hypoxia signalling in cancer and approaches to enforce tumour regression. Nature. 2006;441:437-43.

[62] Singh A, Settleman J. EMT, cancer stem cells and drug resistance: an emerging axis of evil in the war on cancer. Oncogene. 2010;29:4741-51.

[63] Scheel C, Weinberg RA. Cancer stem cells and epithelial–mesenchymal transition: concepts and molecular links. Seminars in cancer biology: Elsevier; 2012. p. 396-403.

[64] Müller V, Stahmann N, Riethdorf S, Rau T, Zabel T, Goetz A, et al. Circulating tumor cells in breast cancer: correlation to bone marrow micrometastases, heterogeneous response to systemic therapy and low proliferative activity. Clinical Cancer Research. 2005;11:3678-85.

[65] Hanahan D, Weinberg RA. Hallmarks of cancer: the next generation. Cell. 2011;144:646-74.

[66] Chiang AC, Massagué J. Molecular basis of metastasis. New England Journal of Medicine. 2008;359:2814-23.

[67] Bednarz-Knoll N, Alix-Panabières C, Pantel K. Plasticity of disseminating cancer cells in patients with epithelial malignancies. Cancer and Metastasis Reviews. 2012;31:673-87.

[68] Christiansen JJ, Rajasekaran AK. Reassessing epithelial to mesenchymal transition as a prerequisite for carcinoma invasion and metastasis. Cancer research. 2006;66:8319-26.

[69] Mesothelioma Diagnosis.

[70] Cristofanilli M, Budd GT, Ellis MJ, Stopeck A, Matera J, Miller MC, et al. Circulating tumor cells, disease progression, and survival in metastatic breast cancer. New England Journal of Medicine. 2004;351:781-91.

[71] Arya SK, Lim B, Rahman AR. Enrichment, detection and clinical significance of circulating tumor cells. Lab on a chip. 2013;13:1995-2027.

[72] Fischer AH. Circulating tumor cells: seeing is believing. Archives of Pathology

& Laboratory Medicine. 2009;133:1367-9.

[73] Farace F, Massard C, Vimond N, Drusch F, Jacques N, Billiot F, et al. A direct comparison of CellSearch and ISET for circulating tumour-cell detection in patients with metastatic carcinomas. British journal of cancer. 2011;105:847-53.

[74] Myung JH, Gajjar KA, Saric J, Eddington DT, Hong S. Dendrimer‐Mediated Multivalent Binding for the Enhanced Capture of Tumor Cells. Angewandte Chemie. 2011;123:11973-6.

[75] Hoshino K, Huang Y-Y, Lane N, Huebschman M, Uhr JW, Frenkel EP, et al. Microchip-based immunomagnetic detection of circulating tumor cells. Lab on a chip. 2011;11:3449-57.

[76] Liu YJ, Guo SS, Zhang ZL, Huang WH, Baigl D, Xie M, et al. A micropillar‐integrated smart microfluidic device for specific capture and sorting of cells. Electrophoresis. 2007;28:4713-22.

[77] Saliba A-E, Saias L, Psychari E, Minc N, Simon D, Bidard F-C, et al. Microfluidic sorting and multimodal typing of cancer cells in self-assembled magnetic arrays. Proceedings of the National Academy of Sciences. 2010;107:14524-9.

[78] Nagrath S, Sequist LV, Maheswaran S, Bell DW, Irimia D, Ulkus L, et al. Isolation of rare circulating tumour cells in cancer patients by microchip technology. Nature. 2007;450:1235-9.

[79] Stott SL, Hsu C-H, Tsukrov DI, Yu M, Miyamoto DT, Waltman BA, et al. Isolation of circulating tumor cells using a microvortex-generating herringbone-chip. Proceedings of the National Academy of Sciences. 2010;107:18392-7.

[80] Wang S, Liu K, Liu J, Yu ZT, Xu X, Zhao L, et al. Highly efficient capture of circulating tumor cells by using nanostructured silicon substrates with integrated chaotic micromixers. Angewandte Chemie. 2011;50:3084-8.

[81] Chen Y, Li P, Huang PH, Xie Y, Mai JD, Wang L, et al. Rare cell isolation and analysis in microfluidics. Lab on a chip. 2014;14:626-45.

[82] Thiery JP. Epithelial–mesenchymal transitions in tumour progression. Nature Reviews Cancer. 2002;2:442-54.

[83] Yu M, Bardia A, Wittner BS, Stott SL, Smas ME, Ting DT, et al. Circulating breast tumor cells exhibit dynamic changes in epithelial and mesenchymal composition. Science. 2013;339:580-4.

[84] Lv P, Tang Z, Liang X, Guo M, Han RP. Spatially gradated segregation and

recovery of circulating tumor cells from peripheral blood of cancer patients. Biomicrofluidics. 2013;7:34109.

[85] Hou HW, Warkiani ME, Khoo BL, Li ZR, Soo RA, Tan DS, et al. Isolation and retrieval of circulating tumor cells using centrifugal forces. Scientific reports. 2013;3:1259.

[86] Sun J, Liu C, Li M, Wang J, Xianyu Y, Hu G, et al. Size-based hydrodynamic rare tumor cell separation in curved microfluidic channels. Biomicrofluidics. 2013;7:11802.

[87] Karabacak NM, Spuhler PS, Fachin F, Lim EJ, Pai V, Ozkumur E, et al. Microfluidic, marker-free isolation of circulating tumor cells from blood samples. Nature protocols. 2014;9:694-710.

[88] Sun J, Li M, Liu C, Zhang Y, Liu D, Liu W, et al. Double spiral microchannel for label-free tumor cell separation and enrichment. Lab on a chip. 2012;12:3952-60.

[89] Gupta V, Jafferji I, Garza M, Melnikova VO, Hasegawa DK, Pethig R, et al. ApoStream™, a new dielectrophoretic device for antibody independent isolation and recovery of viable cancer cells from blood. Biomicrofluidics. 2012;6:024133.

[90] Gascoyne PR, Shim S. Isolation of circulating tumor cells by dielectrophoresis. Cancers. 2014;6:545-79.

[91] Shim S, Stemke-Hale K, Noshari J, Becker FF, Gascoyne PR. Dielectrophoresis has broad applicability to marker-free isolation of tumor cells from blood by microfluidic systems. Biomicrofluidics. 2013;7:011808.

[92] Seal S. A sieve for the isolation of cancer cells and other large cells from the blood. Cancer. 1964;17:637-42.

[93] Khato J, SATO H, SUZUKI M, SATO H. Filtrability and flow characteristics of leukemic and non-leukemic tumor cell suspension through polycarbonate filters in relation to hematogenous spread of cancer. The Tohoku journal of experimental medicine. 1979;128:273-84.

[94] Holdich R, Kosvintsev S, Cumming I, Zhdanov S. Pore design and engineering for filters and membranes. Philosophical Transactions of the Royal Society of London A: Mathematical, Physical and Engineering Sciences. 2006;364:161-74.

[95] Vona G, Sabile A, Louha M, Sitruk V, Romana S, Schütze K, et al. Isolation by size of epithelial tumor cells: a new method for the immunomorphological and molecular characterization of circulating tumor cells. The American journal of pathology. 2000;156:57-63.

[96] Desitter I, Guerrouahen BS, Benali-Furet N, Wechsler J, Jaenne PA, Kuang Y, et al. A new device for rapid isolation by size and characterization of rare circulating tumor cells. Anticancer research. 2011;31:427-41.

[97] Zheng S, Lin H, Liu JQ, Balic M, Datar R, Cote RJ, et al. Membrane microfilter device for selective capture, electrolysis and genomic analysis of human circulating tumor cells. Journal of chromatography A. 2007;1162:154-61.

[98] Tan SJ, Yobas L, Lee GY, Ong CN, Lim CT. Microdevice for the isolation and enumeration of cancer cells from blood. Biomedical microdevices. 2009;11:883-92.

[99] Hosokawa M, Hayata T, Fukuda Y, Arakaki A, Yoshino T, Tanaka T, et al. Size-selective microcavity array for rapid and efficient detection of circulating tumor cells. Analytical chemistry. 2010;82:6629-35.

[100] Zheng S, Lin HK, Lu B, Williams A, Datar R, Cote RJ, et al. 3D microfilter device for viable circulating tumor cell (CTC) enrichment from blood. Biomedical microdevices. 2011;13:203-13.

[101] Hur SC, Mach AJ, Di Carlo D. High-throughput size-based rare cell enrichment using microscale vortices. Biomicrofluidics. 2011;5:022206.

[102] Lim LS, Hu M, Huang MC, Cheong WC, Gan ATL, Looi XL, et al. Microsieve lab-chip device for rapid enumeration and fluorescence in situ hybridization of circulating tumor cells. Lab on a chip. 2012;12:4388-96.

[103] Lin HK, Zheng S, Williams AJ, Balic M, Groshen S, Scher HI, et al. Portable filter-based microdevice for detection and characterization of circulating tumor cells. Clinical cancer research : an official journal of the American Association for Cancer Research. 2010;16:5011-8.

[104] Coumans F, van Dalum G, Beck M, Terstappen L. Filter characteristics influencing circulating tumor cell enrichment from whole blood. PloS one. 2013;8:e61770.

[105] Hosokawa M, Kenmotsu H, Koh Y, Yoshino T, Yoshikawa T, Naito T, et al. Size-based isolation of circulating tumor cells in lung cancer patients using a microcavity array system. PloS one. 2013;8:e67466.

[106] LaBarbera DV, Reid BG, Yoo BH. The multicellular tumor spheroid model for high-throughput cancer drug discovery. Expert opinion on drug discovery. 2012;7:819-30.

[107] Yamada KM, Cukierman E. Modeling tissue morphogenesis and cancer in 3D. Cell. 2007;130:601-10.

[108] Santini MT, Rainaldi G. Three-dimensional spheroid model in tumor biology. Pathobiology. 1999;67:148-57.

[109] Tung YC, Hsiao AY, Allen SG, Torisawa YS, Ho M, Takayama S. High-throughput 3D spheroid culture and drug testing using a 384 hanging drop array. The Analyst. 2011;136:473-8.

[110] Gwak SJ, Choi D, Paik SS, Cho SW, Kim SS, Choi CY, et al. A method for the effective formation of hepatocyte spheroids using a biodegradable polymer nanosphere. Journal of Biomedical Materials Research Part A. 2006;78:268-75.

[111] Ong S-M, Zhao Z, Arooz T, Zhao D, Zhang S, Du T, et al. Engineering a scaffold-free 3D tumor model for in vitro drug penetration studies. Biomaterials. 2010;31:1180-90.

[112] Loessner D, Stok KS, Lutolf MP, Hutmacher DW, Clements JA, Rizzi SC. Bioengineered 3D platform to explore cell-ECM interactions and drug resistance of epithelial ovarian cancer cells. Biomaterials. 2010;31:8494-506.

[113] Ozawa F, Ino K, Arai T, Ramon-Azcon J, Takahashi Y, Shiku H, et al. Alginate gel microwell arrays using electrodeposition for three-dimensional cell culture. Lab on a chip. 2013;13:3128-35.

[114] Torisawa Y-s, Takagi A, Nashimoto Y, Yasukawa T, Shiku H, Matsue T. A multicellular spheroid array to realize spheroid formation, culture, and viability assay on a chip. Biomaterials. 2007;28:559-66.

[115] Mehta G, Hsiao AY, Ingram M, Luker GD, Takayama S. Opportunities and challenges for use of tumor spheroids as models to test drug delivery and efficacy. Journal of controlled release : official journal of the Controlled Release Society. 2012;164:192-204.

[116] Liang Y, Zhang H, Feng Q-S, Cai M-B, Deng W, Qin D, et al. The propensity for tumorigenesis in human induced pluripotent stem cells is related with genomic instability. Chinese journal of cancer. 2013;32:205.

[117] Okita K, Yamanaka S. Induced pluripotent stem cells: opportunities and challenges. Philosophical Transactions of the Royal Society B: Biological Sciences. 2011;366:2198-207.

[118] Lee AS, Tang C, Rao MS, Weissman IL, Wu JC. Tumorigenicity as a clinical hurdle for pluripotent stem cell therapies. Nature medicine. 2013;19:998-1004.

[119] Lutolf M, Hubbell J. Synthetic biomaterials as instructive extracellular microenvironments for morphogenesis in tissue engineering. Nature biotechnology.

2005;23:47-55.

[120] O'brien FJ. Biomaterials & scaffolds for tissue engineering. Materials Today. 2011;14:88-95.

[121] Hench LL. Bioceramics, a clinical success. American Ceramic Society Bulletin. 1998;77:67-74.

[122] Ambrosio A, Sahota JS, Khan Y, Laurencin CT. A novel amorphous calcium phosphate polymer ceramic for bone repair: I. Synthesis and characterization. Journal of biomedical materials research. 2001;58:295-301.

[123] Niinomi M. Recent research and development in titanium alloys for biomedical applications and healthcare goods. Science and technology of advanced Materials. 2003;4:445-54.

[124] PENG D-l, WANG W. Study on the Solidification Structure and Mechanical Property of Ti-Nb-Zr-Mo Alloy Artificial Limb Joint Precision Casting. Foundry. 2012;10:005.

[125] Chen G, Ushida T, Tateishi T. Scaffold design for tissue engineering. Macromolecular bioscience. 2002;2:67-77.

[126] Jones I, Currie L, Martin R. A guide to biological skin substitutes. British journal of plastic surgery. 2002;55:185-93.

[127] Nair LS, Laurencin CT. Polymers as biomaterials for tissue engineering and controlled drug delivery. Tissue engineering I: Springer; 2006. p. 47-90.

[128] Kim I-Y, Seo S-J, Moon H-S, Yoo M-K, Park I-Y, Kim B-C, et al. Chitosan and its derivatives for tissue engineering applications. Biotechnology advances. 2008;26:1-21.

[129] Glowacki J, Mizuno S. Collagen scaffolds for tissue engineering. Biopolymers. 2008;89:338-44.

[130] Cen L, Liu W, Cui L, Zhang W, Cao Y. Collagen tissue engineering: development of novel biomaterials and applications. Pediatric research. 2008;63:492-6.

[131] Lynn A, Yannas I, Bonfield W. Antigenicity and immunogenicity of collagen. Journal of Biomedical Materials Research Part B: Applied Biomaterials. 2004;71:343-54.

[132] Gómez-Guillén M, Pérez-Mateos M, Gómez-Estaca J, López-Caballero E, Giménez B, Montero P. Fish gelatin: a renewable material for developing active biodegradable films. Trends in Food Science & Technology. 2009;20:3-16.

[133] Jain E, Kumar A. Disposable polymeric cryogel bioreactor matrix for therapeutic protein production. Nature protocols. 2013;8:821-35.

[134] Vats A, Tolley N, Polak J, Gough J. Scaffolds and biomaterials for tissue engineering: a review of clinical applications. Clinical Otolaryngology & Allied Sciences. 2003;28:165-72.

[135] Sherwood JK, Riley SL, Palazzolo R, Brown SC, Monkhouse DC, Coates M, et al. A three-dimensional osteochondral composite scaffold for articular cartilage repair. Biomaterials. 2002;23:4739-51.

[136] Uematsu K, Hattori K, Ishimoto Y, Yamauchi J, Habata T, Takakura Y, et al. Cartilage regeneration using mesenchymal stem cells and a three-dimensional poly-lactic-glycolic acid (PLGA) scaffold. Biomaterials. 2005;26:4273-9.

[137] Nisbet D, Yu L, Zahir T, Forsythe J, Shoichet M. Characterization of neural stem cells on electrospun poly (ε-caprolactone) submicron scaffolds: evaluating their potential in neural tissue engineering. Journal of Biomaterials Science, Polymer Edition. 2008;19:623-34.

[138] Pankajakshan D, Philipose LP, Palakkal M, Krishnan K, Krishnan LK. Development of a fibrin composite‐coated poly (ε‐caprolactone) scaffold for potential vascular tissue engineering applications. Journal of Biomedical Materials Research Part B: Applied Biomaterials. 2008;87:570-9.

[139] Zhu X, Cui W, Li X, Jin Y. Electrospun fibrous mats with high porosity as potential scaffolds for skin tissue engineering. Biomacromolecules. 2008;9:1795-801.

[140] Rowlands A, Lim SA, Martin D, Cooper-White JJ. Polyurethane/poly (lactic-co-glycolic) acid composite scaffolds fabricated by thermally induced phase separation. Biomaterials. 2007;28:2109-21.

[141] Park S, Lee HJ, Koh WG. Multiplex immunoassay platforms based on shape-coded poly(ethylene glycol) hydrogel microparticles incorporating acrylic acid. Sensors. 2012;12:8426-36.

[142] Fairbanks BD, Schwartz MP, Bowman CN, Anseth KS. Photoinitiated polymerization of PEG-diacrylate with lithium phenyl-2,4,6-trimethylbenzoylphosphinate: polymerization rate and cytocompatibility. Biomaterials. 2009;30:6702-7.

[143] Lin H, Zhang D, Alexander PG, Yang G, Tan J, Cheng AW, et al. Application of visible light-based projection stereolithography for live cell-scaffold fabrication

with designed architecture. Biomaterials. 2013;34:331-9.

[144] www.bd.com.

[145] http://www.biolamina.com/product-ln-521.

[146] Higuchi A, Ling QD, Ko YA, Chang Y, Umezawa A. Biomaterials for the feeder-free culture of human embryonic stem cells and induced pluripotent stem cells. Chemical reviews. 2011;111:3021-35.

[147] Mahlstedt MM, Anderson D, Sharp JS, McGilvray R, Barbadillo Muñoz MD, Buttery LD, et al. Maintenance of pluripotency in human embryonic stem cells cultured on a synthetic substrate in conditioned medium. Biotechnology and bioengineering. 2010;105:130-40.

[148] Kim S, Ahn SE, Lee JH, Lim DS, Kim KS, Chung HM, et al. A novel culture technique for human embryonic stem cells using porous membranes. Stem cells. 2007;25:2601-9.

[149] www.alvetex.com.

[150] Liu L, Yoshioka M, Nakajima M, Ogasawara A, Liu J, Hasegawa K, et al. Nanofibrous gelatin substrates for long-term expansion of human pluripotent stem cells. Biomaterials. 2014;35:6259-67.

[151] Sargent CY, Berguig GY, McDevitt TC. Cardiomyogenic differentiation of embryoid bodies is promoted by rotary orbital suspension culture. Tissue Engineering Part A. 2009;15:331-42.

[152] Ghaemmaghami AM, Hancock MJ, Harrington H, Kaji H, Khademhosseini A. Biomimetic tissues on a chip for drug discovery. Drug discovery today. 2012;17:173-81.

[153] Phillips BW, Horne R, Lay TS, Rust WL, Teck TT, Crook JM. Attachment and growth of human embryonic stem cells on microcarriers. Journal of biotechnology. 2008;138:24-32.

[154] Chen X, Chen A, Woo TL, Choo AB, Reuveny S, Oh SK. Investigations into the metabolism of two-dimensional colony and suspended microcarrier cultures of human embryonic stem cells in serum-free media. Stem cells and development. 2010;19:1781-92.

[155] Chen CS, Mrksich M, Huang S, Whitesides GM, Ingber DE. Geometric control of cell life and death. Science. 1997;276:1425-8.

[156] Bhatia S, Balis U, Yarmush M, Toner M. Effect of cell–cell interactions in preservation of cellular phenotype: cocultivation of hepatocytes and nonparenchymal

cells. The FASEB Journal. 1999;13:1883-900.

[157] Huang S, Ingber DE. Shape-dependent control of cell growth, differentiation, and apoptosis: switching between attractors in cell regulatory networks. Experimental cell research. 2000;261:91-103.

[158] Chiu DT, Jeon NL, Huang S, Kane RS, Wargo CJ, Choi IS, et al. Patterned deposition of cells and proteins onto surfaces by using three-dimensional microfluidic systems. Proceedings of the National Academy of Sciences. 2000;97:2408-13.

[159] <Scaffold Design for Tissue Engineering.pdf>.

[160] Flanagan TC, Wilkins B, Black A, Jockenhoevel S, Smith TJ, Pandit AS. A collagen-glycosaminoglycan co-culture model for heart valve tissue engineering applications. Biomaterials. 2006;27:2233-46.

[161] Tateishi T, Chen G, Ushida T. Biodegradable porous scaffolds for tissue engineering. Journal of Artificial Organs. 2002;5:77-83.

[162] Khademhosseini A, Langer R, Borenstein J, Vacanti JP. Microscale technologies for tissue engineering and biology. Proceedings of the National Academy of Sciences of the United States of America. 2006;103:2480-7.

[163] Hubbell JA. Biomaterials in tissue engineering. Nature biotechnology. 1995;13:565-76.

[164] Peter S, Miller M, Yasko A, Yaszemski M, Mikos A. Polymer concepts in tissue engineering. Journal of biomedical materials research. 1998;43:422-7.

[165] Schmidt CE, Baier JM. Acellular vascular tissues: natural biomaterials for tissue repair and tissue engineering. Biomaterials. 2000;21:2215-31.

[166] Lanza R, Langer R, Vacanti JP. Principles of tissue engineering: Academic press; 2011.

[167] Chan BP, Leong KW. Scaffolding in tissue engineering: general approaches and tissue-specific considerations. European spine journal : official publication of the European Spine Society, the European Spinal Deformity Society, and the European Section of the Cervical Spine Research Society. 2008;17 Suppl 4:467-79.

[168] Williams DF. On the mechanisms of biocompatibility. Biomaterials. 2008;29:2941-53.

[169] Wulf K, Teske M, Löbler M, Luderer F, Schmitz KP, Sternberg K. Surface functionalization of poly (ε - caprolactone) improves its biocompatibility as scaffold material for bioartificial vessel prostheses. Journal of Biomedical Materials

Research Part B: Applied Biomaterials. 2011;98:89-100.

[170] Hutmacher DW. Scaffolds in tissue engineering bone and cartilage. Biomaterials. 2000;21:2529-43.

[171] Mitragotri S, Lahann J. Physical approaches to biomaterial design. Nature materials. 2009;8:15-23.

[172] Agrawal C, Ray RB. Biodegradable polymeric scaffolds for musculoskeletal tissue engineering. Journal of biomedical materials research. 2001;55:141-50.

[173] Karande TS, Ong JL, Agrawal CM. Diffusion in musculoskeletal tissue engineering scaffolds: design issues related to porosity, permeability, architecture, and nutrient mixing. Annals of biomedical engineering. 2004;32:1728-43.

[174] Karageorgiou V, Kaplan D. Porosity of 3D biomaterial scaffolds and osteogenesis. Biomaterials. 2005;26:5474-91.

[175] Wei J, Yoshinari M, Takemoto S, Hattori M, Kawada E, Liu B, et al. Adhesion of mouse fibroblasts on hexamethyldisiloxane surfaces with wide range of wettability. Journal of Biomedical Materials Research Part B: Applied Biomaterials. 2007;81:66-75.

[176] Charest JL, García AJ, King WP. Myoblast alignment and differentiation on cell culture substrates with microscale topography and model chemistries. Biomaterials. 2007;28:2202-10.

[177] Hyun J, Chen J, Setton LA, Chilkoti A. Patterning cells in highly deformable microstructures: effect of plastic deformation of substrate on cellular phenotype and gene expression. Biomaterials. 2006;27:1444-51.

[178] Lee TC, Niederer P. Basic Engineering for Medics and Biologists: An ESEM Primer: IOS Press; 2010.

[179] Hollister SJ. Scaffold engineering: a bridge to where? Biofabrication. 2009;1:012001.

[180] Mikos A, Lu L, Temenoff J, Tessmar J. Synthetic bioresorbable polymer scaffolds. Elsevier Academic Press: San Diego, CA, USA; 2004. p. 237-45.

[181] Plikk P, Målberg S, Albertsson A-C. Design of resorbable porous tubular copolyester scaffolds for use in nerve regeneration. Biomacromolecules. 2009;10:1259-64.

[182] Huang Y, Mooney D. Gas foaming to fabricate polymer scaffolds in tissue engineering. Scaffoldings in tissue engineering. 2005:159.

[183] Tang Y, Li N, Liu A, Ding S, Yi C, Liu H. Effect of spinning conditions on the

structure and performance of hydrophobic PVDF hollow fiber membranes for membrane distillation. Desalination. 2012;287:326-39.

[184] Tibbitt MW, Anseth KS. Hydrogels as extracellular matrix mimics for 3D cell culture. Biotechnology and bioengineering. 2009;103:655-63.

[185] Azad AK, Sermsintham N, Chandrkrachang S, Stevens WF. Chitosan membrane as a wound‐healing dressing: Characterization and clinical application. Journal of Biomedical Materials Research Part B: Applied Biomaterials. 2004;69:216-22.

[186] Yoo HJ, Kim HD. Synthesis and properties of waterborne polyurethane hydrogels for wound healing dressings. Journal of Biomedical Materials Research Part B: Applied Biomaterials. 2008;85:326-33.

[187] Jafari B, Rafie F, Davaran S. Preparation and characterization of a novel smart polymeric hydrogel for drug delivery of insulin. BioImpacts: BI. 2011;1:135.

[188] Tanigo T, Takaoka R, Tabata Y. Sustained release of water-insoluble simvastatin from biodegradable hydrogel augments bone regeneration. Journal of Controlled Release. 2010;143:201-6.

[189] Bryant SJ, Anseth KS. The effects of scaffold thickness on tissue engineered cartilage in photocrosslinked poly (ethylene oxide) hydrogels. Biomaterials. 2001;22:619-26.

[190] Ashammakhi N, Ndreu A, Yang Y, Ylikauppila H, Nikkola L. Nanofiber-based scaffolds for tissue engineering. European Journal of Plastic Surgery. 2012;35:135-49.

[191] Xu C, Inai R, Kotaki M, Ramakrishna S. Aligned biodegradable nanofibrous structure: a potential scaffold for blood vessel engineering. Biomaterials. 2004;25:877-86.

[192] Venugopal J, Ramakrishna S. Applications of polymer nanofibers in biomedicine and biotechnology. Applied Biochemistry and Biotechnology. 2005;125:147-57.

[193] Norman JJ, Desai TA. Methods for fabrication of nanoscale topography for tissue engineering scaffolds. Annals of biomedical engineering. 2006;34:89-101.

[194] Zeleny J. The electrical discharge from liquid points, and a hydrostatic method of measuring the electric intensity at their surfaces. Physical Review. 1914;3:69.

[195] Zhu N, Chen X. Biofabrication of tissue scaffolds: INTECH Open Access Publisher; 2013.

[196] Sackmann EK, Fulton AL, Beebe DJ. The present and future role of microfluidics in biomedical research. Nature. 2014;507:181-9.

[197] Terry SC, Jerman JH, Angell JB. A gas chromatographic air analyzer fabricated on a silicon wafer. Electron Devices, IEEE Transactions on. 1979;26:1880-6.

[198] Doroszewski J, Skierski J, Przaądka L. Interaction of neoplastic cells with glass surface under flow conditions. Experimental cell research. 1977;104:335-43.

[199] Manz A, Graber N, Widmer Há. Miniaturized total chemical analysis systems: a novel concept for chemical sensing. Sensors and actuators B: Chemical. 1990;1:244-8.

[200] Whitesides GM. The origins and the future of microfluidics. Nature. 2006;442:368-73.

[201] Andersson H, Van den Berg A. Microfluidic devices for cellomics: a review. Sensors and actuators B: Chemical. 2003;92:315-25.

[202] Sia SK, Whitesides GM. Microfluidic devices fabricated in poly (dimethylsiloxane) for biological studies. Electrophoresis. 2003;24:3563-76.

[203] Xiong B, Ren K, Shu Y, Chen Y, Shen B, Wu H. Recent developments in microfluidics for cell studies. Advanced Materials. 2014;26:5525-32.

[204] El-Ali J, Sorger PK, Jensen KF. Cells on chips. Nature. 2006;442:403-11.

[205] Huh D, Gu W, Kamotani Y, Grotberg JB, Takayama S. Microfluidics for flow cytometric analysis of cells and particles. Physiological measurement. 2005;26:R73.

[206] Xia N, Hunt TP, Mayers BT, Alsberg E, Whitesides GM, Westervelt RM, et al. Combined microfluidic-micromagnetic separation of living cells in continuous flow. Biomedical microdevices. 2006;8:299-308.

[207] Nagrath S, Sequist LV, Maheswaran S, Bell DW, Irimia D, Ulkus L, et al. Isolation of rare circulating tumour cells in cancer patients by microchip technology. Nature. 2007;450:1235-9.

[208] Yu M, Stott S, Toner M, Maheswaran S, Haber DA. Circulating tumor cells: approaches to isolation and characterization. The Journal of cell biology. 2011;192:373-82.

[209] Li YQ, Chandran BK, Lim CT, Chen X. Rational Design of Materials Interface for Efficient Capture of Circulating Tumor Cells. Advanced Science. 2015;2.

[210] Pal R, Yang M, Lin R, Johnson B, Srivastava N, Razzacki S, et al. An integrated microfluidic device for influenza and other genetic analyses. Lab on a

chip. 2005;5:1024-32.

[211] Young EW, Beebe DJ. Fundamentals of microfluidic cell culture in controlled microenvironments. Chemical Society Reviews. 2010;39:1036-48.

[212] Jung D, Kapur R, Adams T, Giuliano K, Mrksich M, Craighead H, et al. Topographical and physicochemical modification of material surface to enable patterning of living cells. Critical Reviews in Biotechnology. 2001;21:111-54.

[213] Kim D-H, Provenzano PP, Smith CL, Levchenko A. Matrix nanotopography as a regulator of cell function. The Journal of cell biology. 2012;197:351-60.

[214] Keenan TM, Folch A. Biomolecular gradients in cell culture systems. Lab on a chip. 2008;8:34-57.

[215] Vukasinovic J, Cullen DK, LaPlaca MC, Glezer A. A microperfused incubator for tissue mimetic 3D cultures. Biomedical microdevices. 2009;11:1155-65.

[216] Jiang B, Zheng W, Zhang W, Jiang X. Organs on microfluidic chips: A mini review. Science China Chemistry. 2014;57:356-64.

[217] Douville NJ, Zamankhan P, Tung Y-C, Li R, Vaughan BL, Tai C-F, et al. Combination of fluid and solid mechanical stresses contribute to cell death and detachment in a microfluidic alveolar model. Lab on a chip. 2011;11:609-19.

[218] Huh D, Matthews BD, Mammoto A, Montoya-Zavala M, Hsin HY, Ingber DE. Reconstituting organ-level lung functions on a chip. Science. 2010;328:1662-8.

[219] Griep L, Wolbers F, De Wagenaar B, Ter Braak P, Weksler B, Romero IA, et al. BBB on chip: microfluidic platform to mechanically and biochemically modulate blood-brain barrier function. Biomedical microdevices. 2013;15:145-50.

[220] Miller JS, Stevens KR, Yang MT, Baker BM, Nguyen D-HT, Cohen DM, et al. Rapid casting of patterned vascular networks for perfusable engineered three-dimensional tissues. Nature materials. 2012;11:768-74.

Chapter 2

Technological developments

In this chapter, we present the technological development of this thesis work. Firstly, we describe the electrospinning technique for the fabrication of nanofiber scaffolds. Then, we introduce hydrogel formation techniques, with especial focus on poly(ethylene glycol) (PEG) based hydrogel. Afterwards, we present several lithography techniques lithography techniques for surface patterning and microfluidic device fabrications.

2.1 Electrospinning

Electrospinning is a straightforward but yet simple technique to produce nanofibers with uniform diameter and different materials [1, 2]. Generally, the setup for electrospinning includes three parts: a syringe, a high-voltage power supply and a conductive collector. A polymer solution is first prepared by completely dissolving of polymer in certain solvent. During electrospinning, a syringe is used to feed polymer solution with a constant flow rate controlled by syringe pump. The needle of syringe is connected with a positive electrode, while the negative electrode connects on the collector. During the fiber towards to the collector, the solvent is evaporated and dry fibrous mats are generated on the collector. Several processing parameters are important to the performance of nanofibers, such as the solution composition, the voltage, the distance between needle and collector, as well as the temperature and humidity of environment [3-5]. **Fig. 2.1** shows a typical electrospinning setup used in this work.

Various biodegradable natural or synthetic polymers can be easily used to fabricate submicron fibers. To improve the performance of nanofibers in tissue engineering, the fabricated nanofibers can be treated by surface modification using such as plasma and wet chemical etch, surface graft polymerization, and co-electrospinning of surface active agents and polymers [6-8]. Surfaces of nanofibers can also be chemically modified with attaching specific bioactive ligands to improve cell adhesion, proliferation, and differentiation by mimicking the ECM morphology and functions [6].

A large number of investigations have shown that the cellular behaviors, such as attachment, proliferation and differentiation, can be modulated by regulating the parameters of nanofiber such as chemical composition, fiber morphology, diameter

and alignment [9] (**Fig. 2.2**).

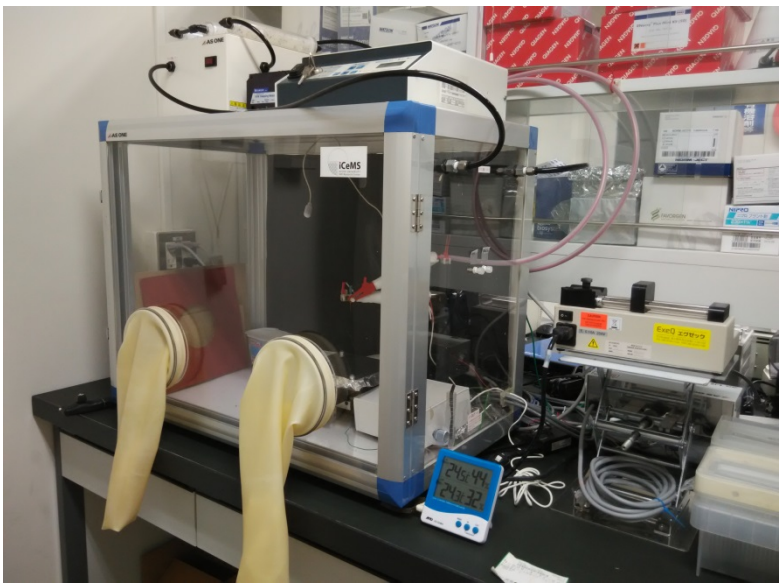

Fig. 2.1 Electrospinning setup used in this work.

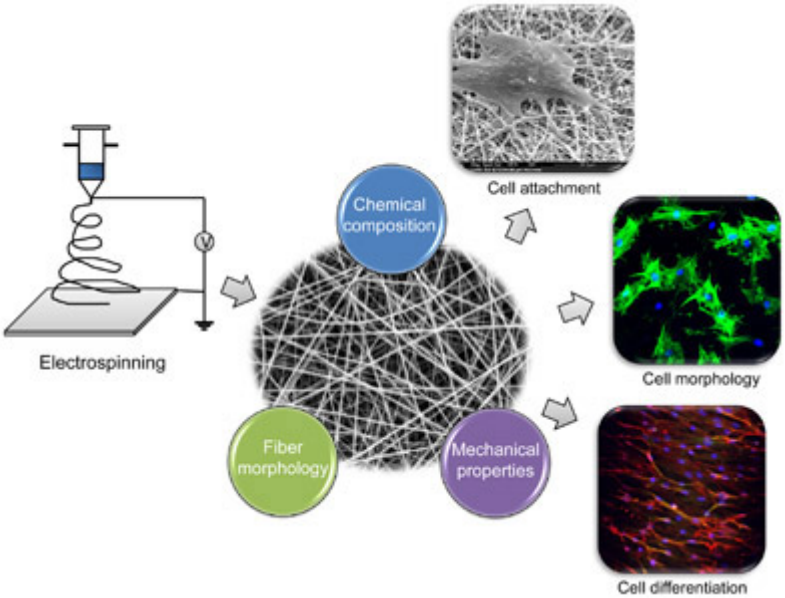

Fig. 2.2 Properties of electrospun nanofibers (ex. chemical composition, fiber morphology and mechanical properties) can influence cellular behaviors (attachment, morphology and differentiation)[9].

Among many others, the porosity of the fiber mat is an important parameter to

control cell migration, cell morphology, cell proliferation as well as phenotypic expression [10-12]. An appropriate porosity of scaffold allows the diffusion of nutrients to the cells and waste product out of cells. The mechanical property of nanofiber, which can be controlled by changing the compositions of materials, also plays a critical role in cell morphology. It has been shown, for example, that the stiffness of scaffold influences cellular behaviors in 3D porous structures [13].

Furthermore, nanofibers can also be used for repairing damaged tissues, including sciatic nerve, heart, tendon, and blood vessel. Shin et al [14] fabricated poly(ε-caprolactone) (PCL) nanofiber scaffold and seeded with mesenchymal stem cells (MSCs), then implanted in the omenta of rats, and they found the nanofiber scaffold with cells maintained their original size and shape after 4 weeks. Nimet et al [15] applied PCL nanofiber mat into rat and found that the diameter of nanofiber significantly influenced the *in vivo* degradation. Manning et al [16] developed a heparin/fibrin-based delivery system (HBDS)/poly(lactic-co-glycolic acid) (PLGA) nanofiber scaffold with growth factor incorporated, and the *in vivo* studies in a large animal tendon model verified the potential of this scaffold for improving tendon healing (**Fig. 2.3**). The injuries recovery of both peripheral and central nervous systems can greatly benefit from the neural tissue engineering strategy with a scaffold or conduit to facilitate the regrowth of nerves [17]. The electrospun collagen nanofibers have been fabricated for skin wound healing, which showed an effective wound-healing accelerators in early-stage wound healing [18].

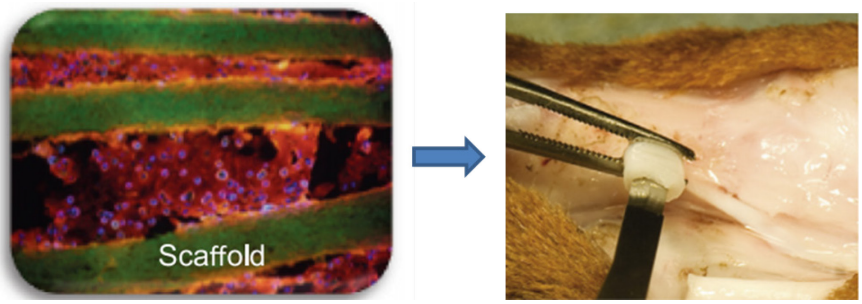

Fig. 2.3 HBDS/PLGA nanofiber scaffold with adipose-derived mesenchymal stem cells (ASC) cultured for in vivo implanting at the site of the flexor tendon for tendon healing. the PLGA was labelled with FITC (green), the HBDS was labeled with Alexa Fluor 546 (red) and the ASC nuclei were labeled with Hoechst 33258 (blue) [16].

Nevertheless, there are still important challenges to meet for real applications of electrospun nanofibers. Due to the relative poor mechanical properties, thin nanofiber scaffolds are general fragile and they have not enough strength for the further *in vitro* cell culture and *in vivo* implantation. This explains why the most of the developed nanofiber scaffolds so far were relatively thick with low porosity which inhibits cell penetration inside the fiber mats. In such a case, the permeability of the scaffold is also poor to prevent the efficient diffusion of nutrient. In this work, we propose a solution to this problem by electrospinning monolayer nanofiber on a stronger supporter (*see chapter 3*).

2.2 Hydrogel formation methods

Hydrogels could be classified into physical- or chemical-stimuli responsive hydrogels. The physical stimuli, includes temperature (such as agarose) and electric or magnetic fields, while chemical stimuli, includes pH, ionic factors (such as alginate) and chemical agents. Hydrogels can be either natural or synthetic [19]. Natural hydrogels are composed of either proteins, such as collagen and gelatin, or polysaccharides, such as alginate and agarose. The main advantages for these hydrogels are the low toxicity, good biocompatibility and biodegradability due to the similar chemical structure to the ECM. Synthetic polymers to form hydrogels are mainly based on chemical polymerization technique, which can control the structures and functions more precisely, such as PEG-based hydrogels made by photo-initiation polymerization [20, 21].

PEG hydrogels are attractive as scaffolds, because not only they can provide 3D environment for tissue, but also the macroscopic physical and microscopic chemical structures of them can be easily tailored and modulated by precise lithography related techniques and chemical synthesis control, respectively. Besides, it is also very simple to modify them to be biodegradable by incorporation of degradable segments or copolymerization with other polymers or biomolecular. The synthesis of PEG-based hydrogels through photo-polymerization is the most common method to convert PEG prepolymer solution into crosslinked insoluble hydrogels, which allows the synthesis of hydrogel scaffolds with spatial and temporal control [22]. The most widely used polymers for photo-polymerization include poly (ethylene glycol)

diacrylates (PEGDA) and poly (ethylene glycol) dimethacrylate (PEGDMA). So far, PEGDA has been widely applied in cell encapsulating [23, 24], cartilage tissue regeneration [25], tissue resurfacing [26] and wound healing [27]. Koh et al [28] presented an easy and effective method for the encapsulation of cells inside PEG-based hydrogel microstructures fabricated using photolithography. Temenoff et al [29] found that changing the molecular weight of PEG in synthesis affected the final tensile and swelling properties of oligo (poly (ethylene glycol) fumarate) hydrogels while the presence of interface did not have a significant effect. **Fig. 2.4** shows PEGDA macroporous scaffold for osteochondral defect regeneration. Besides, these PEG-based hydrogels are inherently resistant to non-specific cell adhesion and protein adsorption, thus they have also been reported a lot for the application in anti-fouling coating and anti-cell adhesive cell spheroids formation [30, 31].

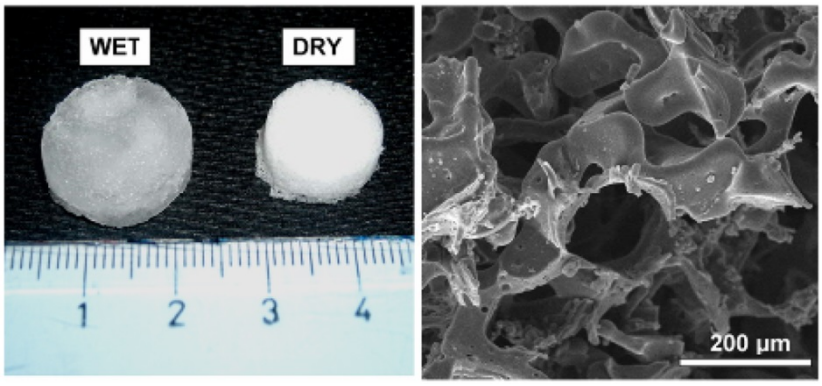

Fig. 2.4 Macroporous scaffolds of poly(ethylene glycol) diacrylate (PEGDA) with high swelling properties for osteochondral defect [32].

2.3 Lithography techniques

Micro- and nanofabrication is utilized to produce micro and nanostructures or features of the sizes in micrometer or nanometer range. It is essential for modern science and technology development. Historically, microfabrication techniques were firstly developed for the semiconductor productions to make devices on various substrates such as silicon wafer, glass, plastic or other types of material. However in present, the conception of miniaturization and integration has been widely applied to other areas, such as physics, chemistry, life science, material science, computer

science, ultra-precision engineering, and equipment design. In this thesis work, we are particular interested in their applications in biological research [33-35].

Among different techniques of microfabrication, lithography is a common patterning method which can also be applied to fabricate micro-topography and microstructures for cell biological research. However, traditional photolithography methods alone can only generate photoresist patterns on a substrate. It is necessary to use pattern transfer techniques to transfer photoresist patterns onto other substrates and materials, such as wet and dry etching, selective deposition and lift-off. More recently, soft lithography has been widely used to produce topographic and chemical patterns on a substrate for cell biological studies. The most commonly used soft lithography techniques include microfluidic patterning, stencil-assisted patterning and micro-contact printing [36].

2.3.1 UV photolithography

Photolithography is a technique to transfer a predesigned pattern on a photomask onto a substrate pre-coated with photoresist involving shining UV light. A main advantage of photolithography is that it can used to fabricate multiple structures at once (i.e. in parallel), producing very complex patterns in relative short time. The schematic of traditional photolithography by using photoresist is shown as **Fig. 2.5**.

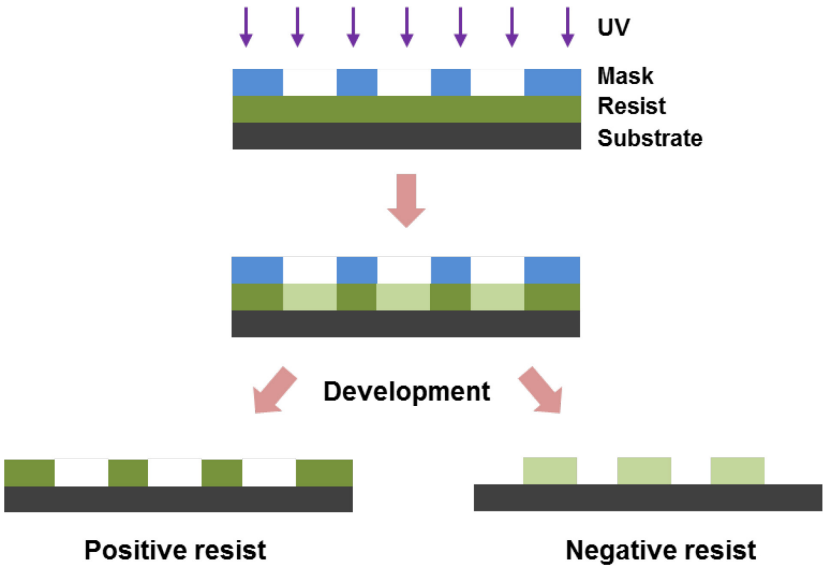

Fig. 2.5 Schematic diagram of conventional photolithography methods (Positive and negative photoresists)

The basic process for UV lithography includes mask preparation, substrate cleaning, photoresist coating, baking, alignment, UV exposure and developing.

Before coating the wafers, the cleaning process should be carried out as following:

For Glass substrate:

- Acetone + Ultrasonic 5 min
- Isopropanol + Ultrasonic 5 min
- Plasma O_2 5 min
- Bake on hotplate (200℃ for 5 min)

For Si wafer substrate:

- Piranha Clean (1:1 96% H_2SO_4 : 30% H_2O_2) : 10~20 min.
- DI water rinse: 15 min (3 baths 5 min each one)
- Sample dry: N2 gun or reactive ion etching (RIE)
- Bake on hotplate (200℃ for 5 min)

After the cleaning process, the photoresist can be spin coated. A certain thickness of liquid photoresist layer is spin-coated on a clean substrate, such as Si wafer and glass. The thickness of resist is controlled by the spinning speed. After coating, a soft bake with certain temperature is processed to remove the solvent in the resist and enhance the adhesion between resist and wafer. After cooling down to room temperature, the substrate is exposed to a UV light with the photomask closely contacting to the resist layer. And the distance between photomask and resist affect the final pattern resolution greatly. The more closely adhesion between resist and mask, the higher resolution will be obtained. During the UV exposure, some chemical reactions occur in the photoresist under the transparent part of mask. For the positive resist, the UV light let the bonds of long chain polymers of the resist broken and become short polymer chains, which will be easily solved and taken away in development process; while in contrast, for negative resists, UV light results in a crosslinking reaction of the resist polymers, which let the resist less soluble while the unexposed resist will be removed by the developer. Notably, for all the negative resist, a post-baking process is needed after UV exposure to further activate cross-linking.

a) Mask design and fabrication

Basically, the masks for UV photolithography include two kinds: optical mask and transparency mask, shown as **Fig. 2.6**. The optical mask is made of a thin layer of chromium on glass or quartz and a high resolution of UV light can be obtained (~1 μm), while transparency mask made of a plastic transparency film with black ink patterns, which can be produced easily by a printer, can reach a relative low resolution (>20 μm).

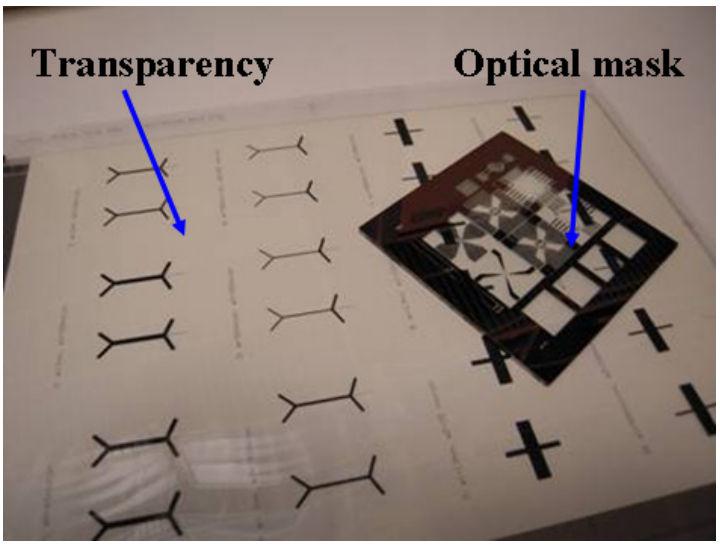

Fig. 2.6 Illustration of transparency mask and standard optical mask

In this work, all the masks are designed by a photolithographic mask design software L-Edit (Tanner research, USA). Then photo masks with micro patterns can be produced by a focused laser beam generator with high precision X-Y stage. In our lab, we use micro pattern generator machine μPG 101 (Heidelberg Instruments) by direct laser writing to fabricate photo masks (**Fig. 2.7**). In brief, the designed pattern is inputted into the machine by μPG 101 software and written onto a commercial blank optical mask, which is a quartz plate coated with 1000 Å thick chrome and a 1 μm layer of AZ1518 positive photoresist on top (Nanofilm, CIPEC Company). The designed pattern can be exposed on the substrate by a laser beam travelling over the surface of substrate. A minimum feature size can reach to 1 μm with an accuracy of 0.1 μm. After the laser exposure, the exposed substrate was developed by immersion into AZ-726 MIF developer (Micro Chemicals) for around 30 s with gentle agitation,

following with DI water rinsing to remove the residual developer. Then the mask was treated with a wet etching process about 45s with gentle agitated Chrome-Etch 3144 (Honeywell) to remove the exposed chrome layer, followed with thorough DI water rinsing. Finally, the remained AZ1518 resist can be removed with a short time acetone ultrasonic bath to obtain a photomask with the designed chrome pattern on top.

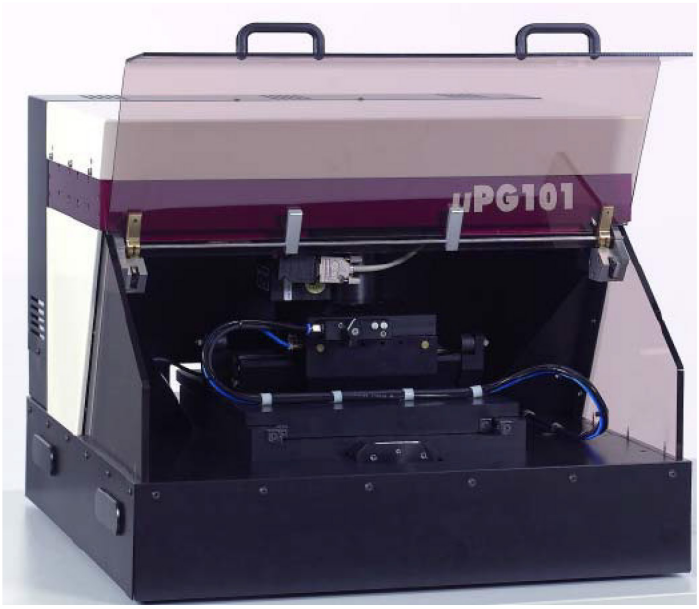

Fig. 2.7 µPG 101 direct laser writer (Heidelberg Instruments) [37].

b) Photoresist

Photoresist is a UV light sensitive material, which is composed of basic materials, UV sensitive initiator and solvent [38]. In this thesis, both positive photoresist (AZ series) and negative photoresist (SU-8 series) were used for either filter or microfluidic fabrications.

AZ40XT photoresist (**Fig. 2.8a**) is a new developed AZ series resist, which a chemically amplified ultra-thick positive resist. The field of application of the AZ 40XT starts at 15-30 µm, where litho-processes with conventional positive resists become very time-consuming due to increasing delays for rehydration of N2-outgassing, both not required for the AZ 40XT. Via single coating, 100 µm resist film thickness can be obtained. Even for very high resist film thicknesses, AZ 40 XT requires only short soft bake times, no delay for rehydration, very small exposure

doses due to its chemical amplification, and shows a high development rate. Therefore, processing of the AZ 40XT goes much faster as compared to conventional thick resists. Compared to most other positive resist, a post exposure bake is obligatory for AZ 40XT to finalize photoreaction and make it developable [39].

The SU-8 series photoresists (**Fig. 2.8b**) are the main negative photoresists, which consists of chemically amplified, epoxy based negative resists that are highly functional, optically transparent and photo imaginable to near UV (365nm) radiation. SU8 resist is a polymer with large distribution of viscosity that can be spun or spread over a thickness ranging from <1 micrometer up to > 300 micrometers. Cured films or microstructures are very resistant to solvents, acids and bases and have excellent thermal and mechanical stability.

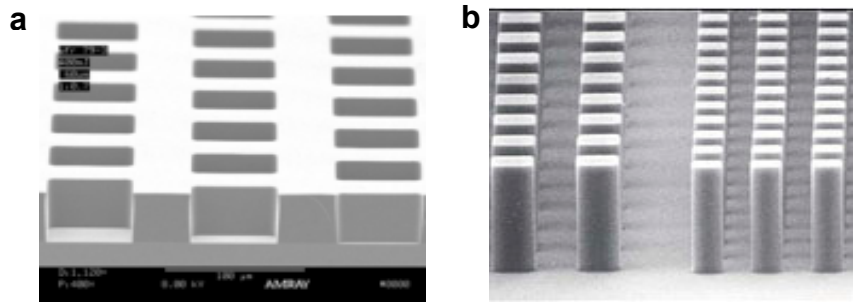

Fig. 2.8 Microtructures generated by photoresist. (a) 60 μm features in AZ 40XT with 40μm thickness; (b) 10μm features in SU-8 2000 with 50μm thickness [39, 40].

2.3.2 Soft lithography

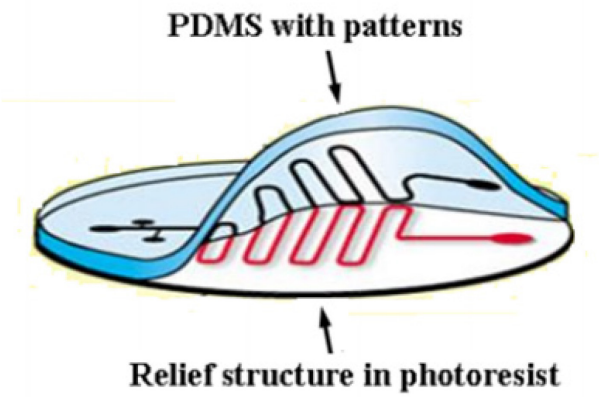

Fig. 2.9 Schematic of soft lithography.

Soft lithography is generally a series of techniques for replicating patterns or structures with "elastomeric stamps, molds, and conformable photomasks" [41]. The features of construct are from nanometer to micrometer scale [42]. The process of soft lithography consists of elastic stamp creating, to transfer the patterns onto glass, silicon or polymer surfaces, shown as **Fig. 2.9**. The most notable material for soft lithography is polydimethylsiloxane (PDMS), which is also the most widely used material and proved to be an efficient and economic method for nano- and micro fabrication [43-48]. Also other elastomers such as polyimides, polyurethanes, and cross-linked Novolac™ resins were used in soft lithography [49].

PDMS is a polymer belonging to polysiloxanes family, which can be characterized by silicon backbone and oxygen atoms [50]. PDMS has outstanding physical properties and chemical stability in wide range of environments. It also has optical transparence about ~300 nm and thermal stability to 150 °C. Especially the low surface energy (21.6×10^{-3} J m^{-2}) of PDMS allows easy release from templates and surfaces [51]. The most widely used two commercial PDMS products for soft lithography are Sylgard 184 from Dow Corning and RTV 615 from GE Toshiba Silicones Co., Ltd. In my thesis, all PDMS is RTV 615, which contains two components: part A and part B (curing agent). The normal ratio of A and B is 10:1 (w/w) and after mixing completely, cured PDMS can be obtained after two hours at 80°C. **Fig. 2.10** shows the schematic of PDMS crosslinking.

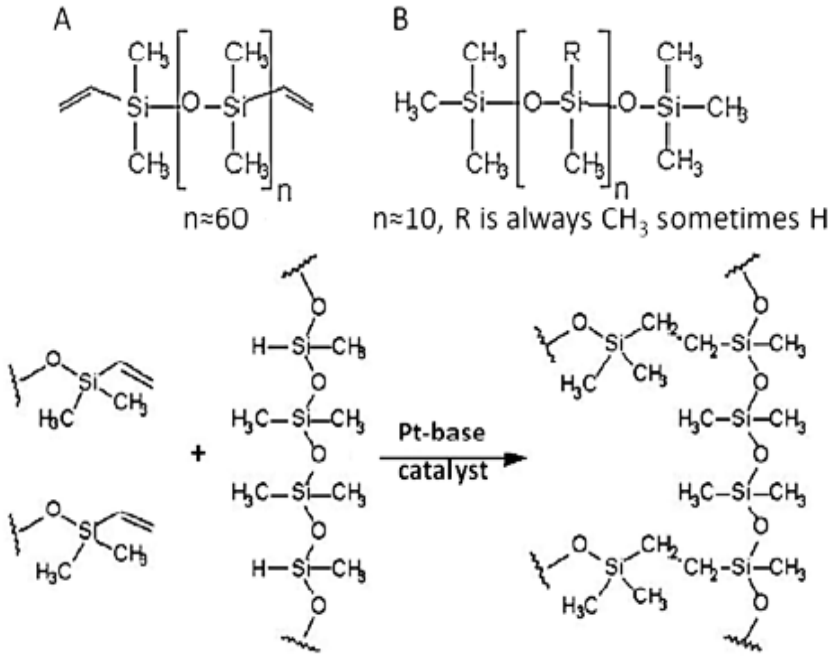

Fig. 2.10 Schematic of PDMS crosslinking [52].

Basically, the PDMS stamp is replicated from a master, which is normally fabricated by photolithography, as well as electron beam and focused ion beam lithography. Although PDMS is safe, it's still a sticky and messy polymer. So it's necessary to wear disposable gloves during working with PDMS. The PDMS mixture of part A and B should be stirred for at least 3 minutes for even mixing. Then the premixed PDMS prepolymer solution is casted on the top of the mold. However this stirring process will cause many air bubbles inside PDMS solution and these bubbles have to be removed before curing. To degas the PDMS, we transfer the PDMS mixture into a vacuum chamber (**Fig. 2.11**). The vacuum will lead the bubbles to expand and rise to the surface of mixture. The degas time is normally depended on the amount of PDMS mixture. After degassing, we can remove it from the vacuum chamber and pouring the PDMS mixture onto from the edge of the master and as low as possible to prevent to create new air bubbles. The PDMS will flow to a uniform height over the mold eventually. Some air bubbles will form again on the surface of the master, especially the area near the turns of the channels. And after about 10 minutes, these small bubbles will float up to the surface, but which will usually burst during the curing process and will not affect the final performance of device.

Fig. 2.11 Photograph of PDMS degassing vacuum chamber in ENS lab.

Then the PDMS mixture and master can be placed in an 80℃ oven for curing to harden. The curing time should be normally at least 2 hours. After curing, the solid PDMS mold can be taken out from the oven and wait for several minutes for cooling

to room temperature, which makes it easier to be peeled off. Then, the solid PDMS with the desired patterns can be peeled away gently and cut carefully with a knife.

However, sometimes especially for the small size patterns, a release agent deposition process generally based on silanization mechanism (**Fig. 2.12**) is necessary for the master to peel PDMS mold off more easily. In my thesis work, we used trichloromethylesilane (TMCS) for surface anti-sticking treatment. The master or mold was evaporated in TMCS vapor for 1~3 min.

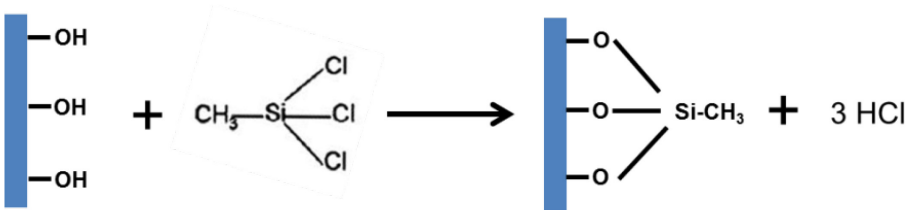

Fig. 2.12 Silanization mechanism of surface treatment with TMCS.

2.4 Microfluidic device fabrication

With advances in microfabrication, microfluidic devices can be easily manufactured which revolutionize both personalized healthcare medicine through point-of-care diagnostics or high-throughput drug discovery.

Among all the polymers used for microfluidic devices fabrication, PDMS is the most popular material. PDMS microfluidic devices can be fabricated by soft lithography, which is also the main technique for rapid prototyping of microfluidic devices [53, 54]. The physical and chemical properties of PDMS are contributory to achieve patterns and structures with high-quality. Clean room facilities are necessary to fabricate features in the size range of 1 to 500 μm typically, which is relevant to microfluidic systems.

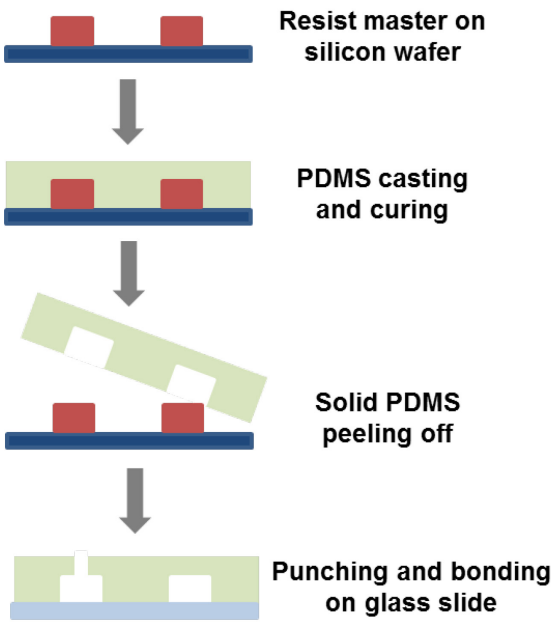

Fig. 2.13 Schematic of PDMS microfluidic chip fabrication.

Fig. 2.13 shows the general process of microfluidic device fabrication. After peeling off from the master or mold, solidified PDMS layer with patterns can be cut into proper size, and the holes with certain sizes for the channels can be punched with biopsy punch. To ensure a good bonding effect and prevent small particles from clogging the channels, the glass slides should be cleaned carefully before bonding. Wearing gloves is necessary throughout the cleaning process to avoid skin oils to stick onto the surface of slide. The surface should be first rinsed with distilled water and then rinsed again with isopropanol. Afterwards a nitrogen gun is used to dry off the residual isopropanol. Then the PDMS and glass slide are treated with low temperature oxygen plasma (**Fig. 2.14**). Inside the plasma machine, the bonding surfaces of the slide and the PDMS device are subjected to high energy plasma which strips away electrons on the surface to transform the surfaces into hydrophilic. Once contact the two surfaces to each other, a strong bond will be generated. Finally half an hour baking in an 80°C oven can enhance and stabilize the bonding.

Fig. 2.14 Photo of plasma cleaner in ENS lab.

2.5 Conclusion

We presented the micro and nanofabrication techniques used in this work. We have chosen hydrogel formation and nanofiber electrospinning techniques for the fabrication of scaffolds because of the biomimetic properties of two candidates. Lithography based fabrication techniques have been chosen for the device fabrication, including conventional UV photolithography and soft lithography. We believe that these fabrication techniques are essentials and compatible to the most of biological studies. We will provide in the following chapters a few examples of their application in the studies of stem cells and cancer cells.

Reference

[1] Reneker DH, Chun I. Nanometre diameter fibres of polymer, produced by electrospinning. Nanotechnology. 1996;7:216.

[2] Frenot A, Chronakis IS. Polymer nanofibers assembled by electrospinning. Current opinion in colloid & interface science. 2003;8:64-75.

[3] Schiffman JD, Schauer CL. A review: electrospinning of biopolymer nanofibers and their applications. Polymer Reviews. 2008;48:317-52.

[4] Huang Z-M, Zhang Y-Z, Kotaki M, Ramakrishna S. A review on polymer nanofibers by electrospinning and their applications in nanocomposites. Composites science and technology. 2003;63:2223-53.

[5] Pham QP, Sharma U, Mikos AG. Electrospinning of polymeric nanofibers for tissue engineering applications: a review. Tissue engineering. 2006;12:1197-211.

[6] Yoo HS, Kim TG, Park TG. Surface-functionalized electrospun nanofibers for tissue engineering and drug delivery. Advanced drug delivery reviews. 2009;61:1033-42.

[7] Luong ND, Moon I-S, Lee DS, Lee Y-K, Nam J-D. Surface modification of poly (l-lactide) electrospun fibers with nanocrystal hydroxyapatite for engineered scaffold applications. Materials Science and Engineering: C. 2008;28:1242-9.

[8] Stendahl JC, Wang L-J, Chow LW, Kaufman DB, Stupp SI. Growth factor delivery from self-assembling nanofibers to facilitate islet transplantation. Transplantation. 2008;86:478.

[9] Kai D, Jin G, Prabhakaran MP, Ramakrishna S. Electrospun synthetic and natural nanofibers for regenerative medicine and stem cells. Biotechnology journal. 2013;8:59-72.

[10] Lowery JL, Datta N, Rutledge GC. Effect of fiber diameter, pore size and seeding method on growth of human dermal fibroblasts in electrospun poly (ε-caprolactone) fibrous mats. Biomaterials. 2010;31:491-504.

[11] Chen M, Patra PK, Warner SB, Bhowmick S. Role of fiber diameter in adhesion and proliferation of NIH 3T3 fibroblast on electrospun polycaprolactone scaffolds. Tissue Engineering. 2007;13:579-87.

[12] Badami AS, Kreke MR, Thompson MS, Riffle JS, Goldstein AS. Effect of fiber diameter on spreading, proliferation, and differentiation of osteoblastic cells on electrospun poly (lactic acid) substrates. Biomaterials. 2006;27:596-606.

[13] Nam J, Johnson J, Lannutti JJ, Agarwal S. Modulation of embryonic mesenchymal progenitor cell differentiation via control over pure mechanical modulus in electrospun nanofibers. Acta biomaterialia. 2011;7:1516-24.

[14] Shin M, Yoshimoto H, Vacanti JP. In vivo bone tissue engineering using mesenchymal stem cells on a novel electrospun nanofibrous scaffold. Tissue engineering. 2004;10:33-41.

[15] Bölgen N, Menceloğlu YZ, Acatay K, Vargel I, Pişkin E. In vitro and in vivo degradation of non-woven materials made of poly (ε-caprolactone) nanofibers prepared by electrospinning under different conditions. Journal of Biomaterials Science, Polymer Edition. 2005;16:1537-55.

[16] Manning C, Schwartz A, Liu W, Xie J, Havlioglu N, Sakiyama-Elbert S, et al. Controlled delivery of mesenchymal stem cells and growth factors using a nanofiber scaffold for tendon repair. Acta biomaterialia. 2013;9:6905-14.

[17] Schmidt CE, Leach JB. Neural tissue engineering: strategies for repair and regeneration. Annual review of biomedical engineering. 2003;5:293-347.

[18] Rho KS, Jeong L, Lee G, Seo B-M, Park YJ, Hong S-D, et al. Electrospinning of collagen nanofibers: effects on the behavior of normal human keratinocytes and early-stage wound healing. Biomaterials. 2006;27:1452-61.

[19] Lee KY, Mooney DJ. Hydrogels for tissue engineering. Chemical reviews. 2001;101:1869-80.

[20] Fairbanks BD, Schwartz MP, Bowman CN, Anseth KS. Photoinitiated polymerization of PEG-diacrylate with lithium phenyl-2,4,6-trimethylbenzoylphosphinate: polymerization rate and cytocompatibility. Biomaterials. 2009;30:6702-7.

[21] Cuchiara MP, Allen AC, Chen TM, Miller JS, West JL. Multilayer microfluidic PEGDA hydrogels. Biomaterials. 2010;31:5491-7.

[22] Ergenç TI, Kizilel S. Recent advances in the modeling of PEG hydrogel membranes for biomedical applications: INTECH Open Access Publisher; 2011.

[23] Starly B, Chang R, Sun W. UV-Photolithography fabrication of poly-ethylene glycol hydrogels encapsulated with hepatocytes. Proceedings of the 17th Annual Solid Freeform Fabrication Symposium, University of Texas at Austin2006. p. 102-10.

[24] Liu VA, Bhatia SN. Three-dimensional photopatterning of hydrogels containing living cells. Biomedical microdevices. 2002;4:257-66.

[25] Musumeci G, Loreto C, Castorina S, Imbesi R, Leonardi R, Castrogiovanni P. New perspectives in the treatment of cartilage damage. Poly (ethylene glycol) diacrylate (PEGDA) scaffold. A review. Italian Journal of Anatomy and Embryology. 2013;118:204-10.

[26] Hern DL, Hubbell JA. Incorporation of adhesion peptides into nonadhesive hydrogels useful for tissue resurfacing. Journal of biomedical materials research. 1998;39:266-76.

[27] Liu SQ, Ee PLR, Ke CY, Hedrick JL, Yang YY. Biodegradable poly (ethylene glycol)–peptide hydrogels with well-defined structure and properties for cell delivery. Biomaterials. 2009;30:1453-61.

[28] Koh W-G, Revzin A, Pishko MV. Poly (ethylene glycol) hydrogel microstructures encapsulating living cells. Langmuir. 2002;18:2459-62.

[29] Temenoff JS, Athanasiou KA, Lebaron RG, Mikos AG. Effect of poly (ethylene glycol) molecular weight on tensile and swelling properties of oligo (poly (ethylene glycol) fumarate) hydrogels for cartilage tissue engineering. Journal of biomedical materials research. 2002;59:429-37.

[30] Ju H, McCloskey BD, Sagle AC, Kusuma VA, Freeman BD. Preparation and characterization of crosslinked poly (ethylene glycol) diacrylate hydrogels as fouling-resistant membrane coating materials. Journal of Membrane Science. 2009;330:180-8.

[31] Karp JM, Yeh J, Eng G, Fukuda J, Blumling J, Suh KY, et al. Controlling size, shape and homogeneity of embryoid bodies using poly(ethylene glycol) microwells. Lab on a chip. 2007;7:786-94.

[32] Guarino V, Gloria A, Raucci MG, Ambrosio L. Hydrogel-based platforms for the regeneration of osteochondral tissue and intervertebral disc. Polymers. 2012;4:1590-612.

[33] Hill TL. Effect of rotation on the diffusion-controlled rate of ligand-protein association. Proceedings of the National Academy of Sciences. 1975;72:4918-22.

[34] Bég OA, Makinde O. Viscoelastic flow and species transfer in a Darcian high-permeability channel. Journal of Petroleum Science and Engineering. 2011;76:93-9.

[35] Nitsche JM, Frasch HF. Dynamics of diffusion with reversible binding in microscopically heterogeneous membranes: General theory and applications to dermal penetration. Chemical Engineering Science. 2011;66:2019-41.

[36] Verhulsel M, Vignes M, Descroix S, Malaquin L, Vignjevic DM, Viovy JL. A review of microfabrication and hydrogel engineering for micro-organs on chips. Biomaterials. 2014;35:1816-32.

[37] http://www.himt.de/.

[38] Madou MJ. Fundamentals of microfabrication: the science of miniaturization: CRC press; 2002.

[39] http://www.microchemicals.com/products/photoresists/az_40xt.html.

[40] http://www.microchem.com/Prod-SU8_KMPR.htm.

[41] Xia YWGM. Soft lithography. Angew Chem Int Ed. 1998;37:550-75.

[42] Rogers JA, Nuzzo RG. Recent progress in soft lithography. Materials today. 2005;8:50-6.

[43] Bessueille F, Pla-Roca M, Mills CA, Martinez E, Samitier J, Errachid A. Submerged microcontact printing (SμCP): An unconventional printing technique of thiols using high aspect ratio, elastomeric stamps. Langmuir. 2005;21:12060-3.

[44] Sadhu VB, Perl A, Péter M, Rozkiewicz DI, Engbers G, Ravoo BJ, et al. Surface modification of elastomeric stamps for microcontact printing of polar inks. Langmuir. 2007;23:6850-5.

[45] Lalo Hln, Vieu C. Nanoscale Patterns of Dendrimers Obtained by Soft Lithography Using Elastomeric Stamps Spontaneously Structured by Plasma Treatment. Langmuir. 2009;25:7752-8.

[46] Kang SJ, Kim B, Kim KS, Zhao Y, Chen Z, Lee GH, et al. Inking Elastomeric Stamps with Micro‐Patterned, Single Layer Graphene to Create High‐Performance OFETs. Advanced Materials. 2011;23:3531-5.

[47] Xia Y, Whitesides GM. Soft lithography. Annual review of materials science. 1998;28:153-84.

[48] Plecis A, Chen Y. Fabrication of microfluidic devices based on glass–PDMS–glass technology. Microelectronic Engineering. 2007;84:1265-9.

[49] Kumar A, Whitesides GM. Features of gold having micrometer to centimeter dimensions can be formed through a combination of stamping with an elastomeric stamp and an alkanethiol ‘‘ink’’followed by chemical etching. Applied Physics Letters. 1993;63:2002-4.

[50] Chandrasekhar V. Polysiloxanes. Inorganic and Organometallic Polymers. 2005:209-48.

[51] Martos C, Rubio F, Rubio J, Oteo J. Surface energy of silica-TEOS-PDMS

ormosils. Journal of sol-gel science and technology. 2001;20:197-210.

[52] Esteves dA, Brokken-Zijp J, Laven J, Huinink H, Reuvers N, Van M, et al. Influence of cross-linker concentration on the cross-linking of PDMS and the network structures formed. Polymer. 2009;50:3955-66.

[53] Anderson JR, Chiu DT, Wu H, Schueller O, Whitesides GM. Fabrication of microfluidic systems in poly (dimethylsiloxane). Electrophoresis. 2000;21:27-40.

[54] Whitesides GM, Ostuni E, Takayama S, Jiang X, Ingber DE. Soft lithography in biology and biochemistry. Annual review of biomedical engineering. 2001;3:335-73.

Chapter 3

Culture and differentiation of pluripotent stem cells

In this chapter, we present a study of culture and differentiation of induced pluripotent stem cells by using culture patch method. We first describe the fabrication of the culture patch which consists of a monolayer of crosslinked gelatin nanofibers formed on a honeycomb frame made of biocompatible polymer. Then, we present the results of cell proliferation on culture patch under off-ground culture condition. Next, we show how human pluripotent stem cells (hiPSCs) can be differentiated into cardiomyocytes and neurons on the culture patch under off-ground culture conditions and how this method is advantageous comparing to the conventional culture dish method.

3.1 Introduction

A major challenge of cell culture is to find suitable substrates with appropriate stiffness, surface morphology and adhesion molecules for down-regulation of cell-matrix tractions. This is particularly important for the cell fate regulation of stem cells which depends critically on the cellular microenvironment. Previously, different culture protocols have been proposed for iPSC culture but few of them were designed to mimic the in vivo organization of extracellular matrix (ECM) proteins and the in vivo hydrodynamic of nutrient and cellular factors. Besides, the stem cells have to be derived to the targeting cells at high purity, high efficiency and yield, high purity. Since these targeting cells are tissue specific, they have to be differentiated on different types of substrates and under different physiological conditions. It is therefore a real challenge to develop a general culture perform for culture and differentiation of iPSCs.

By considering the high potential of iPSCs derived tissues for regenerative medicine [1], we put forward the importance of patch form as a general culture platform. It has recently been demonstrated that cells placed on a gel layer could give a therapy efficacy significantly better than that without a material support. After cell seeding and cultivation, the culture patch can be transformed to functioning cell patch which can be used not only for therapy but also for different types of cell-based assays such as toxicity test and drug screening. In addition, the cell patches of different types of cells derived from iPSCs may be integrated into a microfluidic device, thereby allowing easy control of more realistic physiological

conditions to mimic the *in vivo* body circuitries [2]. Thus the culture patch method should open a new perspective for different types of *in vitro* and *in vivo* assays in advanced biomedical research and drug development.

As example, we designed a culture patch in form of crosslinked monolayer nanofibres supported by honeycomb frame. Biocompatible nanofibers are promising to mimic the *in vivo* organization of ECM proteins for a better understanding of cell-material interaction and prospective applications in regenerative medicine [3, 4]. Among many others, we have chosen to fabricate gelatin nanofibers by electrospinning [5]. Previously, gelatin nanofibrous substrates have been successfully used for cell culture and long term expansion of human pluripotent stem cells (hiPSCs) [6]. To further improve the culture performance, and by considering, in addition, the requests of versatility and flexibility for both *in vivo* and *in vitro* assays, we propose in this part a new type of substrate based on monolayer network of gelatin nanofibers bounded on patterned honeycomb frame of PEGDA for hiPSCs culture, which not only mimic the *in vivo* organization of the ECM but also take into account the hydrodynamic properties of the *in vivo* cellular microenvironments. Besides, this substrate allows off-ground culture with much enhanced permeability and much decreased exogenous contact of cells, due to the extremely high porosity of the patch and extremely low material inclusion. Since cardiac and neuron cells are the mostly important for drug screening and disease therapy, we are mainly interested in hiPSCs differentiation into cardiomyocytes and motor neurons in this work. And the differentiation difference between in off-ground environment and in conventional 2D culture environment is compared.

3.2 Fabrication of culture patch

This culture patch is made of crosslinked monolayer gelatin nanofibers, as shown as **Fig. 3.1**. The patch frame is a honeycomb shaped and highly porous membrane mounted on a ring of the same material for easy handling with sufficient mechanic stability. The crosslinked monolayer nanofibers can be produced by electrospinning while the honeycomb frame can be produced by soft-lithography, both relying batch processes for mass production. In the following, we will give the details of the fabrication process.

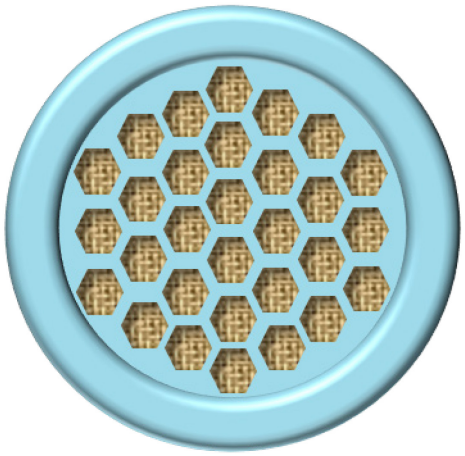

Fig. 3.1 Design of nanofiber patch composed of PEGDA honeycomb frame and monolayer gelatin nanofibers.

3.2.1 PEGDA honeycomb network fabrication

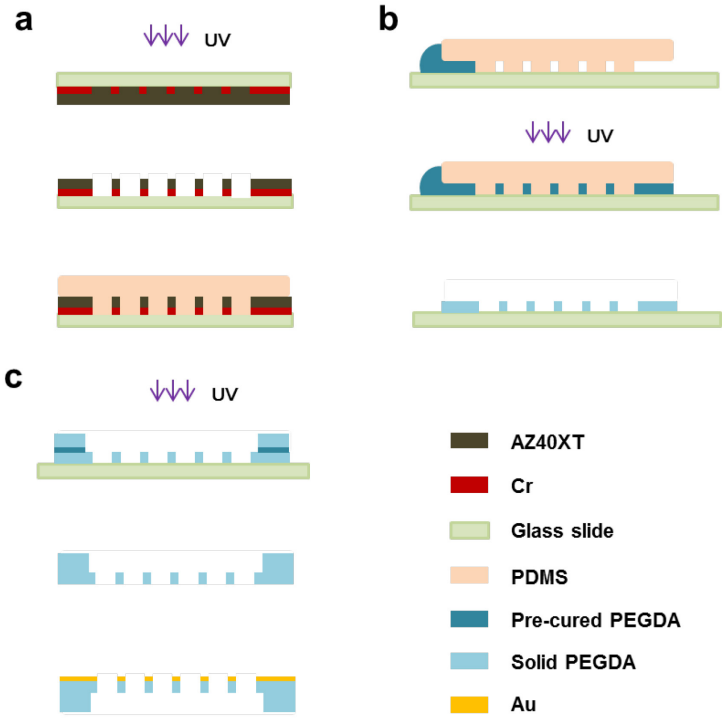

Fig. 3.2 Schematic of PEGDA honeycomb frame fabrication. (a) PDMS mold fabrication by lithography; (b) Aspiration-assisted PEGDA frame production; (c) PEGDA ring mounting and Au deposition.

The fabrication procedure of PEGDA honeycomb network is shown in **Fig. 3.2**.

It includes three steps:

a) PDMS mold fabrication

Chromium mask of honeycomb network arrays of 500 μm diameter and 50 μm width was produced by micro pattern generator (μPG 101, Heidelberg Instruments) with 60% 40mW energy, followed with resist developing (AZ726MIF, 1 min) and 45s chrome etching. After rinsing and removal of residual resist in acetone, a Cr mask with honeycomb pattern can be obtained.

Positive resist AZ40XT was used to generate the master mold by UV lithography. First, 50 μm AZ40XT resist layer was spin-coated on the mask at 500 rpm for 10s and then 1500 rpm for 20s. The resist was then prebaked following the sequence of 1 min at 65°C, 1 min at 95°C and 8 min at 126 °C. After cooled down to room temperature, the mask was backside exposed with UV light (365 nm wavelength and 9.1 mW/cm^2) for 90 s, following with a post-bake process (30 s at 65°C, 30 s at 95°C and 2 min at 105 °C). The mask was then developed in AZ319MIF for 2.5 min with mild agitation. After rinsing with DI water, the mask with patterned resist was dried with nitrogen gun, resulting in AZ40XT master mold.

Next, AZ40XT resist master was evaporated by TMCS for anti-sticking surface treatment for 1-3 min. A PDMS solution was prepared using GE RTV 615 PDMS components A and B at a ratio of 10:1 and then poured on the top of the resist master. After curing at 80°C for 2 h, the PDMS mold can be peeled off (shown as **Fig. 3.3**).

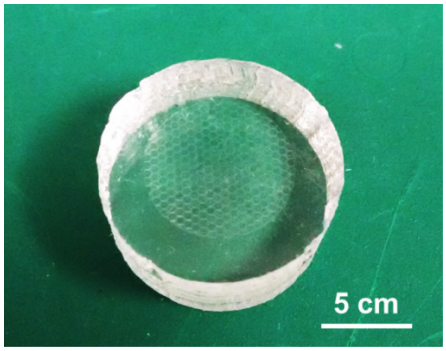

Fig. 3.3 Photograph of PDMS mold for honeycomb frame.

b) Aspiration-assisted PEGDA frame production

PEGDA honeycomb frame was fabricated with PDMS aspiration-assisted molding technique. In brief, the PDMS mold was first placed on a glass slide. Then, the PDMS-glass assembly was placed in a desiccator for degasing during 15 min. At the same time, a PEGDA pre-polymer solution mixed with 1 v/v% Irgacure 2959 as photo-initiator was prepared and used to fill the PDMS-glass cavity by degassing induced micro-aspiration. After the free space of PDMS-glass cavity was filled completely, it was exposed with UV light (365 nm wavelength) at 9.1 mW/cm^2 for 30s. Then the solidified PEGDA network was formed after peeling off PDMS mold.

c) PEGDA ring mounting and Au deposition

To increase the mechanical strength and convenience of handle, 100 μm thick PEGDA rings of 13 mm outer diameter and 9 mm inner diameter were prepared in a similar manner. Firstly, a Cr mask defining the ring geometry was generated with μPG 101 at 60 % 40 mW energy. After development and chrome etching, acetone was applied to remove the residual resist. Then a 100 μm thick SU8-3050 resist was spin-coated on a clean silicon wafer at 500 rpm 10 s and then 1000 rpm for 30s, and then soft-baked at 65 °C for 1 min and 95°C for 45 min. After cooling down to room temperature, the mask was exposed with UV light for 28s. The resist was then post baked at 65°C for 1 min and 95°C for 5 min. After development with SU8 developer and trimethylchlorosilane (TMCS) evaporation, the PDMS mold was produced by soft lithography and placed on a glass slide. Then, the PEGDA solution was injected into the mold and solidified by UV exposure for 30 s. Finally, the ring was mounted on PEGDA frame, using about 10 μl pre-cured PEGDA solution as binder for UV curing. Then the whole frame was immersed into isopropanol ultrasound bath for 10 min and then DI water ultrasound bath for 10 min to remove the residual unreacted PEGDA and photo-initiator. **Fig. 3.4** shows the photo of PEGDA honeycomb frame mounted with a ring.

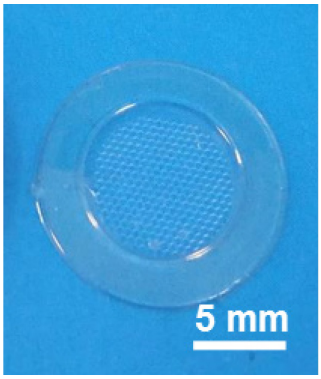

Fig. 3.4 Photograph of PEGDA honeycomb frame mounted with a ring.

Prior to electrospinning, the backside surface of PEGDA frame was deposited with 10 nm thick Au by sputter coater (K675X, EMITECH, Germany) at 25 mA current to obtain more uniform nanofiber layer and enhance the attachment of gelatin nanofiber and PEGDA frame .

3.2.2 Gelatin nanofiber electrospinning

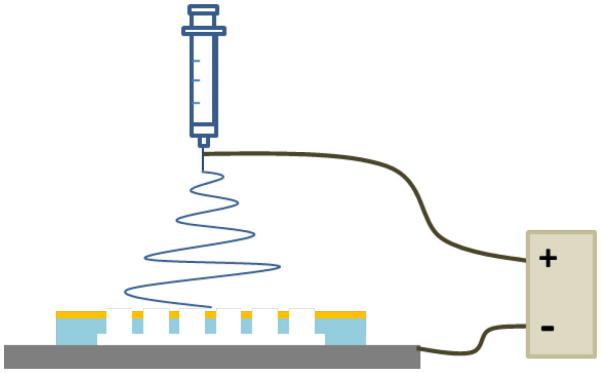

Fig. 3.5 Schematic of electrospinning on PEGDA frame.

The obtained PEGDA frame coated with Au was fixed on a silicon wafer for gelatin nanofiber electrospinning. First, the gelatin solution was prepared. 10 wt% gelatin powder (G2625, Sigma-Aldrich, France) was dissolved in the mixed solution of acetic acid, ethyl acetate and distilled water with a volume ratio of 21:14:10. Then a syringe with gelatin solution was mounted in a syringe pump (KD Scientific). The spinneret was connected to the anode of high potential power supply (TechDempaz, Japan) with bias voltage of 11 KV and the cathode was connected to the grounded silicon wafer. Then the PEGDA substrate with golden surface on top was fixed onto

the silicon wafer to collect nanofibers, shown as **Fig. 3.5**. The pump federate was fixed at 0.2 ml/h and the distance between spinneret tip and collected PEGDA substrate was 10 cm.

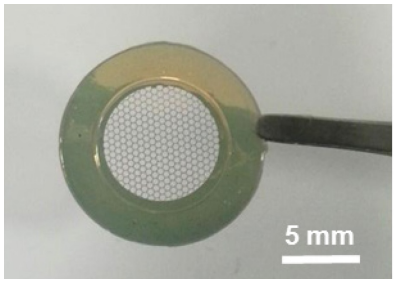

Fig. 3.6 PEGDA frame supported gelatin nanofiber net with a tweezer holding.

After electrospinning, gelatin nanofibers collected on PEGDA substrates were dried in vacuum overnight to evaporate the remaining solvent. Then crosslinking solution was prepared by dissolve 0.2M 1-ethyl-3-(3-dimethylaminopropyl) carbodiimide hydrochloride (EDC) and 0.2 M N-hydroxysuccinimide (NHS) in ethanol completely. The electrospun gelatin scaffolds were cross-linked in the crosslinking solution for 4 h. After crosslinking, samples were rinsed with ethanol three times and then dried in vacuum overnight to remove the remaining chemicals. **Fig. 3.6** shows the final PEGDA frame supported gelatin nanofiber net.

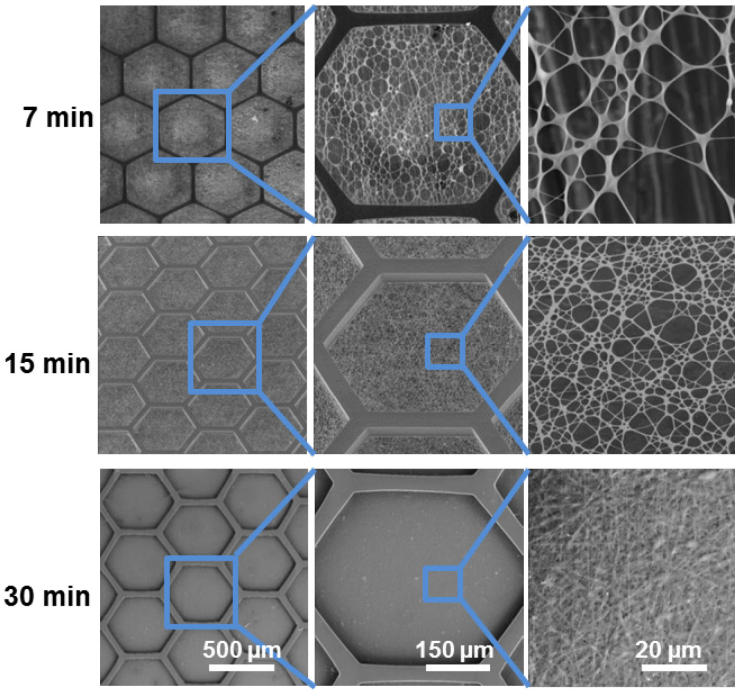

Fig. 3.7 SEM photographs of gelatin nanofiber at different electrospinning time.

To optimize the porosity and pore size of gelatin nanofiber, different electrospinning time was tested based on the other constant parameters. The morphology of fibers observed by SEM was shown as **Fig. 3.7**. For both 7 min and 15 min of spinning time, single layer nanofiber mat can be obtained. But when spinning time was 30 min or more, nanofiber mat becomes multilayers and there was almost no through hole among fibers. The size of pores and porosity of nanofiber mat were analyzed by imageJ from SEM photos, as shown in **Fig. 3.8**. The porosities for 7 min and 15 min of spinning time were 79.8±0.8% and 63.65±1.35%, respectively. Both of them are transparent enough for a final suspension culture system. But for 30 min of electrospinning, the porosity was difficult to measure by software since the multi-layer and the too small pores. The pores for 15 min spinning were mainly less than 5 μm^2 and almost no more than 20 μm^2, while for 7 min of spinning time, the area of most pores was from 0 to 20 μm^2, and some of them were even more than 100 μm^2, which was much larger than the size of cells.

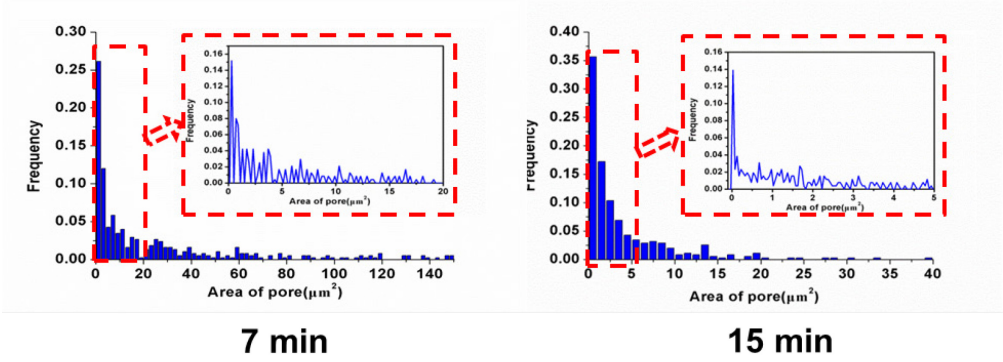

Fig. 3.8 Pore size distribution of gelatin nanofiber at different electrospinning time (7 min and 15 min).

To confirming this effect, the same number (2×10^5) of hiPSCs was seeded on the substrates with different density of fibers. After 24 hours, the adhesion and coverage of cells on gelatin fibers was shown as **Fig. 3.9**. For the nanofiber layers by electrospinning for 15 min and 30 min, adhesive cells almost covered the entire fibrous area with very slight difference between each other. However there were obvious much fewer cells attached on the nanofibers with 7 min electrospinning. Therefore considering both high permeability and enough support for cells, 15 min was chosen as the optimum electrospinning time for the next studies.

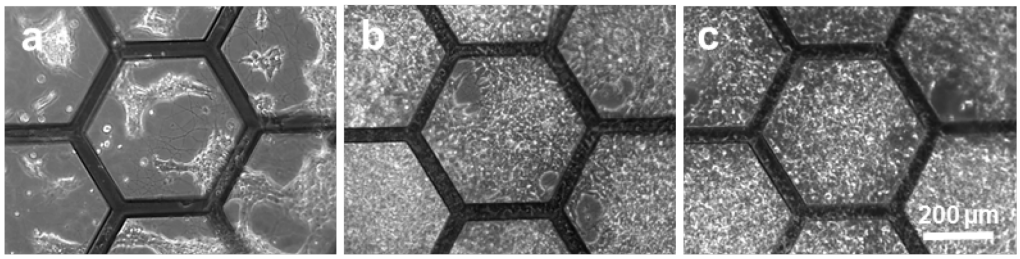

Fig. 3.9 Human iPSCs cultured on gelatin nanofiber substrate with different electrospinning time. (a: 7min; b: 15min; c: 30min)

3.3 Cell characterization methods

3.3.1 SEM observation

Cell samples were fixed in PBS containing 4% formaldehyde for 30 minutes. Then, they were rinsed twice with PBS buffer, and immersed in 30% ethanol (in DI water) for 30 min. Afterward, the samples were dehydrated in a graded series of ethanol solutions with concentrations of 50%, 70%, 80%, 90%, 95%, and 100%, respectively, and in each for 10 min then dried with a nitrogen gas flow. Before observation, a 2 nm thick gold layer was deposited on the samples by sputtering. The observation was performed with a SEM machine (Hitachi S-800) operated at 10 kV.

3.3.2 Immunocytochemistry

For the immunostaining of NIH-3T3 and Hela cells, after culture for 2 days, the cells on nanofiber patch were fixed with 4% paraformaldehyde (PFA) in PBS for 15 min. Then cells were washed with PBS three times. Afterward, cells were permeabilized with 0.5% Triton-X-100 for 10min. After washing with PBS for three times, cells were then blocked in 1% BSA solution for 30 min, followed with PBS washing for three times. Then the cytoskeleton and nuclear of cells were stained with Atto 488 Phalloidin (Sigma) and DAPI (Life technology) for 20 min, respectively. After washed with PBS for three times again, cells can be observed under an inverted optical microscope (Zeiss, Axiovert 200) equipped with a digital CCD camera (Evolution QEI).

For the immunostaining of iPSCs and differentiated cardiomyocytes and neurons, after rinsing with PBS to remove unattached cells, the cells were fixed with

4% paraformaldehyde (PFA) diluted in PBS for 15 min. Then cells were treated with 0.5% Triton X-100 in PBS at 4°C overnight (for antigens inside nuclear) or 10min at room temperature (for antigens outside nuclear) for permeabilization and then incubated in a blocking solution containing 5% v/v normal goat serum, 5% v/v normal donkey serum, 3% v/v bovine serum albumin, and 0.1% v/v Tween 20 in D-PBS overnight at 4 °C to block out non-specific bindings. Cells were then incubated with primary antibodies, i.e., anti-OCT4 (1:100 diluted, Santa Cruz), anti-NANOG (1:100 diluted, Santa Cruz), anti-α-Actinin (Sarcomeric) (1:500 diluted, Sigma), anti-Troponin T-C (1:200 diluted, Santa Cruz), anti-connexin 43 (1:100 diluted, Cell Signaling), anti-MYH6 (1:50 diluted, Santa Cruz), anti-Pax6 (1:100 diluted, Abcam), anti-Sox1 (1:100 diluted, Abcam), anti-Nestin (1:200 diluted, Sigma), anti-Olig2 (1:100 diluted, Abcam), anti-β tubulin III (1:400 diluted, Sigma) and anti-HB9 (1:100 diluted, Abcam) in blocking solution at 4°C overnight. After incubation with the primary antibody overnight at 4 °C, cells were incubated with the appropriate secondary antibody, i.e., Alexa Fluor 488 Donkey anti-rabbit IgG (1:300 diluted, Jackson ImmnoResearch) and Alexa Fluor 594 Donkey anti-mouse IgG (1:300 diluted, Jackson ImmnoResearch) in blocking buffer at room temperature for 1 h. Then, cells were incubated with 300 ng/ml 4'-6-diamidino-2-phenylindole (DAPI) for 30 min for nuclear staining, and finally washed three times with PBS. Then stained cells were observed with an inverted optical microscope (Zeiss, Axiovert 200) equipped with a digital CCD camera (Evolution QEI).

3.3.3 Live/dead assay

Cell viability was studied with live/dead assay. Briefly, cells on substrate were incubated with 2 μM of Calcein AM and 2 μM EthD-1 for live and dead cell staining, respectively. After 30 min incubation at 37°C and 5% CO_2, cells were analyzed with a fluorescence microscope, as described above.

3.3.4 Total RNA purification

Total RNAs from normal cultured hiPSCs, dome-like EBs, hiPSCs derived cardiomyocytes or derived neurons were harvested using the RNeasy Mini Kit (Qiagen, Valencia, CA) following the manufacturer's instructions. mRNA concentrations were measured in a NanoDrop1000 spectrophotometer (Thermo

Fisher).

3.3.5 Reverse transcription-polymerase chain reaction (RT-PCR)

A reaction mixture (25 μL) containing 5 units of Taq DNA polymerase (Takara, Japan), 1 μl cDNA and 0.2 μM PCR primers (shown in **Table 3.1**) in PCR buffer was subjected to amplification in a DNA thermal cycler (Applied Biosystems 7300 Real-Time PCR System). PCR was performed for 30~35 cycles (94 °C, 30 sec; 58 °C, 30 sec; 72 °C, 60 sec) with an initial incubation at 94 °C for 5 min and a final extension at 68°C for 3 min. Amplified products (10 μL) were resolved by 1.2% w/v agarose gel electrophoresis and visualized by ethidium bromide staining. RT-PCR results of glyceraldehyde-3-phosphate dehydrogenase (GAPDH) were used as control.

Table 3.1 Forward and reverse primer sequences used for PCR detection

Primers	Sequence
OCT4 forward	5′-GACAGGGGGAGGGGAGGAGCTAGG-3′
OCT4 reverse	5′-CTTCCCTCCAACCAGTTGCCCCAAAC-3′
NANOG forward	5′-CAGCCCCGATTCTTCCACCAGTCCC-3′
NANOG reverse	5′-CGGAAGATTCCCAGTCGGGTTCACC-3′
PAX6 forward	5′-ACCCATTATCCAGATGTGTTTGCCCGAG-3’
PAX6 reverse	5′- ATGGTGAAGCTGGGCATAGGCGGCAG-3′
BRACHYURY forward	5′-GCCCTCTCCCTCCCCTCCACGCACAG-3′
BRACHYURY reverse	5′-CGGCGCCGTTGCTCACAGACCACAGG-3′
AFP forward	5′-GAATGCTGCAAACTGACCACGCTGGAAC-3′
AFP reverse	5′-TGGCATTCAAGAGGGTTTTCAGTCTGGA-3′
Nestin forward	5’-ATCGCTCAGGTCCTGGAAGG-3’
Nestin reverse	5’-AAGCTGAGGGAAGTCTTGGAG-3’
Olig2 forward	5′-GGGCCACAAGTTAGTTGGAA-3′
Olig2 reverse	5′-GAGGAACGGCCACAGTTCTA-3′
GAPDH forward	5′-AACAGCCTCAAGATCATCAGC-3′
GAPDH reverse	5′-GGTCTCTCTCTTCCTCTTGTGC-3′

3.3.6 Quantitative RT-PCR (q-PCR)

Total RNA was reverse transcribed using the RT First Strand Kit (Qiagen). cDNA was amplified and quantified with Power SYBR Green PCR MasterMix (Life Technologies) and relative primers. Briefly, “hot start” PCRs were carried out with an initial incubation at 95 °C for 10 min, followed by 40 cycles of 95 °C for 15 s and

then 60 °C for 3 min using an Applied Biosystems 7300 Real-Time PCR system (Life Technologies). Data analysis was carried out using Cluster 3.0 in combination with the TreeView 1.1.5 open-source software.

Table 3.1 shows the forward and reverse primer sequences used for q-PCR. qBiomarker Validation PCR Array-Cardiomyocytes Differentiation Kit (Cat. No. 337231 IPHS-102A) was used for cardiomyocytes q-PCR test and gene expression heat map generation.

3.3.7 Flow cytometry

iPSCs differentiated cardiomyocytes on PEGDA supported nanofiber substrates and on glass slide were harvested with TrypLE Express for 5 min at 37°C. Then cells were washed twice with D-PBS and cell numbers were counted. For staining with FITC labeled cTnT antibody, cells were diluted to a final concentration of 1×10^7 cells mL^{-1} in PBS containing 2% fetal calf serum. Then cells were incubated in antibody solution at room temperature for 30 min. A specific isotype control was used as a negative control. After removing the antibodies by centrifugation at 1000 rpm for 5 min, cells were washed with D-PBS containing 2% fetal calf serum. Finally, cell suspensions were applied to a FACS Canto II flow cytometer (BD Biosciences).

3.4 Off-ground culture for enhanced cell proliferation

To demonstrate the advantages of this nanofiber substrate for cell processing, firstly two types of cells, fibroblast NIH-3T3 and cancer cell Hela were cultured on the substrate:

3.4.1 NIH-3T3 and Hela cells culture

Both NIH-3T3 and Hela cells were cultured with a culture medium composed of 89% Dulbecco's Modified Eagle Medium (DMEM), 10% Fetal Bovine Serum (FBS) and 1% penicillin/streptomycin at 37 °C with 5% CO_2 supplementation for 3~4 days until 80~90% confluence, respectively. Then they were dissociated with Trypsin at 37 °C for 5 min. After centrifugation at 1200 rpm for 5 min, cells were re-suspended

in fresh medium at desired density for seeding.

Before cell seeding, the gelatin nanofiber patch was sterilized under UV light for 15 min for both top and bottom surface. Then 50 μl medium containing 2×10^3 cells was added on the top of the substrate and in the center of PEGDA ring. After incubation at 37 °C for 1 h for cell adhesion, 2 ml more fresh medium was added around the patch gently. It's worth mentioning that the nanofiber patch can be suspended inside the medium, which results into an "off-ground" culture for the cells. And without any coating, both these two kind cells can attach on fiber within 2 h.

After two days culture, the cytoskeleton and nuclear of cells were stained. **Fig. 3.10** shows the immunofluorescence images of NIH-3T3 and Hela cells cultured on PEGDA-nanofiber substrate, in which cytoskeleton and nuclear were stained with Phalloidin (green) and DAPI (blue), respectively. And since PEGDA cannot absorb proteins, there is almost no cell attached on PEGDA frame, which demonstrated that cells can be patterned variably by easily changing the shape of PEGDA, on the PEGDA-nanofiber substrate.

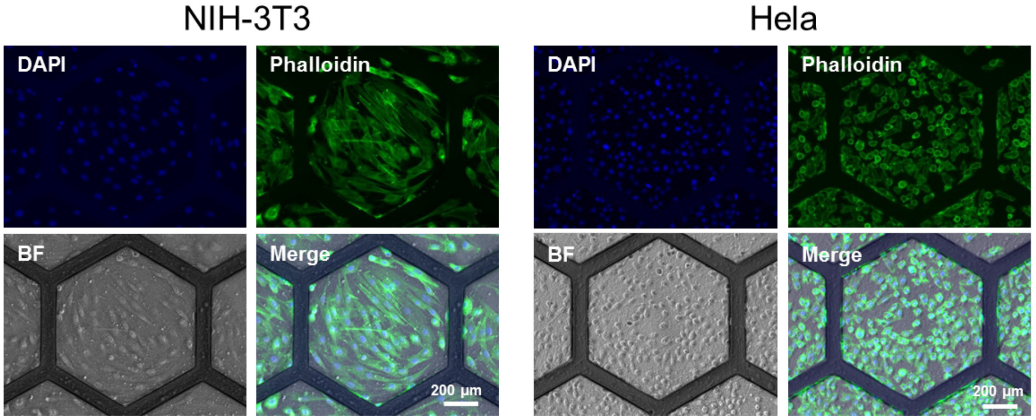

Fig. 3.10 Bright field and immunostaining fluorescence images of NIH-3T3 cells (left) and Hela cells (right) on gelatin nanofiber patch. Green: Phalloidin for cytoskeleton; Blue: DAPI for nuclear.

But comparing to the morphology of cells cultured in normal culture dish, cells on the nanofiber substrate can't elongate as much as in culture dish. Normally, hydrophilic substrate with high surface energy benefits more for the adhesion and spreading of cells. The isoelectric point of cells is around 3~4, which charged negatively in culture medium. Therefore, the absorption of cells increases on positively charged material surface. However the isoelectric point of gelatin is ~4,

negatively charged in medium, while nanofiber's ζ-potential changes little compared to the raw material [7], so gelatin nanofiber should be also negatively charged even if after crosslinking, which decreased the spreading of cells on our gelatin nanofiber substrate compared to positively charged culture dish.

3.4.2 Cell proliferation

Then we compared the population doubling time of NIH-3T3 on our substrate to on multi-well plate. 9 substrates were cultured with the same number of NIH-3T3 cells (2×10^3 cells). Then cells were digested off from one substrate after 24 h, 48 h and 72 h respectively. The number of cells was counted with a hemocytometer. The final data was obtained from the average result of three times repeating experiments (**Fig. 3.11**). The cell number on multi-well plate was counted 24 h similarly.

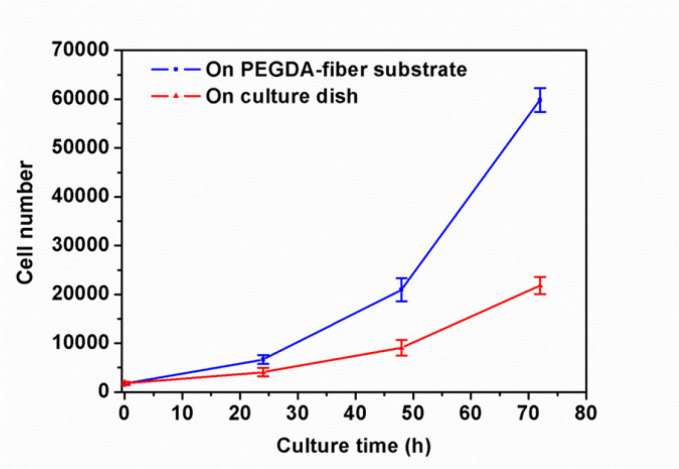

Fig. 3.11 NIH-3T3 cell number increase versus culture time on PEGDA-nanofiber substrate and normal multi-well plate, showing a significant cell proliferation rate difference between the two types of culture substrates.

After calculation, the doubling time of cells on substrate was 15.01 h, shorter than 19.79 h of normal culture, and the growth rates were 0.0462 and 0.035 for cells on substrate and culture plate respectively. It indicates that the proliferation rate of cells can be improved with this kind of off-ground culture substrate, which provides a three dimensional nutrition supply environment for cells, rather than only up-side nutrition supply in normal culture dish.

3.5 Cardiac patch differentiated from hiPSCs for drug test

It's reported that cardiovascular diseases (CVDs) are the main causes of death worldwide (more than 17.3 million deaths every year) [8]. Taking example of Europe, CVD causes over 4 million deaths and over 1.9 million deaths in the European Union (EU), which amount 47% of all deaths in Europe and 40% in the EU [9]. In America, CVDs are reported to be responsible for 800,000 deaths in 2011, which is even less than 600,000 deaths due to all cancers [10]. CVDs are various including stroke, hypertensive heart disease, rheumatic heart disease, cardiomyopathy, atrial fibrillation, congenital heart disease and so on [11]. And the principal reason for CVDs is that unlike other types of cells, cardiomyocytes have very little, or no proliferation ability, which making heart cannot heal itself when there is injury or disease. Thus, it makes the options for cardiac regeneration treatment very limited. Some drug therapies have been proposed to alleviate several factors related to the initial damages, however in fact none of them leads to cardiac repair. For heart transplant, extreme time consuming for waiting and pretty high cost make it not a possible therapy way for most patients.

Tissue engineering attracts much attention currently which serves a promising method for cardiac repair as well as regenerative medicine development. As an outstanding source, human iPSCs can be easily generated with patient-specific cells by reprogramming and differentiate into any cell types of three somatic germ layers including cardiomyocytes, serve as promising tools in disease modeling, cell therapy and regenerative medicine for cardiac disease therapies [12, 13].

A qualified cardiac patch should provide pure cardiac cells and also supply an extracellular matrix (ECM) with good biocompatibility and robust mechanical properties. Here the designed cell culture system with PEGDA as honeycomb frame and the gelatin nanofiber was used for cardiac differentiation from human iPSCs. Both PEGDA and gelatin nanofiber are biocompatible materials and the honeycomb structure of PEGDA has been proved to have a definite elasticity and has been applied to cardiomyocytes culture, which could supply not only strength support but also deformability along with cardiomyocytes contraction [20-22].

In this part, we present a method for generating cardiac patch on the designed gelatin nanofiber substrate. The process is including three steps, shown as **Fig. 3.12**. First, human iPSCs were cultured on the substrate and formed hemisphere

embryonic bodies (EBs) by changing ROCK inhibitor treatment time; Then cardiomyocytes were differentiated from hemisphere EBs directly on the substrate; Finally, by simply transferring the whole cell patch on MEA system, the effect of several cardiac drugs were tested.

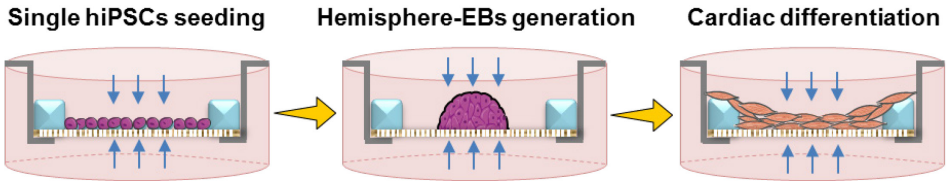

Fig. 3.12 Schematic of hiPSCs differentiation into cardiomyocytes.

3.5.1 Human iPSCs culture and hemisphere EBs generation

Human iPSCs (cell line 253G1 from Kyoto university and human episomal iPSC line from Life Technology) were cultured in complete E8 medium (Life Technology), on vitronectin (Life Technology, 1:100 diluted in DPBS) coated culture dish at 37°C with 5% CO_2 supplementation. The medium was changed every day until cells grow to 70% ~ 80% confluences. For iPSCs harvest, cells were cultured with 0.5 mM EDTA DPBS solution for 5 min at 37 °C.

PEGDA-gelatin substrate was coated with 1:500 vitronectin diluted in PBS solution at room temperature for 1h, then 2×10^5 iPSCs in 50 µl E8 medium with 10 µM Y-27632 was seeded on the substrate and then transferred into incubator. After 1 h incubation for cell adhesion, 2 ml fresh E8 medium with 10 µM Y-27632 were gently added in culture dish. Then cells can attach on nanofiber (coated with 1:500 diluted vitronectin) only inside the PEGDA frame because PEGDA is not protein absorbable. After culturing in the E8 medium with Y-27632 for 1~4 hours, the medium was changed with normal E8 medium without Y-27632. After several hours, inside each honeycomb-like frame, attached monolayer hiPSCs formed a dome-like hemisphere EB gradually, almost in the center of frame, as shown in **Fig. 3.13**.

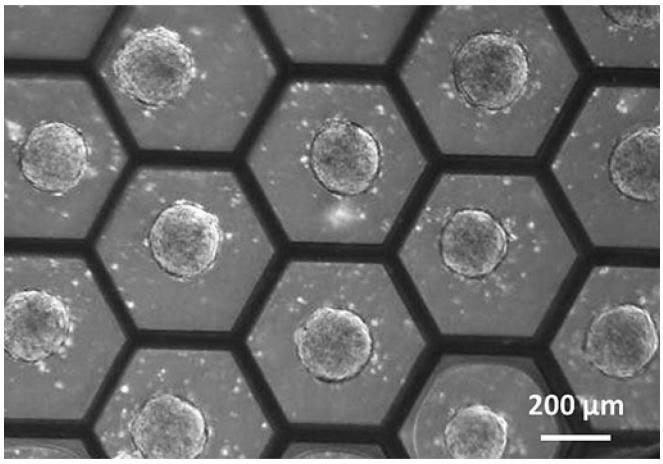

Fig. 3.13 Bright field image of hemisphere EBs on PEGDA honeycomb frame supported gelatin nanofiber substrate.

a) The effect of Y-27632 treatment time

At different Y-27632 treatment time, the flatness of dome-like EBs is different (**Fig. 3.14a**). As the treatment time of Y-27632 increasing, the migration of cells became more difficult, resulted in flatter EBs. When Y-27632 worked for only one hours, as shown as SEM photos (**Fig. 3.14b**), the dome-like EBs were almost hemisphere and had the most highest thickness, which lead to a smaller diameter since the cells' number was constant. There were two reasons for this phenomenon, one is the more diluted vitronection coating, which is an important component of the ECM for hESC or hiPSCs attachment through interactions with a variety of integrin, especially αVβ5 integrin [14]. Compared with 1:100 diluted vitronectin for normal iPSCs culture, 1:500 diluted vitronectin gave a weaker cell attachment on substrate; the other reason is the treatment time of Y-27632. Y-27632 is a selective inhibitor of the Rho-associated kinase p160ROCK and it is mainly used to prevent the dissociation induced apoptosis and promote the survival rate of embryonic stem cells and induced pluripotent stem cells [15]. So treated with Y-27632 is good for increase cells survival. However ROCK is a key regulator of cell migration and also can affect cell-cell adhesion [16], thus decrease of ROCK inhibitor working time will promote cell migration and cell-cell adhesion, which will lead iPSCs to be inclined to form spheroid morphology, while increase of Y-27632 time means increase the inhibition of cell migration and cell-cell interaction, which will make the migration of cells become more difficult, leading to a weaker cell-cell adhesion power and resulting a flat cluster morphology. As statistics, the average diameter of EBs for 1 or

2 hours Y-27632 treatment is similar and around 220 to 230 μm (shown as **Fig. 3.14c**). Therefore, 2 hours of Y-27632 treatment time was applied for the following cardiomyocytes differentiation experiments.

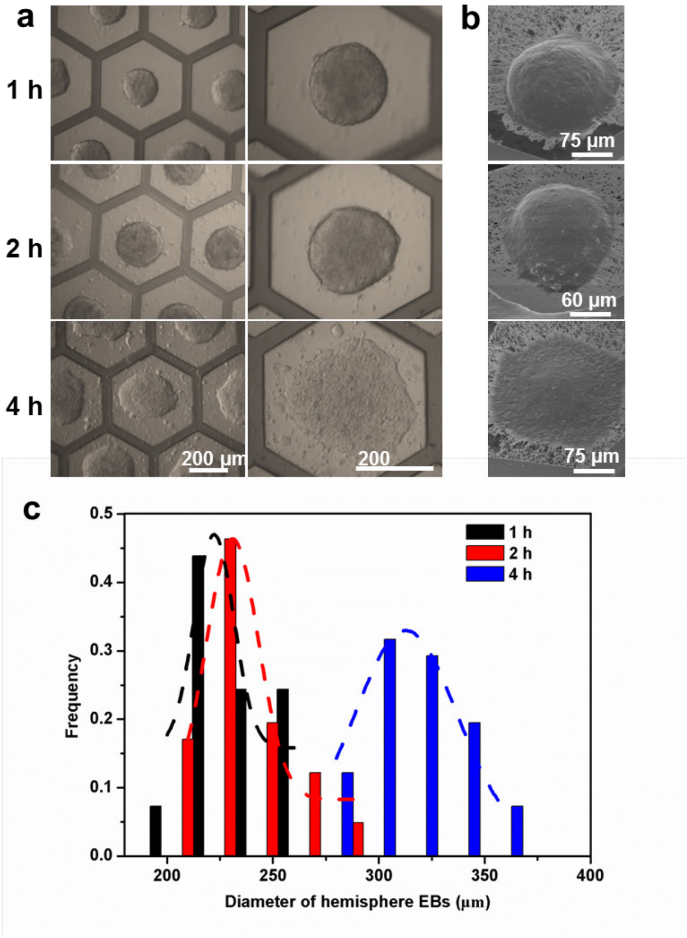

Fig. 3.14 Effect of Y-27632 treatment time on the flatness of iPSC clusters. (a) Bright field images of iPSC clusters at different Y-27632 treatment time; (b) SEM images of iPSC clusters at different Y-27632 treatment time; (c) Diameter distributions of iPSC clusters at different Y-27632 treatment time.

b) Viability of hemisphere EBs

A good beginning cell state is very important for the next differentiation. So we let the hemisphere EBs cultured for two more days, and stained them with Calcein AM and EthD-1 with live/dead assay. As shown in **Fig. 3.15**, almost all the cells of EBs part were live, and there were only few dead cells around EBs, which indicated that there was no obvious effect to the viability of cells when the Y-27632 treatment time was decreased to 2 hours.

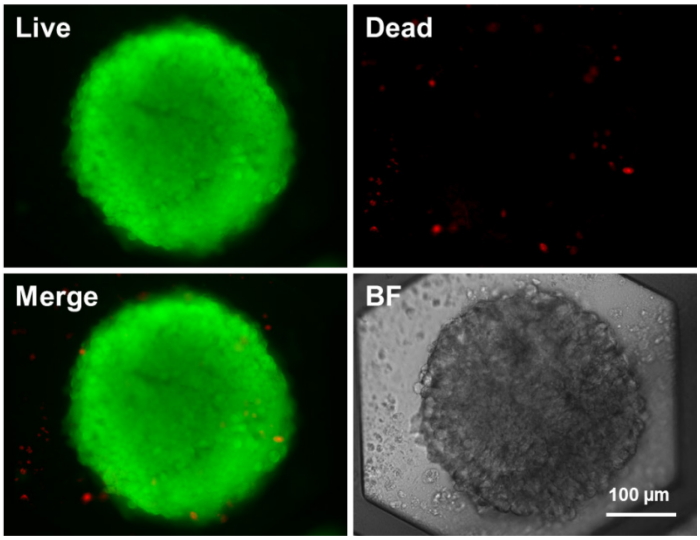

Fig. 3.15 Immunofluorescence staining and bright field images of hemisphere EBs cultured for 48 h after Calcein AM/EthD-1staining for cell viability test.

c) Pluripotency of hemisphere EBs

To evaluate the stemness of hemisphere EBs generated on our PEGDA supported gelatin nanofiber substrate, pluripotent stem cell markers OCT3/4 and NANOG were used to stain the hemisphere EBs. The immunofluorescence results showed a typical hiPSC-like staining pattern, revealed that the expression of these markers was maintained (**Fig. 3.16a**). Reverse transcription-polymerase chain reaction (RT-PCR) analysis shown as **Fig. 3.16b**, demonstrated that the hemisphere EBs still kept to express pluripotency genes (Oct3/4 and NANOG), but not express three-germ differentiation genes (PAX6, BRACHYURY and AFP), which is similar to the undifferentiated hiPSCs cultured on traditional 2D culture dish, confirming that the formation of dome-like EBs on PEGDA supported gelatin nanofiber substrate does not affect the pluripotency of iPSCs.

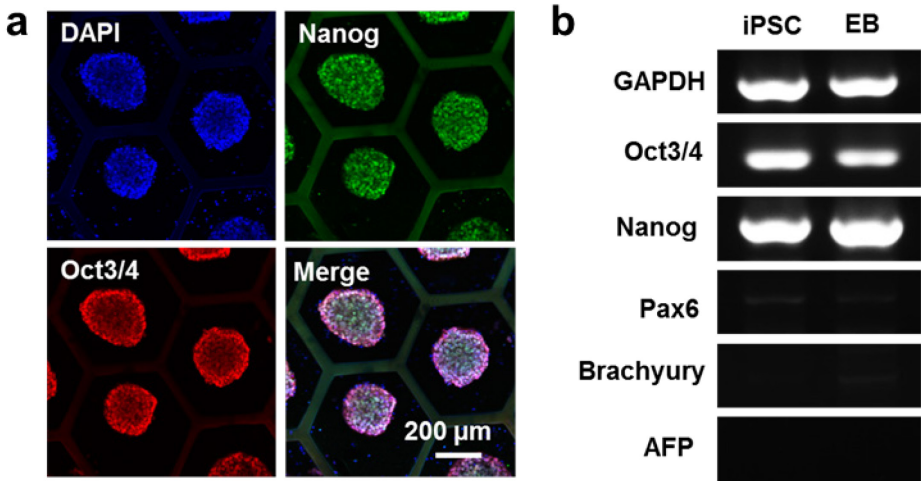

Fig. 3.16 Pluripotency of hemisphere EBs on nanofiber substrate. (a) Immunocytochemistry analysis of Nanog and Oct 3/4 in hemisphere EBs; (b) RT-PCR results of hemisphere EBs and conventional cultured iPSCs.

3.5.2 Cardiomyocytes differentiation from hemisphere EBs

a) Cardiomyocytes differentiation protocol

Once hemisphere EBs formed, cardiomyocytes differentiation was started since the next day, according to GiWi protocol developed by Lian et al [17], by modulating Wnt signaling with small molecules. As shown in **Fig. 3.17a**, 12 μM CHIR99021 in RPMI 1640/B27 without insulin medium was added in dish to change E8 medium, and after 24h of CHIR99021 treatment, the medium was changed with RPMI/B27 without insulin. 72 h after addition of CHIR99021, 5 μM IWP2 RPMI 1640/B27 without insulin medium was added to exchange medium. On day 5 of differentiation, IWP2 was removed by changing new RPMI/B27 without insulin medium. Then every 3 days, change medium with RPMI/B27 medium. Cell morphology during differentiation was recorded by an inverted microscope. Since GSK3 inhibitor was added, many cells stated to migrate out from EBs. As differentiation processing, separated EBs begun to connect to each other to form a thick cell sheet (**Fig. 3.17b**).

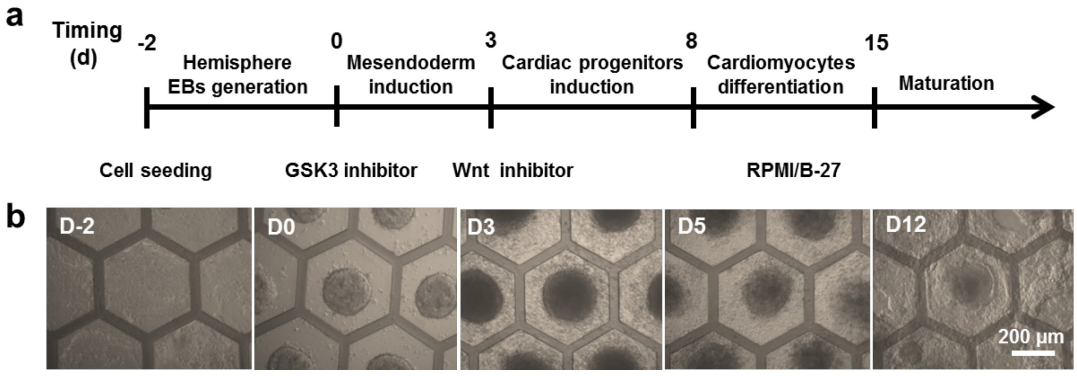

Fig. 3.17 (a) Schematic of the protocol for the differentiation of cardiomyocytes from human iPSCs generated hemisphere EBs; (b) Bright-field images of the typical morphology at day -2, day 0, day 3, day 5 and day 12.

With the same protocol, hiPSCs cultured on glass slide were differentiated into cardiomyocytes at the same time as a control. After treated by GSK3 inhibitor and Wnt inhibitor successively, cell contraction on PEGDA supported nanofiber substrate and glass slide can be observed around Day 7 and Day 8, respectively.

b) Qualitative characterizations

For qualitative analysis the distribution of cardiomyocytes related proteins expression, the differentiated cells on both nanofiber substrate and glass slide at day 20 were stained with cardiomyocytes related antibodies. The immunofluorescence staining images were shown as **Fig. 3.18**. TnnT2, a highly cardiomyocytes-specific protein, was positive for the cells differentiated in both 2D (glass slide) and 3D (nanofiber substrate) environment, while on 3D nanofiber culture system, the expression of TnnT2 showed enhanced sarcomeric organization, which indicated a more mature cardiac cell state. α-MHC is a cardiac muscle-specific protein involved in active force generation. A decreasing expression of α-MHC on 3D substrate was found compared to the cells on 2D glass slide. It has been found that α-MHC expression was dropping along with cardiac maturation [25], which indicated that 3D off-ground differentiation system may promote cardiac maturation. Immunostaining of α-actinin and connexin43 was shown as **Fig. 3.18**. Striated sarcomeres (α-actinin positive) can be observed for the differentiated cells on both 3D substrate and 2D glass slide. Connexin43, for staining gap junction, plays a significant role in the coordination of cells contraction, which showed more positive

for the cells on nanofiber substrate compared to the control.

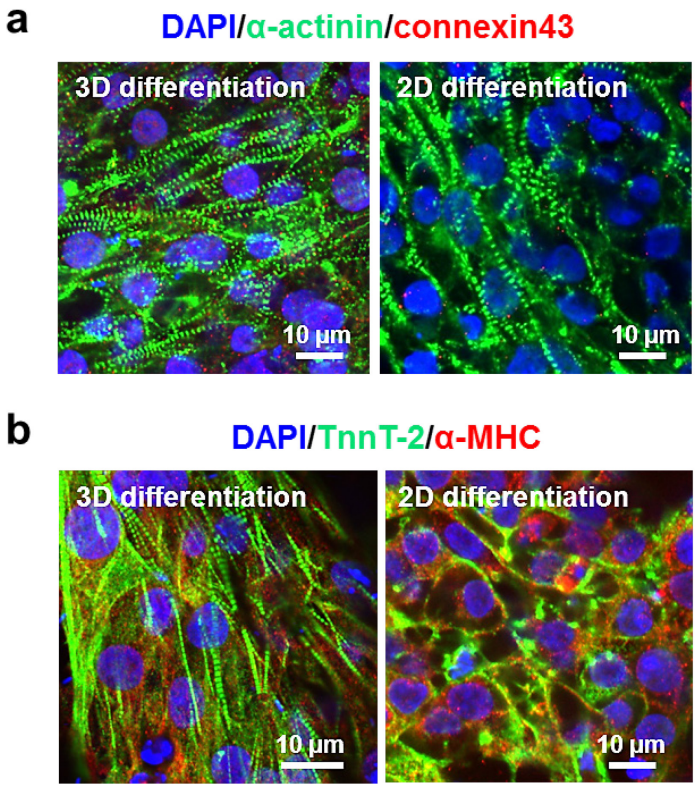

Fig. 3.18 Immunofluorescence staining images of cardiomyocytes derived from hiPSCs on nanofiber substrate (3D) and glass slide (2D). (a) Blue: nuclear; green: α-actinin; red: connexin43; (b) Blue: nuclear; green: TnnT2; red: α-MHC.

c) Quantitative characterizations

Quantitative characterizations were used to further confirm the advantages of nanofiber substrate providing 3D off-ground environment for cardiomyocytes differentiation. As expect, there were 74.7% cTnT positive cardiomyocytes generated on nanofiber substrate compared to 34.5% on 2D glass slide at day 21 according to flow cytometry results (**Fig. 3.19**). The genetic level difference for the cells differentiated in 3D and 2D environment was compared by analyzing the mRNA expression patterns of 22 cardiac differentiation related genes with q-PCR, shown as **Fig. 3.20**. Compared to the cells on day 0, almost all the genes related to differentiation and cardiac were higher expressed for the differentiated cells in both 2D and 3D environments at 9 days. Compared to 2D differentiation, all the cardiac-specific genes, such as NKX2-5, TNNT2, TNNI3 were much higher expressed in 3D off-ground differentiation environment. And the expression of both

the genes related to cardiac structure, such as DES, ACTN2, and genes related to cardiac function, such as PLN, GATA4 was also improved for the cells on nanofiber in 3D differentiation environment. At the same time, the genes related to sodium/calcium/potassium channels which play significant roles during cardiac contraction, such as SLC8A1, RYR2 and KCNQ1 were also increasingly expressed in 3D off-ground differentiation system. Conversely, the expression of ADRB1 gene, which affects the resting heart rate and can be involved in heart failure, was decreased a little compared to 2D control differentiation.

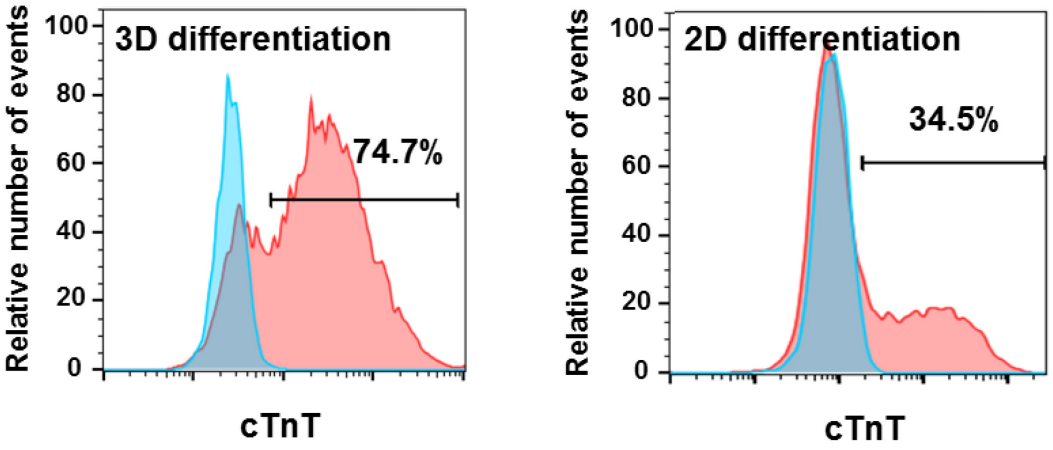

Fig. 3.19 Flow cytometer analysis with specific cardiomyocytes marker cTnT for the cells derived from hiPSCs on nanofiber substrate (3D) and glass slide (2D) at day 21.

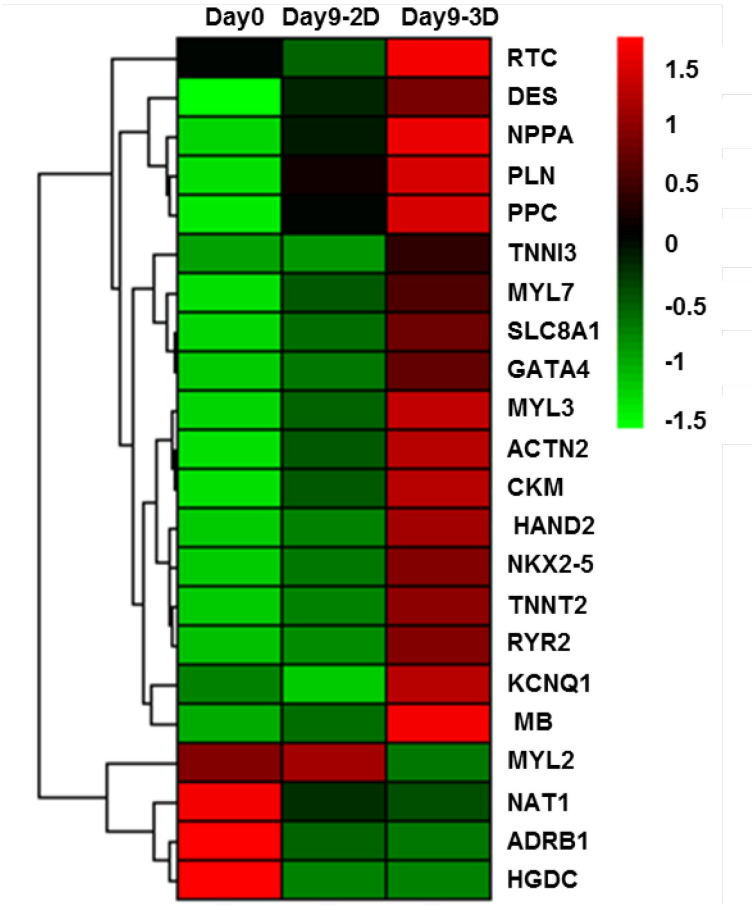

Fig. 3.20 Heat map of 22 cardiac related mRNAs expression of hiPSCs at day 0 and the cardiomyocytes derived from hiPSCs on nanofiber substrate (3D) and glass slide (2D) at day 9, as determined by q-PCR.

3.5.3 Cardiac drug test on multi-electrode array

Extracellular electrical signals recording for derived cardiac patch were performed by using a PC-based data acquisition system (Multi Channel System, Reutlingen, Germany), composed of multi-electrode array (MEA), preamplifiers, filter amplifiers and data acquisition boards (AD Instruments, Japan). The MEA is made of a 50×50 mm glass substrate with a 1.4×1.4 mm matrix of 60 silicon nitride insulated electrodes (30 μm diameter and 200 μm distance) imbedded in the center. Data were recorded at 20 kHz with 16-bit precision.

The functional electrophysiological properties of derived cardiomyocytes on PEGDA supported nanofiber substrate was determined by MEA. At day 21, the substrate with cells can be easily transferred from culture medium to the testing chamber (filled with pre-warmed RPMI/B27 medium) of MEA data acquisition

system by tweezers handling (**Fig. 3.21**). This is clear advantageous due to the fact that the tissues formed on the monolayer nanofibers can serve as more robust barriers to drugs because of tight junctions between cells. The spontaneous field potentials (FPs) of iPSCs derived-cardiomyocytes were monitored by the extracellular recording of MEA system. The testing chamber was always kept at 37 °C by a temperature control system during the whole testing process.

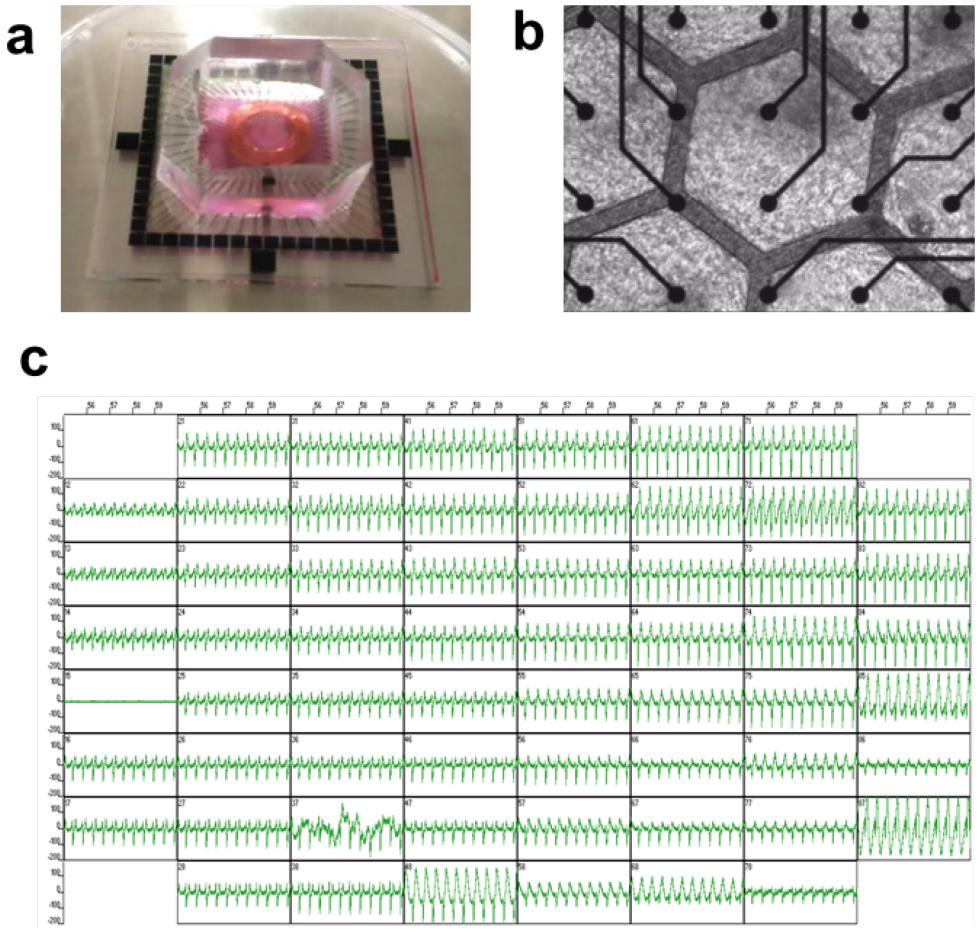

Fig. 3.21 Electrophysiology test of cardiac patch on MEA. (a) Cardiac patch inside MEA testing chamber filled with medium. (b) Bright field image of cardiac patch on the micro electrodes of MEA. (c) Overall view of cardiac-representative field potential on 64 channels recorded from cardiac patch by MEA.

After 15 min for system stability, the original signals of cardiomyocytes on day 21 were obtained. The field potential of contracting cells was simultaneously recorded by an 8×8 electrode grid, and the overall recorded signals of 60 channels were shown as **Fig. 3.21c**. The signals from all channels showed typical cardiac field

potential waveforms with very close synchronism and frequency.

Next, fresh RPMI/B27 medium with 50 nM E-4031 (Sigma, M5060) were added to change the old medium for studying the effect of E-4031 on cardiomyocytes. After 10 min, the reaction FP signal was recorded, following with 10 min treatment of 100 nM E-4031 and signal recording. The introduction of E-4031 showed a prolonged QT interval dependent by the drug concentration (**Fig. 3.22a**). 50 nM and 100 nM E-4031 increased 36% and 52% QR interval, respectively (**Fig. 3.22b**). This was mainly due to the blocking effect of E-4031 on the rapid component of the delayed rectifier potassium current.

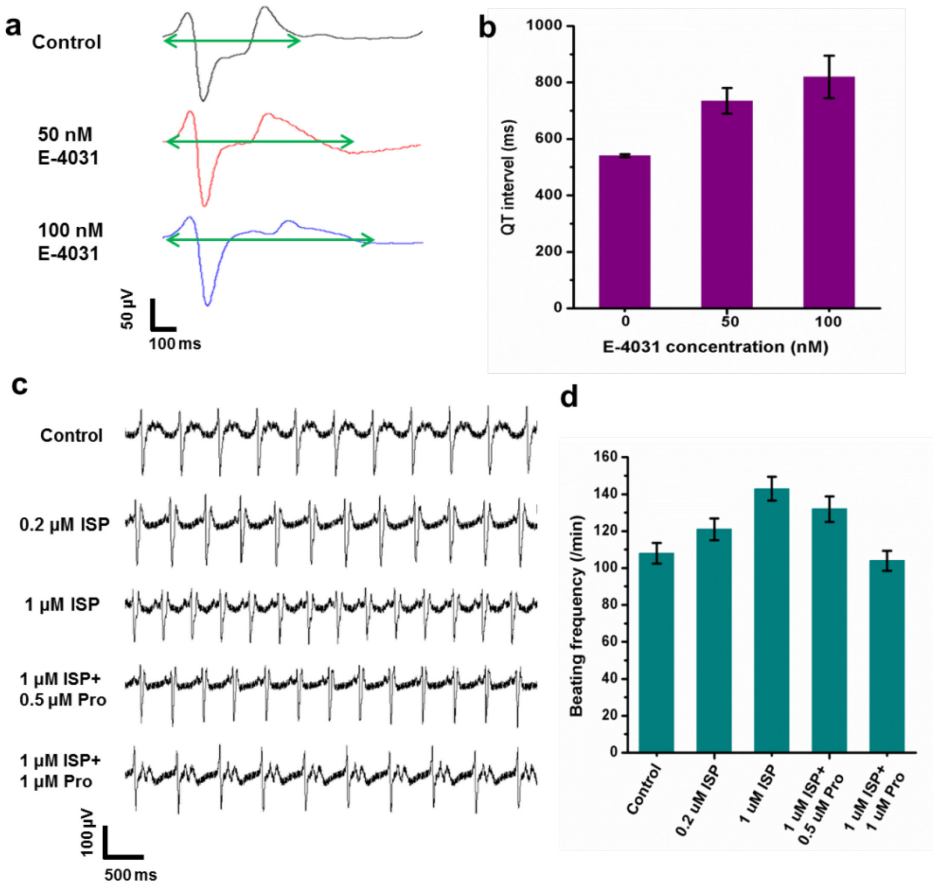

Fig. 3.22 Drug tests of cardiac patch. (a) Effect of 50 nM and 100nM E-4031 on the field potential wave (green lines represent QT interval). (b) QT interval prolonged with the increase of E-4031 concentration. (c) Effect of cardiac drug ISP and Pro concentrations on the field potential wave of cardiac patch. (d) Beating frequency changes with ISP and Pro treatment.

Then, the cell reaction for cardiac drugs, Isoproterenol (ISP) (Sigma, I6504) and Propranolol (Pro) (Sigma, P0884), were tested in the same way. Isoproterenol, a beta-agonist, was introduced to the cells with gradual increased concentrations, which lead to a dose-dependent increase of beating frequency (**Fig. 3.22c**). Then the application of different concentration propranolol, a beta-blocker, resulted in a dose-dependent decrease of beating frequency (**Fig. 3.22d**). The above results of cardiac drug tests indicated a good drug reaction and functional performance of the cardiomyocytes generated on PEGDA frame supported nanofiber substrate.

3.5.4 Discussion

We present a monolayer gelatin nanofiber substrate with PEGDA honeycomb frame supporting, which could provide an off-ground 3D cell culture environment. There have been numerous methods reported for EBs generation [18-21]. They could product uniform EBs by micro-wells or other techniques, and when they started to differentiate EBs to cardiac cells, there were two ways: either they let EBs to dispersed suspended in differentiation medium or reseed EBs in culture dish. The first way resulted in heterogeneous cardiac clusters with irregular shape due to the inevitable fusing of EBs, while these irregular cardiac clusters have different cardiac functional properties, such as beating frequency [18]. Besides, this kind of separated suspended cardiac cluster was also difficult to be applicate, which need to disperse the clusters to single cells for reseeding. And the way of plating the generated EBs on coated culture dish for differentiation changed the 3D state and environment of EBs, and could not control an even distribution of plated EBs. Here to our best knowledge, we generated for the first time homogeneous hemisphere EBs adhesive inside each PEGDA honeycomb frame which allowing efficient cardiomyocytes differentiation to form a relatively uniform functional cardiac sheet directly on the same substrate. Due to both the non-protein adhesion of PEGDA, seeded hiPSCs can be separated into several colonies by the regular PEGDA frame and form dome-like EBs by easily controlling the treatment time of ROCK inhibitor. Unlike traditional suspension EBs which are very easy to merge together and difficult to be manipulated, hemisphere EBs are attached on the nanofiber patch, which can be operated and controlled easily by handling the whole patch.

It has been reported a lot about the advantages of 3D cell culture environment, which can mimic the *in vivo* microenvironments more accurately [22, 23]. Although

in our work the hemisphere EBs was adhesive to the nanofiber, it was not the same as traditional 2D adhesive culture because the nanofiber layer was almost monolayer with very high porosity and large enough pore size which could let the cells located in the bottom of EBs still contacted to the same nutrient and factors as the cells located on the top during culturing and differentiation. Therefore, the environment was similar to the 3D environment of traditional suspension EBs. Lee et al [29] reported a similar PEGDA micropatterned PS/PSMA nanofiber, but their nanofiber layer was very thick and compact, which cannot provide a 3D exposure environment for cells. Following with dome-like EBs generation, the similar pluripotency of cells in EBs, the higher cardiomyocytes differentiation efficiency, genetic and protein specific markers expression levels and better beating uniformity, compared with traditional 2D monolayer cell differentiation were demonstrated. The proliferation enhancement effect of our nanofiber patch for fibroblast was mainly due to the improved permeability of patch, which has been shown before (Part 3.3). Similarly, the remarkable better cardiac differentiation performance may also attribute to this kind of 3D exposure culture environment, which could let cells contact with much more differentiation factors and nutrient not only from the top of EBs but also from the bottom gaps among nanofiber.

After cardiomyocytes differentiation, the contraction of cardiac sheet on nanofiber showed much better synchronism and homogeneity, compared to the control differentiation on glass slide. This is because on nanofiber, cells formed separated homogeneous EBs first before differentiation, and during differentiation, each EB was exposed to the differentiation factors equally all over the whole substrate. Then the cells migrated and connected to form one thick cell layer, leading to a homogeneous beating cardiac sheet. However, on glass, cells were a large flat clone before differentiation and cell migration occurred during differentiation leading to a annular apophysis close to the edge, which was the only beating region, while most areas in the center of the annular apophysis circle were clam with almost no contraction.

For the spontaneous functional electrophysiological performance characterization, no matter 2D monolayer differentiation or conventional EBs differentiation, the dispersing and re-seeding were needed [24, 25]. However this step was troublesome and brought certain unavoidable injury to the cells, and could also destroy the organization structure of cells that has been established. But in our

case, we just need to transfer the device with derived cells on it from culture medium to MEA testing chamber, which made it very convenient to monitoring the function property of derived cardiomyocytes. Furthermore we have demonstrated that this PEGDA supported nanofiber substrate was also a platform, which could be used directly for cardiac drug tests. Our results using MEA mapping technique showed that hiPSC derived cardiomyocytes responded appropriately to three different cardiac drug compounds known to affect QT intervals and chronotropy, which confirmed that the differentiated cells were cardiac-functional and this device could be supplied as a promising human cardiac model platform for drug safety tests.

3.6 Functional motor neuron differentiation from hiPSCs

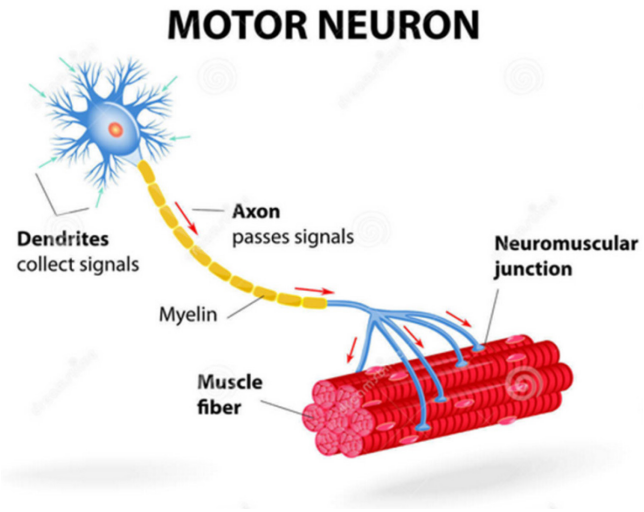

Fig. 3.23 Motor neuron structure, including dendrites, cell body with nucleus, axon, myelin sheath, nodes of Ranvier and motor end plates. The impulses are transmitted through the motor neuron in one direction [26].

Motor neurons are the cells located in spinal cord, projecting their axons outside the spinal cord to control muscles directly or indirectly through neuromuscular junctions [27]. Similar to other type neurons, motor neuron is composed of a cell body (soma), dendrites, and an axon as shown as **Fig. 3.23**, in which dendrites collect signals and then axon passes the signals to the muscles to control the contraction and relaxation of muscle, resulted into the movement. So any problem of motor neuron will affect the movement directly and cause motor neuron diseases

(MNDs). MNDs are neurodegenerative in nature and cause increasing disability and eventually death, such as amyotrophic lateral sclerosis (ALS) and spinal muscular atrophy (SMA) [28]. Unfortunately there is no a cure or efficient treatments for MNDs in present.

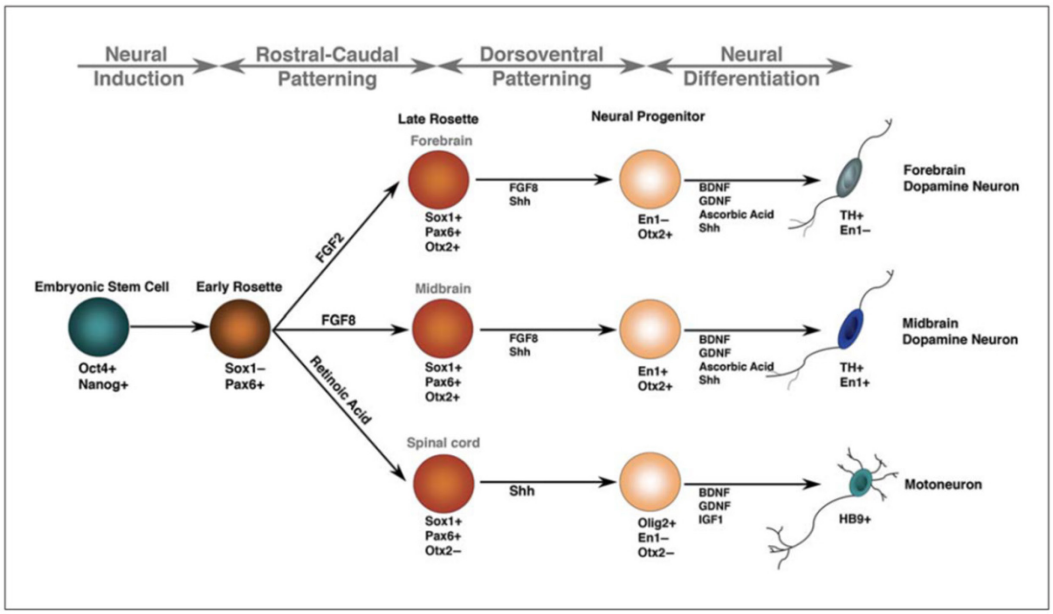

Fig. 3.24 Related factors for hESC or hiPSCs differentiation into neurons. From neural induction of pluripotent stem cells to the expansion and early specification of neural progenitors and the final differentiation into specific neuronal lineages [29].

Due to the of pluripotency and the ability to give rise to any cell type of the organism, ESCs and more recently iPSCs have emerged as powerful tools for the study of neurobiology, and also hold great promises for regenerating complex neural tissues and repairing neuron injury whether from direct damage or from the disease of neuron development and degeneration [30]. Hence, in recent years, the related mechanisms about neural induction, differentiation and specification have been studied widely [31-33]. In the meantime, different subtypes of neurons have been generated by differentiation from stem cells, such as dopaminergic neurons [34, 35], interneurons[36, 37], motor neurons[14, 38, 39] and pyramidal neurons [40]. **Fig. 3.24** outlines the various stages and the related factors of hESC or hiPSCs differentiation into neurons, from neural induction of pluripotent stem cells to the expansion and early specification of neural progenitors and the final differentiation to specific neuronal lineages. For MNDs, human iPSCs derived motor neurons could

be very promising not only for generating reliable MNDs model in regenerative medicine development and pharmaceutical applications, but also for further transplantation and injury repair.

In the past decade, there were several protocols have been developed to differentiate motor neurons from hiPSCs. However, there are still some limitations hindered the application of these protocols, such as time consuming (up to 2 months), genetic manipulation requirement, low efficiency and introduction of unknown factors [38, 39, 41]. In this part, we developed a protocol for motor neuron differentiation on gelatin nanofiber patch. After generate monolayer or hemisphere EBs on the patch, motor neuron differentiation was proceeded following three steps: neuroectrodermal induction based on dual inhibition of SMAD signaling [42], motor neuron differentiation into motor neuron progenitors, and motor neuron maturation, as shown as **Fig. 3.25**.

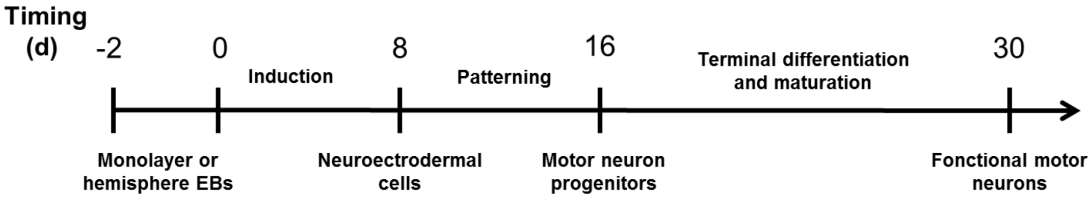

Fig. 3.25 Schematic of the protocol for hiPSCs (either monolayer iPSCs or hemisphere EBs) differentiation into motor neurons.

3.6.1 Motor neuron differentiation protocol

a) Neuroectrodermal induction

The induction medium was prepared with Knockout Serum Replacement (KSR) medium and N2 medium at different ratio. KSR medium contains 20% KSR, 0.1 mM β-mercaptoethanol, 2 mM Glutamax, 1% Non-Essential Amino Acid (NEAA) and 4 ng/ml basic fibroblast growth factor (bFGF) in DMEM/F12. N2 medium contains 1% N2 supplement, 2 mM Glutamx and 1% NEAA in DMEM/F12. The neuron induction of hiPSCs was done by using N2/KSR medium at ratio of 0/100% (day 1-3), 25%/75% (day 4), 50%/50% (day 5-6), 75%/25% (day 7) and100%/0 (day 8), respectively, together with 10 μM SB431542 and 0.1 μM LDN193189 (for dual inhibition of SMAD signaling) for all days.

b) Motor neuron differentiation

From day 9 to 16, cells were treated with N2 medium containing 0.1 μM retinoic acid (RA), 0.5 μM purmorphamine (Pur) and 20 ng/ml bFGF. The medium was changed every two days.

c) Motor neuron maturation

At day 17, motor neuron progenitors were digested with 1 mg/ml Dispase and re-suspended in a maturation medium which is composed of 1:1 mixture of N2 medium and B27 medium with a number of maturation factors. The B27 medium contains neurobasal medium, 2% B27 supplement, and 2 mM Glutamax. The maturation factors include 10 ng/mL brain-derived neurotrophic factor (BDNF), 10 ng/mL glial-derived neurotrophic factor (GDNF), 10 ng/mL insulin-like growth factor 1 (IGF-1), 1 μM cyclic adenosine monophosphate (cAMP), 0.2 μg/mL ascorbic acid (AA), 0.1 μM RA, and 1 μM Pur.

Prior to cell seeding, the nanofiber patch was treated in a laminin solution (1:50 iMatrix511 in PBS, Clontech) at 37℃ overnight while glass slides and multi-electrode array (MEA, Multichannel, Germany) samples were first treated in a solution of poly-ornithine (PO, Sigma P4957) at 37° C for 2h and then in the laminin solution at 37℃ overnight. After cell seeding, the medium was changed every two days.

3.6.2 Effect of beginning cell states and substrates on differentiation

No matter which type differentiation from hiPSCs, the initial cell density is one of the critical parameters deciding the final differentiation efficiency [43, 44]. Here we optimized the seeding density for motor neuron differentiation on vitronectin coated glass slide (Φ15mm，A=2.36 cm^2). We seeded hiPSCs at initial cell number of 4×10^5, 6×10^5 and 8×10^5. After two days, cells were induced and differentiated as the protocol above. During differentiation, the morphology of cells can be divided into four regions from the center to the edge of glass (shown as **Fig. 3.26**). In the center, cells were much denser and it's difficult to observe the morphology of each cell. More close to the edge of glass, lower density and more elongated neuron

morphology can be observed. Interestingly, at day 16, there were neuron spheres appeared in the center of glass slide, and the cells on the edge elongated as neuron-like morphology.

The differentiated cells were stained with neuron specific protein β-tubulin III and motor neuron progenitor specific marker Olig2 at day 16, as shown as **Fig. 3.27**. There were more Olig2 positive motor neuron progenitors in the center than on the edge of glass. And cells differentiated from low seeding density expressed more Olig2, which indicated for our protocol, the optimum seeding density is 4×10^5 cells per 2.36 cm^2.

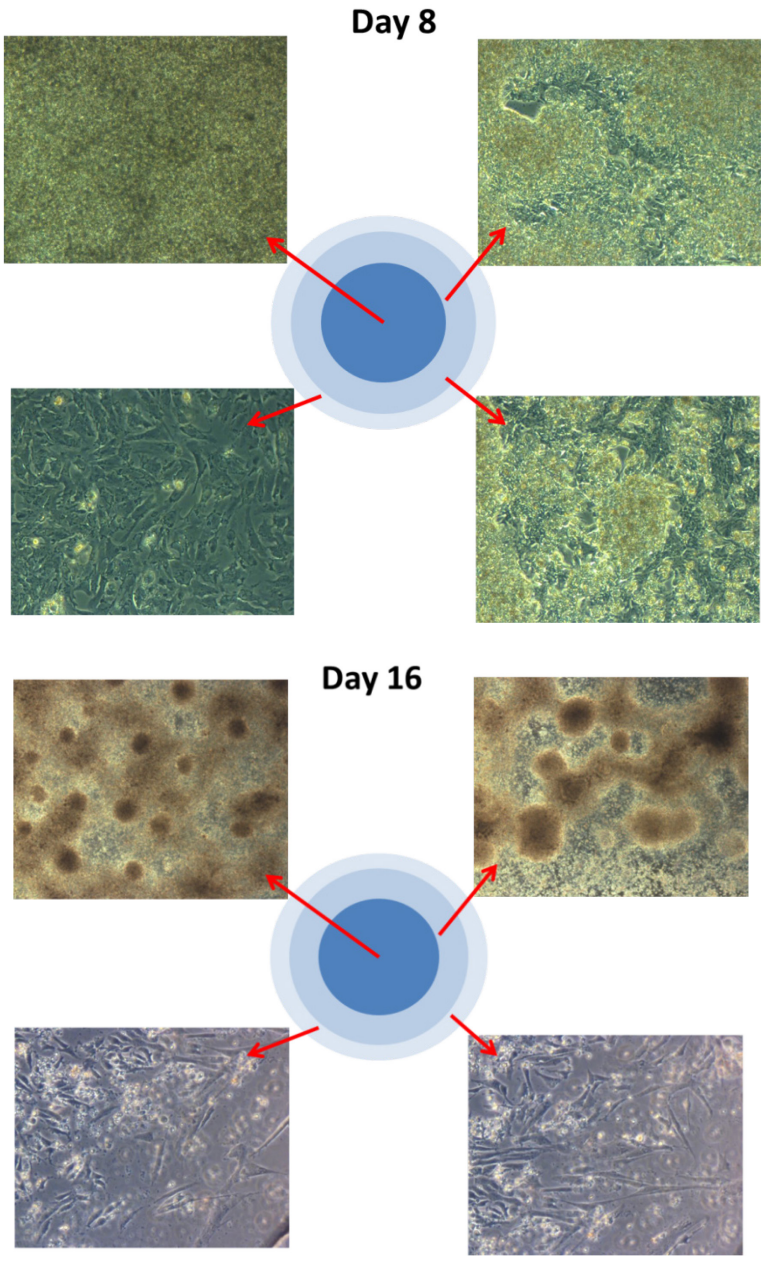

Fig. 3.26 Cell morphologies at different regions of glass slide on day 8 and day 16.

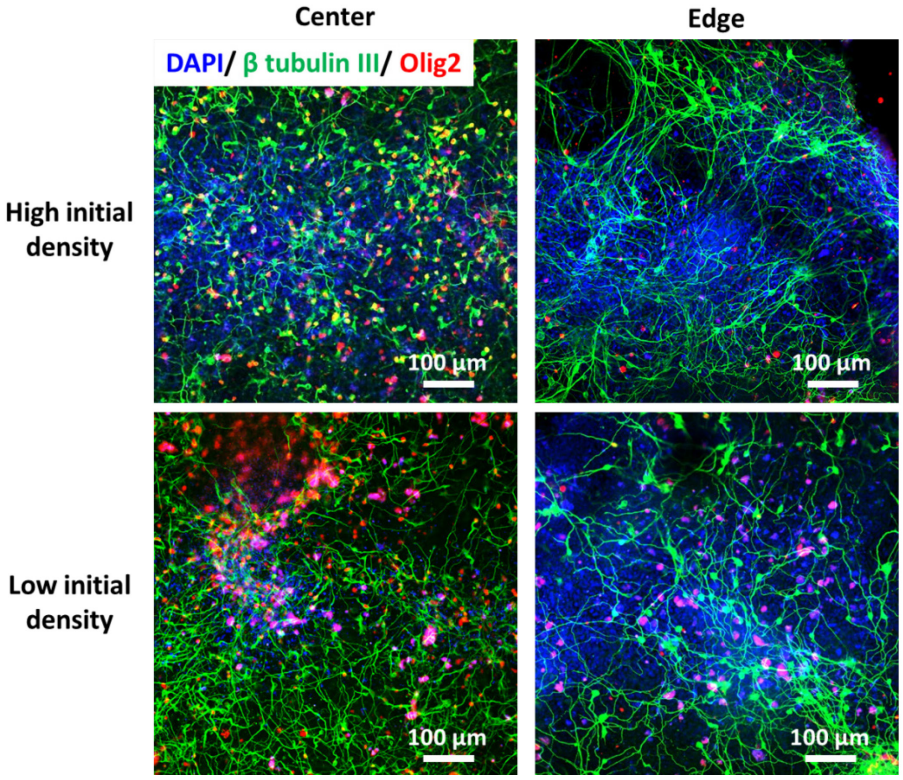

Fig. 3.27 Immunofluorescence staining for neurons derived from different densities of hiPSCs on glass slide. DAPI: nuclear (blue); β-tubulin III: neural microtubule (green); Olig2: motor neuron progenitor (red).

Currently there are lots of protocols for hiPSCs differentiation into neurons, generally the protocols can be divided into two main groups according to the beginning cell state [45, 46]: EBs differentiation or monolayer iPSC colonies differentiation. So far there was no unified opinion yet which method is better. Therefore, in this part, we will compare the differences between EBs and monolayer differentiation into motor neurons on nanofiber patch in off-ground condition, with conventional 2D differentiation on glass slide as control.

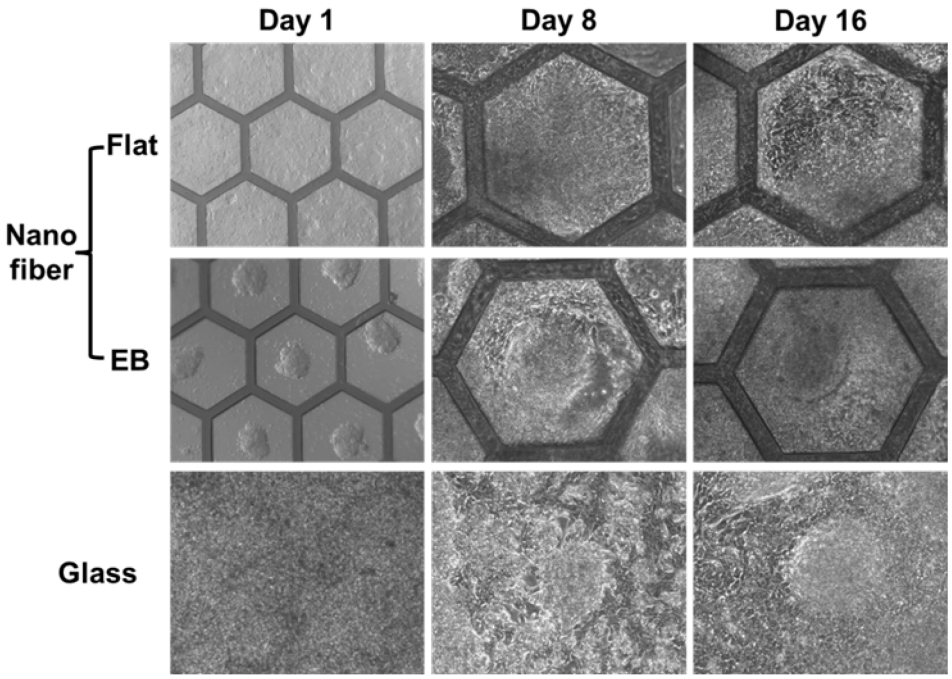

Fig. 3.28 Bright field images of cells during motor neuron differentiation from different beginning cell states at different substrates.

Fig. 3.28 shows the bright field images of differentiating cells at different stages. After the formation of hemisphere EBs or monolayer colonies for two days, the iPSCs were induced to neuroectrodermal cells by inhibition of dual Smad signaling pathway, using TGF-β inhibitor SB431542 and BMP4 inhibitor LDN193189. Typical cell morphology changes can be observed at day 8. Meanwhile, cells started from EB like colonies migrated to the outside of the EB area and then connected to the neighboring ones. The results of immunostaining show that at day 8 most cells became both Pax6 and nestin positive which are neuroectodermal specific transcription factor and common neural progenitor marker, respectively (**Fig. 3.29**). The results of q-PCR revealed a higher nestin expression level of the cells on nanofibers than on glass, suggesting that the off-ground culture with crosslinked monolayer nanofibers lead to a better neuron induction of hiPSCs than conventional culture (**Fig. 3.30**).

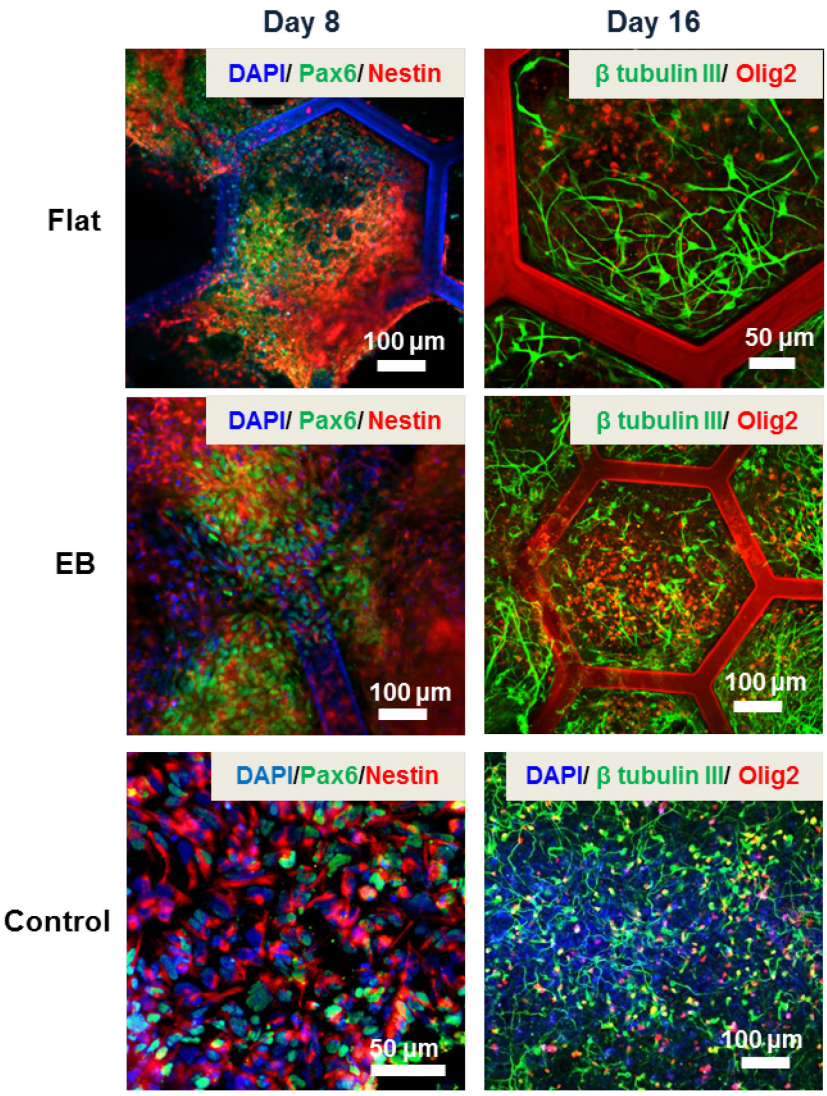

Fig. 3.29 Immunofluorescence staining images of hiPSCs-derived neurons at day 8 and day 16 from different beginning cell status. DAPI: nuclear (blue); Pax6: neuroectrodermal cells (green); Nestin: neuron stem cells (red); β-tubulin III: neural microtubule (green); Olig2: motor neuron progenitor (red).

After day 8, cells were exposed to soluble morphogens RA and Pur for motor neuron specification. At day 16, the immunofluorescence images show clearly neuron specific β-tubulin III stained microtubules and motor neuron progenitor specific transcription factor Olig2. However, the results of q-PCR (**Fig. 3.30**) show a much higher expression level of Olig2 for the cells started from monolayer colonies than that from EB-like ones and on glass (**Fig. 3.29**), suggesting that monolayer iPSCs colonies could be better directed to the motor neurons under off-ground culture conditions.

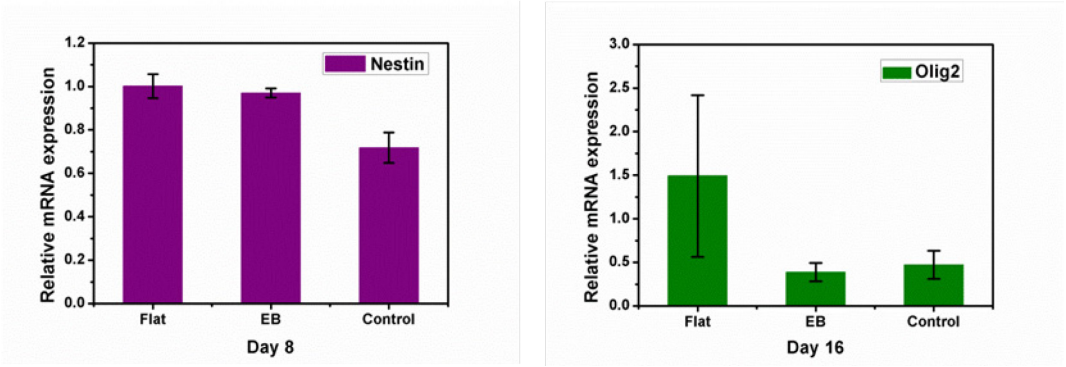

Fig. 3.30 Relative mRNA expression of Nestin at day 8 and Olig2 at day 16 for different beginning cell status of motor neuron differentiation.

3.6.3 Effect of different substrates on motor neuron maturation

After day 16, motor neuron progenitors derived from monolayer iPSCs on the culture patch were digested and reseeded for maturation on three types of substrates, i.e., pre-coated glass slide, MEA or culture patch. **Fig. 3.31** shows the morphology changes of the cells at day 22, 26 and 30 on different culture supports. In the beginning, single neurons started to adhere on the substrate and showed extension of neurites extension. Due to cell proliferation, neuron clusters and even neuron spheres (especially on glass slide) were formed. Then, elongated axons (up to several hundred micrometers) appeared at day 30. However, significant differences in cell/cluster morphology can be observed with different types of culture supports. Apparently, neurons cannot attach on well on MEA, which lead to a poor proliferation. Neurons are also more likely to form large clusters on MEA and glass while they spread on the culture patch due to compartmentation and less stiff substrate. Indeed, neurons are found in the relatively soft tissue of the nervous system, they thrived similarly on softer materials *in vitro* [47, 48]. Compared to the environment of nervous system in vivo, glass and MEA are too rigid for neuron culture, while the culture patch formed by crosslinked monolayer gelatin nanofibers should provide a culture support quite similar to the *in vivo* extracellular matrix for both neuron proliferation and neurites extension.

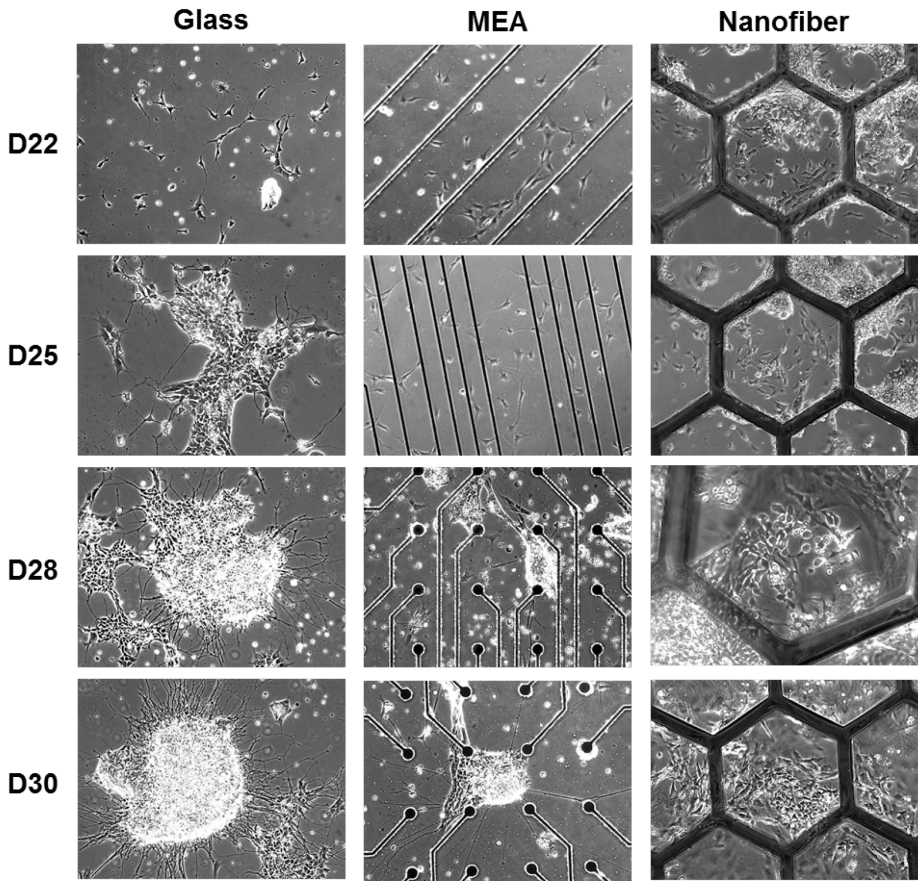

Fig. 3.31 Bright field images of motor neuron morphology reseeded at different substrate and different day.

Cells on glass slide were stained with motor neuron specific transcription factor marker HB9 and neuron specific protein β tubulin III at day 22 and day 30, as shown as **Fig. 3.32**. Most of neurons were HB9 positive motor neurons. We observed β-tubulin III positive neuron networks obviously. But there were also some β-tubulin III positive but HB9 negative neurons existed, especially at day 30.

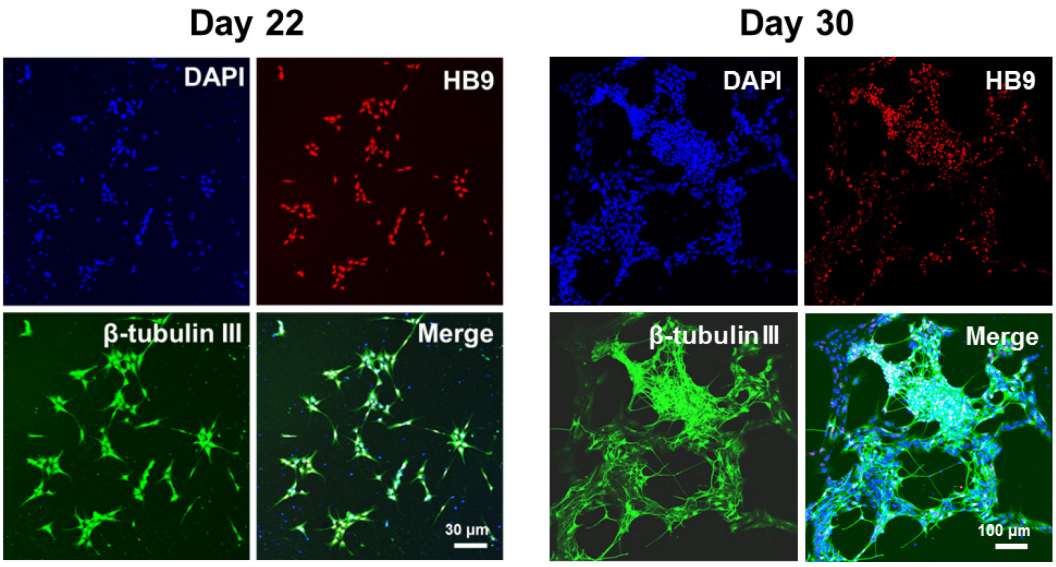

Fig. 3.32 Immunostaining images of motor neurons on glass slide during maturation at day 22 and day 30. DAPI: nuclear (blue); HB9: motor neuron (red); β-tubulin III: neural microtubule (green).

After day 30, neural electrical signals were monitored on real time every two days with MEA system. Similar to the electrophysiology test of cardiac patch, neuron patch can also be handled and transferred easily with a tweezer onto MEA platform (shown as **Fig. 3.33**).

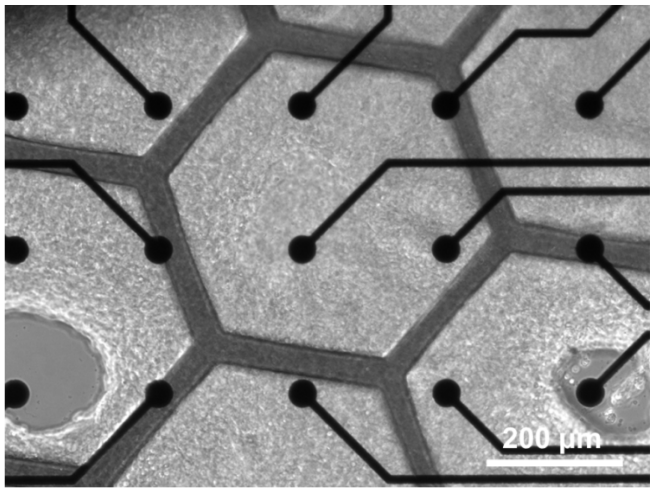

Fig. 3.33 Bright field images of neuron patch on MEA.

Around day 38, there was spontaneous extracellular field potentials could be detected for neuron patch, as shown as **Fig. 3.34**, which proved the neurons became mature enough and formed functional neuron network. But the neuron signals were

not detected on every electrode. It was probably due to either the worse contact of patch and electrodes comparing to the case of neurons directly seeded on MEA, or the various maturity of neurons in different locations. Besides, we should however mention that the patch is not perfectly flat so that the distance between the patch is not in conformal contact with each of the electrodes of MEA, leading to electrode dependent signal intensity. **Fig.3.34 (b-d)** show 10 second recorded signals by electrode 78#, 51# and 46# respectively.

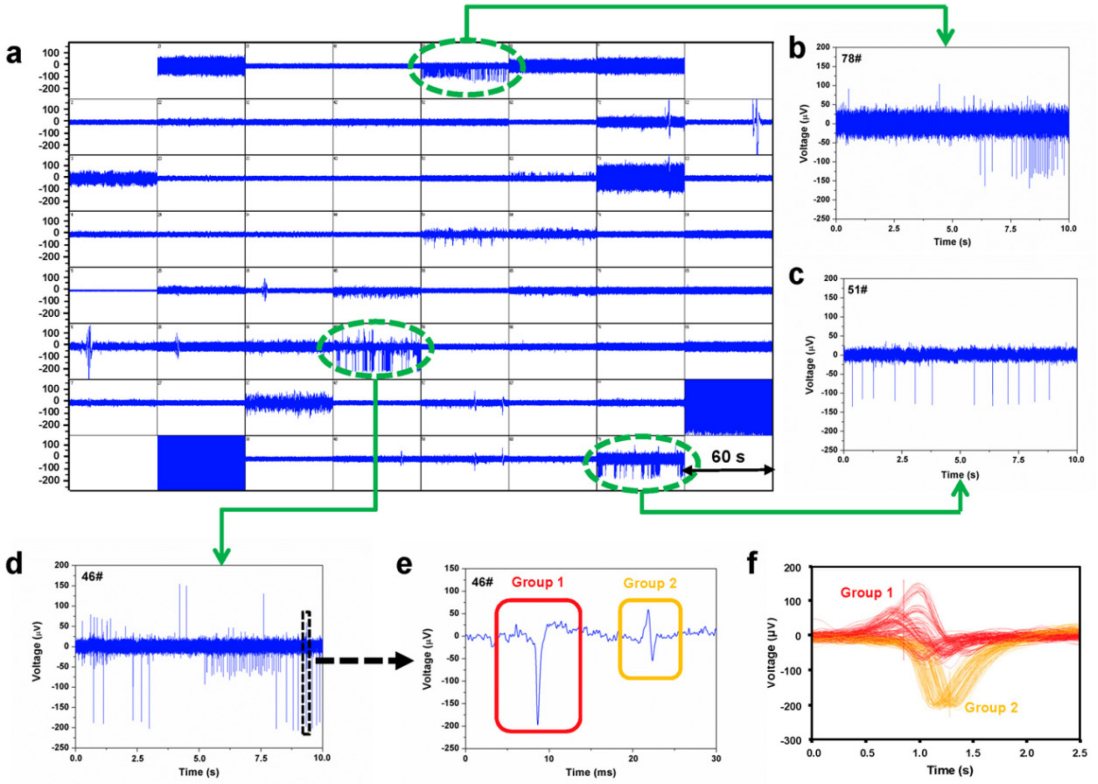

Fig. 3.34 Spontaneous electrical signals of motor neurons on nanofiber patch recorded by MEA. (a) Overall view of spontaneous neuron activity detected on 64 channels recorded. (b) Electrical signals detected by electrode 78# for 10 s. (c) Electrical signals detected by electrode 51# for 10 s. (d) Electrical signals detected on electrode 46# for 10 s. (e) Two typical groups of neuron spike detected by electrode 46#. (f) Spike sorting for the electrical signals detected by electrode 46#.

Taking example of channel 46#, spikes could be detected with a signal-to-noise ratio ranged from 3:1 to 5:1. With spike sorting tool implemented in MC_Rack software, signals from channel 46# can be divided into two main groups of spikes

generated from the activity of 2 neurons according to waveform dissimilarity, shown as **Fig. 3.34 (e-f)**. And the individual spikes typically displayed a negative component of 150~200 μV for the spike group 1, and a negative component of 50~80 μV followed by a positive component of 50~130 μV for group 2. For most of electrodes with spike detected, the signals were attributed to 1~2 neurons per electrode. And the duration of each spike was around 1 ms, which matches the normal neuron signal characteristic.

The electrical signals of cells reseeded on MEA were also monitored every two days, however until day 50, there was no electrical signal detected. It revealed that the off-ground neuron culture system with nanofiber patch can enhance motor neuron maturation, due probably to the more similar *in vivo* extra neural environment compared to the rigid 2D substrates.

3.7 Conclusion

In this chapter, we firstly described the fabrication of the culture patch made of crosslinked monolayer gelatin nanofibers and PEGDA frame. Next, we show the advantage of this culture patch for off-ground culture, which leads to a significant increase of the proliferation rate comparing to that cultured conventionally. We then used the culture patch for the shape control of hiPSCs colonies (varying from monolayer to hemisphere EB-like by changing the Rock inhibitor treatment time). Afterward, the EB-like colonies were used for cardiac differentiation on the culture patch, showing ~74.7% of differentiation efficiency compared to ~34.5% with the culture dish method. When the culture patch with derived cardiomyocytes was placed on a multi-electrode array, we obtained expected field potential signals as well as the drug type and dose dependent responses. Finally, we used the culture patch to control motor neuron differentiation of hiPSCs. Motor neuron progenitors were obtained on the patch, showing the expression of their characteristic proteins. After reseeding to different types of culture support, representative electrical signals could be recorded at day 30 with the patch, due to spontaneous firing of neurons, but no firing was detected with for the neurons reseeded on MEA device until day 50. Our results also show that the differentiation efficiency of hiPSCs to neurons is higher when started from flat iPSCs colonies comparing to that of EB-like ones.

Over-all, the culture patch we proposed in this work can be used for advanced studies of cardiac and neuronal differentiation and electrophysiological recordings. Comparing to the more conventional culture dish methods, the culture patch method could be a more efficient alternative for process optimization and thus a large variety of applications.

Reference

[1] Lutolf M, Hubbell J. Synthetic biomaterials as instructive extracellular microenvironments for morphogenesis in tissue engineering. Nature biotechnology. 2005;23:47-55.

[2] Bhatia SN, Ingber DE. Microfluidic organs-on-chips. Nature biotechnology. 2014.

[3] Rho KS, Jeong L, Lee G, Seo B-M, Park YJ, Hong S-D, et al. Electrospinning of collagen nanofibers: effects on the behavior of normal human keratinocytes and early-stage wound healing. Biomaterials. 2006;27:1452-61.

[4] Liu S-J, Kau Y-C, Chou C-Y, Chen J-K, Wu R-C, Yeh W-L. Electrospun PLGA/collagen nanofibrous membrane as early-stage wound dressing. Journal of Membrane Science. 2010;355:53-9.

[5] Li S, Shi J, Liu L, Li J, Jiang L, Luo C, et al. Fabrication of gelatin nanopatterns for cell culture studies. Microelectronic Engineering. 2013;110:70-4.

[6] Liu L, Yoshioka M, Nakajima M, Ogasawara A, Liu J, Hasegawa K, et al. Nanofibrous gelatin substrates for long-term expansion of human pluripotent stem cells. Biomaterials. 2014;35:6259-67.

[7] Cho D, Lee S, Frey MW. Characterizing zeta potential of functional nanofibers in a microfluidic device. Journal of colloid and interface science. 2012;372:252-60.

[8] Alwan A. Global status report on noncommunicable diseases 2010: World Health Organization; 2011.

[9] http://www.ehnheart.org/cvd-statistics.html.

[10] Mozaffarian D, Benjamin EJ, Go AS, Arnett DK, Blaha MJ, Cushman M, et al. Heart disease and stroke statistics-2015 update: a report from the american heart association. Circulation. 2015;131:e29.

[11] Naghavi M, Wang H, Lozano R, Davis A, Liang X, Zhou M, et al. Global, regional, and national age-sex specific all-cause and cause-specific mortality for 240 causes of death, 1990-2013: a systematic analysis for the Global Burden of Disease Study 2013. Lancet. 2015;385:117-71.

[12] Chong JJ, Yang X, Don CW, Minami E, Liu YW, Weyers JJ, et al. Human embryonic-stem-cell-derived cardiomyocytes regenerate non-human primate hearts. Nature. 2014;510:273-7.

[13] Yamanaka S. Induced pluripotent stem cells: past, present, and future. Cell stem

cell. 2012;10:678-84.

[14] Hu W, He Y, Xiong Y, Lu H, Chen H, Hou L, et al. Derivation, Expansion, and Motor Neuron Differentiation of Human-Induced Pluripotent Stem Cells with Non-Integrating Episomal Vectors and a Defined Xenogeneic-free Culture System. Molecular neurobiology. 2015.

[15] Li X, Meng G, Krawetz R, Liu S, Rancourt DE. The ROCK inhibitor Y-27632 enhances the survival rate of human embryonic stem cells following cryopreservation. Stem cells and development. 2008;17:1079-85.

[16] Riento K, Ridley AJ. Rocks: multifunctional kinases in cell behaviour. Nature reviews Molecular cell biology. 2003;4:446-56.

[17] Lian X, Zhang J, Azarin SM, Zhu K, Hazeltine LB, Bao X, et al. Directed cardiomyocyte differentiation from human pluripotent stem cells by modulating Wnt/beta-catenin signaling under fully defined conditions. Nature protocols. 2013;8:162-75.

[18] Dahlmann J, Kensah G, Kempf H, Skvorc D, Gawol A, Elliott DA, et al. The use of agarose microwells for scalable embryoid body formation and cardiac differentiation of human and murine pluripotent stem cells. Biomaterials. 2013;34:2463-71.

[19] Mohr JC, Zhang J, Azarin SM, Soerens AG, de Pablo JJ, Thomson JA, et al. The microwell control of embryoid body size in order to regulate cardiac differentiation of human embryonic stem cells. Biomaterials. 2010;31:1885-93.

[20] Kempf H, Olmer R, Kropp C, Ruckert M, Jara-Avaca M, Robles-Diaz D, et al. Controlling expansion and cardiomyogenic differentiation of human pluripotent stem cells in scalable suspension culture. Stem cell reports. 2014;3:1132-46.

[21] Burridge PW, Thompson S, Millrod MA, Weinberg S, Yuan X, Peters A, et al. A universal system for highly efficient cardiac differentiation of human induced pluripotent stem cells that eliminates interline variability. PloS one. 2011;6:e18293.

[22] Yamada KM, Cukierman E. Modeling tissue morphogenesis and cancer in 3D. Cell. 2007;130:601-10.

[23] Pampaloni F, Reynaud EG, Stelzer EH. The third dimension bridges the gap between cell culture and live tissue. Nature reviews Molecular cell biology. 2007;8:839-45.

[24] Minami I, Yamada K, Otsuji TG, Yamamoto T, Shen Y, Otsuka S, et al. A small molecule that promotes cardiac differentiation of human pluripotent stem cells under

defined, cytokine- and xeno-free conditions. Cell reports. 2012;2:1448-60.

[25] Mehta A, Verma V, Nandihalli M, Ramachandra CJ, Sequiera GL, Sudibyo Y, et al. A systemic evaluation of cardiac differentiation from mRNA reprogrammed human induced pluripotent stem cells. PloS one. 2014;9:e103485.

[26] Wada T, Honda M, Minami I, Tooi N, Amagai Y, Nakatsuji N, et al. Highly efficient differentiation and enrichment of spinal motor neurons derived from human and monkey embryonic stem cells. PloS one. 2009;4:e6722.

[27] Love S, Louis D, Ellison DW. Greenfield's Neuropathology Eighth Edition 2-Volume Set: CRC Press; 2008.

[28] http://www.dreamstime.com/.

[29] Gaspard N, Vanderhaeghen P. From stem cells to neural networks: recent advances and perspectives for neurodevelopmental disorders. Developmental medicine and child neurology. 2011;53:13-7.

[30] Altmann CR, Brivanlou AH. Neural patterning in the vertebrate embryo. International review of cytology. 2001;203:447-82.

[31] Levine AJ, Brivanlou AH. Proposal of a model of mammalian neural induction. Developmental biology. 2007;308:247-56.

[32] Chambers I, Tomlinson SR. The transcriptional foundation of pluripotency. Development. 2009;136:2311-22.

[33] Swistowski A, Peng J, Liu Q, Mali P, Rao MS, Cheng L, et al. Efficient generation of functional dopaminergic neurons from human induced pluripotent stem cells under defined conditions. Stem cells. 2010;28:1893-904.

[34] Doi D, Samata B, Katsukawa M, Kikuchi T, Morizane A, Ono Y, et al. Isolation of human induced pluripotent stem cell-derived dopaminergic progenitors by cell sorting for successful transplantation. Stem cell reports. 2014;2:337-50.

[35] Maroof AM, Keros S, Tyson JA, Ying SW, Ganat YM, Merkle FT, et al. Directed differentiation and functional maturation of cortical interneurons from human embryonic stem cells. Cell stem cell. 2013;12:559-72.

[36] Wonders CP, Anderson SA. The origin and specification of cortical interneurons. Nature reviews Neuroscience. 2006;7:687-96.

[37] Li XJ, Du ZW, Zarnowska ED, Pankratz M, Hansen LO, Pearce RA, et al. Specification of motoneurons from human embryonic stem cells. Nature biotechnology. 2005;23:215-21.

[38] Hu BY, Zhang SC. Differentiation of spinal motor neurons from pluripotent

human stem cells. Nature protocols. 2009;4:1295-304.

[39] Espuny-Camacho I, Michelsen KA, Gall D, Linaro D, Hasche A, Bonnefont J, et al. Pyramidal neurons derived from human pluripotent stem cells integrate efficiently into mouse brain circuits in vivo. Neuron. 2013;77:440-56.

[40] Denham M, Dottori M. Signals involved in neural differentiation of human embryonic stem cells. Neuro-Signals. 2009;17:234-41.

[41] Hester ME, Murtha MJ, Song S, Rao M, Miranda CJ, Meyer K, et al. Rapid and efficient generation of functional motor neurons from human pluripotent stem cells using gene delivered transcription factor codes. Molecular therapy. 2011;19:1905-12.

[42] Chambers SM, Fasano CA, Papapetrou EP, Tomishima M, Sadelain M, Studer L. Highly efficient neural conversion of human ES and iPS cells by dual inhibition of SMAD signaling. Nature biotechnology. 2009;27:275-80.

[43] Lian X, Bao X, Al-Ahmad A, Liu J, Wu Y, Dong W, et al. Efficient differentiation of human pluripotent stem cells to endothelial progenitors via small-molecule activation of Wnt signaling. Stem cell reports. 2014;3:804-16.

[44] Wilson HK, Canfield SG, Hjortness MK, Palecek SP, Shusta EV. Exploring the effects of cell seeding density on the differentiation of human pluripotent stem cells to brain microvascular endothelial cells. Fluids and Barriers of the CNS. 2015;12:13.

[45] Watanabe K, Kamiya D, Nishiyama A, Katayama T, Nozaki S, Kawasaki H, et al. Directed differentiation of telencephalic precursors from embryonic stem cells. Nature neuroscience. 2005;8:288-96.

[46] Zhang S-C, Wernig M, Duncan ID, Brüstle O, Thomson JA. In vitro differentiation of transplantable neural precursors from human embryonic stem cells. Nature biotechnology. 2001;19:1129-33.

[47] Balgude A, Yu X, Szymanski A, Bellamkonda R. Agarose gel stiffness determines rate of DRG neurite extension in 3D cultures. Biomaterials. 2001;22:1077-84.

[48] Tessier-Lavigne M, Goodman CS. The molecular biology of axon guidance. Science. 1996;274:1123-33.

Chapter 4

Isolation and culture of cancer cells

In this chapter, we present a study of isolation and culture of cancer cells. We first describe the development of a CTCs isolation technique by using conical shape holes and microfluidic device. The processing parameters such as flow rate and cell density are studied for different types of tumor cells. Cell culture is also performed after isolation to show the post-isolation capability of the proposed device. Afterward, clinical trials are performed and mechanical analysis is used to theoretically demonstrate the advantages of the conical shape holes of the filter and the microfluidic design. Finally, we describe a multi-well device for tumor spheroids formation. The performances of the culture with three different types of materials are compared, showing the suitability of agarose formed device. Then, we show the drug effects on the tumor spheroids formation.

4.1 Introduction

Cancer is one of the leading causes of mortality and every year it accounts for millions of deaths all over the world [1]. It has been proven that the early diagnosis of cancers is the key to against cancer diseases. Circulating tumor cells (CTCs) in the peripheral blood of cancer patients are promising biomarkers for cancer detection and diagnosis [2]. However, CTCs are extremely rare in the blood, which is about only 1~10 CTCs among 1 billion blood cells, leading to the main technical challenge to capture them [3]. To address this, efforts have been made by several research groups [4-8]. However, there are still problems influence the isolation process or the further analyze and have to be solved, such as write blood cells contamination, low cell viability after capture, low operation speed. After the CTCs isolation, the further culture of CTCs is significant for phenotypic and genotypic analyze of single CTC to understand in depth cancer metastasis.

On the other hand, as we know that malignant cells in neoplastic tissue, like healthy cells in normal tissue, are organized in complex 3D networks displaying nutrient and signal gradients, cell–cell contact, as well as cell–extracellular matrix (ECM) interactions [9]. Therefore, generating an organotypic model mimicking *in vivo* solid tumor tissue, such as 3D tumor spheroids, benefit for drug delivery, toxicity, and metabolism, compared to conventional 2D cultures, due to their more physiological cell–cell contact geometry, mass transport, and mechanical properties

[10, 11]. However, the available systems are mostly appropriate for small size spheroid formation, which cannot efficiently recapture the spheroid complexity of solid tumours. And to facilitate the diffusion of nutrients, drugs and other factors into the spheroid area, it is also important to form the 3D assays with the materials of high permeability [10].

4.2 CTCs capture

4.2.1 Device fabrication

Capture of CTCs from peripheral blood of cancer patients has major implications for metastatic detection and therapy analyses. Here we designed and fabricated a microfluidic device with the integration of a filter with conical-shaped microhole array and a micro-injector with cross-flow components for size dependent capture of tumor cells (shown as **Fig. 4.1**). During operation, A filter made of PEGDA with conical holes is sandwiched between two patterned PDMS layers and the sample was loaded from inlet 1 and collected from outlet 2, passing through the filter with a syringe pump for constant pulling speed.

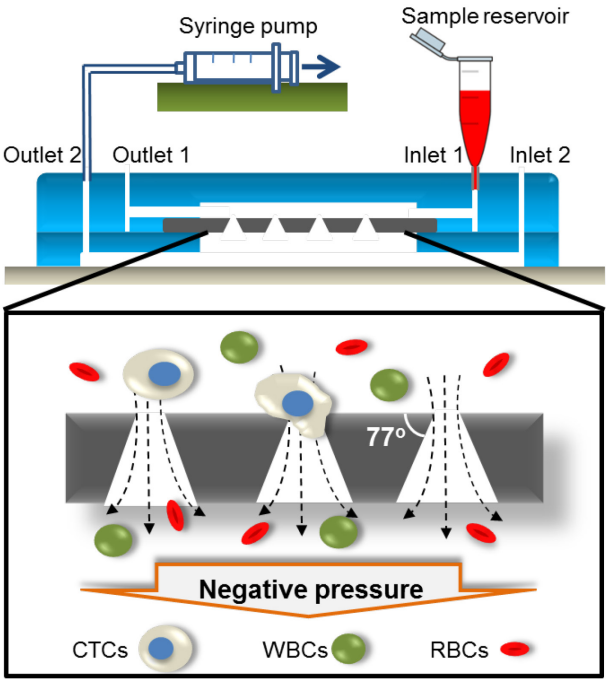

Fig. 4.1 Schematic of the experimental setup of microfluidic device with integrated conical-hole filter for capture of circulating tumor cells.

Both filter and microfluidic device were made of biocompatible materials (poly(ethylene glycol) diacrylate (PEGDA) and polydimethylsiloxane (PDMS), respectively) with rather standard fabrication processes. PDMS is now widely used for the fast prototyping of microfluidic devices whereas PEGDA can be easily functionalized to tune the protein or cell adhesion properties of the filter surfaces. Next we will give the details for the fabrication of PEGDA filter and the integration in microfluidic chips.

a) Fabrication of conical-hole microfilters

The fabrication procedure of PEGDA microfilter is shown in **Fig. 4.2**. It includes three main steps: PDMS mold generation, PEGDA micro-filter production and PEGDA ring mounting.

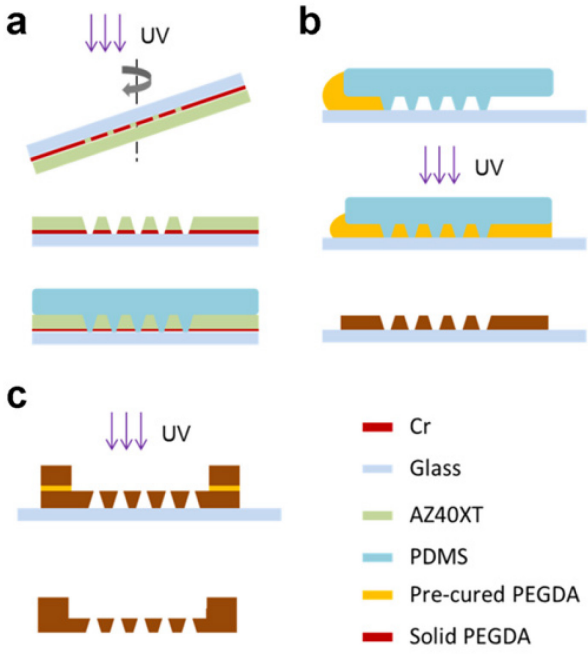

Fig. 4.2 Fabrication procedure of conical-hole filters. (a) Fabrication of PDMS mold with conical pillars; (b) Replication of PDMA pattern into PEGDA thin membrane, the same replication process is used for the fabrication of PEGDA ring; (c) UV assisted bonding of PEGDA membrane and ring.

a) PDMS mold generation by lithography

We designed a dots arrays of 5.5 or 6.5 or 8.0 μm diameter and 30 μm period by L-Edit software. Then a chromium mask of relevant holes arrays was produced by micro pattern generator (μPG 101, Heidelberg Instruments) with 40 mW and 60% energy followed with resist developing (AZ726MIF, 1 min) and 45 s chrome etching.

50 μm AZ40XT resist layer was spin-coated on the mask and prebaked following the sequence of 1 min at 65°C, 1 min at 95°C and 10 min at 126°C. After cooled down to room temperature, the mask was backside exposed with UV light (9.1 mW/cm^2) for 250 s at an incident angle of 20° (for a final of half conical angle of 13°) and a rotation speed of 3 rpm. Following with a post-bake (30 s at 65°C, 30 s at 95°C and 3 min at 105 °C), the mask was developed with AZ319MIF for 3 min. After development, conical holes of bottom and top diameters of 5.5, 6.5, 8.0 μm and 19.4, 20.4, 21.9 μm were obtained. After rinsing with DI water, the mask with patterned resist was dried with nitrogen gun.

Then the resist surface on mask was evaporated with TMCS for surface anti-sticking. A PDMS solution was prepared using GE RTV 615 PDMS components A and B at a ratio of 10:1 and then poured on the top of the resist master, followed with a curing process at 80°C for 2 h. The SEM photos of PDMS mold with conical shape pillars are shown as **Fig. 4.3**.

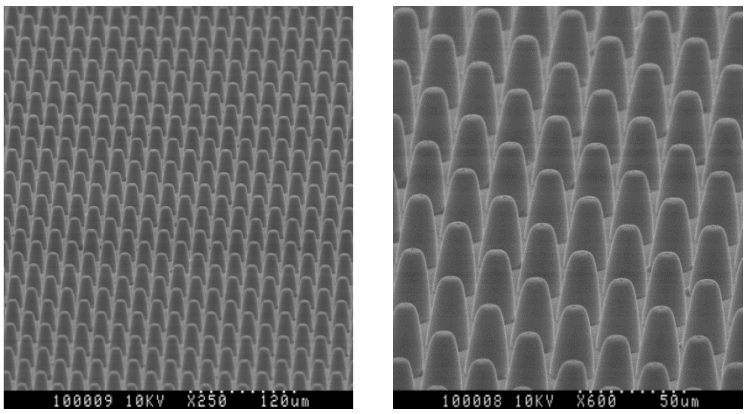

Fig. 4.3 SEM photos of PDMS mold with conical pillars.

b) PDMS aspiration-assisted molding for PEGDA filter

Then the solid PDMS mold layer with conical pillars was placed on a glass slide. The PDMS-glass assembly was placed in a desiccator for degassing for 15 min. Meanwhile, a PEGDA solution mixed with 1 v/v% 2-hydroxy-2

-methylpropiophenone (HOMPP) as photo-initiator was prepared protected from light and used to fill the PDMS-glass cavity by degassing induced micro-aspiration, followed by UV exposure at 9.1 mW/cm^2 for 30s. Finally, the solidified PEGDA filter was peeled off, resulting in a microfilter with conical holes and a porosity of 3.6%. **Fig. 4.4** shows the SEM photos of PEGDA filter with conical holes.

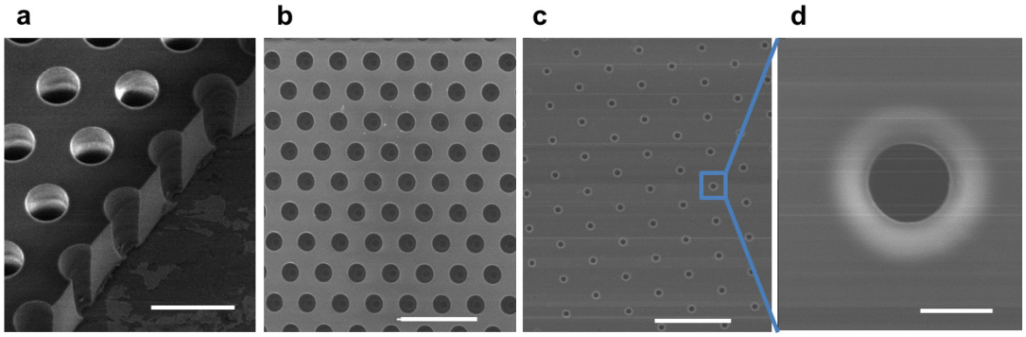

Fig. 4.4 SEM images of PEGDA filter with conical-hole array. (a) Cross section of a conical holes array; (b, c) Bottom and top view of SEM images of conical-hole array, respectively; (d) Top view SEM image of a single conical hole. Scale bar: (a) 40 μm (b, c) 100 μm (d) 5 μm.

c) PEGDA ring mounting

To increase the mechanical strength and handle the filter easily, 100 μm thick PEGDA rings of 13 mm outer diameter and 6 or 9 mm inner diameter were prepared in a similar manner. Briefly, a 100 μm thick SU8-3050 resist was exposed with a Cr mask defining the ring geometry. After development and trimethylchlorosilane (TMCS) evaporation, the PDMS mold was produced by soft lithography and placed on a glass slide. Then, the PEGDA solution was injected into the mold and solidified by UV exposure. Finally, the ring was mounted on the filter, using pre-cured PEGDA solution as binder for UV curing. For comparison, filters of cylindrical holes were obtained using UV lithography at normal incident angle without rotation. **Fig. 4.5** shows the photo of final PEGDA filter mounted with ring.

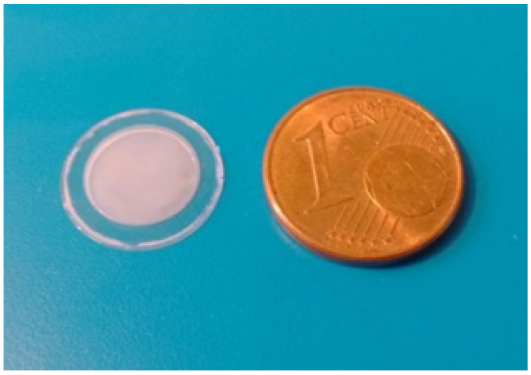

Fig. 4.5 Photograph of a 9 mm diameter PEGDA filter mounted with PEGDA ring aside a 1 cent euro coin.

b) Microfluidic device integration

The microfluidic chip for micro-filter integration was composed of two layers. The sample was loaded into the microfluidic device from the inlet of the top chamber (inlet 1) and collected from the outlet of the bottom chamber (outlet 2), passing through the microfilter sandwiched between the two structured PDMS layers. The layouts of the upper and bottom PDMS layers are shown in **Fig. 4.6**.

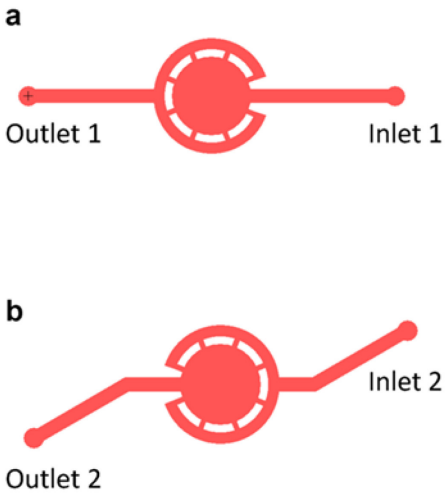

Fig. 4.6 Layout for the fabrication of upper (a) and bottom (b) PDMS layers.

Here the upper PDMS was produced by soft lithography with a mold fabricated by a CNC milling system. First, a two level pattern was produced on a PMMA plate. The first level is a cavity of 13 mm diameter and 130 µm in depth, designed for embedment of PEGDA filter. The second level includes a 6 mm or 9 mm chamber, 8

radial channels of 400 µm width, the inlet, the outlet and the ring channels of 1 mm width, all having a depth of 400 µm. After machining, the mold was ultrasonic washed with isopropanol. Then, the pattern was replicated twice into PDMS by soft lithography and both inlet and outlet holes were punched, resulting in the desired upper layer.

The bottom layer was fabricated by standard soft lithography with a mold fabricated by UV lithography. First, a chromium mask was produced by µPG 101 and then replicated into a 100 µm thick photoresist (SU8-3050, Micro resist). After development and evaporation of TMCS, PDMS was poured on the SU8 mold with a thickness of ~ 1 mm and cured at 80°C for 2 h. After peeling off, the main chamber of diameter of 6 mm or 9 mm was punched.

The surfaces of upper and bottom PDMS layers were treated by oxygen plasma shortly and the PEGDA filter was sandwiched between the two PDMS layer, following by a thermal bonding at 80°C for 30 min. Finally, the inlet and outlet of the bottom layer were punched and the PDMS-PEGDA assembly was irreversibly bonded to a glass slide after plasma treatment of the PDMS layer. **Fig. 4.7** shows a microfluidic device operating with blood sample.

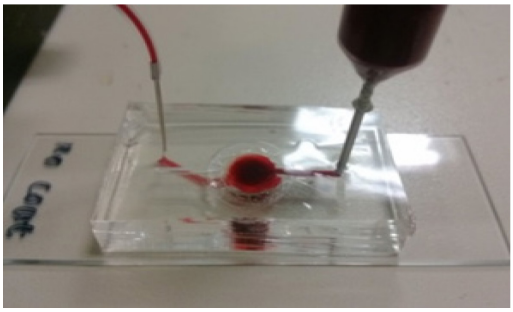

Fig. 4.7 Photograph of a microfluidic device operating with a test blood sample.

4.2.2 Experimental

a) CTC isolation process

Three cell lines (MCF-7, HT-29 and U87) were prepared in 10% FBS and 1% penicillin/streptomycin with their respective media, McCoy's 5A Modified Medium and Dulbecco's Modified Eagle Medium (DMEM) at 37°C with 5% CO_2 supplementation for 3-4 days. Prior to filtration tests, cells grown to confluence were

detached by Trypsin at 37°C for 3 min. After centrifugation at 1200 rpm for 5 min, cells were resuspended in PBS or PBS diluted healthy human blood (V_{PBS}:V_{blood}= 1:1) to the desired density. Human blood was collected from healthy donors in collection tube with EDTA to prevent coagulation and used within 24 h.

Before isolation, a metallic needle was mounted on the bottom of an Eppendorf tube and then inserted in the inlet of the upper layer of the device to facilitate injection. Before sample introduction, the device was rinsed with PBS first. Then, the sample was introduced from the Eppendorf tube by negative pressure generated with a syringe pump connected the outlet of the bottom layer. By varying the speed of the syringe pump, the flow rate of the sample across the filter could be controlled. After filtration of blood samples, the device was rinsed with 300 µl PBS once from inlet 1 to outlet 2 and once from inlet 2 to outlet 2 for more clear observation.

b) Immunostaining and microscopic imaging

The captured cells were fixed and treated inside the device. 4% paraformaldehyde (PFA) diluted in PBS at 10 µl/min for 15min was injected from inlet 1 to outlet 2, followed by PBS rinsing at 50 µl/min for 6 min. Similarly, 0.2% Triton X-100 in PBS was injected into the device at 10 µl/min for 10 min for permeabilization and 300 µl 1% BSA in PBS was introduced at 10 µl/min for 30 min to block out non-specific bindings. Afterwards, cells were stained with dye solutions (passing from inlet 1 to outlet 1). First, 600 µl immunostaining solution, containing 5 µg/ml Anti-Pan-cytokeratin (AE1/AE3) Alexa Fluor 488- (1:100 diluted in PBS; eBioscience SAS) and Anti-Human CD45 PE (1:20 diluted in PBS, eBioscience SAS, France), was injected at 10 µl/min for 1 h to stain tumor cells and WBCs, respectively. Then, the nucleus were stained by 4',6-diamidino-2-phenylindole (DAPI,100 nM, Life Technologies) at 10 µl/min for 10 min. Finally, the device was rinsed by 300 µl PBS for 6 min and fluorescence images were obtained with an inverted optical microscope (Zeiss, Axiovert 200) equipped with a digital CCD camera (Evolution QEI).

c) Cell culture after capture

A filter of 6.5 µm hole-diameter treated with Maxgel ECM mixture (1:25 diluted

in complete McCoy's 5A medium, Sigma-Aldrich) at 37°C for 1 h was used for culture test. After filtration of HT-29 cells spiked in PBS at a flow rate of 0.2 ml/min, the upper PDMS layer could be peeled off and the filter was took out gently and placed into a petri dish. 70 µl culture medium was dropped on the filter in the center of the ring and then incubated for 1h for cell attachment. Then, 1.5 ml medium was added gently around the ring for culture at 37°C in a 5% CO_2 incubator.

d) Cell viability assay

After 3 days culture of captured tumor cells on the filter, the viability of cells was studied by live/dead assay with LIVE/DEAD® viability/cytotoxicity kit (L-3224, Thermofisher Scientific). Briefly, 2 µM of Calcein AM and 2 µM EthD-1 in PBS was used to replace the culture medium for live and dead cell staining, respectively. After 30 min incubation at 37°C and 5% CO_2, fresh PBS was used to replace the staining solution. Cells were then observed and analyzed with a fluorescence microscope, as described above. Live cells were Calcein AM positive with green color, while dead cells were EthD-1 positive with red color. Cell viability was calculated by live cells number divided by total cells number.

e) Scanning electron microscopy observation

Samples were fixed in PBS containing 4% formaldehyde for 30 minutes. Then, they were rinsed twice with PBS buffer, and immersed in 30% ethanol (in DI) for 30 minutes. Afterward, the samples were dehydrated in a graded series of ethanol with concentrations of 50%, 70%, 80%, 90%, 95%, and 100%, respectively, each for 10 min and dried with a nitrogen gas flow. Before observation, a 2 nm thick gold layer was deposited on the samples by sputtering. The observation was performed with a scanning electron microscope (Hitachi S-800) operated at 10 kV.

f) Hydrodynamic simulation

Numerical simulation has been performed with commercial software (COMSOL Multiphysics). For simplicity, cylindrical- and conical-holes were replaced by a linear array of rectangular or trapezoidal slits, respectively, keeping the other

geometrical parameters as the same of two-dimensional filters (6.5 µm entrance size, 30 µm thickness, and 30 µm pitch size). The results were obtained with a transfilter pressure of 100 Pa and water viscosity of $\sim 1 \times 10^{-3} Pa.s$ without cells.

g) Definition of capture efficiency, purity and cell viability

The capture efficiency of the device for the targeting tumor cells was defined as the ratio of tumor cells found on the filter, n_c, to the initial tumor cells injected into the device, n_i,

$$TcCE = \frac{n_c}{n_i} \times 100\% \quad (1)$$

The capture purity of the device for the targeting tumor cells was defined as the ratio of tumor cells found on the filter, n_c, and the total number of cells found on the filter, $n_c + n_{wbc}$,

$$TcCP = \frac{n_c}{n_c + n_{wbc}} \times 100\% \quad (2)$$

where n_{wbc} is the number WBCs found on the filter.

The cell viability of the tumor cells captured by the filter was defined as the ratio of live tumor cells, n_{cl}, and dead tumor cells n_{cd}, both being found on the filter

$$TcCP = \frac{n_{cl}}{n_{cl} + n_{cd}} \times 100\% \quad (3)$$

4.2.3 Results

a) Cancer cell capture

We fabricated 30 µm thick PEGDA filter with 30 µm pitch conical holes at constant angle of 13°. For comparison, filters with conical holes of three different entrance diameters (5.5, 6.5 and 8.0 µm) were produced over an area of disk of two different diameters (6 and 9 mm). For demonstration, HT-29 cancer cells were spiked in a diluted blood sample of a healthy person at concentration of 10^3 cells/ml and the filtration experiments were performed with a filter of 6.5 µm conical holes at a constant flow rate, controlled with a syringe pump at a constant pulling speed. As results, we recovered the most of the spiked HT-29 cells on the filter with a limited number of normal blood cells (**Fig. 4.8**). Here, fluorescence images were recorded

after immunostaining (green for CK positive, red for CD45 positive, blue for nuclei of all cells). By counting the total cell number injected into the device and those of CK and CD45 positive for tumor cells and leukocytes respectively on the filter, we obtained a capture efficiency of ~95% and a capture purity of ~86%.

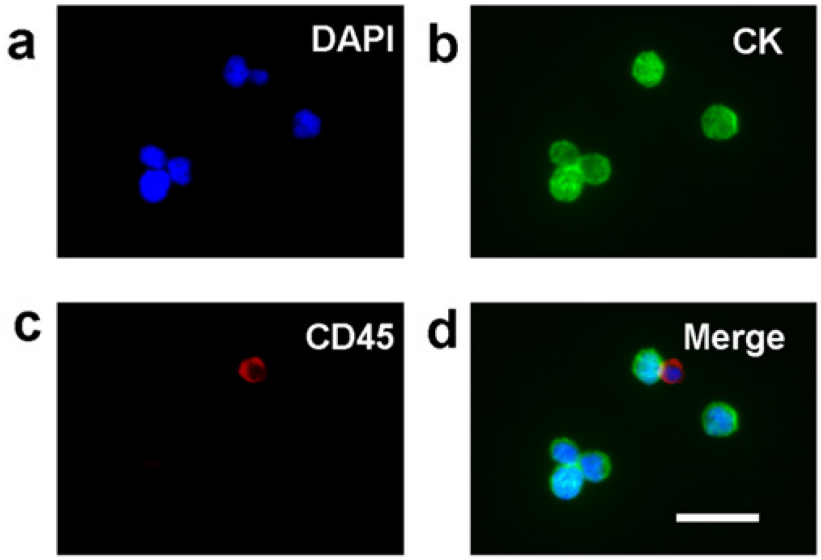

Fig. 4.8 HT-29 cells on the surface of a filter. (a-c) Fluorescence images of HT-29 cells and WBCs stained with anti-CK-AlexaFluor 488 (green) and anti-CD45-PE (red), respectively. Nuclei were stained in blue with DAPI. Here HT-29 cells were spiked in a blood sample and the filtration was done with a filter of 6.5 µm hole diameter. (d) Merged image of (a), (b) and (c). Scale bar: (a-d) 30 µm.

b) Validation with clinical samples

Blood samples donated by 14 cancer patients and 6 healthy donors were used to test the potential clinical relevance of the device. The volume of each blood sample was 2 ml. Without red blood cells lysing, we diluted all samples in PBS at a volume ratio of 1:2 before filtration. The filtration experiments were performed with a filter of 6.5 µm conical holes at a flow rate of 0.2 ml/min. After filtration and immunostaining, fluorescence images of the cells captured on the filters were recorded (green for CK positive, red for CD45 positive, blue for nuclei of all cells). **Fig. 4.9** shows one example of the fluorescence images obtained with the blood sample of a lung cancer patient. Again, both cancer cells ($DAPI^+/CK^+/CD45^-$) and white blood cells (WBCs, $DAPI^+/CK^-/CD45^+$) were captured, validating the

feasibility of CTC capture by using our device.

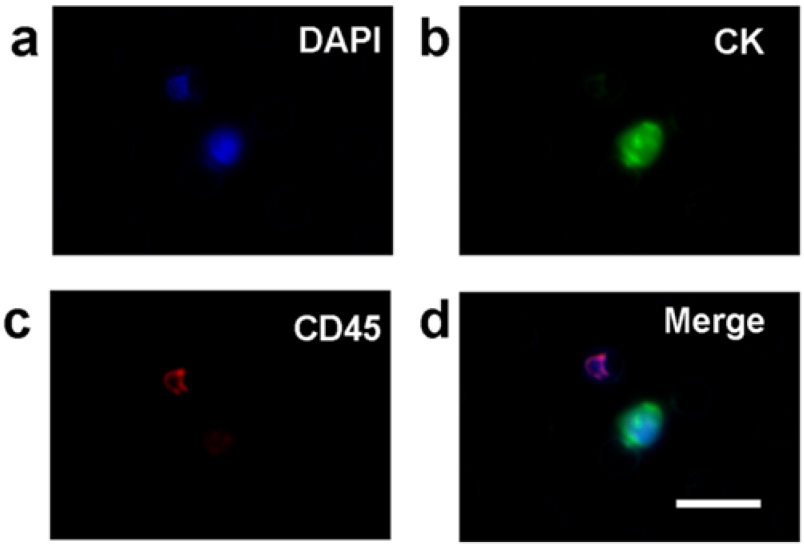

Fig. 4.9 CTCs of a cancer patient. (a) Fluorescence Nucleus staining with DAPI (blue). (c, b) Fluorescence of a CTC after staining with anti-CK-AlexaFluor 488 (green) and anti-CD45-PE (red), respectively. (d) Merge image of (a-c). Scale bar: 30 μm.

Statistically, CTCs could be detected in the blood samples of a large portion of cancer patients but not in that of healthy donors (shown as **Table 4.1**). Among 14 blood samples of the cancer patients, only 5 did not show up the CTC signature, due probably to the limited volume of our blood samples. Previously, it has been reported that even with 7.5 ml blood samples of cancer patients, no CTC could be detected in some samples [12]. Similar to the capture of cancer cells spiked in blood samples, only a limited number (a few of hundreds) of WBCs were found on the surface of the filter (**Fig. 4.10**), which made easy the fluorescence imaging and enumeration of CTCs. In addition to the cancer cells and WBCs, some other types of cells which are neither CK nor CD45 positive may show up, but their presence did not affect the detection of CTCs. More systematic analyses will be conducted for a more detailed clinical validation of the device.

Table 4.1 Validation of the method with clinical samples. CTC enumeration after filtration with 2 ml blood samples diluted in PBS at a volume ratio of 1:2.

	Blood sample	CTC number
Healthy donors	1#	0
	2#	0
	3#	0
	4#	0
	5#	0
	6#	0
Lung cancer	7#	2
	8#	1
	9#	4
	10#	0
	11#	2
	12#	6
	13#	2
	14#	0
Nasopharynx cancer	15#	1
	16#	0
Mediastinal tumor	17#	1
	18#	2
Cardia cancer	19#	1
Cervical cancer	20#	0
Breast cancer	21#	0

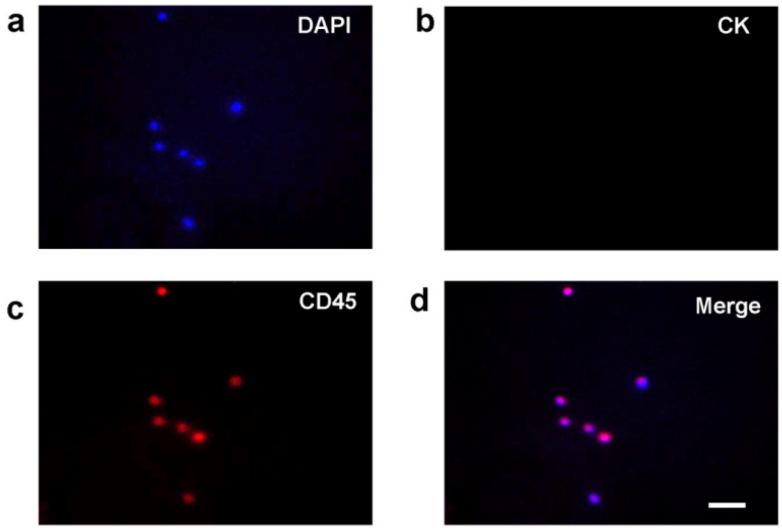

Fig. 4.10 Fluorescence images of WBCs of a healthy donor on the filter. (a) Fluorescence of nuclei staining with DAPI (blue). (c, b) Fluorescence of after staining with anti-CK-AlexaFluor 488 (green) and anti-CD45-PE (red), respectively. (d) Merge image of (a-c). Scale bar: (a-d) 30 μm.

c) Flow rate and cell density dependencies

To quantitatively evaluate the performance of the method, experiments were performed with HT-29 cells spiked in PBS at a concentration of 5×10^4 cells/ml. After filtration, cells were stained by DAPI and CK, showing a clear coincidence of these two types of fluorescence (shown as **Fig. 4.11**).

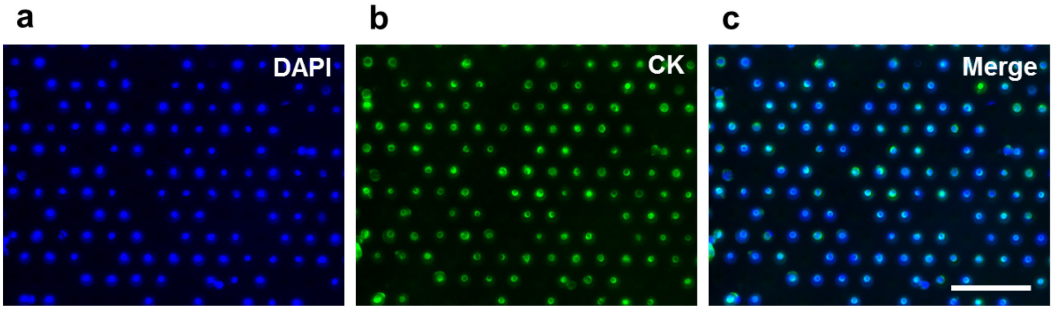

Fig. 4.11 Fluorescence images of tumor cells on the filter. (a) HT-29 cell nuclei are stained with DAPI (blue). (b) HT-29 cells were stained with anti-CK-AlexaFluor 488 (green). (c) Merged image of (a) and (b). The tumor cells were spiked in PBS at a 104 cells/ml concentration of. Scale bar: 100μm.

The flow rate dependency of the cell capture efficiency was studied by using

HT-29 cells spiked into PBS at 100 cells/ml concentration. In the range of flow investigation (0.2~2.0 ml/min with filters of 6.5 μm holes diameter and 6 mm diameter filter area), we observed an increase of the capture efficiency with the decrease of the flow rate (**Fig. 4.12**). A further increase of the capture efficiency (>95%) was possible with a smaller flow rate. For the same capture efficiency (95%), the flow rate was increased by a factor of 2.25 when the 6 mm diameter filter was replaced by the 9 mm diameter filter, which corresponds to a decrease of the filtration time from 18 min to 8 min for a 6 ml sample.

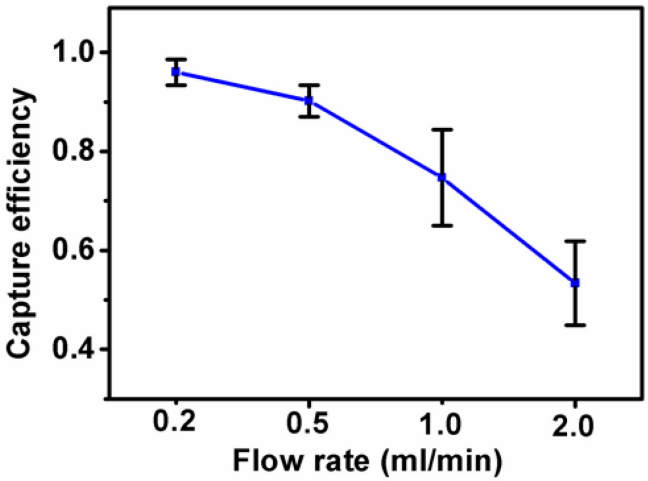

Fig. 4.12 Capture efficiency as a function of flow rate. The error bars represent the standard derivation (s.d.) of three measurements.

Similarly, we evaluated the cell density dependency of the capture efficiency (**Fig. 4.13**) by enumerating cell on the 6 mm diameter filter after immunostaining. As expected, the capture efficiency of our device is almost the same for different cell densities due to the fact that the number of captured cell (10~100) is much less than the number of the holes of the filter (~10^4) and there should be no change of the pressure across the filter under given experimental conditions.

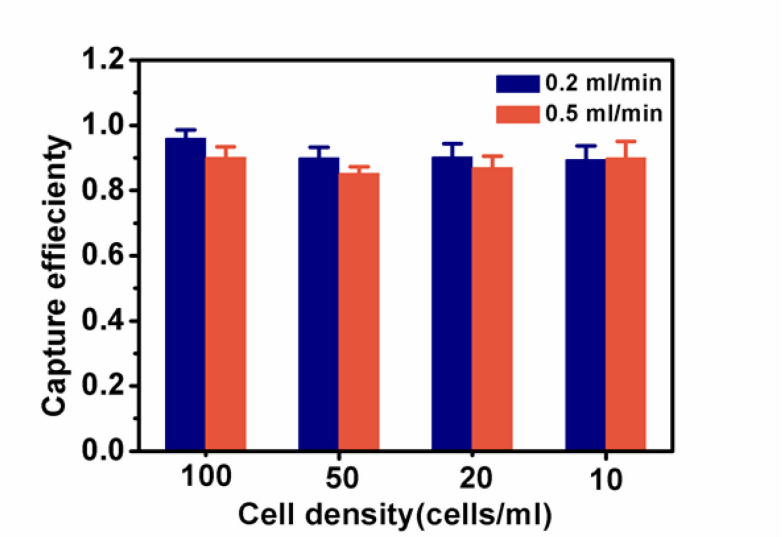

Fig. 4.13 Capture efficiency of 10, 20, 50, 100 HT-29 cells spiked in 1 ml PBS at a flow rate of 0.2 or 0.5 ml/min, respectively. The error bars represent the standard derivation (s.d.) of three measurements.

d) Cell type and hole size dependencies

To assess the reliability of our device for different tumor cell types, the capture efficiency has been evaluated for three cell lines (MCF-7, HT-29 and U87), each spiked in PBS at a 100 cells/ml concentration and injected into the device at a flow rate of 0.2 or 0.5 ml/min. Not surprisingly, remarkable differences of the capture efficiency could be observed due to the size differences of these tumor cells (**Fig. 4.14**). Here, three types of filters of different hole diameters (5.5, 6.5, 8.0 μm) were used, which also allowed us to evaluate the hole size dependency of the capture efficiency. Clearly, the smaller the hole size, the higher the capture efficiency. Using the filters of 5.5 μm diameter holes, a capture efficiency of 98%, 96% and 85% could be achieved for MCF-7, HT-29 and U87, respectively. Increasing the hole size from 5.5 μm to 6.5 μm has negligible effect on the capture of MCF-7 but the filter of 8.0 μm diameter holes resulted in a much decreased capture efficiency, suggesting an optimal size (~6.5 μm) of conical holes for MCF-7 capture. The filters of 6.5 μm diameter holes could also be accepted for HT-29 capture but filters of 5.5 μm in diameter or smaller is preferable for U87 capture.

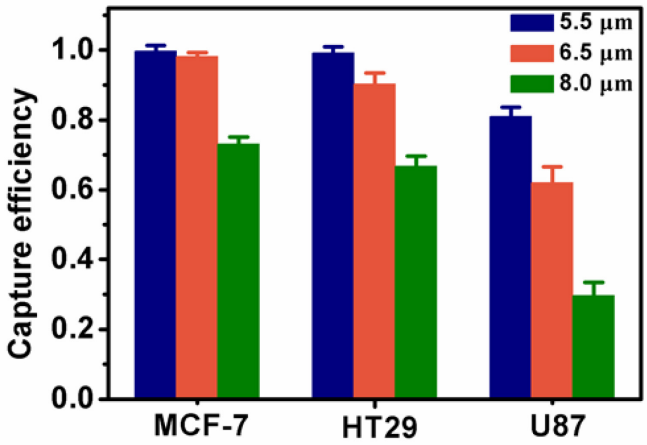

Fig. 4.14 Cell-type dependency of capture with filter of different hole sizes at a flow rate of 0.5 ml/min. The error bars represent the standard derivation (s.d.) of three measurements.

To understand the observed cell type dependencies of micro-hole capture, the size of each cell type and their nuclei were determined (**Fig. 4.15**) by analyzing the bright field images of suspended cells and the fluorescence of the cell nuclei stained with 0.5 µg/ml Hoechst 33342 in a suspension of cells in PBS. As expected, MCF-7 has the largest size of cell body and nuclei, giving rise to the best capture efficiency for the given hole size of the filter (6.5 µm). U87 and HT-29 have comparable cell sizes, but U87 has much smaller nuclei, which led to capture efficiency significantly lower than that of HT-29 using the same filter of 6.5 µm hole diameters. Since the nuclei are much more difficult to deform than the cytoplasm, the entrance diameter of conical holes for filtration should be correlated to the size of corresponding nucleus rather than the size of the cell.

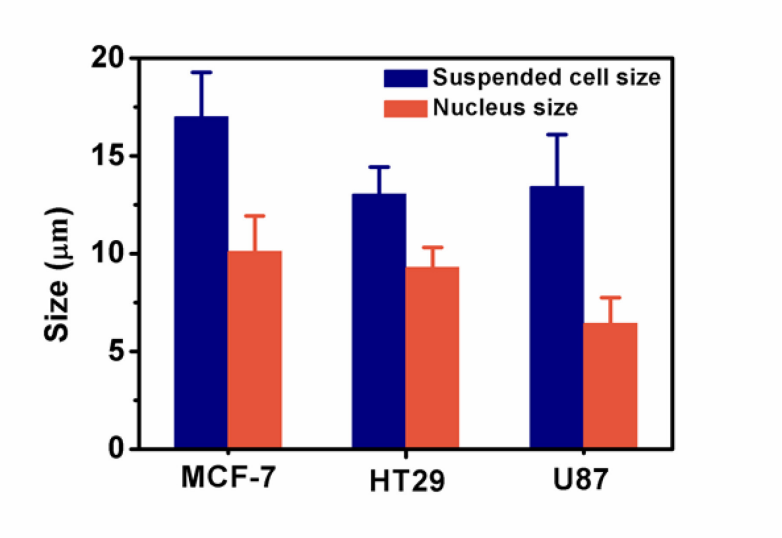

Fig. 4.15 Cell and nuclei sizes measured with a suspension of cells stained by Hoechest33342. The error bars represent the standard derivation (s.d.) of three measurements.

e) Cell viability assessment

We took SEM photos of tumor cells captured on filter after one hour (**Fig. 4.16**). From the photos, there were a lot of tentacle-like pseudopodia prolongation shown as the yellow arrows, which means cells started to adhere on the filter for proliferation and migration.

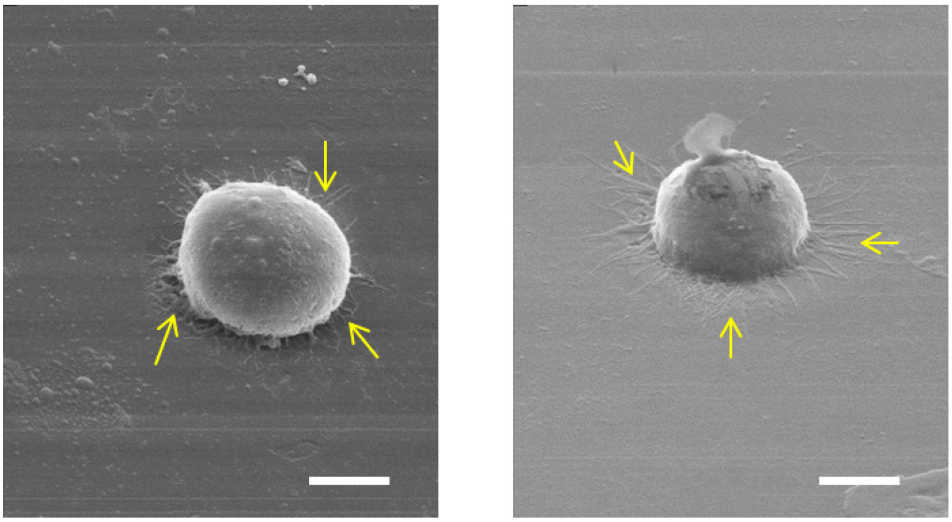

Fig. 4.16 SEM photos of captured tumor cells after one hour (scale bar: 5 μm).

HT29 cells spiked in PBS were used to evaluate the cell viability after filtration with 6.5 μm conical-hole filters. In total, about 90% cells could be captured for 10^4 injected cells. Calcein AM and EthD-1 were used to stain live and dead cells respectively, indicating that more than 95% of captured HT-29 cells were alive. Cell culture was tested with the same filter after filtration (**Fig. 4.17a and b**).

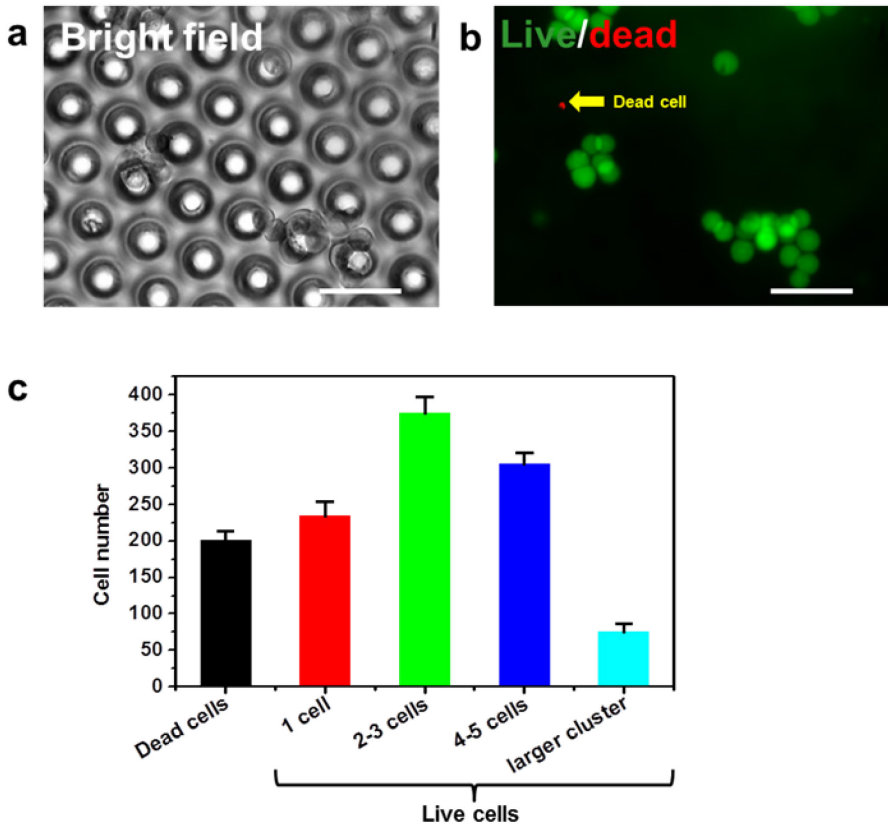

Fig. 4.17 Cell culture and viability test. (a) Bright field image of cells on the PEGDA filter after capture and culture for 3 days. (b) Immunostaining fluorescence of HT-29 cells after Calcein AM/EthD-1staining. (c) Statistic data of cell number per cluster at day 4. Scale bar: (a) and (b) 50 μm. The error bars represent the s.d. of three times of counting with a number of randomly selected areas.

After 3 days, live cells localized on the surface of the filter formed cell clusters due to growth (**Fig. 4.17c**). As can be seen, most of the clusters have a cell number less than 6, due probably to the single cell proliferation initially captured on the filter at different places. Considering a doubling time of ~23 h, not all captured cells are capable to expand. Some of cells need time for adaptation or repairing, some others could be lost during culture medium exchange, etc. Among the larger clusters, half

have more than 8 cells per cluster, which is due probably to the capture of more than one cell in close proximity to each other.

4.2.4 Discussion

We put forward the novel design of the filter with high density conical holes to achieve the best compromise between the capture efficiency, purity and viability of CTCs. In general, the capture efficiency of CTCs increases with the decrease of the hole-size but a too much small hole size will lead to poor capture purity because of the accumulation of undesired blood cells on the filter. The optimal hole-size preventing the loss of precious cells should be comparable or smaller than the nuclei size of the CTCs, which can also be smaller or overlap with the size of erythrocytes. Considering however the fact that the shapes of erythrocytes can be extensively changed under the influence of mechanical forces in a flow or restraint area of circulation, erythrocytes may easily penetrate into the hole under influence of applied transfilter pressure. The question is how erythrocytes escape from the hole. The red blood cells (RBCs) are non-nucleated cells in form of disks of 6.2~8.2 μm diameters and 0.8~2.5 μm thickness. Although abundant, they can pass quickly through microholes of comparable sizes. WBCs have comparable or larger sizes. Once penetrated, their retention depends mainly on the transfilter pressure which cannot be large for high viability of captured CTCS, the interaction with hole wall and the shape of the hole. To illustrate the advantage of using conical holes, we consider a model of soft particles squeezed in two types of holes (cylindrical and conical) with the same size at the entrance. In simplified geometries shown in **Fig. 4.18**, one can relate the built-up pressure to the surface tension of the particle according to Laplace's law,

$$\Delta P = 2\gamma\left(\frac{1}{R_1} - \frac{1}{R_2}\right)$$

(1)

where γ is the surface tension, R_1 and R_2 are respectively the radius of the curvature of the tailing and leading edges of the particle. Thus, $\Delta P = 0$ for cylindrical holes and $\Delta P > 0$ for conical holes because of the difference between the two curvatures. With a surface tension[47] of ~3.0×10^{-5} N/m and a radius of curvature of tailing and leading edge R_1=3.25 μm and R_2=$2R_1$, respectively, ΔP ~ 9.2 Pa. Although this built-up pressure is rather small, it may efficient stimulate WBCs to escape the conical holes,

suggesting a better clearance of the conical-hole filter than that of the cylindrical ones.

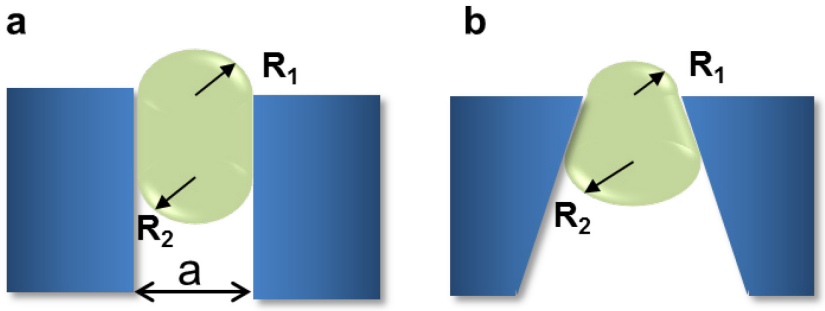

Fig. 4.18 Schematic of cell retention in a cylindrical (a) and conical hole (b): Cells squeezed in two filter types can have different built up pressure due to the difference in surface tension of their leading and tailing edges.

For comparison, our model was tested by performing capture of tumor cells under the same experimental conditions but using the two types of filtration holes. HT-29 cells were spiked into blood samples and then loaded into the devices at a flow rate of 0.2 ml/min. After capture and immunostaining, we deduced a capture efficiency of 96% (98%) and a capture purity of 86% (39%) with a conical (cylindrical) hole filter (**Fig. 4.19**). As expected, the capture efficiencies of both filters were pretty high but much more WBCs were found on the filter of cylindrical holes (**Fig. 4.20**). The retention of WBCs and other blood cells may have other side effects such aggregation due to the release of clogging factors from the deformed or lysed cells, making the cylindrical-hole clearance more difficult and thus increasing the transfilter pressure which is undesirable for a constant-flow filtration.

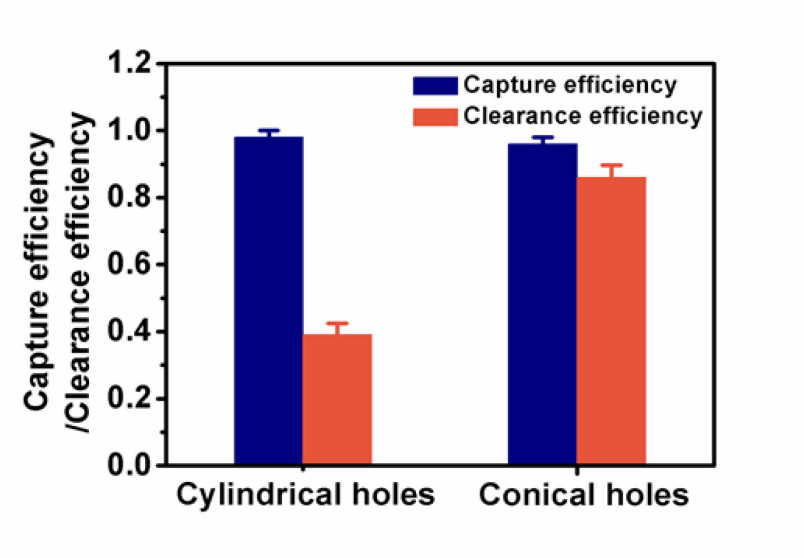

Fig. 4.19 Comparison of cylindrical- and conical-hole filters on the capture efficiency and purity of tumor cells at a flow rate of 0.2 ml/min. The error bars represent the S.D. of three measurements.

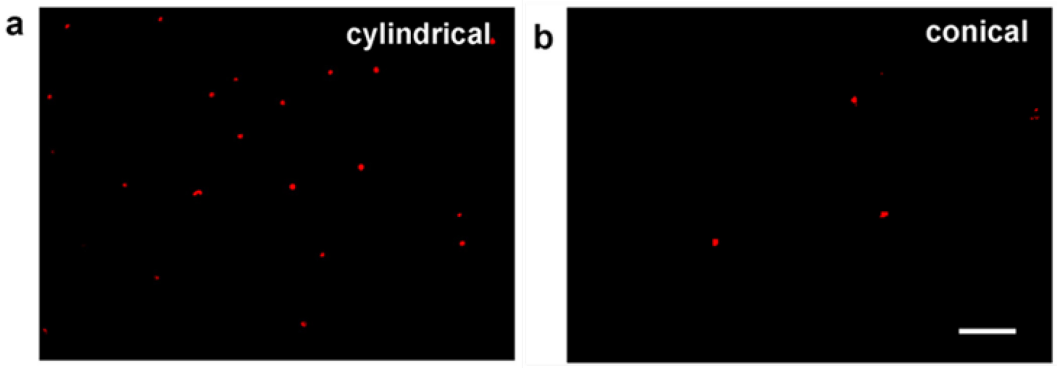

Fig. 4.20 Fluorescence images of WBCs on the filter. Blood samples of a healthy person were diluted in PBS at 1:1 (v/v%). After filtration and anti-CD45 staining, fluorescence images were taken, showing a much reduced WBC retention by conical holes (a) than cylindrical ones (b). Scale bar: 100 μm.

The cell viability is one of the most critical issues in current research of CTC capture since living cells can be expanded and needed for downstream phenotypic and genotypic analyses. In principle, a low transfilter pressure should be applied during filtration to avoid the stress induced cellular damage. In our experiments, the transfilter pressure was controlled by the flow rate with a syringe pump. Consider a non-Newtonian fluid through a cylindrical hole at a constant flow rate, the trans filter

pressure can be calculated by [13]

$$\Delta P = \frac{3\eta Q}{a^3}\left[1 + \frac{8L}{3\pi a}\right] \quad (2)$$

where a is the hole radius and L is the thickness of the hole, η the viscosity and Q the flow rate of the liquid. For given a, η and Q, ΔP increases with L.

In the case of conical holes, the calculation is more complex. In the limit of very large aperture angles, the thickness of the hole can be considered as infinitely small so that a minimal transfilter pressure is obtained. For the filter composed by an array of holes, the transfilter pressure should be inversely proportional to the number of holes. In our case, the number of holes in a 6 (9) mm diameter filter is 3.6×104 (8.2×104), which is huge comparing to the number of tumor cells that can be captured. With a flow rate of 0.2 ml/min and a blood sample of viscosity of $3\sim4\times10^{-3}$ Pa·s, we obtained a transfilter pressure of 213~284 (95~126) Pa for a 30 μm thick cylindrical-hole filter of 6 (9) mm diameter. In the case of conical holes with very large angles, the thickness of the filter can be considered to be very small (L~0). Accordingly, we obtained a transfilter pressure of 24~32 (10~14) Pa, which is one order of magnitude lower than that obtained with the 30 μm thick cylindrical-hole filter. Such a decrease of transfilter pressure can lead to a significant increase of the cell viability [5, 14-16], proving again the advantage of conical-hole filters. Moreover, such a small transfilter pressure will remain the same during filtration if the clearance of the filter is efficient. Note also that the small transfilter pressure resulting from the flow rate we applied should be significantly smaller than the stiffness of the most of tumor cells, which guarantees high cell viability during and after filtration. As expected, the most of captured tumor cells were immobilized in the hole area but on the surface of the filter due to the small size of the hole and the low transfilter pressure (**Fig. 4.21**).

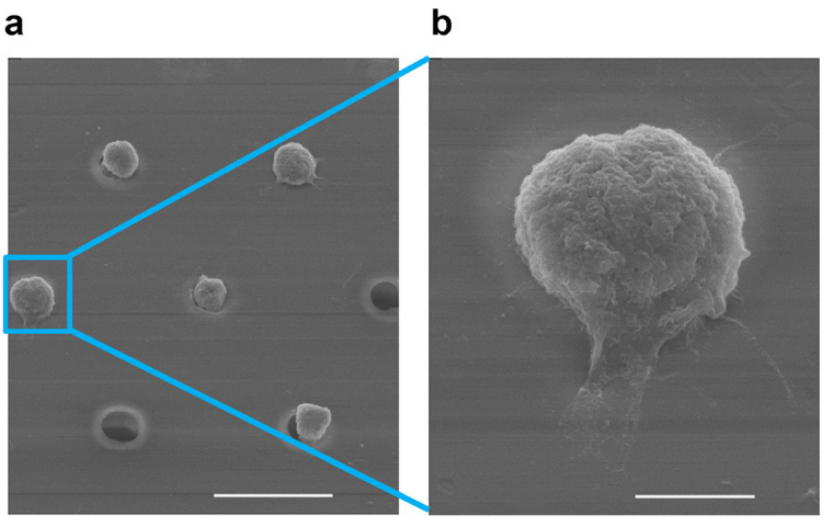

Fig. 4.21 SEM image of tumor cells on the filter. HT-29 cells were spiked in PBS at a 10^4 cells/ml concentration. After filtration, cells were fixed by dehydration and coated by 2nm thick gold. Scale bar: 100µm.

Finally, numeric simulation has been performed to compare the flow dynamics with the two types of filters using simplified geometry and boundary conditions (**Fig. 4.22**). The results show that for the same transfilter pressure the flow rate across the conical holes is significantly larger than that across the cylindrical ones. In other words, under conditions of constant flow rate, the transfilter pressure of the conical holes should be significantly smaller than that of cylindrical ones, in agreement with the above analyses. Streamlines are also shown, illustrating a flow focusing effect, i.e., no flow goes to the areas at equidistance of neighboring holes. These results also show a clearly flow focusing effect, suggesting the necessity of introducing a cross-flow component to flush gently away the cells accidently deposed on the surface of dead areas at equidistance of neighboring holes to void clogging of blood cells. In our devices, this has been done by designing a number of radial channels connected between the inlet channel and the upper chamber. Effectively, this design which is different from the previous ones allowed us to gain in capture purity of tumor cells. Nevertheless, this cross flow component should also be small enough to avoid additional flow stress. For a flow rate of 0.2 ml/min and a filter of 6.5 µm holes and 9 µm diameter, the maximum value of induced shear stress is ~ 8 Pa for a cell size of 15 µm diameter, which is reasonably small to avoid the cell damage but sufficient to flush away the non-adherent cells. Note also that once a tumor cell is captured by a hole the flow can bypass this cell, reducing further the pressure and/or shear stress induced cell

damage.

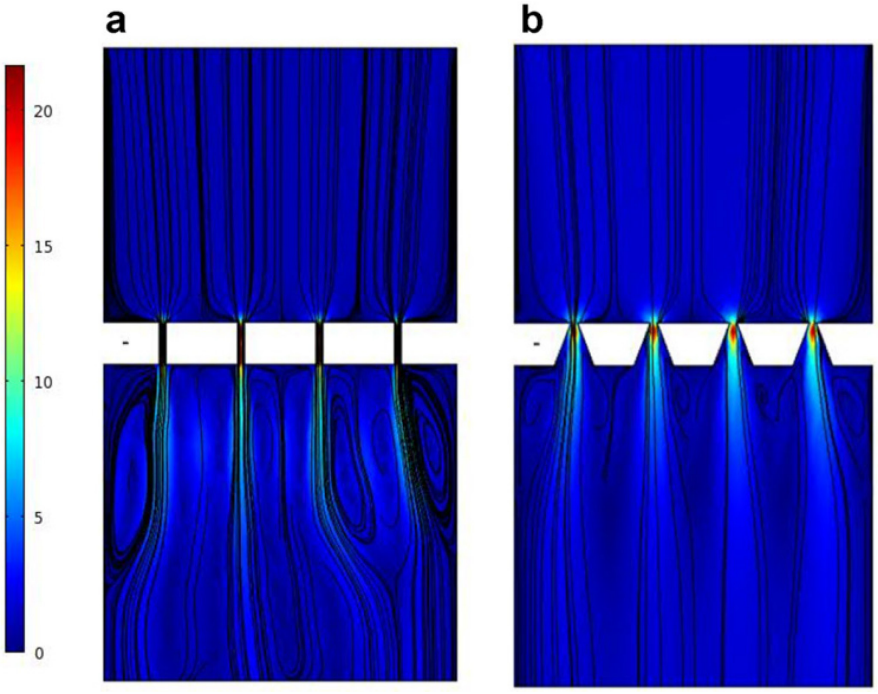

Fig. 4.22 Hydrodynamic simulation of flow focusing. The same transfilter pressure (100 Pa) were applied, showing both flow focusing but a higher flow rate through trapezoidal slits than through rectangular ones.

4.3 Tumor spheroids formation

4.3.1 Device fabrication

Fig. 4.23 shows the schematic process flow of multi-well array fabrication. A flat PDMS film of 2 mm thickness was prepared by casting a mixture of PDMS pre-polymer and cross-linker (GE RTV 615) at ratio of 10:1 on a silicon wafer. After curing at 80°C for 1 h, the PDMS layer was peeled-off and an array of holes was created on the PDMS layer using a computer numeric controlled (CNC) milling machine and a biopsy punch of 2 mm diameter. Afterward, the PDMS layer was exposed in trimethylchlorosilane (TMCS) vapour for 1 min. This PDMS layer with holes was then used as master to cast a second layer of PDMS with posts. After curing at 80℃ for 2 h, the second PDMS layer was peeled off.

The agarose multi-well arrays were produced by using the second layer PDMS as mold. A solution of 5% agarose in DI water was dissolved at 120°C for 5 min and

then immediately casted on the PDMS mold. After cooling down to room temperature and waiting for 10 min, a solid agarose layer was obtained by gelatinization. Then, the agarose layer was gently removed from the PDMS mold, resulting in a multi-well device for spheroid culture.

For comparison, PDMS multi-well arrays were prepared similarly, while PEGDA multi-well arrays was produced by UV assisted casting with a PEGDA (average M_n=250) solution mixed with 1 v/v% Irgacure 2959 as photo-initiator.

Prior to cell seeding, all multi-well devices were sterilized by UV irradiation and then equilibrated with culture medium for at least 15 min.

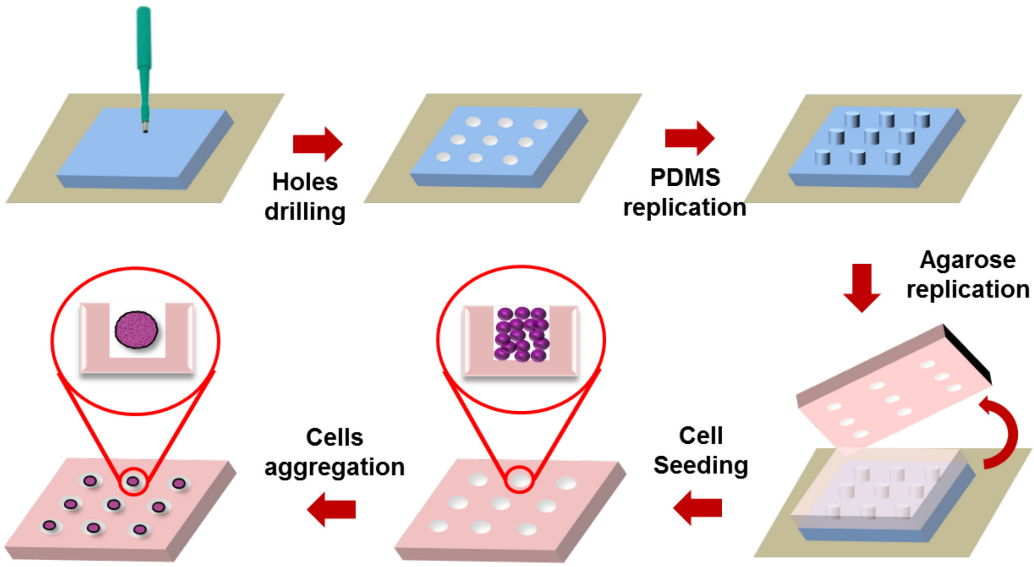

Fig. 4.23 Schematic fabrication process flow of agarose multi-well arrays and tumor spheroid formation.

4.3.2 Experimental

a) Cell seeding and tumor spheroid formation

Here we chose human glioblastoma cell line U-87 for tumor spheroid studies. U-87 cells were prepared in Dulbecco's Modified Eagle Medium (DMEM) completed with 10% FBS and 1% penicillin/streptomycin at 37°C with 5% CO_2 supplementation for 3~4 days. After proliferated to confluence, cells were detached by Trypsin at 37 °C for 3 min and centrifuged before re-suspended in a culture medium at a density of 5×10^6 or 10^7 cells/ml. The multi-well devices were placed in

a culture dish and each well of the device was then filled with 50 μl cell containing medium. After 15 min incubation for cells settling inside the wells, 2 ml more medium was added gently around the device. Finally, the culture dish with the multi-well device was transferred into incubator. After 24 h incubation, tumor spheroids can be observed in each well.

b) Drug test and live/dead assay

At day 2 or day 4, the old culture medium was changed with new culture medium contained with 10^{-7} M anti-cancer drug Combretastatin A4 (CA4). After another 2 days, apoptotic cells can be observed around cancer spheroids.

Cell viability was studied by live/dead assay. Briefly, PBS solution with 2 μM of Calcein AM and 2 μM EthD-1 was used to change the medium for live and dead cell staining, respectively. After 30 min incubation at 37°C and 5% CO_2, fresh PBS was used to wash out the residual dyes for 2 times. Stained cell spheroids were transferred on a glass slide for fluorescence observation with an inverted optical microscope (Zeiss, Axiovert 200) equipped with a digital CCD camera (Evolution QEI).

4.3.3 Results and discussions

a) Materials comparisons of multi-wells

Fig. 4.24 shows the microphotographs of tumor spheroids formed in multi-wells made of PDMS, PEGDA and agarose. After 2 days, spheroid shaped cell aggregates could be found in all three types of wells. As can be observed, no cell attached on the agarose well but a large number of cells attached on PDMS both inside and outside the well (indicated by red arrows), due to the different surface properties. More interestingly, the spheroid in PDMS well is likely composed by three smaller aggregates, suggesting strong attachment to the surface of each of them during the growth phase. In PEGDA well, a flatten spheroid was observed, together with some spread cells on the board of the well. And due to the worse optical transparency of PEGDA, it's difficult to observe the tumor spheroids clearly by microscope. Agarose, a typical hydrogel, is low-cost, transparent and not toxic to cells [17]. The quite

smooth and hydrophilic surface, as well as the highly soft nature of agarose makes the well not adhesive to cells, which results a much easier cell aggregation than other two types of wells. More interestingly, agarose is permeable to gas and small biomolecules, which facilitate diffusion of nutrients, drug and other cell factors. Therefore, agarose was chosen as an ideal material of multi-wells for tumor spheroid generation and spheroid culture under physiological conditions.

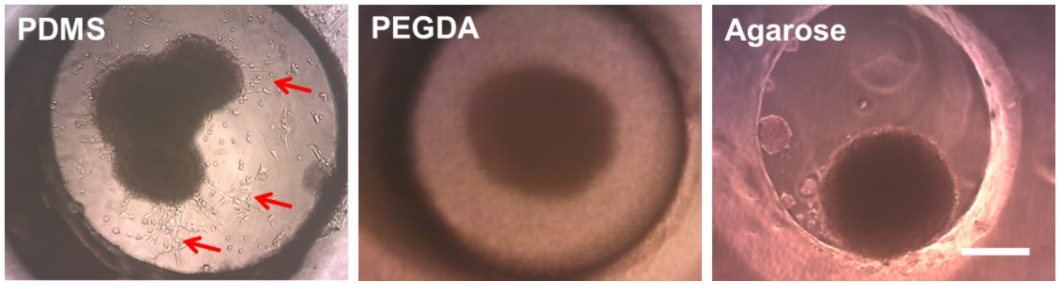

Fig. 4.24 Microphotographs of tumor spheroids in multi-wells made of PDMS, PEGDA and agarose, respectively. Scale bar: 0.5 mm.

b) Generation and growth of tumor spheroids in agarose wells

Fig. 4.25 shows the growth of tumor spheroid in agarose wells. As expected, tumor cells aggregated first in the well and then formed compact spheroids. Afterwards, the spheroid grew until day 10 due to cell proliferation. After 10 days, the size of the spheroid remained almost the same (about 1.4 mm). Interestingly, the size of the spheroid decreases during the first 4 days. This decrease can probably be attributed to the sharp change from hemisphere-like aggregation to spheroid and the compact of cells due to strong cell-cell interaction. It is also interesting to note that increasing the cell seeding density has no effect on the final size of the spheroid which was always about 1.4 mm, due probably to the limitation of diffusion length. In fact, when the size of the spheroid becomes too large, there will be no sufficient nutrient diffused to the center area. The spheroid can be considered as a self-organized entity in which the proliferation of cells should be strongly affected or regulated by cell-cell interaction in the whole entity. More details analyses have to be developed for further studies.

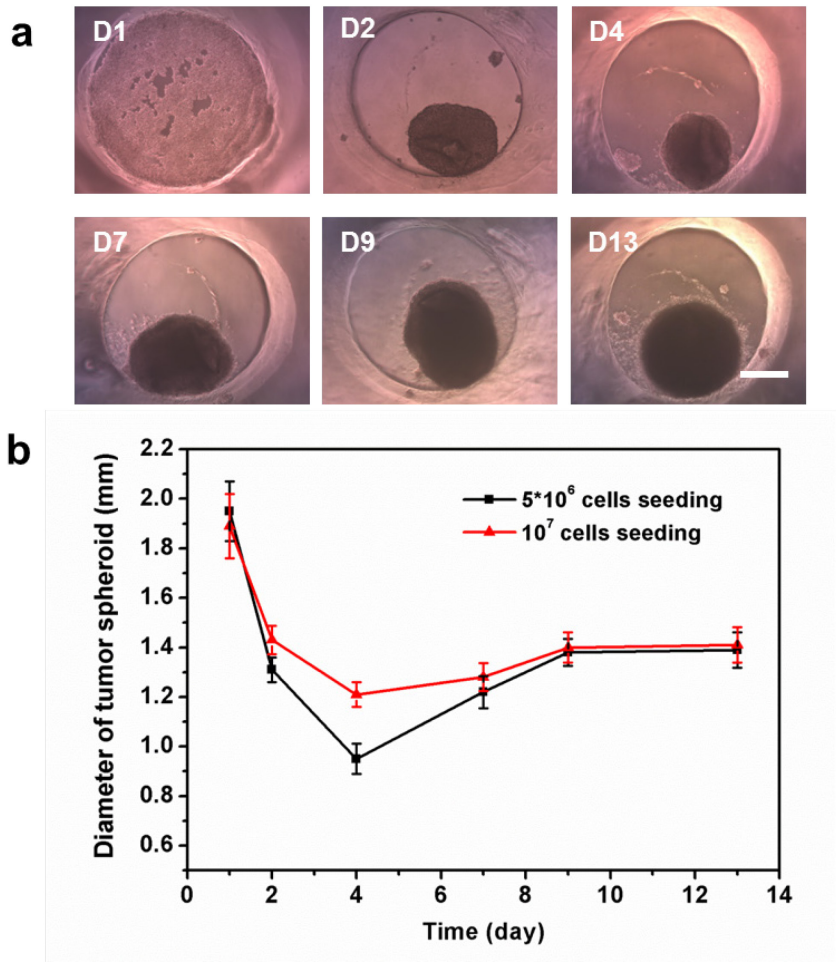

Fig. 4.25 (a) Tumor spheroid formation in an agarose well at different time; scale bar: 0.5 mm; (b) Size variation of the spheroid as a function of time.

c) Combretastatin A-4 effects on tumor spheroids growth

To study the anticancer drug effect, CA4 was added in the medium at day 4, which is a stilbene inhibits tubulin polymerization at the colchicine-binding site of tubulin and high cytotoxic against a variety of human cancer cells including some multidrug resistant cancer cell lines [18, 19]. As expected, the spheroid stopped to grow and some of the cells were detached from the spheroid (**Fig. 4.26**). The live/dead cell staining images showed that in the culture medium with the drug, many cells were dead after three days drug treatment, whereas no matter at day 4 or day 7, almost all cells were alive in the medium without CA4. But for the different time of addition drug, there was difference on drug effect. From the live/dead staining results, for drug adding at day 2, there were dead cells on both the area next to the edge and the central area of the spheroid after three days, but for drug adding

at day 4, there were fewer dead cells compared to earlier drug adding, which were mainly distributed only on the edge area of the spheroid at day 7. In the process of the tumor spheroid growth, beginning from single separated cells, cells keep aggregation until day 4, shown as **Fig. 4.26**. It means that when the drug was added at day 2, the tumor spheroid was not organization enough, which will let drug penetrate into the center of spheroid to effect on the cells, whereas for drug added at day 4, the tumor sphere was compact and became a self-organized entity, it will be more difficult for drug to effect in the center of spheroid. It has also been reported that these cell–cell contacts and ensuing communication in closely packed 3D cell structures can influence the response of cells to drugs [20, 21].

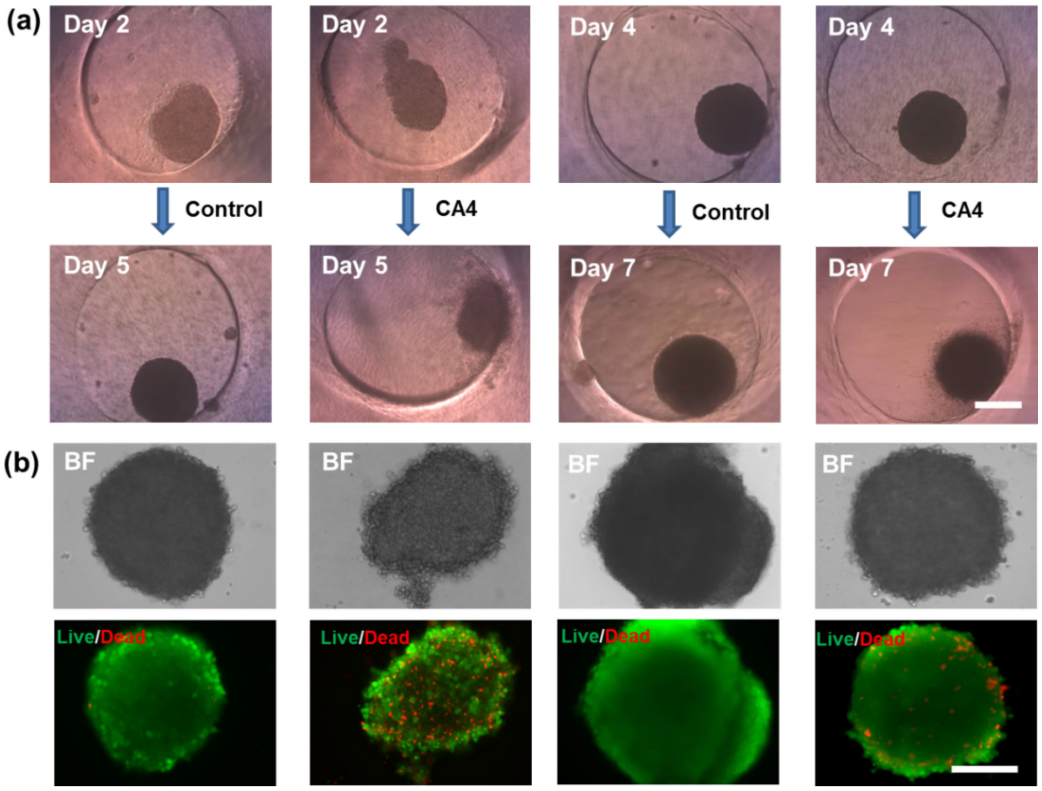

Fig. 4.26 Effect of anticancer drug CA4 on the morphology of tumor spheroids and cell viability. (a) Morphology change of the tumor spheroid with or without CA4 adding for drug added at day 2 and day 4 respectively. Scale bar: 0.5 mm. (b) Bright field and live/dead cell staining microphotographs of the spheroid after 3 days with or without CA4 treatment added at day 2 and day4 respectively. Scale bar: 0.5 mm.

4.5 Conclusion

In conclusion, we developed a microfluidic device with a conical-shaped microhole array and a micro-injector with cross-flow components for CTCs isolation. This device was first validated by filtration of tumor cells spiked in blood and then used for detection of CTCs in blood samples of cancer patients. Furthermore, three tumor cell lines were tested with microhole arrays of different hole-sizes, showing a clear cell-type dependency of the capture efficiency and suggesting a (cell) nuclei size dependent design of microholes. As results, we achieved a capture efficiency of ~95% and a capture purity of ~86%, respectively. Finally, tumor cells after filtration were cultured on the same filter for several days, showing a cell viability of ~95%, thereby providing a solid base for downstream phenotypic and genotypic analyses. Together with the simplicity of the method and the possibility to integrate other microfluidic functions into the same device, more systematic studies are warranted to elucidate the underlying cellular and molecular mechanism of CTCs and to promote the clinical relevance of current efforts on microfluidics.

On the other hand, we also developed a simple but reliable technique for tumour spheroids formation by using agarose multi-wells. In 2 mm diameter agarose wells, 1.4 mm diameter U87 tumour spheroids can be formed and cultured for many days. Interestingly, the size of the tumour spheroids does not change with the further increase of seeding cell density. Anti-cancer drug CA4 added at different stages of tumour spheroid formation have different drug effect. More systematic studies are expected for more clear and mechanistic understanding of spheroid formation and anti-cancer drug effect on tumors.

References

[1] Jemal A, Bray F, Center MM, Ferlay J, Ward E, Forman D. Global cancer statistics. CA: a cancer journal for clinicians. 2011;61:69-90.

[2] Yu M, Stott S, Toner M, Maheswaran S, Haber DA. Circulating tumor cells: approaches to isolation and characterization. The Journal of cell biology. 2011;192:373-82.

[3] Fischer AH. Circulating tumor cells: seeing is believing. Archives of Pathology & Laboratory Medicine. 2009;133:1367-9.

[4] Yusa A, Toneri M, Masuda T, Ito S, Yamamoto S, Okochi M, et al. Development of a new rapid isolation device for circulating tumor cells (CTCs) using 3D palladium filter and its application for genetic analysis. PloS one. 2014;9:e88821.

[5] Harouaka RA, Nisic M, Zheng S-Y. Circulating tumor cell enrichment based on physical properties. Journal of laboratory automation. 2013;18:455-68.

[6] Hosokawa M, Hayata T, Fukuda Y, Arakaki A, Yoshino T, Tanaka T, et al. Size-selective microcavity array for rapid and efficient detection of circulating tumor cells. Analytical chemistry. 2010;82:6629-35.

[7] Hou HW, Warkiani ME, Khoo BL, Li ZR, Soo RA, Tan DS, et al. Isolation and retrieval of circulating tumor cells using centrifugal forces. Scientific reports. 2013;3:1259.

[8] Hur SC, Mach AJ, Di Carlo D. High-throughput size-based rare cell enrichment using microscale vortices. Biomicrofluidics. 2011;5:022206.

[9] Kelm JM, Timmins NE, Brown CJ, Fussenegger M, Nielsen LK. Method for generation of homogeneous multicellular tumor spheroids applicable to a wide variety of cell types. Biotechnology and bioengineering. 2003;83:173-80.

[10] Mehta G, Hsiao AY, Ingram M, Luker GD, Takayama S. Opportunities and challenges for use of tumor spheroids as models to test drug delivery and efficacy. Journal of controlled release : official journal of the Controlled Release Society. 2012;164:192-204.

[11] Haycock JW. 3D cell culture: a review of current approaches and techniques. 3D Cell Culture: Springer; 2011. p. 1-15.

[12] Hosokawa M, Kenmotsu H, Koh Y, Yoshino T, Yoshikawa T, Naito T, et al. Size-based isolation of circulating tumor cells in lung cancer patients using a microcavity array system. PloS one. 2013;8:e67466.

[13] Holdich R, Kosvintsev S, Cumming I, Zhdanov S. Pore design and engineering for filters and membranes. Philosophical Transactions of the Royal Society of London A: Mathematical, Physical and Engineering Sciences. 2006;364:161-74.

[14] Lim C, Zhou E, Quek S. Mechanical models for living cells—a review. Journal of biomechanics. 2006;39:195-216.

[15] Kuo JS, Zhao Y, Schiro PG, Ng L, Lim DS, Shelby JP, et al. Deformability considerations in filtration of biological cells. Lab on a chip. 2010;10:837-42.

[16] Harouaka RA, Zhou M-D, Yeh Y-T, Khan WJ, Das A, Liu X, et al. Flexible micro spring array device for high-throughput enrichment of viable circulating tumor cells. Clinical chemistry. 2014;60:323-33.

[17] Dahlmann J, Kensah G, Kempf H, Skvorc D, Gawol A, Elliott DA, et al. The use of agarose microwells for scalable embryoid body formation and cardiac differentiation of human and murine pluripotent stem cells. Biomaterials. 2013;34:2463-71.

[18] Liou J-P, Chang Y-L, Kuo F-M, Chang C-W, Tseng H-Y, Wang C-C, et al. Concise synthesis and structure-activity relationships of combretastatin A-4 analogues, 1-aroylindoles and 3-aroylindoles, as novel classes of potent antitubulin agents. Journal of medicinal chemistry. 2004;47:4247-57.

[19] Sanna VK, Jaggi M, Kumar V, Burman AC. Evaluation of 5-hydroxy-2,3-diaryl (substituted)-cyclopent-2-en-1-ones as cis-restricted analogues of combretastatin A-4 as novel anti angiogenic and anticancer agents. Investigational new drugs. 2010;28:363-80.

[20] Olive PL, Durand RE. Detection of hypoxic cells in a murine tumour with the use of the comet assay. Journal of the National Cancer Institute. 1992;84:707-11.

[21] Oloumi A, Lam W, Banath J, Olive P. Identification of genes differentially expressed in V79 cells grown as multicell spheroids. International journal of radiation biology. 2002;78:483-92.

Chapter 5

Conclusion and Perspective

This thesis work aimed at development of new devices and new methods for biomedical research, drug testing, regenerative medicine and disease diagnosis. Induced pluripotent stem cells and cancer cells have been chosen for demonstration of the high potential of our microengineering approaches.

Firstly, we demonstrated a patch form made of monolayer gelatin nanofiber on biodegradable PEGDA micro-frame, to provide off-ground culture conditions and tools for easy handling that can be used for various downstream analyses and implantation. As expected, we found a significant improvement of the proliferation rate of normal mammalian cells, comparing to that cultured conventionally. When used for human induced pluripotent stem cells (hiPSCs) culture, we could be able to tune precisely the shape of hiPSC colonies (from monolayer to hemisphere EBs), which is desired for the proliferation of hiPSCs. The hemisphere EBs had comparable pluripotency to the traditional cultured iPSCs. The generated hemisphere EBs on patch were then differentiated into cardiomyocytes by modulating Wnt signaling with small molecules. ~74.7% of differentiation efficiency was obtained on the nanofiber patch compared to ~34.5% of traditional 2D differentiation. RT-PCR results indicated that cardiomyocytes cells derived on PEGDA supported nanofiber substrate showed also higher cardiac related gene expression. This cardiac patch can be easily handled and transferred into multi-electrode array (MEA) system for cardiac drug test by field potential monitoring. The derived cardiac sheet showed corresponding reaction to different drugs and different drug dose, which indicated the cardiomyocytes derived on nanofiber patch, had a good functional performance. Similarly, we did also motor neuron differentiation of hiPSCs on this patch, which performed an enhanced differentiation efficiency compared to on glass slides. And after comparison of motor neuron differentiation from monolayer iPSC colony and hemisphere EBs on nanofiber patch, we found a much better differentiation efficiency of monolayer differentiation. After achieving motor neuron progenitors at day 16, the progenitor cells were digested off from patch and reseeded on different substrates for maturation. At day 38, neuron representative electrical signals and firing were detected for neuron patch; however no signal detected for the motor neurons reseeded on MEA until day 50, which revealed that the off-ground neuron culture system with nanofiber net can enhance motor neuron maturation.

Secondly, our work for cancer cell study is composed of two parts: cancer diagnosis and *in vitro* tumor model building. On one hand, for cancer diagnosis, we

demonstrated a microfluidic device for high efficiency and high purity capture of circulating tumor cells (CTCs). The key novelty of this approach lies on the integration of a filter with conical-shaped microhole array and a micro-injector with cross-flow components for size dependent capture of tumor cells without significant retention of non-tumor cells. First, this device was validated by filtration of tumor cells spiked in blood and then used for detection of CTCs in blood samples of cancer patients. Additionally, three tumor cell lines were tested with microhole arrays of different hole-sizes, showing a clear cell-type dependence of the capture efficiency and suggesting a (cell) nuclei size dependent design of microholes. As results, we achieved a capture efficiency of ~95% and a capture purity of ~86%, respectively. Then, tumor cells after filtration were cultured on the same filter for several days, showing a cell viability of ~95%, thereby providing a solid base for downstream phenotypic and genotypic analyses. Then more systematic studies are warranted to elucidate the underlying cellular and molecular mechanism of CTCs. Together with the advantage of easy operation, low-cost and high potential of functional integration, this approach offers unprecedented opportunities for metastatic detection and cancer treatment monitoring. On the other hand, for *in vitro* tumor model building, multicellular tumor spheroid has been proved to be a promising method. In this work, we developed a simple but reliable technique for the fabrication of multi-well array for tumor spheroids formation. After comparison of different materials for the multi-wells, agarose was found to be the best material. In 2 mm diameter agarose wells, 1.4 mm diameter U87 tumor spheroids can be formed and cultured for many days. Interestingly, the size of the tumor spheroids does not change with the further increase of seeding cell density. Anti-cancer drug CA4 added at different stages of tumor spheroid formation have different drug effect. More systematic studies are expected for more clear and mechanistic understanding of spheroid formation and anti-cancer drug effect on tumors.

To conclude this thesis work, we have successfully demonstrated several microdevices for advanced study in cell biology and biomedical research. Accordingly, the microengineering techniques developed in this work should allow gaining new knowledges in this interdisciplinary and emerging field. We believe that the results we obtained in this work could contribute to the progress of micro-engineered devices and that much more can be done along this promising research direction.

Though this thesis work is limited to proof-of-concept, we believe in the high application potential of our approaches, as discussed below.

Nanofiber patch for iPSCs studies:

Our findings suggest that this new type of monolayer nanofiber culture substrate can be used not only for off-ground culture but also for a variety of cell-based assays and *in vivo* evaluation, due to the versatility and the flexibility offered by the patch form of the stadium. It can also be used for drug assays which minimize the animal models since the tissue formed on monolayer nanofibers can more accurately simulate normal cell morphology, proliferation, differentiation and migrations, as compared to the conventional cell culture. To this regard, it is important to note that although different animal models, including murine and non-human primates could be used to evaluate the effect of hiPSCs but in many cases it is not relevant to translate animal data into clinical assays due to their clear differences (ex. the beating rate and timing of maturation). Thus, the proposed patch can also be used to study personal disease models since hiPSCs have also high potential to model different disease states by using hiPSCs issued from patients.

Besides, this patch is very easy to be integrated into microfluidic device (such as the similar device for CTCs capture), meanwhile, the pluripotency of iPSCs provides diversity of cell types. Both of these advantages make the further organ-on-chip study possible, for more flexible and accurate studying the physiological and pathophysiological processes in living organs, and operating drug screening and assessment.

Due to the flexibility of this patch, it will be also a promising tool for tissue engineering and regeneration medicines. It can be very simple to replace PEGDA to other biodegradable materials, such as poly(lactic-co-glycolic acid) (PLGA). Although gelatin is already a natural biomaterial, which can be biodegraded *in vivo*, it's also very simple to change it to other materials case by case, such as collagen. After *in vitro* specific differentiation of iPSCs, the whole cell patch will be very flexible for *in vivo* transplantations and therapy.

The iPSCs proliferation and differentiation are both sophisticated and complex. For example, the manipulator has to change medium every day during the iPSC proliferation and various mediums have to be prepared every one or two days during

the iPSC differentiation. In addition, the processes of iPSCs proliferation and differentiation are often non-producible due to lot-to-lot variation as well as uncertainly of human factors. Thus, it is highly desirable to develop automatic culture and differentiation systems, together with the nanofiber patches or other advanced stem cell devices. Most recently, a prototype system has been proposed along this direction, as shown in **Fig. 5.1**. **Fig. 5.1a** is a medium storage container with temperature controlling system. There is also a UV sterilization system inside the container (**Fig.5.1b**). The six-well plate can be settled on the culture platform (**Fig.5.1c**) and then transferred into incubator during culture. For the medium changing during the culture and differentiation, the program can be pre-set on the control panel. The next step will be a systematic evaluation of the proposed apparatus and then push it for large scale applications by creating a dedicated startup company.

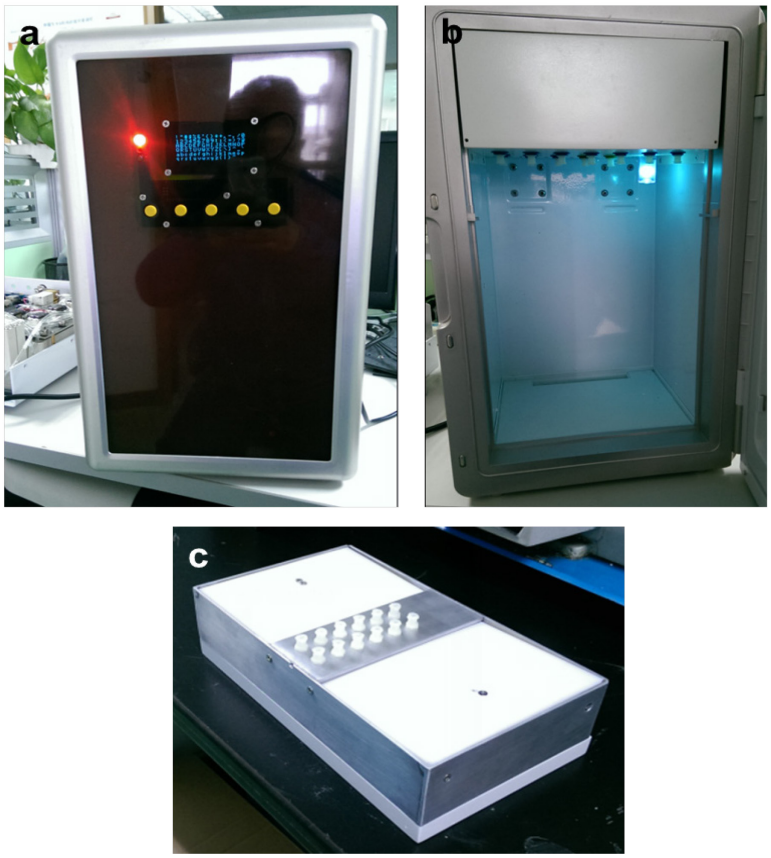

Fig. 5.1 Automatic culture and differentiation system. (a) Medium container; (b) Inside chamber of container during UV sterilization; (c) Culture platform with two positions for 6-well plate.

CTCs isolation related studies:

For more careful and systematic studies of CTC isolation as well as post-CTC isolation and/or clinic applications, automatic systems and standard protocols have to be proposed. In collaboration with other partners, the ENS Laboratory for Microfluidics has also been worked along this direction. A prototype of automatic isolation and staining has been proposed, shown as in **Fig. 5.2**. Here, two plastic layers with cross-flow microfluidic channels (**Fig. 5.2a**) can be fixed separately in the top and bottom part of a steel holder or clamp (**Fig. 5.2b**). The conical filter for CTCs isolation can then be inserted between the two plastic layers by nut screw fixation. The sealing of the filter is achieved with two elastomer layers pre-mounted on the two plastic layers. Then, the filtration (and immunostaining process) can be performed in an automatic way with the prototype apparatus (**Fig. 5.2c**). After processing, the filter with cells can be moved away from the device for microscopic observation and/or down-stream analyses.

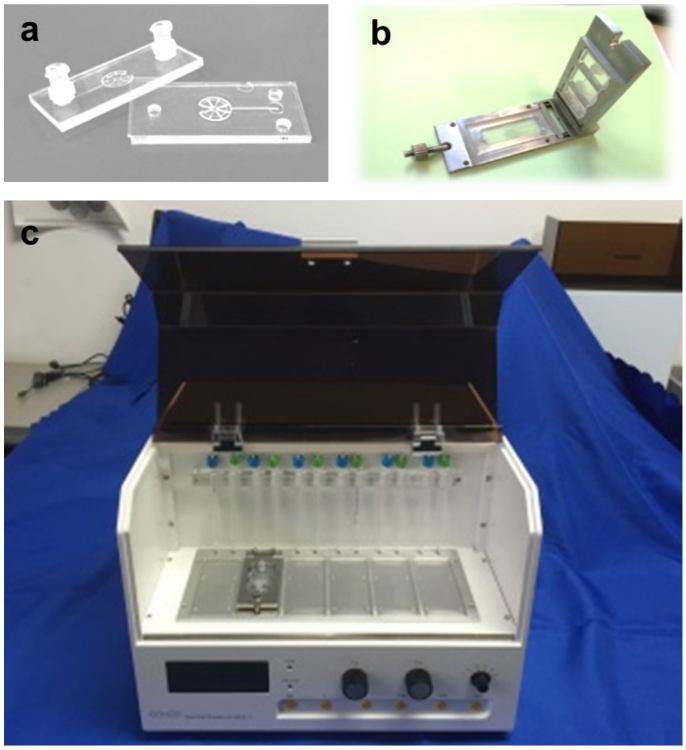

Fig. 5.2 Commercial CTCs detection products and equipment. (a) mass produced microfluidic chip; (b) Steel holder for chip; (c) CTCs detection equipment.

CTCs enumeration is significant for cancer diagnosis, in practice, numbers alone

correlate with outcomes, as in the case of breast cancer, where greater than 5 CTCs in 7.5 ml of blood is indicative of clinical progression [1]. However besides CTCs detection, we expect to get beyond simple enumeration, thus there are a lot of further downstream studies we can do with the captured CTCs.

Unlike other antibody affinity-based capture methods, the CTCs captured by our device are capable for further molecular biological analyze. First, the isolated CTCs provide researchers another route for biomarker discovery. In oncology, such work usually relies on archival tumor tissue, but often samples aren't available, as in the case of inoperable cancers, or where biopsies are difficult to obtain [2]. CTCs offer a noninvasive way for samples collection. Besides, CTCs can provide to researchers an update of what mutations are driving the cancer. Researcher can study the genetic mutation and molecular cytogenetic profile and understand in depth epithelial mesenchymal transition (EMT) during metastasis by immunological and molecular studies, such as fluorescence in situ hybridization (FISH) analysis.

On the other hand, the CTCs captured with our device show good viability and which were also cultured successfully after isolation, making it possible for monitoring the biological response of a tumor or treatment, and evaluation of its resistance to therapies. Since the most present therapy and drugs can kill the primary tumor to some extent, while the main problem sabotaged conquering cancer is to prevent metastasis efficiently. On this point, CTC is also useful tool for the development of novel drugs specialized metastasis, while efficient control of metastasis will largely prolong the survival time of patient and decrease cancer death, which is promising for cancer curing.

Tumor spheroids formation related studies:

We have demonstrated an agarose multi-well array for tumor spheroids formation and also preliminarily tested the effect of anti-cancer drug CA4. Many interesting studies can be done by using such as device. For example, one can observe the inner structure of the tumor organoids and then compare it with the layered structure of the *in vivo* spheroids [3]. Accordingly, one can also follow the spheroids formation under drug treatment. In general, the tumor growth is restricted by nutrient and oxygen supplying [4]. In order to mimic the *in vivo* tumor organization, it is essential to introduce vascular-like structures to improve the exchange of nutrient and gas inside spheroids. In this respect, microfluidic should be

an efficient tool for performing tumor-on-chip studies as well as more efficient anti-cancer drugs assessment.

Reference

[1] Eroglu Z, Fielder O, Somlo G. Analysis of Circulating Tumor Cells in Breast Cancer. Journal of the National Comprehensive Cancer Network. 2013;11:977-85.

[2] Kling J. Beyond counting tumor cells. Nature biotechnology. 2012;30:578-80.

[3] Deutsch A, Dormann S. Cellular automaton modeling of biological pattern formation2005.

[4] Hu G, Li D. Three-dimensional modeling of transport of nutrients for multicellular tumor spheroid culture in a microchannel. Biomedical microdevices. 2007;9:315-23.

Appendix A

Graphene Oxide (GO) incorporated gelatin nanofiber substrate fabrication

1. Introduction

Graphene and graphene oxide (GO) have drawn much attention in the field of tissue engineering due to their outstanding chemical, electrical and mechanical properties [1-3]. In particular, GO is a novel one-atom-thick two-dimensional carbon material, with many unique physicochemical properties, such as large surface area, sp2 carbon domains, and hydrophilic functional groups [4].

GO functionalized substrates serve as a structural reinforcement with high elasticity and flexibility, and has been demonstrated to enhance the proliferation and differentiation of various stem cell lines, including iPSCs, mesenchymal stem cells and neuron stem cells[1, 5-7].

In this thesis, we have developed a PEGDA frame supported gelatin nanofiber net in Chapter 2, which has been demonstrated to supply an off-ground culture environment for cells to improve cell proliferation and iPSCs differentiation in Chapter 4. Considering the above advantages of GO, we will try to develop a method to deposit GO on the nanofiber substrate, which should further enhance cell growth and differentiation.

2. Experimental

PEGDA frame and gelatin nanofiber net was fabricated as shown as chapter 2. After crosslinking, nanofibers were rinsed with ethanol for three times to remove residual EDC and NHS, then washed with DI water for three times to remove ethanol. GO solution (1 mg/ml) was supplied by Institute of Nanotechnology and biotechnology. Then GO solution was diluted into desired concentration and dispersed by ultrasound machine for 10 min.

We tried two methods for GO deposition:

1) Drop 100 μl 0.3 mg/ml GO solution on the top of substrate and then dried under vacuum over night to remove all the solvent.
2) Immerse substrate inside 0.5 mg/ml GO solution for 15 min, and then dried under vacuum overnight to remove all the solvent.

3. Results

After drying, there was GO deposited on the substrates by both methods. But GO distributed much more even on the substrate treated with the second method. **Fig. 1** shows the Ramen spectrum result of GO modified substrate by the second method. There are two peaks for GO incorporated nanofiber compared to normal nanofiber substrate, which are conformed to the characteristic peaks of GO. D band located at 1350 cm^{-1} and G band at 1600 cm^{-1} indicate the presence of GO on nanofiber substrate.

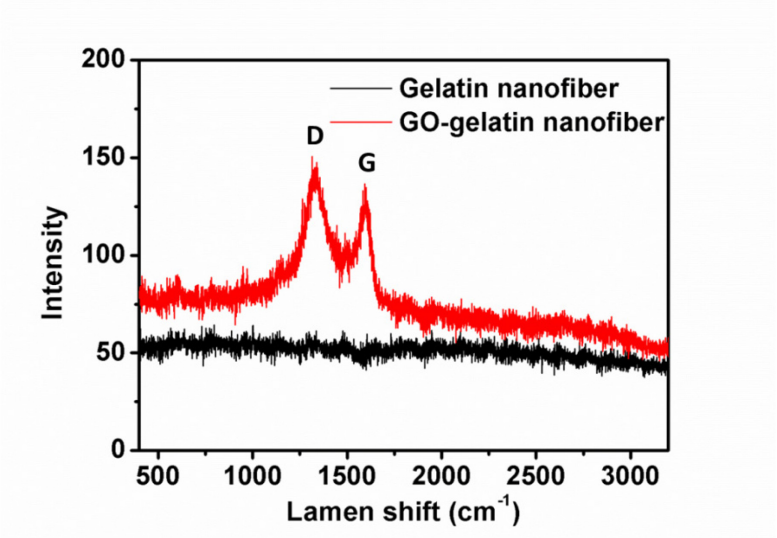

Fig. 1 Raman spectra of gelatin nanofibrous substrate (black) and GO incorporated gelatin nanofibrous substrate (red).

4. Perspective

We are looking forward to use this GO incorporated gelatin nanofiber substrate for cell culture and iPSCs differentiation.

Reference

[1] Kim T-H, Lee K-B, Choi J-W. 3D graphene oxide-encapsulated gold nanoparticles to detect neural stem cell differentiation. Biomaterials. 2013;34:8660-70.

[2] Huang YL, Baji A, Tien HW, Yang YK, Yang SY, Ma CC, et al. Self-assembly of graphene onto electrospun polyamide 66 nanofibers as transparent conductive thin films. Nanotechnology. 2011;22:475603.

[3] Shah S, Yin PT, Uehara TM, Chueng ST, Yang L, Lee KB. Guiding stem cell differentiation into oligodendrocytes using graphene-nanofiber hybrid scaffolds. Adv Mater. 2014;26:3673-80.

[4] Luo Y, Shen H, Fang Y, Cao Y, Huang J, Zhang M, et al. Enhanced Proliferation and Osteogenic Differentiation of Mesenchymal Stem Cells on Graphene Oxide-Incorporated Electrospun Poly(lactic-co-glycolic acid) Nanofibrous Mats. ACS applied materials & interfaces. 2015.

[5] Lee WC, Lim CHY, Shi H, Tang LA, Wang Y, Lim CT, et al. Origin of enhanced stem cell growth and differentiation on graphene and graphene oxide. ACS nano. 2011;5:7334-41.

[6] Chen G-Y, Pang D-P, Hwang S-M, Tuan H-Y, Hu Y-C. A graphene-based platform for induced pluripotent stem cells culture and differentiation. Biomaterials. 2012;33:418-27.

[7] Nayak TR, Andersen H, Makam VS, Khaw C, Bae S, Xu X, et al. Graphene for controlled and accelerated osteogenic differentiation of human mesenchymal stem cells. ACS nano. 2011;5:4670-8.

Appendix B

French Summary

1. Introductions

La recherche biomédicale a connu un essor phénoménal au cours des dernières décennies, grâce au développement des nouvelles méthodes et technologies telles que l'imagerie à haute résolution, les puces à ADN et les séquenceurs ADN, la PCR, le criblage à haut début, les cellules souches pluripotentes induites, etc. Parmi des approches diverses-et-variées, un bon nombre de progrès ont été faits avec l'accompagnement des structures et dispositifs micro-fabriqués. Par exemples, des biomatériaux de plus en plus sophistiqués ont été réalisés par la micro- et nanofabrication pour la culture cellulaire et l'ingénierie tissulaire. De même, les dispositifs microfluidiques ont été réalisés pour manipuler les échantillons de très faible quantité biologique.

Nous nous intéressons particulièrement au contrôle du microenvironnement cellulaire d'un tissu, ce qui implique l'organisation des matrices extracellulaires (ECM), la gestion de facteurs solubles, l'ordonnance des contacts cellulaires, etc. A priori, le comportement d'une cellule est déterminé non seulement par l'ensemble de gènes, de protéines et d'autres espèces sous-cellulaires mais aussi par l'environnement immédiat de la cellule. L'ECM, par exemple, fournit un support structurel et biochimique de la cellule qui est déterminant pour l'adhérence, la prolifération, la migration et la différenciation des cellules. En raison de la complexité de l'ECM et la variation dynamique des facteurs solubles et de l'interaction cellule-ECM, une compréhension approfondie du rôle du microenvironnement cellulaire est important dans la culture de tissus fonctionnels.

Traditionnellement, les cellules isolées d'un tissu corporel et mises en culture ne sont plus dans un milieu naturel (*in vivo*) mais plutôt dans un milieu artificiel (*in vitro*) sur une plateforme de culture telle que des boîtes de culture, des flacons, des plaques multi-puits, etc. Même si les processus cellulaires peuvent être maintenus ou modifiés, les marges de manipulation ou de contrôle sont très limitées. D'une part, les surfaces dans de ces plateformes sont généralement plates ou bi-dimensionnelles. Quels que soient les traitements (revêtement ou microstructuration), ces supports de culture est toujours très différents de ceux réellement présents *in vivo*. D'une part, la configuration dynamique des facteurs solubles autours d'une cellule mise en culture est loin d'être comparable à la configuration *in vivo*. En effet, la plupart des cellules dans un tissu sont au voisinage des capillaires pour échanger les facteurs solubles,

les nutriments et les produits métaboliques par diffusion autour de ces capillaires mais le milieu de culture *in vitro* est souvent statique ou perfusé. Ces grandes différences ont laissé à penser que les approches conventionnelles pour la culture *in vitro* ne sont pas idéales. Faute de mieux, on ajoute les actifs pour augmenter le taux de réussite et corriger le comportement des cellules. En effet, cela est le cas pour la plupart des cellules différentiées et maturées.

La culture et la manipulation *in vitro* des cellules souches pluripotentes telles que les cellules embryonnaires et les cellules pluripotentes induites est beaucoup plus critique en raison de leur plus grande sensibilité aux microenvironnements cellulaires. Ces cellules souches peuvent devenir d'autres types de cellules de façon spontanée ou dériver en cellules cancéreuses, ce qui s'accompagne de problèmes de survie, d'instabilité des gènes, d'hétérogénéité, etc. Des approches diverses et variées ont été proposées telles que la co-culture avec les cellules nourricières (*feeder cells*), les substrats recouverts d'une couche de gel de protéines ou de polymères, les substrats micro- et nano-structurées etc. Une question cruciale reste en suspens: quelle est l'approche la plus adéquate ? Pour mieux répondre à cette question, nous devons travailler sur le grand principe de mimétisme qui consiste à imiter le microenvironnement cellulaire d'un tissu et reconstruire ce tissu en considérant son organisation. Comme « la nature ne fait rien de vain, rien d'inutile » (Aristote), nous pensons que la meilleure approche découle de ce grand principe pour réaliser un nouveau support ou une nouvelle plateforme de culture cellulaire intégrant l'ensemble des paramètres mentionnés plutôt que d'améliorer les approches existantes.

Toutefois, il est normalement difficile d'imiter exactement la composition et le fonctionnement complexe d'ECM dans un tissu natif. Nous devons retenir quelques principes de base à partir de nos expériences précédentes : i) minimiser les contacts exogènes des cellules avec les matériaux 'artificiels' (verre, plastique, etc.), ii) maximaliser la perméabilité ou les échanges des cellules avec le milieu, iii) construire le support avec des protéines de matrixe extracellulaire naturelle.

Par ailleurs, nous sommes également intéressés par le diagnostic biomédical et en particulier le diagnostic du cancer. L'idée est d'apporter une nouvelle solution pour isoler les cellules tumorales circulantes en utilisant un filtre micro-fabriqué et un dispositif microfluidique conçus à partir des analyses de micro-écoulement hydrodynamiques et de migration des cellules à travers un trou conique.

Ce travail de thèse vise à développer de nouveaux supports/dispositifs pour des applications biomédicales, y compris l'ingénierie tissulaire, la médecine régénérative, le diagnostic, etc. Les supports/dispositifs sont utilisés pour contrôler la culture et la différentiation des cellules souches pluripotentes induites et l'isolation et l'analyse de cellules tumorales circulantes. Nous allons d'abord proposer un patch de culture en forme monocouche de nanofibres réticulées, permettant de cultiver et de différentier les cellules souches pluripotentes induites humaines (hiPSCs) "hors sol". Puis, nous démontrerons la possibilité de former des tissus cardiaques et neuronaux sur patch à partir de hiPSCs. Ensuite, nous développerons un dispositif microfluidique avec une membrane composée de trous de forme conique pour isoler les cellules tumorales circulantes et cultiver les cellules ainsi isolées. Enfin, nous évaluerons l'effet de drogues anticancéreuses sur la formation des sphéroïdes tumoraux en utilisant des multi-puits d'agarose micro-fabriqués. Finalement, nous espérons contribuer au progrès des techniques de la micro-ingénierie vers les applications à grande échelle et cliniques.

2. Étude de cellules souches

2.1 Introductions

Les cellules souches et les cellules souches pluripotentes en particulier sont essentielles pour développer de nouvelles méthodes et outils de l'ingénierie tissulaire et la médecine régénérative. Par définition, les cellules souches embryonnaires (ESCs) sont pluripotentes, puisqu'elles sont à l'origine de tous les types de cellules maturées ou différentiées de nos corps. En 2006, un nouveau type de cellules souches pluripotentes a été réalisé par le Prof. Yamanaka de l'Université de Kyoto (prix Nobel de 2012 de médecine), à partir d'une cellule de peau en utilisant quatre facteurs de gènes bien choisis. Ce type de cellules ressemble à des cellules souches embryonnaires, appelées par conséquent "cellules souches pluripotentes induites" (iPSCs). Cette mise au point a ouvert une grande porte au progrès de l'ingénierie tissulaire et à la thérapie de transplantation, puisque les problèmes d'éthiques, de ressources cellulaires et du rejet immunologique sont désormais relégués au second plan.

Comme les ESCs, les iPSCs sont capables de se proliférer infiniment et de se différencier en cellules ectodermique, mésodermiques et endodermiques. En plus, les

ESCs et les iPSCs ont presque les mêmes caractéristiques au niveau de l'expression de gènes et la production de protéines, du temps de doublement, des profils de méthylation de la chromatine, de la formation du corps embryonnaire, de la formation de chimère viable, et de la capacité de différentiation (leur différence est en cours d'évaluation). Cependant, l'utilisation des ESCs provenant de l'embryon humain est strictement interdite dans de nombreux pays, de sorte que le nombre de lignées de cellules souches embryonnaires approuvées pour la recherche est très limité. Cette interdiction entrave la possibilité de répondre à certains besoins des plus urgents, notamment ceux relatifs à la modélisation et à la thérapie de maladies. Les iPSCs peuvent probablement supplémenter les ESCs dans le cadre de la médicine régénérative. Les iPSCs de patients fournissent une plate-forme spécifique à partir de laquelle il est possible d'obtenir des informations mécanistiques de diverses maladies, de mener à bien le criblage de médicaments, d'évaluer leurs potentiels thérapeutiques et d'explorer la réparation des gènes couplée à la thérapie cellulaire.

Toutefois, aucune méthode générique n'est encore disponible pour la production de masse des iPSCs humaine de haute qualité, sans risque d'instabilité génétique et de tumorigénicité. De nombreuses études ont été faites sur l'effet du milieu de culture et/ou des facteurs solubles, mais relative peu ont été consacrés sur l'influence de substrat de culture. On ne sait même pas quelles sont les meilleures rigidités du matériau et quelles sont les meilleures morphologies de surface du substrat pour la culture et la différentiation des iPSCs.

La première préoccupation est la prolifération des iPSCs, à savoir, ces iPSCs devraient se propager sur de nombreuses générations sans perdre leur pluripotence, leur pureté et leur qualité. Dans des conditions de culture classiques, les hiPSCs sont impures et présentent souvent des anomalies chromosomiques importantes et à haut risque de tumorigénicité. En ajoutant des cellules nourricières ou en utilisant un substrat couvert de Matrigel, la qualité de hiPSCs pourrait être largement améliorée, malheureusement ces deux solutions ne sont pas pertinentes pour les applications cliniques en raison de la présence de facteurs d'origine animale. Ce problème a été surmonté en utilisant des substrats revêtus de protéines recombinantes telles que la laminine, la vitronectine, l'E-cadhérine ou des polymères synthétiques. Ces études, ainsi que des essais supplémentaires en utilisant des substrats non plans, soulignent l'importance de l'utilisation des protéines / molécules des ECMs et surfaces texturées

qui prennent en compte une partie de la spécificité de microenvironnement cellulaire *in vivo*.

La deuxième préoccupation est la différenciation contrôlée des iPSCs. Précédemment, les iPSCs ont été différenciées en plusieurs types de tissus somatiques, y compris les cardiomyocytes, les neurones, des ilots d'hépatocytes, etc., mais les méthodes et les protocoles proposés sont encore en pleine évolution. A priori, les cellules différentiées telles que les cellules cardiaques et les neurones ont des différences morphologies et ont des réponses variables aux propriétés mécaniques et physicochimiques des substrats, ce qui impose l'utilisation de différents types de substrats. Par ailleurs, il est préférable que les cellules souches différenciées soient organisées en forme de tissus pour les applications cliniques envisagées, ce qui souligne l'importance de l'interaction cellule-cellule par rapport à l'interaction cellule-substrat.

Dans cette étude, nous proposons une nouvelle plateforme de culture, le patch de culture, pour cultiver et différentier les iPSCs en cellules cardiaques et neuronales.

2.2 Fabrications de patch de culture

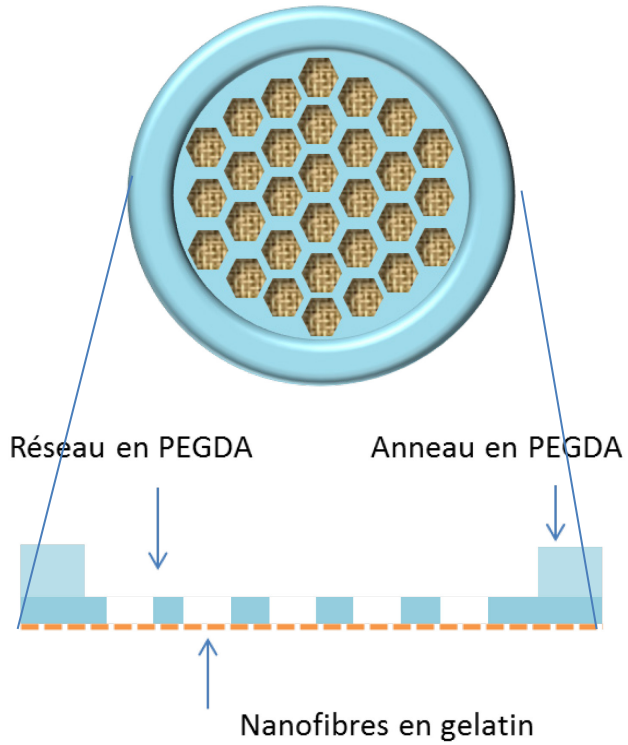

Figure 1. Schéma du patch de culture en filet de gélatine sur un réseau de PEGDA en forme de nid d'abeille.

Le patch de culture que nous développons est sous forme de filet ou monocouche de nanofibres de gélatine réticulées avec des tailles de pores inférieures à celles des cellules déposés sur un réseau de PEGDA en forme de nid d'abeille (Figure 1).

Fabrication du support en PEGDA : Un masque optique de chrome est fabriqué par un faisceau laser focalisé. Puis, une couche de résine (AZ40XT, Microresist) est déposée sur le masque, suivi par un recuit de 10 min à 125°C. Après avoir été irradiée par une lumière UV à travers le masque, la couche de résine est développée, résultant en un moule de résine.

Après avoir été exposé au triméthylchlorosilane (TMCS) comme traitement antiadhésif, un mélange des composants A et B de PDMS (GE RTV 615) dans un rapport de 10: 1 est appliqué au moule. Cette étape est suivie d'un recuit à 80°C pendant 2 h. Puis la couche de PDMS est décollée et posée, côté structuré en contact avec une lame de verre. L'ensemble PDMS-verre est placé dans un dessiccateur pour dégazage pendant 15 min. Puis, la cavité PDMS-verre est remplie par effet de microaspiration avec un mélange de PEGDA avec 1% (en volume) d'Irgacure 2959 (photo-amorceur), suivi d'une exposition aux UV à 12mW / cm^2 pendant 30 sec. Enfin, la couche de PDMS est retirée, résultant en un réseau de PEGDA solidifié en forme de nid d'abeille.

Pour augmenter la résistance mécanique de ce réseau, un anneau de PEGDA est ajouté au-dessus du nid d'abeille. Cet anneau a été préparé selon le protocole décrit ci-dessus et collé sous UV sur le réseau de nid d'abeille en utilisant la solution de PEGDA comme adhésif.

Dépôt des nanofibres de gélatine: Les nanofibres de gélatine sont directement fabriquées sur le nid d'abeille de PEGDA par électrofilature. Une solution de gélatine de 10% en poids est préparée par dissolution des poudres de gélatine (G2625, Sigma-Aldrich, France) dans une solution mixte d'acide acétique, d'acétate d'éthyle et d'eau distillée selon un rapport volumique de 21:14:10. L'électrofilature est faite en utilisant une pompe à seringue, une source d'alimentation de haut potentiel et une plaquette de silicium comme support de dispositif PEGDA et de collecteur de nanofibres. Les nanofibres de gélatine sont obtenues sur l'échantillon de PEGDA en plaçant la plaquette de silicium à une distance de 10 cm de l'aiguille de la seringue chargée de la solution de gélatine et en appliquant une tension de polarisation de 11KV entre l'aiguille (anode) et la plaquette (cathode),. Le flux

d'injection de la solution de gélatine est fixé à 0,2 ml / h. Après récupération, les nanofibres de gélatine sont séchées sous vide pendant une nuit afin d'évaporer le résidu de solvant. Les nanofibres sont ensuite réticulées dans une solution d'éthanol avec 0,2 M d'EDC (1-éthyl-3-(3-diméthylaminopropyl) carbodiimide) et 0,2 M de NHS (N-hydroxysuccinimide, référence) pendant 4 h. Après réticulation, l'échantillon est rincé trois fois à l'éthanol avant d'être séché pendant une nuit sous vide pour éliminer les produits chimiques restants.

La figure 2 montre un patch de culture qui formé de nanofibers de gélatine de diamètre 100-500 nm et une structure de PEGDA de hauteur et largeur 50 µm,

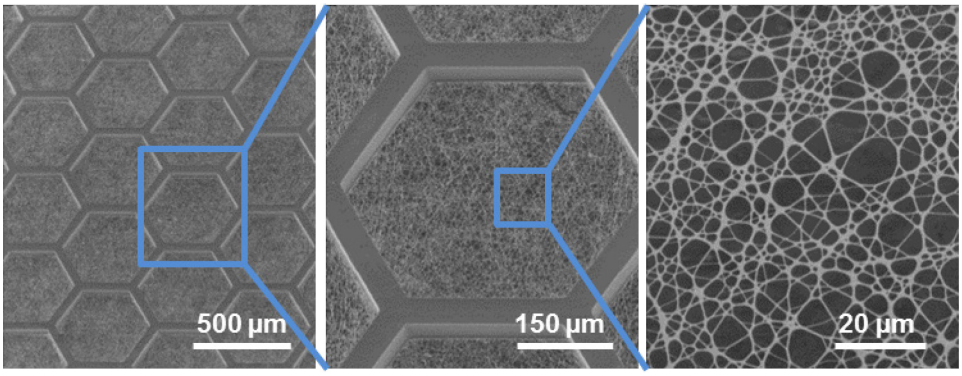

Figure 2. Images de microscope électronique à balayage d'un filet de gélatine déposé sur un réseau en forme de nid d'abeille.

2.3 Culture des cellules de référence sur patch

Pour démontrer l'avantage du filet, deux types de cellules, des fibroblastes NIH-3T3 et des cellules cancéreuses Hela, ont été cultivées en même temps sur les patchs de culture et les boîtes de culture.

Ces cellules sont d'abord préparées séparément pendant 3-4 jours dans un milieu Eagle modifié par Dulbecco (DMEM) avec 10% de FBS et 1% de pénicilline / streptomycine à 37°C avec 5% de CO_2. Puis les cellules cultivées à confluence ont été détachées avec de la trypsine. Cinquante µl de milieu contenant approximativement 2×10^4 de cellules sont déposés à l'intérieur de l'anneau d'un patch placé dans une boîte de culture. Les cellules sont incubées pendant 1 h pour l'adhésion puis 2 ml de milieu de culture sont ajoutés. La culture est réalisée à 37 °C dans un incubateur à 5% de CO_2.

Les résultats montrent que les deux types de cellules peuvent se fixer sur les filets en moins de 2 h et que le nombre de cellules augmente plus vite sur le filet que

sur la boîte de Pétri. La figure 3 montre les images d'immunofluorescence de deux types de cellules cultivées sur patchs, dans lesquelles les cytosquelettes et les noyaux ont été colorés à la phalloïdine-FITC (vert) et au DAPI (bleu), respectivement. Du fait que les protéines ne peuvent pas être déposées sur le PEGDA, aucune cellule n'adhère sur le réseau de PEGDA. Enfin, nous avons observé que le nombre de cellules augmente presque deux fois plus vite sur le filet que sur boîte de Pétri (figure 4).

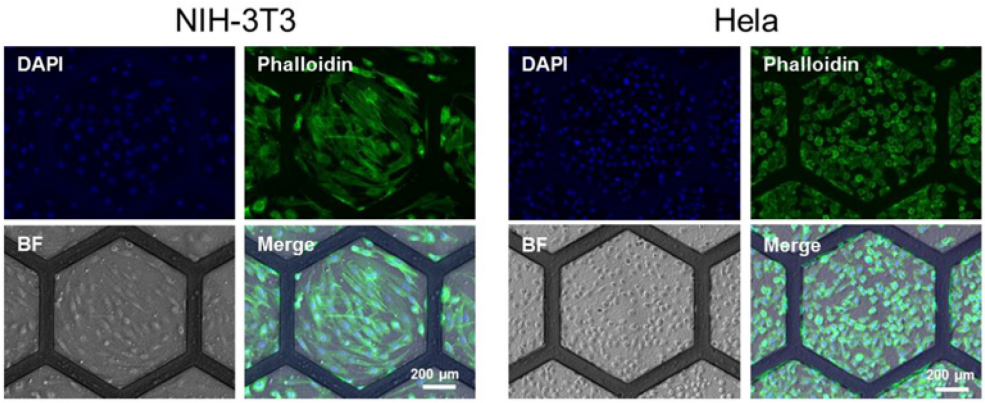

Figure 3. Images en fond clair et de fluorescence des cellules NIH-3T3 (à gauche) et les cellules HeLa (à droite) sur filets de gélatine. Vert: Phalloïdine pour cytosquelette; Bleu: DAPI pour noyau.

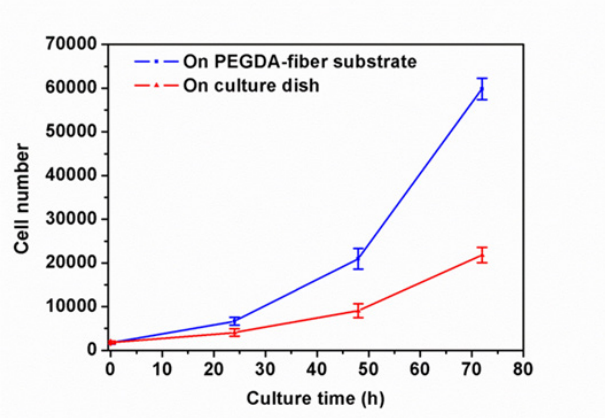

Figure 4. Augmentation du nombre de cellules NIH 3T3 sur deux types de supports en fonction du temps de culture.

2.3 Contrôle de l'agrégation des iPSCs sur patch

Préparation des iPSCs : Les iPSCs sont d'abord mises dans une boîte de

culture revêtue de vitronectine et remplie d'un milieu de culture « E8 complet » (Life technologies). Les cellules sont incubées à 37 °C avec 5% CO_2. Le milieu est alors changé une fois par jours jusqu'à 70% ~ 80% de confluence. Les cellules sont enfin détachées avec une solution de 0,5 mM EDTA dans du DPBS.

Contrôle de l'agrégation des iPSCs : Le patch est d'abord traité dans une solution de vitronectine diluée 500 fois dans du PBS à température ambiante pendant 1 h. 50 µl de milieu de culture E8 contenant 2×10^5 des iPSCs et 10 µM d'Y-27632 (inhibiteur de ROCK) sont alors déposés à l'intérieur de l'anneau du patch placé dans une boîte de culture. Après avoir incubé 1 h pour l'adhésion cellulaire, 2 ml de milieu E8 frais avec 10 µM d'Y-27632 est ajouté dans la boîte de culture. Le milieu de culture est ensuite remplacé 1 à 4 h après par du E8 sans Y-27632, suivi d'une nouvelle incubation de 24 h. On observe alors la formation des colonies d'iPSCs au centre de chaque compartiment du réseau de nid d'abeille en forme d'hémisphère si le traitement d'Y-27632 dure 1 h à 2 h ou d'hémisphère aplati si le traitement dure 4 h. Une fois les colonies formées, les facteurs de différentiation peuvent être ajoutés directement dans le milieu de culture pour produire, par exemple, des cellules cardiaques et des progéniteurs de neurones, sur les filets (Figure 5).

Figure 5. Schéma de la formation de colonies et la différenciation des iPSCs dans un compartiment de nid d'abeille d'un patch de culture.

La figure 6 montre des colonies d'iPSCs de différentes formes, obtenues avec presque le même nombre de cellules mais avec temps de traitement d'Y-27632 différents (1, 2 et 4 h). Les colonies à gauche et au milieu ont une forme d'hémisphère, tantdis que celles à droite ont plutôt une forme très aplatie (barre d'échelle 250 µm).

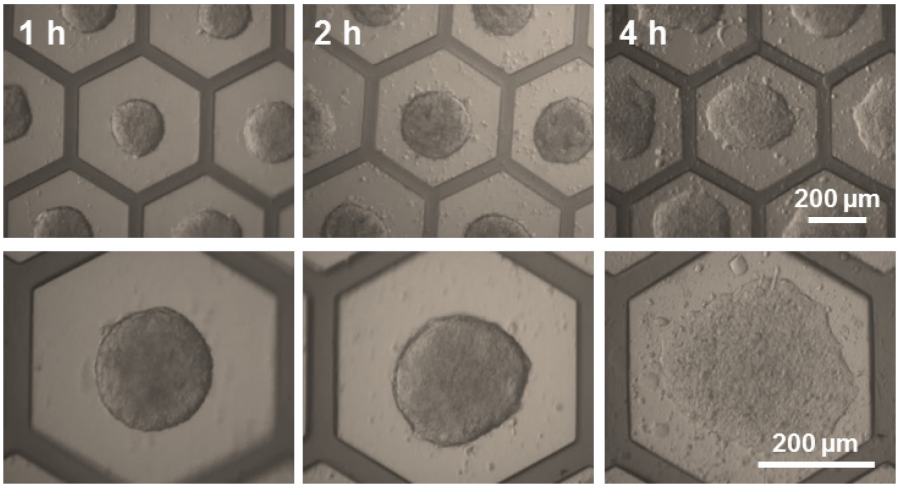

Figure 6. Microphotographie des colonies d'iPSCs de différentes formes, contrôlée par le temps de traitement au Y-27632 à 1 h, 2 h et 4 h, respectivement.

Les colonies formées dans les compartiments du patch sont similaires en taille et en forme. En plus, elles démontrent toutes une bonne viabilité et les expressions caractéristiques de la pluripotence des iPSCs (Figure 7).

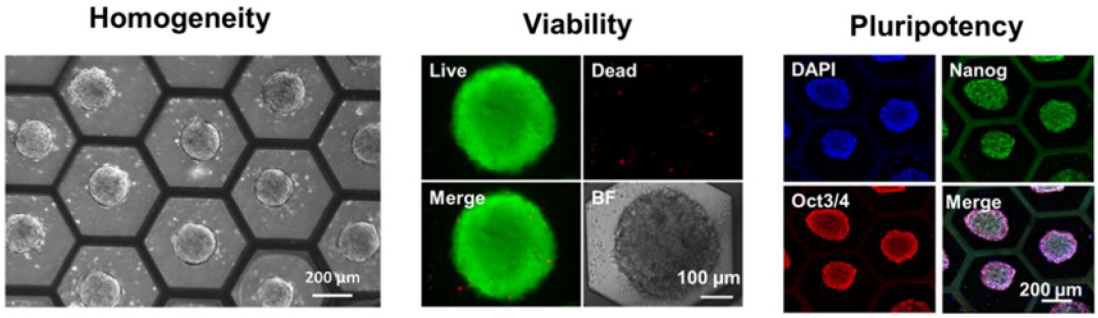

Figure 7. Colonies hémisphériques des iPSCs dans les compartiments d'un patch de culture, montrant une bonne homogénéité, une bonne viabilité et une bonne pluripotence cellulaire.

2.4 Production de patch cardiaque

Une fois que les colonies hémisphériques sont formées, la différentiation des iPSCs sur patch de culture peut se faire de la manière suivante (Figure 8) : Le milieu de culture E8 est d'abord remplacé par RPMI 1640/B27 sans insuline avec 12 µM de CHIR99021. Après 24 h d'incubation, le milieu est remplacé par RPMI 1640/B27 sans insuline (jour 1). Après 48 h d'incubation, le milieu est remplacé par RPMI 1640/B27 sans insuline avec 5µM d'IWP2 (jour 3). Après 48 h d'incubation, le milieu est remplacé par RPMI 1640/B27 sans insuline (jour 5). Puis, le milieu est

changé tous les 3 jours par RPMI / B27. Normalement, la contraction des cellules peut être observée pendant la période de jour 8 à jour 12.

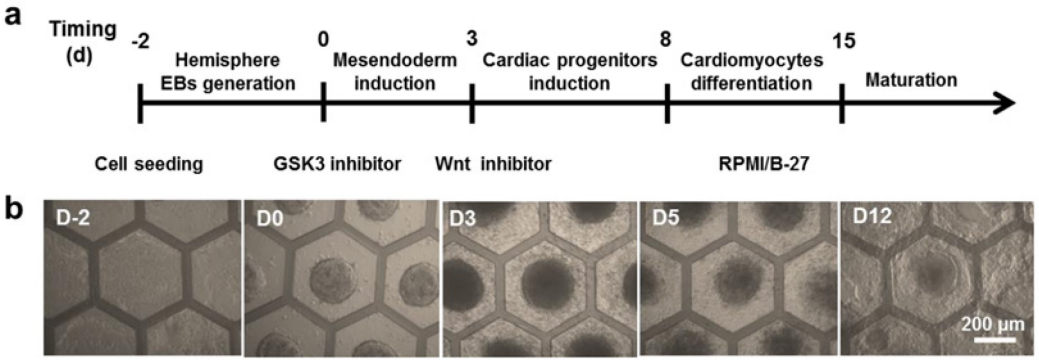

Figure 8 (a) Protocole de différentiation des hiPSCs pour réaliser un patch cardiaque. (b) Image de microphotographie des colonies des iPSCs vers cardiomyocytes à jour -2, 0, 3, 5 et 12.

On observe que ces cellules sont en contraction avec une fréquence de battement de ~1 Hz, indiquant une maturation après différentiation de 4 semaines en utilisant le protocole (Lian et al, Nature Protocole 8, 162, 2013) (barre d'échelle : 20µm).

La figure 9 montre les images de fluorescences des protéines liées aux expressions des cardiomyocytes dérivés des iPSCs au jour 20 sur un patch de culture et sur une lame de verre pour comparaison (bleu : DAPI, vert : a-Actinin ; rouge : TnnT2). Ces images montrent clairement la formation de sarcomères, suggérant que le patch favorise la maturation cardiaque. La figure 9 montre aussi les résultats de la cytométrie en flux, montrant que 74,7 % de cellules sont positives en TnnT2 sur patch mains que seulement 34,5% de cellules sont positives en TnnT2 sur verre au jour 21. Enfin, les résultats de q-PCR montrent une plus forte expression des gènes liés aux fonctions cardiaques sur patch par rapport au contrôle.

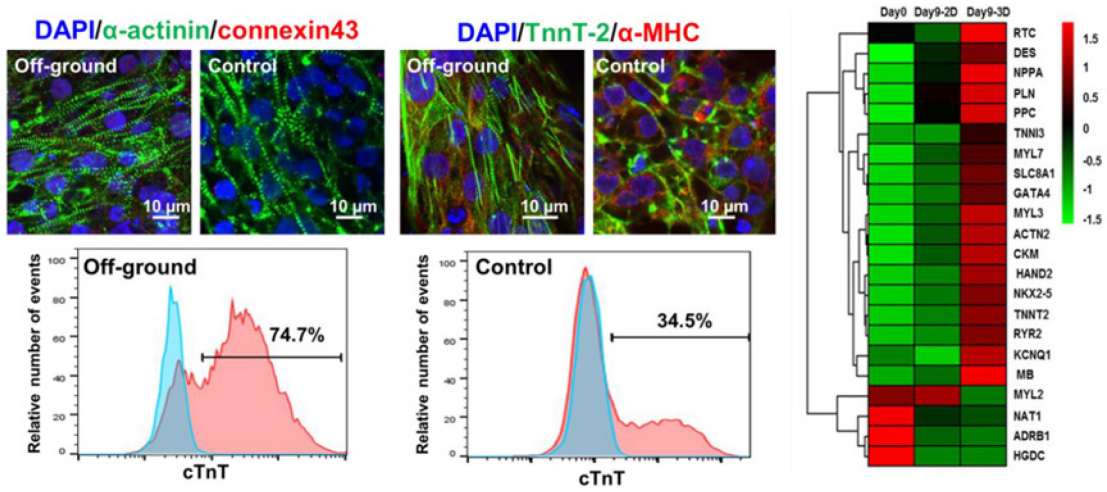

Figure 9 Comparaison des images d'immunofluorescence, de la cytométrie en flux, et de la q-PCR des cardiomyocytes différenciés sur patch et sur lame de verre.

Une fois que le patch cardiaque est obtenu, il peut être placé sur une surface des multi-électrodes (MEA) pour évaluer l'effet de drogues, par exemple, par mesures électrophysiologiques (Figure 10). Nous avons observé un effet des drogues très similaire, la variation de l'intervalle des ondes T et Q et la variation de fréquence de battement étant dépendant du type et de la dose de drogue utilisés. Ainsi, le patch cardiaque que nous proposons est prêt à être utilisé comme une nouvelle plateforme pour évaluer la toxicité des drogues.

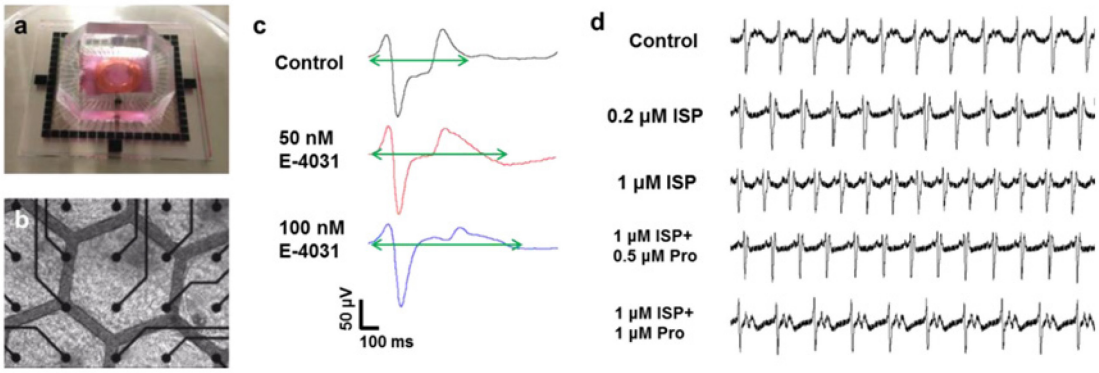

Figure 10. Caractérisation électrophysiologie d'un patch cardiaque pour évaluer les effets de drogues. (a,b) Le patch est placé sur un réseau de multi-électrodes. (c) Variation de l'intervalle QT en fonction de la dose d'E-4031 (0, 50 et 100 nM) (d) Variation de fréquence de battement en fonction de la dose d'ISP et de Pro.

2.5 Production de patch neuronal

De la même manière, les iPSCs sont différenciées en neurones moteurs sur patch

de culture. Le protocole présenté dans la figure 11 suggère trois étapes de production de patch neuronal, i.e ., production des cellules neuroectrodermales par l'inhibition de la signalisation SMAD, production des progéniteurs des neurones moteurs et maturation des neurones moteurs.

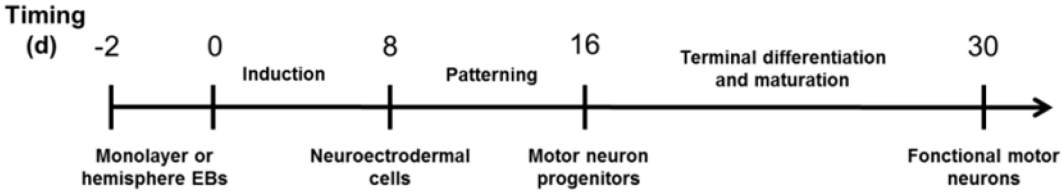

Figure 11. Schéma du protocole de différentiation des iPSCs vers des neurones moteurs.

La figure 12 montre les images de fluorescences des progéniteurs de neurones dérivées des iPSCs sur patch (bleu : DAPI, vert : Nestin ; rouge : β-Tubulin III), indiquant un taux de différentiation relativement élevé après 2 semaines de culture dans un milieu de culture contenant 10 µM d'acide rétinoïque).

Après 16 jours de différentiation, les progéniteurs des neurones moteurs sur patch sont réensemencés sur lame de verre, réseau de multi-électrodes et patch de culture pour maturation. Les figures 13a et 13b montrent les images de microphotographie et d'immunofluorescence des cellules sur lame de verre au cours de la maturation. La figure 13c montre une image d'un patch neuronal sur un réseau de multi-électrodes (MEA) et les signaux électriques représentatifs des neurones au jour 38, ce qui prouve que le patch de culture est tout à fait apte à la production des neurones moteurs et adéquat dans le cadre d'une caractérisation par mesures électrophysiologiques.

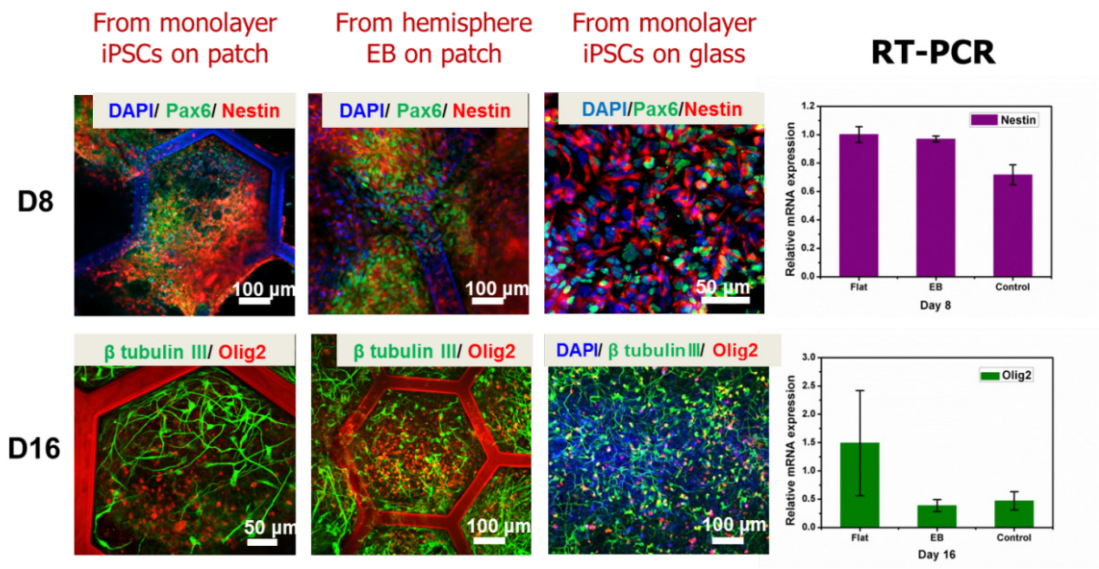

Figure 12. Immunofluorescence des iPSCs différentiées aux jours 8 et 16. DAPI : Nucléaire (bleu); Pax6 : Cellules de neuro-ectoderme (vert); Nestine : Cellules souches neuronales (rouge); β-tubuline III: Microtubules neuronaux (vert); Olig2: Progéniteurs de neurones moteurs (rouge). Expression relative de l'ARNm de Nestine au jour 8 et d'Olig2 au jour 16.

3. Étude des cellules cancéreuses

3.1 Introduction

Le cancer est l'une des principales causes de mortalité avec plusieurs millions de morts dans le monde chaque année. Parmi toutes les mortalités liées au cancer, le cancer métastasé représente 90% des décès. La métastase est la propagation d'une tumeur d'un organe à un autre qui n'est pas directement connecté au premier. La métastase du cancer est un processus complexe, son mécanisme n'est pas encore complètement compris. Typiquement, une métastase comprend les étapes suivantes : la transition épithéliales mésenchymateuses (EMT) et l'invasion, la propagation hématogène et l'extravasation, la transition mésenchymateuses épithéliales (MET) et la colonisation métastatique. Il a été prouvé que dans la métastase, des cellules tumorales circulantes (CTC) jouent un rôle essentiel.

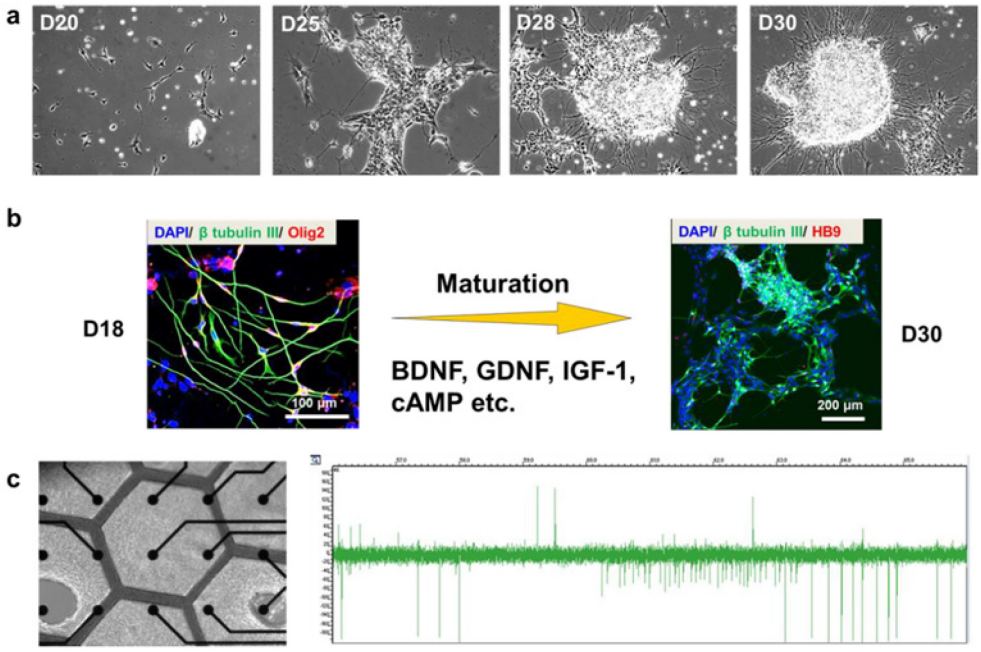

Figure 13. Patch neuronal. (a) Images de microphotographie de neurones moteurs réensemencés au cours de la maturation sur un lame de verre; (b) Image d'immunofluorescence des neurones moteurs sur lame de verre aux jours 18 et 30. DAPI: Nucléaire (bleu); HB9: Neurone motrice (rouge); Olig2: Progéniteurs des neurones moteurs (rouge); β-tubulin III: Microtubules neuronaux (vert) ; (c) Image d'un patch neuronal sur un réseau de multi-électrodes (MEA) et signaux électriques représentatifs des neurones au jour 38.

Le diagnostic précoce de la tumeur primaire, permettant de réduire au mieuxla métastase, est considéré comme l'arme clé pour gagner la guerre contre le cancer. Actuellement, trois techniques principales, i.e. l'imagerie, la biopsie et l'analyse de sang, sont utilisées pour le diagnostic du cancer. Parmi ces trois techniques, l'analyse du sang, i.e. des molécules ou des CTCs présentes dans le sang périphérique d'un patient, est maintenant en développement rapide. La détection des CTCs est particulièrement intéressante pour la détermination caractéristique du cancer. Le problème est que les CTCs sont rares et très rares dans le sang d'un patient, environ 1 ~ 10 CTC sur 1 milliard de cellules de sang. Par conséquent, le principale défi technique est de les isoler ou de les capturer. Pour ce faire, de nombre essais ont été menés. La capture par affinité est basée sur l'interaction immunochimique entre les billes magnétiques ou les surfaces structurées et les cellules tumorales qui expriment des marqueurs de surface spéciaux tels que l'EpCAM, une molécule d'adhésion des cellules épithéliales surexprimée par la majorité des cellules

tumorales. Ces méthodes sont efficaces pour capturer les CTCs de phénotypes épithéliaux mais inapplicable à celles qui n'ont pas ces marqueurs épithéliaux. On sait maintenant que lorsqu'une cellule tumorale entre dans le sang, elle pourra perdre son identité à cause de la transition épithéliale-mésenchymateuse, ce qui signifie que cette approche est intrinsèquement problématique. En revanche, les méthodes physiques telles que la centrifugation, la diélectrophorétique et la filtration sont capables d'isoler les deux types de phénotypes, (épithélial et mésenchymateux). A priori, ces méthodes sont plus appropriées pour les analyses de l'hétérogénéité de tumeurs, de la résistance aux médicaments des tumeurs, etc. Cependant, ces approches sont technologiquement biaisées et il est souvent difficile de parvenir à un compromis entre l'efficacité de la capture, la pureté et la viabilité des cellules. Par exemple, la méthode de filtration a été développée depuis quelques décennies en utilisant presque le même genre de dispositif (filtre de polycarbonate par gravure pré-irradié par des ions très énergiques). Le problème de cette approche est la contamination : on bloque les cellules du sang en même temps des cellules tumorales si la taille de trous du filtre est suffisamment petite pour efficacement isoler les CTCs. En outre, les trous dans ce filtre sont répartis de façon aléatoire et il se peut que deux ou plusieurs trous soient joints; dans ce cas, des CTCs peuvent passer à travers le filtre. Afin de surmonter ce problème, les techniques de microfabrication ont été utilisées pour la fabrication de filtres avec des trous beaucoup mieux définis. Aucune d'entre elles ne sont jusqu'à présent en mesure de répondre aux exigences de l'application clinique.

Non seulement il manque des méthodes efficaces pour capturer les CTCs mais très peu d'études ont été menées sur les CTCs capturés. A ce propos, il sera intéressant d'avoir des modèles in vitro en réalisant, par exemple, des sphénoïdes tumoraux à partir des CTCs capturés pour voir les processus de formation sous l'effet de drogues. Les cellules malignes dans les tissus néoplasiques, comme les cellules saines dans les tissus normaux, sont organisées en 3D in vivo. Ainsi, la génération des sphéroïdes tumoraux en 3D est nécessaire afin de se rapprocher des formes et propriétés physiques du contexte in vivo. Actuellement, les études in vitro sont effectuées sur des sphéroïdes de petites tailles, ce qui ne peut reprendre efficacement la complexité sphéroïde de tumeurs solides. Pour imiter les tumeurs in vivo, il faut aussi considérer les conditions physiologiques du site telles que les caractéristiques et les distributions de nutriments et des facteurs des cellules dans la zone sphéroïde.

La culture en suspension est fréquemment utilisée pour réaliser des sphéroïdes mais il est difficile de contrôler leur uniformité et de les manipuler pour des études systématiques. L'utilisation d'un ballon rotatif ou de bioréacteurs peut améliorer l'uniformité de sphéroïdes mais aussi introduit des contraintes de cisaillement indésirables. L'utilisation des gouttes suspendues peut aussi améliorer l'uniformité de sphéroïdes. Le problème est que la manipulation de gouttes suspendues pour les essais de drogues nécessite beaucoup de temps pendant la progression sphéroïde. Plus récemment, des substrats à motifs 2D et 3D ont été proposés pour soutenir la formation de sphéroïdes. Afin de faciliter la diffusion des nutriments, des médicaments et d'autres facteurs dans la zone sphéroïde, nous avons choisi de travailler sur un modèle à multiples puits microfabriqués en utilisant agarose, un matériau poreux et hydrophobique, permettant d'avoir une meilleure croissance de sphéroïdes ainsi que le criblage à haut débit.

3.2 Capture de CTCs

Nous avons conçu et fabriqué un dispositif microfluidique intégrant un filtre avec un réseau de micro-trous de forme conique et un micro-injecteur avec des composants à courant transversal (Figure 14).

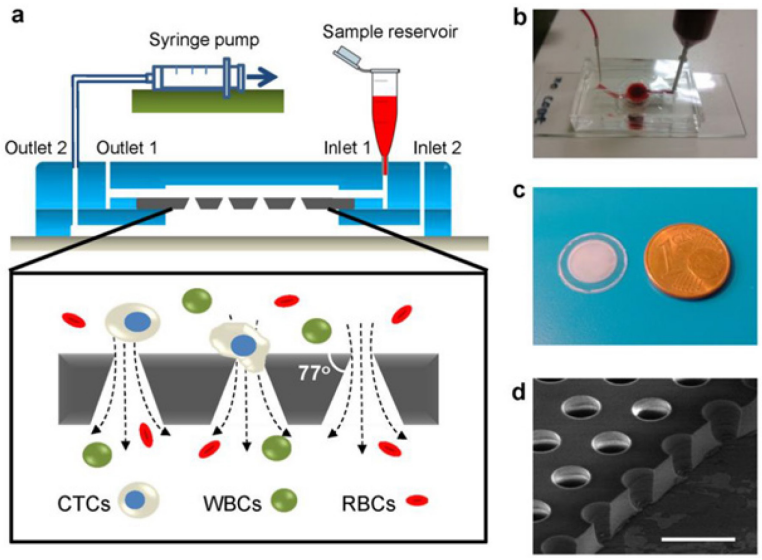

Figure 14 Dispositif microfluidique avec un filtre de trous coniques pour la capture des cellules tumorales circulantes. (a) Schéma du dispositif de filtration des CTCs. (b) Photographie d'un dispositif fonctionnant avec un échantillon de sang. (c) Photographie d'un filtre de diamètre de 9 mm. (d) Image de microscopie électronique à balayage d'un filtre avec des trous coniques. Barre d'échelle: 40µm.

Pour étudier les performances de ce dispositif, des cellules HT-29 ont été dispersées dans un échantillon de sang d'une personne en bonne santé. Les expériences de filtration ont été contrôlées par un pousse-seringue à une vitesse de traction constante. Comme résultat, nous avons récupéré la plupart des cellules HT-29 sur le filtre avec un nombre limité de cellules sanguines normales (Figure 15), montrant une efficacité de capture de ~ 95% et une pureté de capture de ~ 86%. Des échantillons de sang donnés par 14 patients atteints de cancer et 6 donneurs sains ont été utilisés pour tester la pertinence clinique de la méthode. Statistiquement, aucun CTCs n'a pu être détecté dans les échantillons de sang de donneurs sains mais une à plusieurs CTCs ont été capturées pour la plus part des patients atteints de cancer.

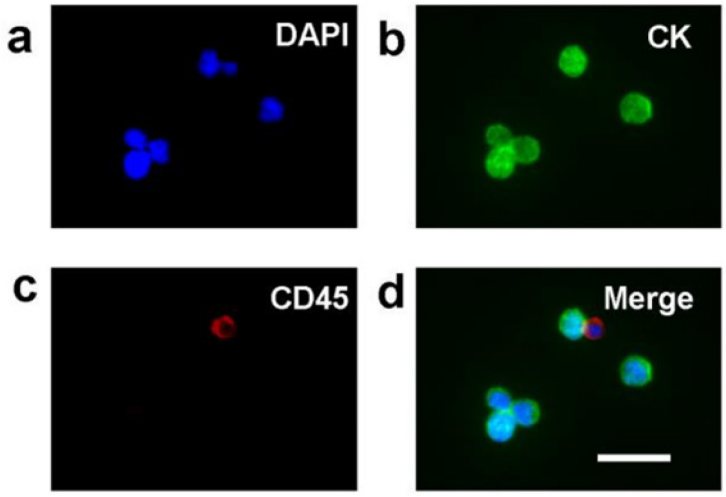

Figure 15. Image d'immunofluorescence des cellules HT-29 sur la surface d'un filtre après avoir été dispersées dans le sang puis filtrées. HT-29 : anti-CK-AlexaFluor 488 (vert) et globine blanc : anti-CD45-PE (rouge) ; Noyaux : DAPI (bleu). Barre d'échelle : 30 µm.

Pour évaluer quantitativement la performance de cette méthode, une étude systématique a été effectuée avec des cellules HT-29 dispersées dans du PBS. Nous avons observé une augmentation de l'efficacité de capture avec la diminution de la vitesse d'écoulement (Figure 16a). Nous avons aussi constaté que l'efficacité de capture est pratiquement la même pour les échantillons de différentes densités cellulaires du fait que le nombre de cellules dispersées (10~100) est bien inférieur au nombre des trous du filtre (~10^4) (Figure 16b). Puis, nous avons remarqué que l'efficacité de capture dépend fortement du type de cellule et que la taille de trous du filtre doit être corrélée à la taille de noyaux des cellules (Figure 16c-d). Une fois

capturées, les cellules ont été cultivées sur le même filtre pendant trois jours. La plupart des cellules sont viables et le nombre de cellule a augmenté de façon remarquable à cause de la prolifération (Figure 16e-f).

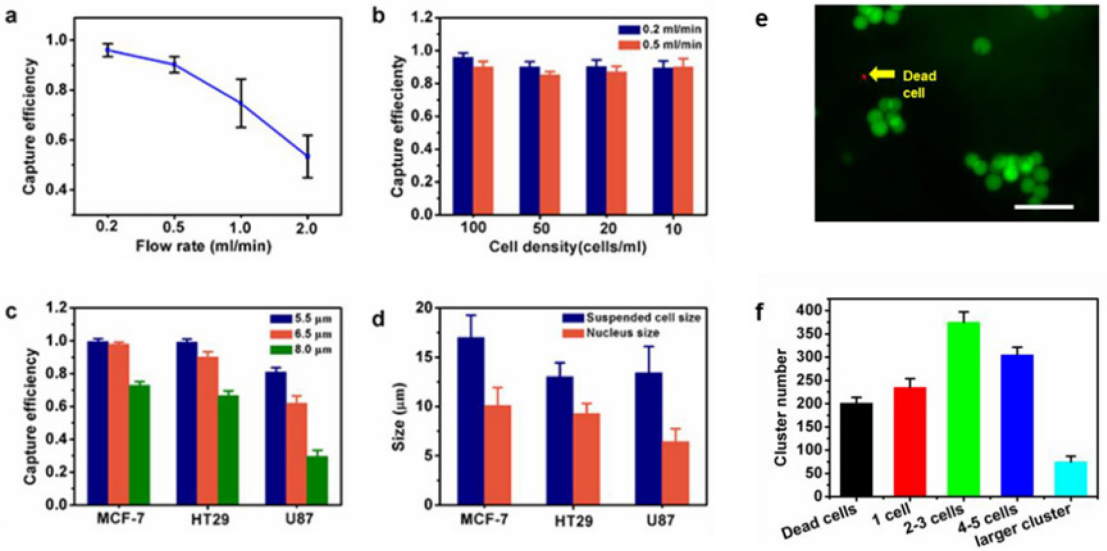

Figure 16: Performances des filtres avec des trous coniques. (a) Efficacité de capture en fonction de la vitesse d'écoulement. (b) Efficacité de capture pour 10, 20, 50, 100 cellules HT-29 dispersées dans 1 ml de PBS, mesurée avec un écoulement de 0,2 ou 0,5 ml/min, respectivement. (c) Dépendance de la capture au diamètre de trous pour un débit de 0,5 ml/min. (d) Taille des noyaux et taille des cellules mesurées avec une suspension de cellules. (e) Immunofluorescence des cellules HT-29 après coloration à la calcine AM / EthD-1. (f) Nombre de cellules par grappe au jour 4. Barre d'échelle: 50 µm. Les barres d'erreurs représentent l'écart type (SD) de trois mesures.

Nous avons également développé une analyse théorique pour expliquer les avantages de ce dispositif (Figure 17). D'une part, un filtre avec des trous coniques permet d'égarer plus facilement les globines blanches par rapport à celui avec des trous cylindrique. Conformément à la loi de Laplace, lorsqu'une vésicule (WBC) entre dans un trou cylindrique, elle ne peut pas s'échapper sans pression à cause de la symétrie de courbure aux deux extrémités. Par contre, lorsque cette vésicule entre dans un trou conique, elle peut s'échapper rapidement sans pression puisque les courbures aux deux extrémités ne sont plus les mêmes (Figure 17a). Il en résulte théoriquement une meilleure sélectivité ou pureté de capture, ce que nous avons prouvé par l'expérience (Figure 17b). D'autre part, un filtre avec des trous coniques permet d'avoir une différence de pression des deux côtés de la membrane relativement faible par rapport au filtre de trous cylindriques, ce qui garantie une

meilleure stabilité des CTCs capturés ainsi qu'une meilleure viabilité cellulaire. Enfin, si le flux entre directement dans les trous sans composant tangentiel, il y aura des zones mortes entre les tous puisque, d'après nos simulations numériques, les lignes d'écoulement ne passent presque pas par ces zones, . Ceci explique l'intérêt d'utiliser un flux avec composants tangentiels grâce au canal circulaire avec multi-entrées radicales (Figure 17c). Là encore, nous améliorerons la sélectivité ou la pureté de capture (Figure 17d).

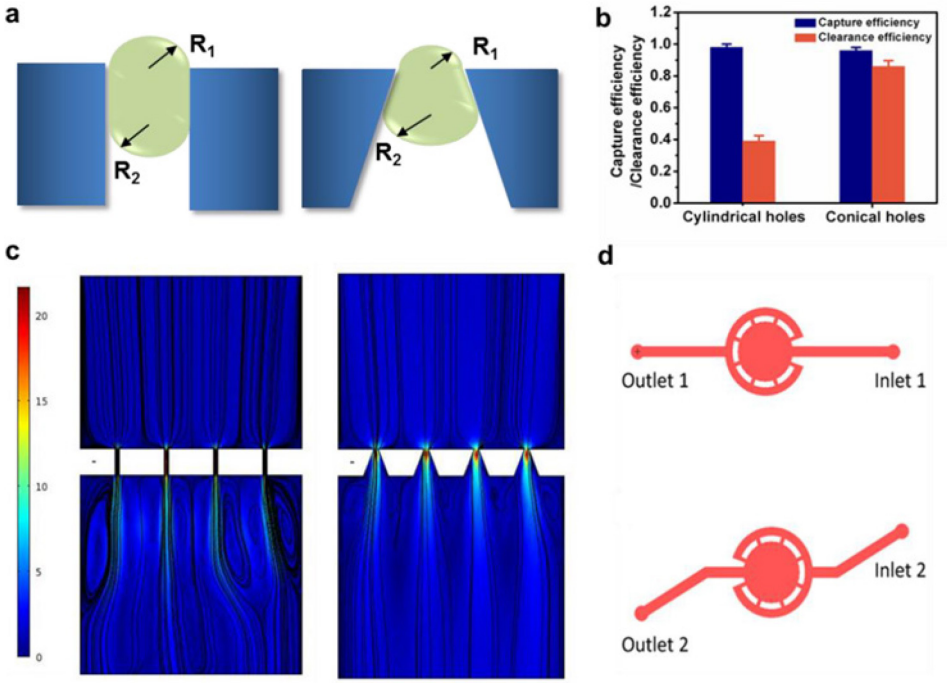

Figure 17. Modèle et comparaison entre les filtres de trous cylindriques et coniques (a) Schéma de la rétention des cellules dans un trou cylindrique et conique; (b) Efficacité de capture et pureté des cellules tumorales pour une filtration au débit de 0.2 ml/min; (c) Simulation de l'écoulement hydrodynamique de focalisation; (d) Canaux microfluidiques de la partie haute et la partie basse du dispositif.

3.3 Formation de sphéroïdes tumoraux

Nous avons développé une technique simple mais fiable pour la formation des sphéroïdes tumoraux (Figure 1). Un réseau de puits a été réalisé par les techniques de moulage en utilisant trois types de matériaux, PDMS, PEGDA et agarose.

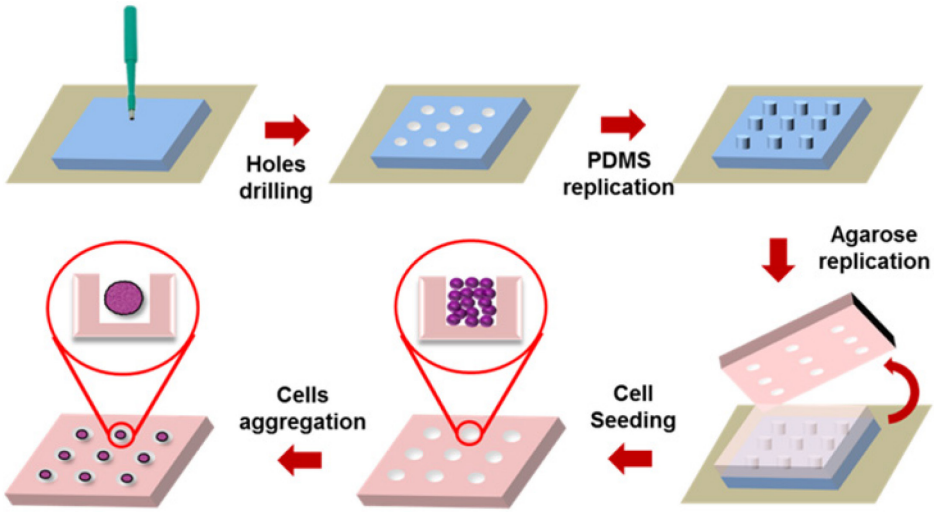

Figure 18. Schéma de procédé de fabrication d'un réseau de multi-puits d'agarose et de formation de sphéroïde tumoral.

Nous avons d'abord comparé les performances de formation de sphéroïdes dans les puits de ces trois types de matériaux (Figure 19a). Clairement, l'utilisation des puits d'agarose est avantageuse en raison de la surface hydrophobe et la perméabilité élevée de ce matériau. Nous avons remarqué que même dans les puits d'agarose les sphéroïdes tumoraux ont cessé de croitre après cette taille quelle que soit la densité cellulaire initiale (Figure 19b). Dans des puits de 2 mm de diamètre d'agarose, des sphéroïdes tumoraux U87 de diamètre de 1,4 mm peuvent être formés après culture pendant 10 jours. Pour étudier l'effet du médicament anti-cancer, la Combretastatine A-4 (CA4) a été ajoutée au jour 2 ou jour 4, montrant des effets clairs sur la formation de sphéroïdes et la viabilité des cellules tumorales (Figure 19c). Plus important encore, nos résultats suggèrent qu'un traitement précoce de médicament était plus efficace pour interdire la croissance du sphéroïde tumoral.

4. Conclusion et perspectives

Ce travail a pour but de mettre au point des nouvelles techniques et outils pour la recherche avancée sur les cellules souches et les cellules cancéreuses. Nous avons d'abord proposé un patch de monocouche de nanofibres réticulées, permettant de cultiver et de différentier les cellules souches pluripotentes induites humaines (hiPSCs) "hors sol". Puis, nous avons démontré la formation des tissus cardiaques et neuronaux sur patch à partir d'hiPSCs. Ensuite, nous avons développé un dispositif microfluidique avec une membrane composée de trous de forme conique pour

d'abord isoler les cellules tumorales circulantes (CTCs) puis les cultiver. Enfin, nous avons évalué l'effet de drogues anticancéreuses sur la formation des sphéroïdes tumoraux en utilisant des multi-puits d'agarose micro-fabriqués. En conclusion, nous avons progressé sur les techniques de la micro-ingénierie dédiées aux applications à grandes échelles et cliniques.

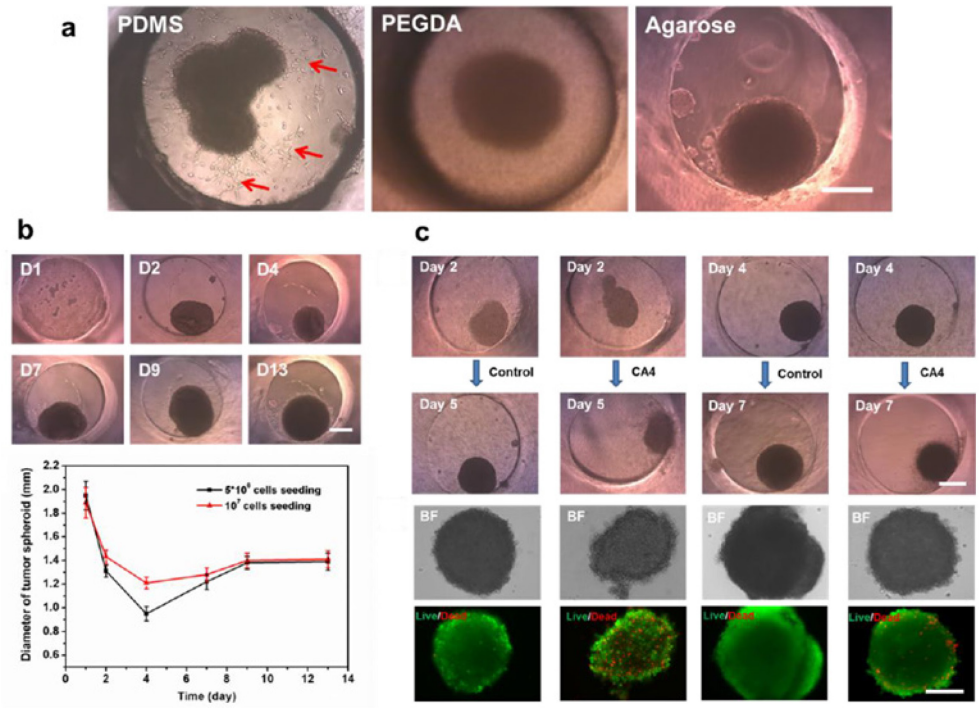

Figure 19. (a) Formation des sphéroïdes tumorales dans multi-puits de PDMS, PEGDA et agarose, respectivement; (b) Formation de sphéroïde tumorale dans un puits d'agarose et variation de taille du sphéroïde en fonction du temps; (c) Effet du médicament anticancéreux CA4 sur la morphologie des sphéroïdes tumorale et viabilité des cellules. Barre d'échelle: 0.5 mm.

List of Abbreviations

2D	Two-dimensional
3D	Three-dimensional
AA	Ascorbic acid
ALS	Amyotrophic lateral sclerosis
BDNF	Brain-derived neurotrophic factor
BF	Bright field
bFGF	Basic fibroblast growth factor
CA4	Combretastatin A4
CAM	Cellular adhesion molecules
cAMP	Cyclic adenosine monophosphate
CNC	Computer numeric controlled
CTCs	Circulating tumor cells
CVD	Cardiovascular diseases
DAPI	4’-6-diamidino-2-phenylindole
DMEM	Dulbecco’s Modified Eagle Medium
EB (EBs)	Embryonic body (Embryonic bodies)
ECF	Extracellular fluid
ECM	Extracellular matrix
EGF	Epithelial growth factor
EMT	Epithelial to mesenchymal transition
ESCs	Embryonic stem cells
FACs	Fluorescence-activated cell sorting
FBS	Fetal Bovine Serum
FGF	Fibroblast growth factor
FISH	Fluorescence in situ hybridization
FPs	Field potentials
GDNF	Glial-derived neurotrophic factor
HA	Hydroxyapatite
HOMPP	2-hydroxy-2-methylpropiophenone
HSCs	Hematopoietic stem cells
IGF-1	Insulin-like growth factor 1

iPSCs	Induced pluripotent stem cells
KSR	Knockout Serum Replacement
MEA	Multi-electrode array
MEA	Multi-electrode array
MEMS	Micro-electromechanical systems
MET	Mesenchymal to epithelial transition
MND	Motor neuron disease
MRI	Magnetic resonance imaging
MSCs	Mesenchymal stem cells
NEAA	Non-Essential Amino Acid
PCL	Poly(ε-caprolactone)
PCR	Polymerase chain reaction
PDMS	Polydimethylsiloxane
PEG	Poly(ethylene glycol)
PEGDA	Poly(ethylene glycol) diacrylate
PEGDMA	Poly(ethylene glycol) dimethacrylates
PET	Positron emission tomography
PFA	Paraformaldehyde
PGA	Polyglycolic acid
PLA	Poly(lactic acid)
PLGA	Poly-dl-lactic-co-glycolic acid
PLLA	Poly-l-lactic acid
PO	Polyornithine
Pur	Purmorphamine
RA	Retinoic acid
RBCs	Red blood cells
RT-PCR	Reverse transcription-polymerase chain reaction
SMA	Spinal muscular atrophy
TCP	Tri-calcium phosphate
TMCS	Trichloromethylesilane
VEGF	Vascular endothelial growth factor
WBCs	White blood cells
μTAS	Miniaturized total chemical analysis system

Publication list

1. **Yadong Tang**, Jian Shi, Sisi Li, Li Wang, Yvon E. Cayre & Yong Chen. Microfluidic device with integrated microfilter of conical-shaped holes for high efficiency and high purity capture of circulating tumor cells. Scientific reports, 2014, 4.
2. **Yadong Tang**, Yong Chen, Li Wang, Jian Shi：Cell culture device. [Patent]. European Patent: EU 15175960.2
3. **Yadong Tang**, Jianmiao Liu, Yong Chen. Agarose multi-wells for tumor spheroid formation and anti-cancer drug test. Microelectronic engineering. Submitted.
4. **Yadong Tang**, et al. Off-ground culture using a net of nanofibers for the formation of cardiac patch derived from human induced pluripotent stem cells. In preparation.
5. **Yadong Tang**, et al. Off-ground motor neuron differentiation from induced pluripotent stem cells. In preparation.
6. Bin Wang, Jian Shi, **Yadong Tang**, Jin Wei, Xiaolong Tu, Yong Chen. Microelectronic engineering. Submitted.
7. Jin Wei, Jian Shi, Bin Wang, **Yadong Tang**, Xiaolong Tu, Emmanuel Roy, Benoit Ladoux, Yong Chen. Fabrication of Adjacent Micropillar Arrays with Different Heights for Cell Studies. Microelectronic engineering. Submitted.
8. Xiaolong Tu, Lina Wang, Jin Wei, Bin Wang, **Yadong Tang**, Jian Shi, Zhijun Zhang, Yong Chen. 3D printed PEGDA microstructures for gelatin scaffold integration and neuron differentiation. Microelectronic engineering. Submitted.

Abstract:

This work aimed to provide new tools and methods that can be used for advanced studies of stem cells and cancer cells. We first developed a patch method for off-ground culture and differentiation of human induced pluripotent stem cells (hiPSCs). The culture patch we proposed consists of crosslinked monolayer gelatin nanofibers on a honeycomb frame to ensure minimal exogenous material contact and maximum permeability. Then, we demonstrated the formation of cardiac tissue constructs and motor neurons on the patch, started from embryoid-body like and monolayer hiPSC colonies, respectively. We also developed a microfluidic device with integrated filter for isolation of circulating tumor cells (CTCs), showing high capture performances in terms of efficiency, selectivity and cell viability. Finally, we evaluated the anti-cancer drug effect on the formation of tumor spheroids by using microfabricated agarose multi-wells. All together, we progressed in micro-engineering toward large scale applications.

Keywords: Stem cell; Cancer cell; Nanofibers; Microfluidics

Résumé:

Ce travail a pour but de mettre au point des nouvelles méthodes pour la recherche avancée sur les cellules souches et les cellules cancéreuses. Nous avons d'abord développé une méthode de patch pour la culture et la différentiation des cellules souches pluripotentes induites humain (hiPSCs) "hors sol". Ce patch de culture est constitué des monocouches de nanofibres réticulées de gélatine sur un support en nid d'abeilles pour assurer un minimum de contact de matériel exogène et un maximum de perméabilité. Puis, nous avons démontré la formation des tissues cardiaques et des neurones moteurs sur le patch, partis de colonies des hiPSCs en forme d'embryoïdes et de monocouches respectivement. Nous avons également développé un dispositif microfluidique avec filtre intégré pour isoler les cellules tumorales circulantes (CTCs), montrant une haute performance de capture en termes d'efficacité, de sélectivité et de viabilité cellulaire. Enfin, nous avons évalué l'effet de drogue anticancéreuse à la formation des sphéroïdes tumoraux en utilisant des multi-puits d'agarose micro-fabriqués. Tous ensembles, nous avons progressé dans la micro-ingénierie vers des applications à grande échelle.

Mots clés: Cellule souche; Cellule cancéreuse; Nanofibres; Microfluidique